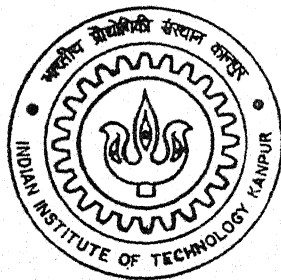# AN INVERSE TECHNIQUE FOR ESTIMATING THE FORCED CONVECTIVE HEAT TRANSFER COEFFICIENT ABOVE FLAT AND RIBBED SURFACES

By

Malay Kumar Das

DEPARTMENT OF MECHANICAL ENGINEERING

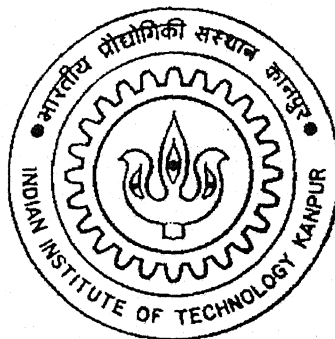## Indian Institute of Technology Kanpur

APRIL, 2003

AN INVERSE TECHNIQUE FOR ESTIMATING THE FORCED CONVECTIVE HEAT TRANSFER COEFFICIENT ABOVE FLAT AND RIBBED SURFACES

A Thesis Submitted
in Partial Fulfilment of the Requirements
for the Degree of
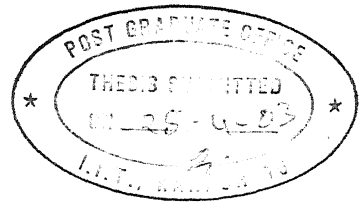Master of Technology

by
Malay Kumar Das

to the
DEPARTMENT OF MECHANICAL ENGINEERING
INDIAN INSTITUTE OF TECHNOLOGY KANPUR
INDIA
April 2003

CERTIFICATE

It is certified that the work contained in the thesis entitled "**An Inverse Technique for Estimating the Forced Convective Heat Transfer Coefficient above Flat and Ribbed Surfaces**", by Malay Kumar Das, has been carried out under my supervision and that this work has not been submitted elsewhere for a degree.

Dr. K. Muralidhar
Department of Mechanical Engineering
I.I.T. Kanpur
India

April, 2003

To Pradipta....

ACKNOWLEDGMENT

Abstract

The present research is concerned with the determination of the local Nusselt number for fluid flow and heat transfer from flat and ribbed surfaces. The determination of local Nusselt number for a surface with known temperatures requires the temperature in the vicinity of the wall. This is equivalent to solving the energy equation with proper initial and boundary conditions. In turn, it calls for the accurate measurement of surface temperatures or surface heat fluxes. In practice, the surface temperature or surface heat flux measurements are generally prone to substantial amount of spatial and temporal errors. The present work shows that the local Nusselt number can be estimated with a good degree of accuracy, even from the noisy surface temperature data, if additional high quality data is available within a favorable region of the flow field. The improvement has been effected by an inverse forced convection formulation in the present work and solved by the conjugate-gradient approach.

The present investigation is restricted to steady laminar flow of an incompressible Newtonian fluid with negligible viscous dissipation and mechanical work. The thermal field is allowed to evolve in time. The scope includes algorithm development, assessment of the numerical performance and experimental validation. The finite-difference method of discretization is used for the numerical solution of differential equations, while liquid crystal thermography and hot-wire anemometry are employed in the experiments. Air is considered as the working fluid for all the analysis.

The conjugate gradient method relies upon iterative updating of the unknown

functions or parameters through the minimization of a functional. The functional is generated in terms of the difference between the computed and measured data. Adjoint and sensitivity problems are formulated as intermediate steps to compute the gradient of the functional and the step size. The adjoint and sensitivity problems also expedite the physical understanding of the problem by enforcing the mirror image of the natural law and by estimating the influence of the prescribed data on the unknown function or parameter.

The effectiveness of any inverse technique is considerably dependent upon the method of stabilization used. Several tools falling in the category of iterative regularization are discussed, devised and employed in the present work.

The results show that the inverse convection technique is capable of estimating the surface information if noise in the additional high quality data is less than 10%. It is also realized that the additional data must be in the regions of high sensitivity. Inverse convection technique has thus been found to be a promising tool to bring out useful information from the noisy experimental data.

Contents

List of Figures

Nomenclature

Dimensional quantities

x^*	Stream-wise distance, m
y^*	Cross stream-wise distance, m
z^*	Transverse distance, m
L	Characteristic length, m
l^*	Length of the Computational domain, m
H	Height of computational domain, m
W	Plate width, m
U	Fluid inlet velocity, m/s
u^*	Fluid velocity in x direction, m/s
v^*	Fluid velocity in y direction, m/s
T_∞	Fluid inlet temperature, ^{o}C
T_0	Plate (or reference) temperature, ^{o}C
T	Computed fluid temperature, ^{o}C
Tm	Measured fluid temperature, ^{o}C
k_f	Thermal conductivity of the fluid, W/m ^{o}K
k_s	Thermal conductivity of the solid, W/m ^{o}K
h	Convective heat transfer coefficient, W/m ^{o}K

Greek Symbols

ρ	Fluid density, kg/m^3
ν	Kinematic viscosity of fluid, m^2/s
α_f	Thermal diffusivity of the fluid, m^2/s
α_s	Thermal diffusivity of the solid, m^2/s
τ	Time, s
τ_f	Final time of estimation, s

Non-dimensional quantities

x	x^*/L	Stream-wise distance.
y	y^*/L	Cross stream-wise distance .
z	z^*/L	Transverse distance.
l	l^*/L	Length of computational domain.
d	H/L	Height of computational domain.
r	W/L	Plate width.
t	$\tau L/U$	Time.
t_f	$\tau_f L/U$	Final time of estimation.
u	u^*/U	Fluid velocity in x direction.
v	v^*/U	Fluid velocity in y direction.
Y	$(T - T_\infty)/(T_0 - T_\infty)$	Measured fluid temperature.
Re	UL/ν	Reynolds number.
Pr	ν/α	Prandtl number.
Pe	UL/α	Peclet number.
Nu	$\left[-\frac{\partial T}{\partial y}/(T - T_\infty)\right]_{y=0}$	Local Nusselt number.
J	(Equation 2.14)	Functional.
w		Weight assigned to measured temperature.
P		Descent direction.

Greek Symbols

θ	$(T - T_\infty)/(T_0 - T_\infty)$	Computed non-dimensional fluid temperature.
$\triangle\theta$		Sensitivity.
λ		Lagrange multiplier.
δ		Dirac delta function.
β		Search step size.
γ		Weight to calculate descent direction.
ϵ		Small real number close to zero.
σ		Standard deviation of measured data.

Special symbols

$\lvert \ldots \rvert$	Absolute value.
$\langle \ldots \vert \ldots \rangle$	Inner product.
$\lVert \ldots \rVert$	Norm.

Subscripts

w	Value of variables at the wall.
m	Value of variables at measurement points.

Superscripts

$\prime$	Gradient.
k	Iteration counter.

Chapter 1

Introduction

While solving a set of partial differential equations, the initial and boundary conditions must be known. In addition the parameters appearing in the equations as well as in the initial and boundary conditions must be specified. Many problems of practical interest are governed by partial differential equations. Often they suffer from the problem of inadequacy of initial and boundary conditions or the knowledge of the required set of parameters. The information may be completely unavailable or supplied with substantial scatter. A reasonable solution can however be derived if additional good quality data of limited size is supplied. In most practical cases, these extra data are also corrupted with some noise. The task of an inverse analyst is to come up with an acceptable solution from the body of low and high quality data.

When a physical system is investigated experimentally, the signals generated by the measurement devices can hardly be free of any noise. The signal quality is quantified by the signal-to-noise ratio. If this ratio is less than 1, the experimental method needs improvement. If it is greater than 10, filtering techniques are adequate to suppress the noise. If this ratio is in between 1 to 10, the inverse technique proves effective to subdue the effect of noise. Qualitatively, the scatter in raw data can be divided into the following groups: systemic, operational, bias, random and sporadic. Poor design of experiment and human factors are responsible for the systemic and operational scatter, allowing no room to filter it out. The bias, random and sporadic scatter are generated from several uncertainties associated with the experiment. Fortunately, these types of scatter follow a statistically predictive behavior, authorizing some mathematical tools, such as the inverse technique, to dampen their corruptive effect.

Inverse calculations for thermal problems are of great practical importance for scientists and engineers. In thermal sciences, the inverse approach is largely applied to determine thermophysical properties and surface heat fluxes. The identification of robust and accurate methods for inverse thermal problems started in the 1960s. Different methods emerged, each with built-in advantages and disadvantages. In the last decade, attempts have been made to generalize these methods. A new and powerful technique based on the conjugate gradient method has emerged as a promising tool for inverse thermal problems. The conjugate gradient method has several disadvantages as well. They can be overcome by studying the performance of the algorithm in the context of a variety of complex applications.

Inverse thermal problems can be divided broadly into two categories: (1) Parameter estimation and (2) Function estimation. In (1), the aim is to determine an unknown parameter in the governing equation and/or initial and boundary conditions. The determination of initial and boundary conditions are generally posed as a function estimation problem. In addition, the determination of thermophysical properties such as thermal conductivity and heat capacity as functions of temperature requires a formulation for function estimation. Occasionally there is an overlap. If *a-priori* information is available regarding the functional form of the boundary conditions, the function estimation problem can be posed as a parameter estimation problem. The present work deals with inverse function estimation problem and all the discussions and formulations are confined to this category.

1.1 Literature Review

A survey of the available literature reveals that various aspect of the inverse technique have been addressed. These has been presented below as per the following sections: (1) Mathematical theory of inverse techniques, (2) Inverse heat conduction, (3) Inverse convection techniques.

1.1.1 Mathematical Theory of Inverse Techniques

The fundamental objective of an inverse procedure is to generate a solution with acceptable accuracy and stability from noisy experimental data. Hadamard [1923]

introduced the concept of a well-posed problem, originating from the philosophy that the mathematical model of a physical problem has to have the properties of uniqueness, existence and stability of the solution. Inverse problems generally violate these requirements. Often, existence and uniqueness can be forced by enlarging or reducing the solution space. For restoring stability, however, one has to change the topology of the spaces, which in many cases cannot be enforced due to the presence of scatter in the experimental data. The method of regularization, introduced by Tikonov [1963] is a watershed in the history of inverse techniques. Extensive review of different regularization methods can be found in the work of Engl *et al.* [1990], Bakushinsky *et al.* [1990], Kirsch [1996] and Glasko [2000].

Iterative regularization is the best available option at present as an inverse estimation technique. It is based on guessing the function to be estimated and improving it by matching the corresponding flow and thermal fields with experimental data. In other words the inverse problem can be posed as an optimization, specifically the minimization, of a functional. The very nature of the inverse algorithm suggests that small scatter in the measurement can cause enormous, perhaps unbounded error in the inverse solution. The method of regularization essentially adds an additional parameter to the functional to force a stable solution. While the regularization method has a firm mathematical background [Kirsch, 1996, Engl *et al.*, 1990, Bakushinsky *et al.*, 1990] the choice of the regularization parameter still needs to be finalized by trial and error. Iterative methods on the other hand, always add an error term with the functional and gradually reduce the overall error. Iterative regularization stops the iteration at some level where this residual error induces stability of the algorithm. However, in this method the question of where to stop the iteration, is not clearly understood. The most general approach is to assume equal standard deviation for all the measured data in the sense that at convergence, absolute error in each data is less than or equal to the standard deviation. While the assumptions regarding the stopping criterion of iterative regularization (also known as *discrepancy principle*) is not universally valid, it is quite popular due to ease of implementation and versatility.

Steepest descent and conjugate gradient methods are commonly used for iterative regularization. Different aspects of these methods are extensively discussed by Gilyazov *et al.* [2000]. The conjugate gradient method has the property of rapid convergence and a smaller probability of being confined to local minima.

This method is now the most accepted for the solution of inverse problems. Hanke [1995] has addressed the mathematical basis of the conjugate gradient method, the discrepancy principle and their applicability to ill-posed problems.

1.1.2 Inverse Heat Conduction

Inverse heat conduction problems are generally formulated to find the surface heat flux or thermophysical properties of a solid from interior temperature measurements. Mathematical models for inverse heat conduction are standardized and well-discussed [Alifanov, 1979, Beck *et al.*, 1985, Kurpisz *et al.*, 1995, Ozisik *et al.*, 2000]. They are also extensively in use.

Alifanov [1979] was the first to formulate the inverse heat transfer equations using the conjugate gradient method. Jarny *et al.* [1991] outlined the general optimization method for solving multidimensional inverse heat conduction equations. The idea was to estimate the unknown initial or boundary or conditions from internal measurements. They used the conjugate gradient method with the adjoint equation. The conjugate gradient method proved to be very efficient even without any *a-priori* assumption about the form of the unknown function. An *a-priori* assumption about the unknown functional serves as a special implementation of their formulation.

Huang *et al.* [1999] used the conjugate gradient formulation to solve the unsteady heat conduction equation in three dimensions. Using the formulation of Jarny *et al.* [1991] they successfully estimated the surface heat flux. This was the first published general solution of inverse heat conduction using the conjugate gradient method.

It is to be realized that the conjugate gradient method is not flawless. One major difficulty is to apply perfect stopping criterion of the iterations. Some discussions on this topic have been carried out by Khachfe *et al.* [2000]. They have pointed out that the minimum value of the functional that will ever be attained depends on the amount of error and the initial guess if the data error is substantial.

Khaliday [1998] used a space marching algorithm for inverse heat conduction. In the algorithm, stability is achieved by smoothing the measurement data using Gram orthogonal polynomials.

Lin *et al.* [2002] successfully coupled inverse technique and transient liquid crystal experiment to find the convective heat transfer co-efficient over a surface. They solved the inverse conduction equation using the Newton root-finding technique, ignoring the need for stabilization.

1.1.3 Inverse Convection Techniques

Moutsoglou [1989,1990] published the first ever work on inverse convection. She applied the function specification method of Beck [1962] in the whole domain as well as in a sequential manner.

Huang *et al.* [1992] used the conjugate gradient method to determine the unknown wall heat flux in laminar flow with steady forced convection through a parallel plate duct. They solved the energy equation for fully developed velocity field and developing temperature field. Interior temperature data, very close to the plate, were used to construct the functional and to retrieve the boundary condition, the unknown wall heat flux in this study. They further simplified the problem neglecting the streamwise second derivative term in the energy equation. Nevertheless, this simplified approach is the first published work on inverse convection using the conjugate gradient method. Their study proved the utility of the conjugate gradient method in solving inverse convection equations. The authors also pointed out that conjugate gradient method fails to improve the initial guess at some points where the adjoint function becomes zero and proposed a modified conjugate gradient approach to circumvent this difficulty.

Huang *et al.* [1999] solved a set of unsteady three dimensional inverse forced convection equations and estimated the time varying surface heat flux by conjugate gradient approach. They used commercial software to solve the unsteady momentum, energy, adjoint and sensitivity equations in this context.

Li *et al.* [2000] applied the inverse forced convection technique to estimate the time varying surface heat flux in an annular duct. The energy equation solved here was taken to be parabolic in both time and space. The authors used simulated temperature measurements at the outer wall of the duct and successfully estimated unknown wall heat flux using the conjugate gradient method.

Colaco *et al.* [2001] used a two dimensional inverse forced convection approach for estimating boundary heat fluxes in irregularly shaped channels. They used

elliptic grid generation procedure for the irregular geometry and determined two boundary heat fluxes simultaneously using the conjugate gradient method. The solutions were accomplished for time-dependent, spatially dependent and both time and spatially dependent heat fluxes.

1.2   Scope of the Present Work

In summarizing the previous work on inverse convection technique, it has been realized that a few test problems have been addressed and successfully modeled. The critical evaluation of the conjugate gradient approach and the inverse convection technique as a whole, is yet to be presented. In all the previous work discrepancy principle is considered as the stabilization method; other techniques have remained unaddressed. Furthermore, previous work have used only numerically generated data perturbed with random noise as the simulated experimental measurements. It is too early to draw conclusions about the performance of inverse convection approach in absorbing the noisy data from real life experiments, for which the inverse technique is ultimately called for. Also the potential of the sensitivity analysis, in the context of inverse convection is yet to be exploited.

The present work is concerned with the extraction of useful information from raw experimental data using the inverse technique. In this work, the performance of the conjugate gradient approach and several stabilization techniques have been extensively studied. The inverse algorithm has been applied to simulated as well as experimental data. Sensitivity analysis has been carried out to substantiate the results. All calculations pertaining to the solution of the partial differential equations have been numerically carried out.

With simulated data, the algorithm has been used for estimating the local Nusselt number for flow over flat and ribbed surfaces under conditions of forced convection. The idea here is to find the local Nusselt number distribution when on one hand the surface temperature carries substantial noise, but additional high quality but limited data is available within the flow field. In the context of simulation, high quality data is generated from the solution of the direct problem with an error-free plate temperature. The following test cases have been considered in the present study. The direct numerical solvers required at intermediate stages of the inverse calculation are also indicated.

1. Flow and heat transfer over a flat plate:

   (a) Two dimensional parabolic solver for velocity and temperature;

   (b) Two dimensional flow field with three dimensional temperature field both determined by a parabolic solver;

   (c) Two dimensional flow field with a parabolic solver with three dimensional elliptic solver for temperature.

2. Flow and heat transfer over a flat plate with a single rib:

   (a) Two dimensional elliptic solver for velocity and temperature;

   (b) Two dimensional flow with three dimensional temperature both by elliptic solver.

   (c) Two dimensional elliptic solver for velocity and temperature with transient plate temperature.

In each case the velocity field is considered to be two-dimensional. For flat plate geometry, velocity field is solved through the boundary-layer approximation. Flow over a surface mounted rib can only be solved in an elliptic framework. The elliptic flow solver is based on stream function-vorticity approach.

In the experimental part of the study, an inverse technique has been presented to estimate the local Nusselt number distribution for flat and ribbed surfaces in the laminar flow. The transient temperature field over the surface has been imaged by liquid crystal thermography. Two different Reynolds numbers for a plate with a solid rib have been considered.

1.3 Thesis Organization

The present thesis has been organized in the following manner:

1. Chapter 1 presents introduction, literature review and scope of the present research.

2. Chapter 2 describes the inverse model in conceptual terms.

3. Chapter 3 presents the formulation of inverse heat transfer from a flat plate.

4. Chapter 4 presents the formulation of inverse heat transfer from a ribbed surface.

5. Chapter 5 is a description of the experimental apparatus.

6. Chapter 6 presents the experimental data reduction technique.

7. Chapter 7 reports major results for heat transfer from the flat plate, with simulated data.

8. Chapter 8 reports major results for heat transfer from the ribbed surface.

9. Chapter 9 carries conclusions of this study and scope of future work.

10. Appendices contain details of numerical treatment and discretization, code validation and grid independence.

Chapter 2

Mathematical Formulation: an Outline

The fundamentals of inverse problem and the mathematical tools used to solve the resulting equations are described in this chapter. The application of the mathematical formulation to specific geometries will be presented in subsequent chapters.

2.1 Fundamentals of Inverse Problem

Following Keller [1976], two problems are said to be inverse to each other if the formulation of one involves the other. For mostly historic reasons, one might call one of these problems (usually the simpler one or the one that was studied earlier) the direct problem; the other is the inverse problem. However, in the real-world, there lies, in most cases, a natural distinction between the direct and the inverse problems. If one wants to predict the future behavior of a physical system from knowledge of its present state and physical laws (including concrete values of all relevant parameters), it will be called a direct problem. Possible inverse problems are the determination of the past state from present-day observations (i. e., the calculation of the evolution of the system backward in time) or the identification of physical parameters from observations of the evolution of the system (parameter identification). Thus inverse problems are associated with determining the cause from the desired or an observed effect.

The detailed classification of inverse problems is given by Kozdoba[1982]. In general, they fall into the following categories:

1. Inverse Boundary Value Problems.

2. Parameter Estimation.

3. Inverse Initial Value Problems.

4. Inverse Geometry Problems.

5. Others.

In the present work the inverse problem is formulated as an inverse boundary value problem. Inverse boundary value problems can be viewed as the recovery of boundary conditions of a partial or ordinary differential equation from complete or partial interior information. In heat transfer, this generally refers to estimation of surface heat flux history of a body from transient temperature measurements at some interior locations.

2.2   Ill-posedness of inverse problem

Hadamard [1923] introduced the concept of a well-posed problem, originating from the philosophy that, the mathematical model of a physical reality has to have the properties of uniqueness, existence and stability of the solution. If one of the properties fails to hold, the problem was called ill-posed. Let us define a problem by the operator equation

$$Db = e \qquad\qquad (2.1)$$

where $b \in B$ and $e \in E$, E and B are metric spaces and D is an operator so that $DB = E$. In general, b can be a vector that characterizes a model of a phenomenon and e can be the observed attributes of the phenomenon. A correctly posed problem must meet the following requirements:

1. The solution of Equation 2.1 must exist for any $e \in E$.

2. The solution of Equation 2.1 must be unique.

3. The solution of Equation 2.1 must be stable with respect to perturbations on the right-hand side, i.e. the operator D^{-1} must be defined in the space E and be continuous.

Let us assume that the values of e cannot be exactly measured and only the approximate values of $e_\delta \in E$. If the error is bounded

$$\|e - e_\delta\|_E \leq \delta \qquad (2.2)$$

where $\|...\|$ is the Euclidian norm, defined in a metric space E. If the problem is correctly posed the following condition holds:

$$\|b - b_\delta\|_E \to 0 \ \text{ if } \ \delta \to 0 \qquad (2.3)$$

where b is the solution of equation Equation 2.1 for an accurate vector e and

$$b_\delta = D^{-1}e_\delta \qquad (2.4)$$

This result (Equation 2.3) is not true when ill-posed problems are encountered. For ill-posed problems the inverse operator D^{-1} defined throughout its domain $DB \in E$ is not continuous, it means that the solution of Equation 2.1 does not depend continuously on the data. Thus, the element $b_\delta = D^{-1}e_\delta$, even if it is exists, is not an approximate solution, because b_δ may arbitrarily deviate from the exact solution b even for small δ.

A lot of problems of optimum control, linear algebra, integral equations, the summation of Fourier series with approximately specified coefficients and the minimization of functionals are ill-posed and they are extremely sensitive to parametric and measurement errors.

The ill-posed nature in a mathematical sense of inverse problems originate from physics. Two effects should be mentioned here: damping and lagging. In the direct problems of heat transfer, the temperature fluctuations are diminished internally in comparison with the surface temperature changes. This is a damping effect. In particular, the higher frequency components of the boundary conditions are damped at a higher rate than the lower frequency components. In the inverse problem the higher frequency components of the measurements are amplified as the measurements are projected to the surface. As a result, the surface condition predictions might be overwhelmed by the noise in the measurements.

A large time delay or lag in the internal response to the changes in the boundary conditions should also be noticed. As an example, let us consider the problem of heating a symmetrical slab of thickness $2l$. The Biot number is defined as

Bi $= hl/k$ and the Fourier number is defined as Fo $= \alpha t/l^2$, where h is the heat transfer coefficient, t represents time, α stands for the thermal diffusivity and k is thermal conductivity of slab material. It can be proved that if the boundary condition of the third kind is prescribed on the surface of the slab, the temperature on the axis of the slab remains almost unchanged until Fo ≈ 0.05. At the same time the surface temperature for example, Bi=4 becomes equal to one half of the temperature for the steady-state. As a result the surface temperature cannot be estimated from the temperature measurements on the axis of the body within such a time interval.

Another question that arises in inverse thermal problems concerns the uniqueness of surface condition as predicted by discrete internal measurements. The natural way to overcome this difficulty is to obtain the maximum amount of information from the measurements. For transient problems, this implies minimizing time steps between two subsequent measurements. However, small steps may cause instabilities in the two subsequent measurements, causing instabilities in the solution. This observations is contrary to the direct problem where stability can be improved by reducing the time steps. As a consequence, for inverse problems the upper and the lower limits for time steps need to be specified.

The ill-posed nature of an inverse formulation causes elegant methods of direct problems be inapplicable. Special numerical techniques must be employed to stabilize the calculations. Any procedure for inverse problems, given in the literature without discussion on the question of stability is, in fact, without value.

2.3   Methods of Solution

Since numerous inverse methods have been proposed in the literature, some criteria for their evaluation are needed. The criteria listed are those proposed by Beck [1985]:

1. The predicted temperatures and heat fluxes should be accurate if measured data is of high accuracy.

2. The method should be insensitive to measurement errors.

3. The method should be stable for small time steps or intervals. This permits the extraction of more information regarding the time variation of surface

conditions than is permitted by large time steps.

4. Temperature measurements from one or more sensors should be permitted.

5. The method should not require continuous first order time derivatives of the surface heat flux. Furthermore, step changes or even more abrupt changes in the surface heat fluxes should be permitted.

6. Knowledge of the precise starting time of the application of the surface heat flux should not be required.

7. The method should not be restricted to any fixed number of observations.

8. Composite solids should be permitted.

9. Temperature dependent properties should be permitted.

10. Contact conductances should not be excluded.

11. The method should facilitate easy computer programming.

12. The computer cost should be moderate.

13. The user should not have to be highly skilled in mathematics in order to use the method.

14. The method should be capable of treating various multidimensional coordinate systems.

15. The method should permit extension to more than one heating surfaces.

16. The method should have a statistical basis and permit various statistical assumptions for the measurement errors.

Though the above criteria are proposed for inverse conduction problems, majority of these are applicable for inverse convection as well. The formulation used in the present work meets most of these conditions (with the exception of (12)).

While solving direct thermal problem one has to formulate and analyze governing partial differential equations of the related phenomenon. These equations must be supplemented with appropriate initial and boundary conditions. All

coefficients in the governing equations, and initial and boundary conditions including thermal conductivity, density and specific heat as well as the capacity and the location of internal heat sources, if they exist, have to be specified. Also, geometry of the physical domain must be fully specified. The main objective here is to find the temperature distribution within a domain initial and boundary disturbances.

For inverse problems, some of the above listed input data are missing. Thus, the mathematical description of the direct problem becomes incomplete and defies its solution. To make the solution of the inverse problem available, additional information is required. Usually, this data is obtained from measurements at interior points of a domain. The general strategy of solving inverse problems can be summarized by the following steps:

1. Make the mathematical description of the boundary value problem complete by assuming arbitrary values as required by the direct problem but not specified in the input data of the inverse problem.

2. Solve the direct problem by an analytical or a numerical method.

3. Compare the calculated and measured values and modify the assumed input data to ensure the best match between these quantities. This essentially calls for an optimization scheme to minimize the functional created from the difference of the computed and the measured data.

4. Stop iteration at a level where maximum information and minimum noise is passed to the numerical solution.

Following this strategy of solving inverse thermal problems, one not only discovers the cause from a known result but also retrieves missing information. Particular methods of solution of inverse problems differ way the assumed input data is modified. The techniques for solving an inverse problem can be loosely classified under the following groups:

1. Integral equation approach.

2. Integral transformation techniques.

3. Series solution approach.

4. Polynomial approach.

5. Hyperbolization of the heat conduction equation.

6. Space marching technique with filtering of the noisy input data, such as the mollification method.

7. Iterative filtering techniques.

8. Steady-state techniques.

9. Beck's sequential function specification method.

10. Levenberg-Marquardt method for the minimization of the least-square norm.

11. Tikonov's regularization approach.

12. Iterative regularization methods for parameter and function estimations.

13. Neural networks and genetic algorithms.

The details review of these methods can be found in the works of Alifanov [1979], Beck *et al.* [1985], Kurpisz [1995] and Ozisik *et al.* [2000]. Presently, the iterative regularization method has become popular among researchers, due to its simplicity and versatility. In the present work iterative regularization method has been used with some traditional and modified schemes of stabilization.

2.3.1 Iterative Regularization

The iterative regularization method, developed by Alifanov [1979], essentially converts the inverse problem into a statement of optimization problem. It is solved through a series of direct problems and a suitable stopping criteria. For well posed problems the iterations are carried out as long as the discrepancy between two successive steps becomes sufficiently small. For ill-posed problems the number of iterations P must be coordinated with the data error δ. In that sense, the number P acts as a regularization parameter. The iterative regularization can be applied to inverse boundary value problems as well as others.

Let the problem to be solved be expressed by an operator equation

$$Db = e_\delta \qquad (2.5)$$

If the operator D^{-1} is not continuous then the problem becomes ill-posed. To overcome the ill-posed nature of the problem two questions have to be answered:

1. What iterative algorithm should be employed?

2. How many iteration steps should be performed?

Numerous iterative algorithms [Kurpisz, 1995] can be applied to solve Equation 2.5 for b. Some of them are listed below:

1. $b^{p+1} = b^p - (Db^p - e_\delta), b^0 = e_\delta, p = 1, 2, \ldots P$

   where P stands for the total number of iterations and p refers to the current iteration level.

2. $b^{p+1} = (I - \nu D^* D)b^p + \nu D^* e_\delta, b^0 = D^* e_\delta, p = 1, 2, \ldots P$

   where D stands here for a matrix operator, b is a vector, I is an identity matrix, D^* is the conjugate of matrix D, ν is a coefficient that satisfies

$$0 < \nu < 2/\|D^* D\|$$

3. $b^{p+1} = \frac{1}{p+1} \sum_{n=0}^{p} [(I - \nu D)b^p + \nu e_\delta]$

The problem of solving an operator equation can be transformed into the problem of minimizing the functional

$$J = \|Db_\delta - e_\delta\| \tag{2.6}$$

It leads to the successful iterative methods, called the gradient search techniques. The general form of an iterative algorithm can be written as follows:

$$b_\delta^{p+1} = R(b_\delta^p, \delta) \tag{2.7}$$

The iterative algorithm is termed as regularized if it satisfies the following conditions:

1. For any $b^0 \in B$ the iterative sequence tends to the exact solution when $\delta = 0$

2. The transition operator $R(b_\delta^p, \delta)$ is continuous for each element b when $\delta = 0$

These conditions are satisfied by the following well-known methods:

1. Steepest Descent.

2. Conjugate Gradient.

Application of the steepest descent method results in the following iterative formula:

$$b^{p+1} = b^p - \beta_p J_b', \quad p = 0, 1 \ldots P \tag{2.8}$$

$$\beta_p = \frac{\|J_b'^p\|_B^2}{2\|DJ_b'^p\|_E^2} \tag{2.9}$$

The conjugate gradient method produces the following algorithm:

$$b^{p+1} = b^p - \beta_p \Omega^p, \quad p = 0, 1 \ldots P \tag{2.10}$$

$$\beta_p = \frac{(J_b'^p, \Omega^p)_B}{2\|D\Omega^p\|_E^2} \tag{2.11}$$

$$\Omega^p = J_b'^p + \alpha_p \Omega^{p-1}, \quad \alpha_0 = 0, \quad \alpha_p = \frac{\|J_b'^p\|_B^2}{\|J_b'^{p-1}\|_B^2} \tag{2.12}$$

where

$$J_b'^p = 2D^*(Db_\delta^p - e_\delta)$$

is a gradient of the functional

$$J^p = \|Db_\delta^p - e_\delta\|$$

with respect to b if the operator D is linear. The symbol D^* stands for the conjugate operator, whereas the notation (a, b) stands for a scalar product. Similar formulas can be written for cases when the operator D is nonlinear but the convergence of the iterations must be established via numerical experiments.

As indicated, the number of iteration steps P must correspond with input data errors and to evaluate its value the discrepancy principle can be used. This means that to determine P we have to take the first solution at the P the iteration level that satisfies

$$\|Db_\delta^p - e_\delta\| \leq \alpha\delta \tag{2.13}$$

where $\alpha > 1$ is a fixed constant.

2.4 Conjugate Gradient Approach

The gradient of a function is a very important property. The partial derivative of a function f with respect to each of the n independent variables are collectively called the gradient of a function and is denoted by $\bigtriangledown f$. If we move along the gradient direction from any point in n-dimensional space, the function value changes at the greatest rate. Hence the direction is called the direction of steepest ascent. Since the gradient vector represents the direction of steepest ascent, the negative of gradient vector denotes the direction of steepest descent. Thus any method that makes use of the gradient vector as a descent direction can be expected to yield rapid convergence. The steepest descent method for minimization of a functional is based on this criterion. Unfortunately, the direction of steepest descent is a local property, and not a global one. Many improvements have been suggested to the steepest descent method. One of them is to consider both the present and the previous descent directions to find the new descent direction. This technique is known as the conjugate gradient method. In the present work this technique is used to solve the inverse convection equation. The conjugate gradient method has been used to optimize the functional formed by the difference between measured and computed temperatures and the governing partial differential equation with the boundary and/or initial conditions serving as the constraints. The entire algorithm is divided into a number of subproblems as described below.

2.4.1 Direct Problem

The direct problem is to solve the governing partial differential equation with the proper boundary and/or initial conditions. In the context of an Inverse calculation, guessing the missing informations, which are continuously updated.

2.4.2 Inverse Problem

If θ and Y are the computed and measured temperatures respectively the following functional can be formed:

$$J = \int_{\Omega} (\theta - Y)^2 \delta(y - y_1) \tag{2.14}$$

where, δ is the Dirac delta function and y_1 indicates the plane of measurement. The integration is carried out over this plane. The solution is generated by seeking

the function $\theta(x, y)$ that minimizing J.

2.4.3   Sensitivity Problem

The sensitivity problem is obtained by perturbing the governing equation and the initial and boundary conditions of the direct problem. The sensitivity function $\Delta\theta$ is the solution of sensitivity problem, and is defined as the directional derivatives of the temperature θ in the direction of perturbation. In the algorithm, the sensitivity function is used only to determine the step size. The solution procedure of the sensitivity problem is similar to that of the direct problem, but the physical implication of the sensitivity function is enormous. This function dictates the dependence of temperature on the unknown quantity to be estimated (here, the local Nusselt number). Specially in thermally developing flows, the importance of the sensitivity function is revealed because temperature within only a very small region of the domain is influenced by the local Nusselt number distribution. The sensitivity function discovers the interior region where the boundary information is contained. In this way, it helps in designing the experiment for high quality measurement. The sensitivity function also indicates the influence of data error on the final solution and helps in selecting the best method of stabilization.

2.4.4   Adjoint Problem and Gradient Equation

The formulation of the adjoint problem proceeds by using the principle of variational calculus. Here the concept of Lagrange multiplier is introduced. The Lagrange multiplier is obtained by solving the the adjoint equation with initial and boundary conditions. The Lagrange multiplier serves as the input to the gradient equation to evaluate the gradient of the functional. The gradient in turn is used to find the descent direction.

2.4.5   Step size computation

The gradient of the functional serves as an input to the sensitivity problem. The step size is computed in relation to the sensitivity coefficient and the differences of the measured and computed temperature, with the requirement that the step size applied to the gradient would bring the functional to its minimum.

2.5 Algorithm Stabilization

Stabilization is the method of imposing stability to the inverse algorithm, specifically the flow of scatter into the final solution. The aim is to resist unbounded changes in the solution for a small change in the input data. Clearly, if the experimental data is completely free of error, no stabilization procedure is required and minimization of the functional would produce the correct result. Unfortunately, in practice, experimental data can hardly be exact. The idea of regularization involves (1) modifying the functional before carrying out optimization or (2) premature stopping of the minimization process. A few approaches used in the present work are discussed below.

2.5.1 Discrepancy Principle

The discrepancy principle is used by both Tikonov [1963] and Alifanov [1979]. Presently this is the most widely used method of stabilization. The principle is based on the following assumptions:

1. Standard deviation (σ) of all measurements are equal.

2. The value of this standard deviation is known.

The iterative procedure is stopped when the following criterion is satisfied

$$|Y - \theta| \leq \sigma \qquad (2.15)$$

The limitations of this procedure comes from the assumptions. Data scatter in different portion of the physical region may not be less than the standard deviation. Even if they are comparable, their standard deviation may not be known in advance.

2.5.2 Additional Measurement Approach

This method proposed by Ozisik [2000] circumvents the limitations of the discrepancy principle. Here two sets of data are used for constructing functionals J_1 and J_2. While minimization of J_1 is continued, the value of J_2 initially decreases. At some point the value of J_2 starts to increase, revealing the onset of instability. Iteration is generally stooped at this stage.

While this method has a number of advantages over the traditional discrepancy principle, it needs a large number of data. It can fail to give satisfactory results if the orders of magnitude of data scatter are different.

2.5.3   Smoothing of Measurement Data

The stability of inverse algorithm is hampered by the high frequency components of the measured data. If the high frequency components can be cut out to some extent, the solution can be stable. This idea has been exploited by Khaliday [1998] for inverse conduction.

2.5.4   Present Approach

In the present work, two types of data has been handled: numerically simulated data and experimentally generated data. Different methodologies are employed for these data types.

Numerically Generated Data

Here the standard deviation of the data set are not all the same. A large number of data with high error, whereas number of high quality data is less. If we use the stopping criteria described above the solution would be overwhelmed by the data with high error and small number of high quality data would fail to refresh the solution. To circumvent this difficulty, the following definition is used to formulate the functional.

$$J = \int_{\Omega} [w(\theta - Y)^2 \delta(y - y_1) + (\theta - Y)^2 \delta(y - y_2)] \qquad (2.16)$$

where w is a weight assigned to the high quality data.

The data at $y = y_2$ is taken to contain substantial error while the data at $y = y_1$ is of high quality. Before constructing the functional all data is filtered using Gram orthogonal polynomial filtering. With due weightage through the parameter w and filtering, the functional is minimized to yield the inverse solution.

The determination of the parameter w is very crucial. This determines the effect of different levels of error on the final solution. The method of minimization of the functional through the conjugate gradient method has shown that the minimum value of the functional (J_{min}) depends upon the data scatter (Figure

2.1). This phenomenon was addressed by Khachfe *et al.* [2000]. J_{min} reaches a value close to zero if the scatter is negligibly small. As the data scatter increases the absolute value of J_{min} increases. Though the mathematical basis of this observation is yet to be addressed, this property is exploited in this present work to evolve an idea of the value of w.
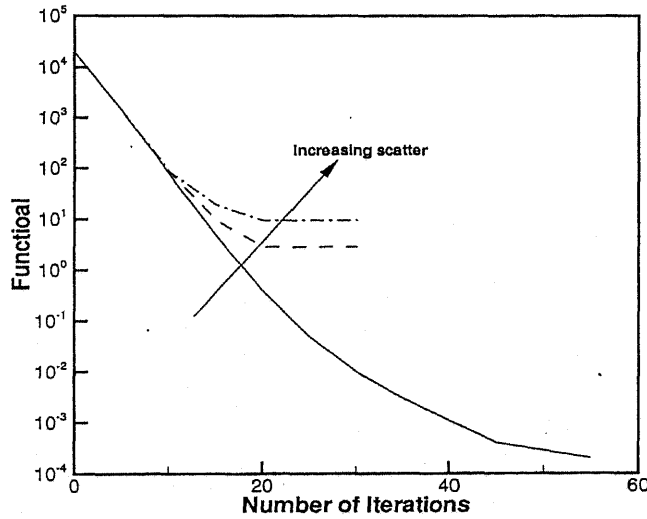
Figure 2.1: The variation of functional with iterations as shown by Khachfe *et al.* [2000]

Starting from an arbitrary initial guess, let the minimum value of the functional be J_{1min}, when data with high scatter is used and J_{2min}, when only data with low scatter is used. Allowing both the data set to influence the final solution equally, we can use

$$w_{optimum} \approx \frac{J_{1min}}{J_{1min}} \qquad (2.17)$$

If $w << w_{optimum}$ the noisy data will influence the solution very much and there will be little recovery of the local Nusselt number. If $w >> w_{optimum}$ the noisy data is practically kept out of any use and the solution is based on very few high quality data points. This set might not be capable of producing uniqueness to the solution. Observations of the present work show that the range $w = (10 - 100)w_{optimum}$ gives the best estimations with accuracy and uniqueness both being reasonably maintained.

Experimentally Generated Data

For experimentally generated data the standard deviation of the data is not clearly known. A large amount of data is available. Additional Measurement Approach, described in Section 2.5.2, has been used here.

2.6   Filtering of Data

The objective of filtering (or, smoothing) is to cut out the high frequency components from the measured data. The high frequency components accentuate the errors in the solution of the inverse problem to a great extent. As shown in the work of N. A. Khalidy [1998] and also of J. Taler *et al.* [1999], the filtered data does stabilize the algorithm. The present work also supports this observation.

Several filtering techniques are presented in the literature to eliminate the noise from the measured data. Examples are inclusion of digital filters in the inverse algorithm. Hanning, triangular, Gaussian, Tukey, Savitzky-Golay and Gram orthogonal polynomial are examples of such filters. In the present work, the performance of Hanning and Gram orthogonal polynomial filtering have been tested and the later is chosen.

2.6.1   Hanning Filter

Hanning filter uses the concept of frequency domain filtering using fast Fourier transform. This is extremely suitable for cases where the number of data points is large. A stringent requirement of this filtering technique is that, for using the fast Fourier transform algorithm, it needs number of data to be equal to 2^n, where n is a positive integer. The fast Fourier transform transfers the data into frequency domain. After cutting out the highest frequency portion (approximately 10% of the area under the power spectrum), the data is again transfered to time or space domain by means of inverse Fourier transform to get the smoothed data. This method has other difficulties such as aliasing and distortion of phase information, and should be carefully employed.

2.6.2   Gram Orthogonal Polynomial Filter

Least squares approximation is very well suited for the recovery of a smooth function from noisy information. It is possible to chose an appropriate function which is flexible enough to reconstruct the underlying noise-free function and its derivatives while still being orthogonal to the noise, i.e., fails to follow the oscillations in the measured data. The Gram orthogonal polynomial filtering, a popular methodology of stabilization of inverse problem [Khalidy, 1998], follows the principle. It uses weighted averaging of several past and future (spatially or temporally) data for smoothing. Thus the filter replaces each data value T_i by a combination of itself and certain adjacent points by fitting a piecewise polynomial using the least squares method to find the coefficients of the polynomial. It can be shown that,

$$f_n(x_i) = \sum_{j=0}^{n} b_j p_j(i) \tag{2.18}$$

where, $f_n(x_i)$ is the smooth representation of the measured temperature at $x = x_i$. Let L be the number of points used to the left and to the right of the central point $x = x_i$. (Notice that Equation 2.16 can be used for smoothing the data spatially as well as in time.) The subscript n refers to the total number of data points used for the smoothing the process ($n = 5$ for $L = 2, n = 7$ for $L = 3$, and so on). The parameters in Equation 2.16 can be calculated as [Korn, 1968],

$$b_j = \frac{\sum_{i=-L}^{L} T(i) p_j(i)}{\frac{(2L+j+1)!(2L-j)!}{(2j+1)\{(2L)!\}^2}} \tag{2.19}$$

$$\text{and,} \quad p_j(i) = \sum_{m=0}^{j} \frac{(-1)^{m+j}(m+j)^{[2m]}(L+i)^{[m]}}{(m!)^2 (2L)^{[m]}} \tag{2.20}$$

where $y^{[m]} = y(y-1)(y-2)........(y-m+1)$ and $m = 1, 2.....$ This type of smoothing is also called moving window averaging. Choice of number of data points is generally heuristic; 7 to 11 points are expected to yield reasonably good approximation.

Gram orthogonal filtering by 7 points moving window averaging is employed in the present study. In this method a piecewise polynomial is set through the first 7 points and these 7 points are smoothed. The next 7 points are then taken into account. It is assumed that at the beginning and the end the data points

are fixed. Using the above Equations 2.16, 2.17 and 2.18 the smoothed values of f_n can be computed as:

$$f_n(x_{i-3}) = \frac{1}{42}(39T_{i-3} + 8T_{i-2} - 4T_{i-1} - 4T_i + T_{i+1} + 4T_{i+2} - 2T_{i+3}) \quad (2.21)$$

$$f_n(x_{i-2}) = \frac{1}{42}(8T_{i-3} + 19T_{i-2} + 16T_{i-1} + 6T_i - 4T_{i+1} - 7T_{i+2} + 4T_{i+3}) \quad (2.22)$$

$$f_n(x_{i-1}) = \frac{1}{42}(-4T_{i-3} + 16T_{i-2} + 19T_{i-1} + 12T_i + 2T_{i+1} - 4T_{i+2} + T_{i+3}) \quad (2.23)$$

$$f_n(x_i) = \frac{1}{21}(-2T_{i-3} + 3T_{i-2} + 6T_{i-1} + 7T_i + 6T_{i+1} + 3T_{i+2} - 2T_{i+3}) \quad (2.24)$$

$$f_n(x_{i+1}) = \frac{1}{42}(T_{i-3} - 4T_{i-2} + 2T_{i-1} + 12T_i + 19T_{i+1} + 16T_{i+2} - 4T_{i+3}) \quad (2.25)$$

$$f_n(x_{i+2}) = \frac{1}{42}(4T_{i-3} - 7T_{i-2} - 4T_{i-1} + 6T_i + 16T_{i+1} + 19T_{i+2} + 8T_{i+3}) \quad (2.26)$$

$$f_n(x_{i+3}) = \frac{1}{42}(-2T_{i-3} + 4T_{i-2} + T_{i-1} - 4T_i - 4T_{i+1} + 8T_{i+2} + 39T_{i+3}) \quad (2.27)$$

Near the end of the domain, the number of points available may not be sufficient to carry out this formulation. Reasonable results can still be obtained by extrapolating the measured data set[1998]

2.7 Computational scheme and Discretization

For the numerical solution of direct, sensitivity and adjoint problem the governing partial differential equations and boundary conditions have been discretized using finite difference technique. For two and three dimensional parabolic equations the Crank-Nicholson scheme is used; fully implicit scheme has been used for elliptic problems. For the flat plate, the velocity field is computed using the boundary-layer approximation. For the ribbed plate, a vorticity-stream function approach is employed for the velocity field using an explicit scheme for the vorticity equation. In all cases the flow field is assumed to be laminar and buoyancy forces have been neglected. Steady and unsteady forced convection heat transfer conditions have been considered. The numerical solution of the direct problem is discussed in Appendix A.

Chapter 3

Flow and Heat Transfer over a Flat Plate

The mathematical procedure of the inverse technique based on iterative regularization method is presented in this chapter for flow over flat plate. The original algorithm, using conjugate-gradient gradient method for conduction problem was developed by Alifanov [1979], which was later applied to convection problem by Huang *et al.* [1992, 1999]. The following assumptions have been employed throughout:

1. The fluid is Newtonian and incompressible.

2. The fluid properties are constant with respect to temperature.

3. The flow is laminar.

4. The velocity field is steady and two-dimensional.

5. The fluid inlet temperature is spatially uniform and temporally constant.

6. Viscous dissipation and mechanical work terms are negligibly small.

7. Forced convection is predominant; hence the momentum and energy equations are not coupled.

8. The flat plate temperature is temporally a constant.

9. Plate temperature data is available with some scatter whose characteristics are known; in addition, limited but high quality temperature data is available within the flow field.

The algorithms described in this chapter, consists of the following basic steps:

1. Smooth the given temperature data using Gram orthogonal polynomial filter through the seven point moving window averaging scheme.

2. Solve the continuity and momentum equations to find the velocity field.

3. Take an initial guess of local Nusselt number distribution over the plate.

4. Compute the temperature field using a guessed local Nusselt number as the boundary condition at the plate.

5. Compute the optimization functional.

6. If the value of the functional conforms to the stopping criteria, stop iterations and present the results.

7. Otherwise, solve the adjoint problem and find the gradient of the functional.

8. Find the search direction.

9. Solve the sensitivity problem and find the search step size.

10. Update the local Nusselt number values over the plate surface.

11. Return to 4 and continue.

3.1   Velocity Computation

The boundary layer approximations are assumed to be applicable for the velocity field, i.e. the streamwise second derivatives in the momentum equation are neglected. This step converts the original elliptic momentum equation into a parabolic form, thus enabling a marching solution. However, this restricts the investigation to high Reynolds number. The boundary-layer form of continuity and momentum equations in the non-dimensional form can be written as:

$$\frac{\partial u}{\partial x} + \frac{\partial v}{\partial y} = 0 \tag{3.1}$$

$$\frac{\partial (u^2)}{\partial x} + \frac{\partial (uv)}{\partial y} = \frac{1}{\text{Re}} \frac{\partial^2 u}{\partial y^2} \tag{3.2}$$
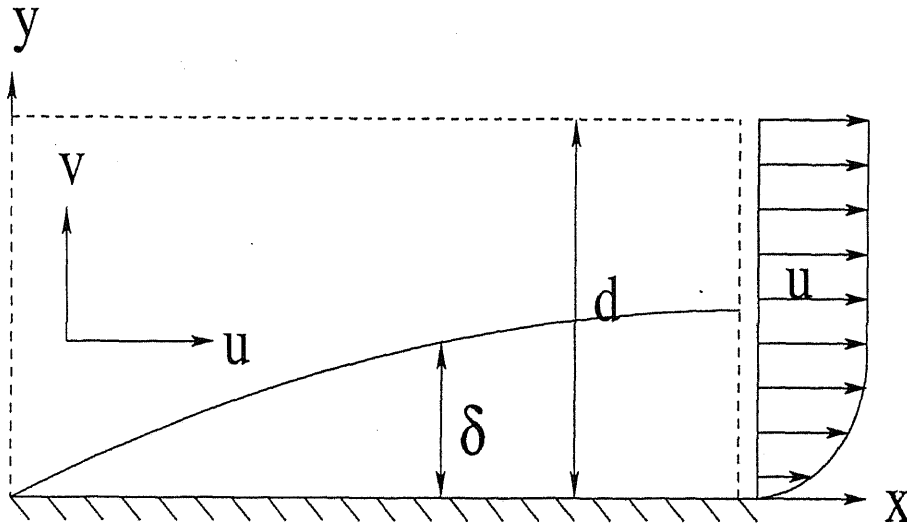
Figure 3.1: Flow over a Flat Plate

The boundary conditions with reference to Figure 3.1 are:

$$x = 0, \ u = 1, \ v = 0 \tag{3.3}$$

$$y = 0, \ u = 0, \ v = 0 \tag{3.4}$$

$$y = d, \ u = 1 \tag{3.5}$$

3.2 Steady Two-Dimensional Temperature Field

The inverse formulation for a steady thermal field is presented first.

3.2.1 Assumptions

1. Temperature field is two-dimensional, i.e. the plate temperature is varies only with length x but not z or time.

2. The temperature field is everywhere steady.

3. Boundary layer approximations are applicable to the thermal energy equation.
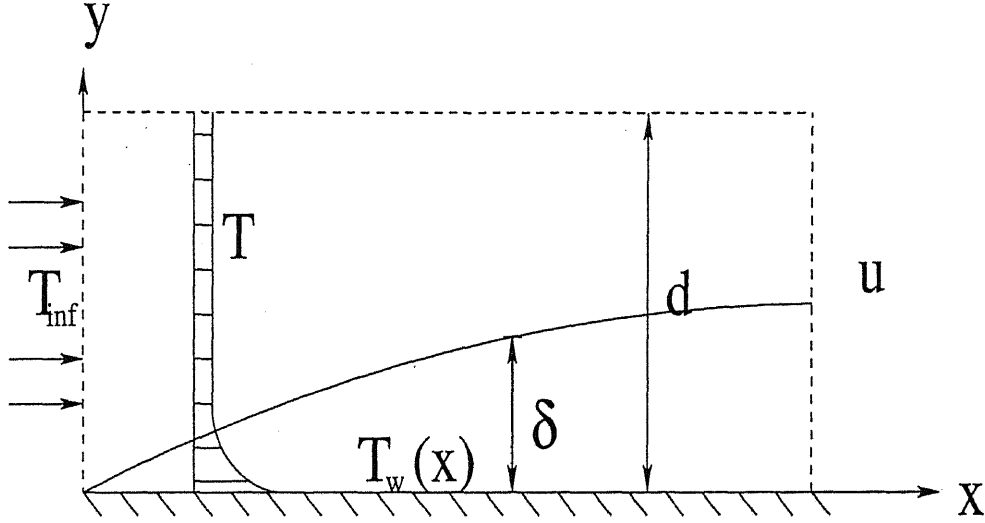
Figure 3.2: Heat Transfer over a Flat Plate

3.2.2   Direct Problem

The direct problem solves the following energy equation:

$$\frac{\partial(u\theta)}{\partial x} + \frac{\partial(v\theta)}{\partial y} = \frac{1}{\text{Pe}}\frac{\partial^2\theta}{\partial y^2} \qquad (3.6)$$

The boundary conditions with reference to Figure 3.2 are:

$$x = 0, \ \theta = 0 \qquad (3.7)$$

$$y = 0, \ \frac{\partial\theta}{\partial y} = -\text{Nu} \qquad (3.8)$$

$$y = d, \ \theta = 0 \qquad (3.9)$$

where Nu is the local Nusselt number. In an overall inverse calculation, local Nusselt number values are updated with the iterations.

3.2.3   Inverse Problem

The inverse problem is posed in the form of minimization of the following functional:

$$J = \int_0^1 \left[(\theta_w - Y_w)^2 + w(\theta_m - Y_m)^2\right]dx \qquad (3.10)$$

where θ_w and Y_w are the computed and measured temperatures at the wall, θ_m and Y_m are the computed and measured temperatures in the interior and w is the weight assigned to the high quality data.

3.2.4   Sensitivity Problem

The sensitivity problem determines the the dependence of the temperature on the unknown local Nusselt numbers. To formulate the sensitivity problem, a perturbation of $\Delta\theta$ is given to θ and θ is replaced by $\theta + \Delta\theta$ in Equation 3.6 to yield

$$\frac{\partial[u(\theta + \Delta\theta)]}{\partial x} + \frac{\partial[v(\theta + \Delta\theta)]}{\partial y} = \frac{1}{\text{Pe}}\frac{\partial^2(\theta + \Delta\theta)}{\partial y^2} \tag{3.11}$$

Now, subtracting Equation 3.6 from Equation 3.11, we have the following sensitivity problem

$$\frac{\partial(u\Delta\theta)}{\partial x} + \frac{\partial(v\Delta\theta)}{\partial y} = \frac{1}{\text{Pe}}\frac{\partial^2(\Delta\theta)}{\partial y^2} \tag{3.12}$$

In the boundary condition, Nu is replaced by Nu+ΔNu and θ by $\theta + \Delta\theta$; thus we have:

$$x = 0, \ \theta + \Delta\theta = 0 \tag{3.13}$$

$$y = 0, \ \frac{\partial(\theta + \Delta\theta)}{\partial y} = -(\text{Nu} + \Delta\text{Nu}) \tag{3.14}$$

$$y = d, \ \theta + \Delta\theta = 0 \tag{3.15}$$

Now, subtracting Equations 3.7, 3.8, 3.9 from Equations 3.13, 3.14, 3.15 respectively, we get the following boundary conditions for the sensitivity problem:

$$x = 0, \ \Delta\theta = 0 \tag{3.16}$$

$$y = d, \ \Delta\theta = 0 \tag{3.17}$$

$$y = 0, \ \frac{\partial(\Delta\theta)}{\partial y} = -\Delta\text{Nu} \tag{3.18}$$

3.2.5   Adjoint Problem

Let, λ be the Lagrange multiplier that is associated with the constraint. We can write the functional

$$J = \int_0^1 \int_0^d \left[(\theta_w - Y_w)^2 + w(\theta_m - Y_m)^2\right] dx dy +$$
$$\int_0^1 \int_0^d \lambda \left[\frac{1}{\text{Pe}}\frac{\partial^2\theta}{\partial y^2} - \frac{\partial(u\theta)}{\partial x} - \frac{\partial(v\theta)}{\partial y}\right] dx dy \tag{3.19}$$

In Equation 3.19, setting $\theta + \triangle\theta$ in place of θ and $J + \triangle J$ in place of J, we have

$$
J + \triangle J = \int_0^1 \int_0^d \left[(\theta + \triangle\theta - Y)^2 \delta(y) + w(\theta + \triangle\theta - Y)^2 \delta(y - y_1) \right] dx dy +
$$
$$
\int_0^1 \int_0^d \lambda \left[\frac{1}{\text{Pe}} \frac{\partial^2 (\theta + \triangle\theta)}{\partial y^2} - \frac{\partial \{ u(\theta + \triangle\theta) \}}{\partial x} - \frac{\partial \{ v(\theta + \triangle\theta) \}}{\partial y} \right] dx dy
$$
$$(3.20)$$

where, $\delta(y - y_0)$ is the Dirac delta function centered around y_0

Subtracting Equation 3.19 from Equation 3.20 and neglecting the terms involving squares of $\triangle\theta$, we have

$$
\triangle J = 2 \int_0^1 \int_0^d \triangle\theta \left[w(\theta - Y)\delta(y) + (\theta - Y)\delta(y - y_1) \right] dy dx +
$$
$$
\int_0^1 \int_0^d \lambda \left[\frac{1}{\text{Pe}} \frac{\partial^2 (\triangle\theta)}{\partial y^2} - \frac{\partial (u\triangle\theta)}{\partial x} - \frac{\partial (v\triangle\theta)}{\partial y} \right] dx dy \qquad (3.21)
$$

Using the boundary conditions from sensitivity problem, we get

$$
\int_0^1 \int_0^d \lambda \frac{\partial^2 (\triangle\theta)}{\partial y^2} dx dy = \int_0^1 \left[\lambda \int \frac{\partial^2 (\triangle\theta)}{\partial y^2} dy - \int \left(\frac{\partial \lambda}{\partial y} \int \frac{\partial^2 (\triangle\theta)}{\partial y^2} dy \right) dy \right]_{y=0}^{y=d} dx
$$
$$
= \int_0^1 \left[\lambda \frac{\partial (\triangle\theta)}{\partial y} \right]_{y=0}^{y=d} dx - \int_0^1 \int_0^d \frac{\partial (\triangle\theta)}{\partial y} \frac{\partial \lambda}{\partial y} dx dy
$$
$$
= \int_0^1 \left[\lambda \frac{\partial (\triangle\theta)}{\partial y} \right]_{y=0}^{y=d} dx - \int_0^1 \left[\triangle\theta \frac{\partial \lambda}{\partial y} - \int \frac{\partial^2 \lambda}{\partial y^2} \triangle\theta dy \right]_{y=0}^{y=d} dx
$$
$$
= \int_0^1 \left[\lambda \frac{\partial (\triangle\theta)}{\partial y} \right]_{y=0}^{y=d} dx + \int_0^1 \left[\frac{\partial \lambda}{\partial y} \triangle\theta \right]_{y=0} dx +
$$
$$
\int_0^1 \int_0^d \triangle\theta \frac{\partial^2 \lambda}{\partial y^2} dx dy \qquad (3.22)
$$

Further

$$
\int_0^1 \int_0^d \lambda \frac{\partial (u\triangle\theta)}{\partial y} dx dy = \int_0^d \left[\lambda u \triangle\theta - \int \lambda u \triangle\theta \right]_{x=0}^{x=1} dy
$$
$$
= \int_0^d [\lambda u \triangle\theta]_{x=0}^{x=1} dy - \int_0^1 \int_0^d \frac{\partial \lambda}{\partial y} u \triangle\theta dx dy
$$
$$
= \int_0^d [\lambda u \triangle\theta]_{x=1} dy - \int_0^1 \int_0^d \frac{\partial \lambda}{\partial y} u \triangle\theta dx dy \qquad (3.23)
$$

Also

$$\int_0^1 \int_0^d \lambda \frac{\partial(v\triangle\theta)}{\partial y}dxdy = \int_0^1 [\lambda v\triangle\theta]_{y=0}^{y=d}dx - \int_0^d \left[\int_0^1 \frac{\partial\lambda}{\partial y}v\triangle\theta dx\right]_{x=0}^{x=1}dy$$

$$= -\int_0^1 \int_0^d \frac{\partial\lambda}{\partial y}v\triangle\theta dxdy \qquad (3.24)$$

Now combining Equations 3.20 to 3.24, we have

$$\triangle J = \int_0^1 \int_0^d \left[\frac{1}{Pe}\frac{\partial^2\lambda}{\partial y^2} + u\frac{\partial\lambda}{\partial x} + v\frac{\partial\lambda}{\partial y}\right]\triangle\theta dxdy +$$

$$2\int_0^1 \int_0^d [w(\theta-Y)\delta(y) + (\theta-Y)\delta(y-y_1)]\triangle\theta dxdy +$$

$$\int_0^1 \triangle\theta\frac{1}{Pe}\left[\frac{\partial\lambda}{\partial y}\right]_{y=0}dx + \frac{1}{Pe}\int_0^1 \left[\lambda\frac{\partial(\triangle\theta)}{\partial y}\right]_{y=0}^{y=d}dx +$$

$$\int_0^d [\lambda u\triangle\theta]_{x=1}dy$$

$$= \int_0^1 \int_0^d \left[\frac{1}{Pe}\frac{\partial^2\lambda}{\partial y^2} + \frac{\partial(u\lambda)}{\partial x} + \frac{\partial(v\lambda)}{\partial y} + 2(\theta-Y)\delta(y-y_1)\right]\triangle\theta dxdy +$$

$$\int_0^1 [\lambda u\triangle\theta]_{x=1}dy + \frac{1}{Pe}\int_0^1 \left[\lambda\frac{\partial(\triangle\theta)}{\partial y}\right]_{y=0}^{y=d}dx$$

$$\int_0^1 \left[\frac{1}{Pe}\frac{\partial\lambda}{\partial y} + 2w(\theta_w - Y_w)\right]_{y=0}\triangle\theta dx \qquad (3.25)$$

where, θ_w and Y_w are computed and measured temperatures at the plate, respectively. For $\triangle J \to 0$, the following adjoint equation and boundary conditions can be deduced,

$$\frac{1}{Pe}\frac{\partial^2\lambda}{\partial y^2} + \frac{\partial(u\lambda)}{\partial x} + \frac{\partial(v\lambda)}{\partial y} + 2(\theta-Y)\delta(y-y_1) = 0 \qquad (3.26)$$

$$x = 1, \ \lambda = 0 \qquad (3.27)$$

$$y = 0, \ \frac{\partial\lambda}{\partial y} = -2w Pe(\theta_w - Y_w) \qquad (3.28)$$

$$y = d, \ \lambda = 0 \qquad (3.29)$$

Since

$$\triangle J = -\frac{1}{Pe}\int_0^1 [\lambda(-\triangle Nu)]_{y=0}dx \qquad (3.30)$$

and the definition of gradient

$$\triangle J = \int_0^1 J'(-\triangle Nu)dx \qquad (3.31)$$

From Equations 3.30 and 3.31, we have the following expression for the gradient of the functional,

$$J' = \lim_{\triangle \mathrm{Nu} \to 0} \frac{\triangle J}{\triangle \mathrm{Nu}} = -\frac{\lambda(x,0)}{\mathrm{Pe}} \qquad (3.32)$$

The adjoint equation deduced above has negative diffusion. It has no initial condition either. These are circumvented by the transformation $x = 1 - x$, which coverts the equation to a well behaved form, generates an initial condition and makes the diffusion term to be positive.

3.2.6   Determination of Search Step Size.

If the value of the functional is J^k after k-th iteration and it is J^{k+1} after temperatures are updated through a step size of β^k, the condition for the optimum step size will be given by:

$$\frac{\partial J^{k+1}}{\partial \beta^k} = 0 \qquad (3.33)$$

Recalling the expression of functional,

$$J^k = \int_0^1 \int_0^d \left[w(\theta - Y)^2 \delta(y - y_1) + (\theta - Y)\delta(y) \right] dxdy \qquad (3.34)$$

$$
\begin{aligned}
min_\beta J^k(-\triangle Nu)^k = \ & min_\beta \int_0^1 \int_0^d \{ w[\theta\{(-\triangle Nu)^k - \beta^k P^k\} - Y]^2 \delta(y - y_1) \\
& + [\theta\{(-\triangle Nu)^k - \beta^k P^k\} - Y]^2 \delta(y) \} dxdy
\end{aligned}
\qquad (3.35)
$$

Linearizing by the Taylor's series expansion,

$$
\begin{aligned}
J^{k+1}[(-\triangle Nu)^{k+1}] = \ & w \int_0^1 \int_0^d \{ \theta[(-\triangle Nu)^k - \beta^k \triangle\theta(P^k)] - Y \}^2 \delta(y - y_1) dxdy \\
& + \int_0^1 \int_0^d \{ \theta[(-\triangle Nu)^k - \beta^k \triangle\theta(P^k)] - Y \}^2 \delta(y) dxdy \\
= \ & \int_0^1 \int_0^d \{ (\theta - Y) - \beta^k \triangle\theta \}^2 \{ w\delta(y - y_1) + \delta(y) \} dxdy
\end{aligned}
$$
$$(3.36)$$

$$\frac{\partial J^{k+1}}{\partial \beta^k} = 2 \int_0^1 \int_0^d \triangle\theta(\theta - Y - \beta^k \triangle\theta)\{ w\delta(y - y_1) + \delta(y) \} dxdy \qquad (3.37)$$

Using Equation 3.33 and 3.37, we have the following equation for the step size:

$$\beta^k = \frac{\int_0^1 \int_0^d \triangle\theta(\theta - Y)\{ w\delta(y - y_1) + \delta(y) \} dxdy}{\int_0^1 \int_0^d (\triangle\theta)^2 \{ w\delta(y - y_1) + \delta(y) \} dxdy} \qquad (3.38)$$

3.2.7 Complete Inverse Algorithm.

The complete inverse algorithm for calculation the Nusselt number distribution over flat surface is summarized below:

1. Solve the continuity and momentum equations to get the velocity field.

2. Filter the imperfect plate temperature data using Gram orthogonal polynomial filter.

3. Solve the energy equation using the following boundary conditions:

$$x = 0, \ \theta = 0 \tag{3.39}$$

$$y = 0, \ \theta = \theta_w \ \text{(filtered)} \tag{3.40}$$

$$y = d, \ \theta = 0 \tag{3.41}$$

4. Get the values of local Nusselt numbers. Take an initial guess of Nusselt number based on the distribution obtained. Initialize $J = 0$

5. Solve energy equation using the following boundary conditions (with Nusselt number from step 4):

$$x = 0, \ \theta = 0 \tag{3.42}$$

$$y = 0, \ \frac{\partial \theta}{\partial y} = -\text{Nu} \tag{3.43}$$

$$y = d, \ \theta = 0 \tag{3.44}$$

Find the temperatures at the plate as well as the plane of high quality data.

6. Compute the functional

$$J = \int_0^1 \int_0^d \{(\theta_w - Y_w)^2 + w(\theta_m - Y_m)^2\} dx dy \tag{3.45}$$

7. Check the stopping criterion

$$|J^k - J^{k-1}| < \epsilon \tag{3.46}$$

where, ϵ is a predetermined real number, very close to zero.

If it is satisfied, stop iterations. Otherwise

8. Solve the adjoint problem

$$\frac{1}{\text{Pe}}\frac{\partial^2\lambda}{\partial y^2} + \frac{\partial(u\lambda)}{\partial x} + \frac{\partial(v\lambda)}{\partial y} + 2(\theta - Y)\delta(y - y_1) = 0 \qquad (3.47)$$

with

$$x = 1, \ \lambda = 0 \qquad (3.48)$$

$$y = 0, \ \frac{\partial\lambda}{\partial y} = -2w\text{Pe}(\theta_w - Y_w) \qquad (3.49)$$

$$y = d, \ \lambda = 0 \qquad (3.50)$$

9. Compute the gradient

$$J' = -\frac{\lambda(x, 0)}{\text{Pe}} \qquad (3.51)$$

10. Compute the descent direction

$$P^k = \gamma^k P^{k-1} + J'^k \qquad (3.52)$$

where

$$\text{for the first iteration } \gamma^k = 0 \qquad (3.53)$$

$$\text{otherwise } \gamma^k = \frac{\langle J^k - J^{k-1} | J^k \rangle}{\|J^{k-1}\|^2} \qquad (3.54)$$

11. Solve the sensitivity problem

$$\frac{\partial(u\triangle\theta)}{\partial x} + \frac{\partial(v\triangle\theta)}{\partial y} = \frac{1}{\text{Pe}}\frac{\partial^2(\triangle\theta)}{\partial y^2} \qquad (3.55)$$

with

$$x = 0, \ \triangle\theta = 0 \qquad (3.56)$$

$$y = 1, \ \triangle\theta = 0 \qquad (3.57)$$

$$y = 0, \ \frac{\partial(\triangle\theta)}{\partial y} = -\triangle\text{Nu} = P^k \qquad (3.58)$$

12. Compute the step size

$$\beta^k = \frac{\int_0^1 \triangle\theta(\theta - Y)\left[\sum_{j=1}^{mp} w_j\delta(y - y_j) + \delta(y)\right]dx}{\int_0^1 (\triangle\theta)^2\left[\sum_{j=1}^{mp} w_j\delta(y - y_j) + \delta(y)\right]dx} \qquad (3.59)$$

where mp indicates number of measurement planes and w_j is the weight assigned to the data from the j-th plane of measurement.

13. Compute the new local Nusselt number

$$(-\text{Nu})^{k+1} = (-\text{Nu})^k - \beta^k P^k \qquad (3.60)$$

14. Go to 5 and continue till convergence.

3.3   Steady Three-Dimensional Temperature Field

The formulation of Section 3.2 is now presented for a steady three dimensional temperature over a flat plate.

3.3.1   Assumptions

1. Temperature field is three-dimensional, i.e. the plate temperature is varying with x and z coordinates

2. The temperature field is steady.

3. Boundary-layer approximations are applicable for the energy equation.

4. The flow field continues to be two dimensional and the z component of velocity is zero.

3.3.2   Direct Problem

The direct problem solves the following energy equation in dimensionless form:

$$\frac{\partial(u\theta)}{\partial x} + \frac{\partial(v\theta)}{\partial y} = \frac{1}{\text{Pe}}\left(\frac{\partial^2\theta}{\partial y^2} + \frac{\partial^2\theta}{\partial z^2}\right) \tag{3.61}$$

The boundary conditions are:

$$x = 0, \ \theta = 0 \tag{3.62}$$

$$y = 0, \ \frac{\partial\theta}{\partial y} = -\text{Nu} \tag{3.63}$$

$$y = d, \ \theta = 0 \tag{3.64}$$

$$z = 0, \ \frac{\partial\theta}{\partial z} = 0 \tag{3.65}$$

$$z = r, \ \frac{\partial\theta}{\partial z} = 0 \tag{3.66}$$

where, Nu is the local Nusselt number distribution.

3.3.3   Inverse Problem

The inverse problem is posed in the form of minimization of the following functional:

$$J = \int_0^1 \int_0^r \left[(\theta_w - Y_w)^2 + w(\theta_m - Y_m)^2 \right] dx dz \qquad (3.67)$$

where θ_w and Y_w are the computed and measured temperatures at the wall, θ_m and Y_m are the computed and measured temperatures in the interior and w is the weight assigned to the high quality data.

3.3.4   Sensitivity Problem

The sensitivity problem determines the the dependence of the temperature on the local Nusselt numbers. To formulate the sensitivity problem, a perturbation of $\Delta\theta$ is given to θ and θ is replaced by $\theta + \Delta\theta$ in Equation 3.61 to yield

$$\frac{\partial[u(\theta + \Delta\theta)]}{\partial x} + \frac{\partial[v(\theta + \Delta\theta)]}{\partial y} = \frac{1}{\text{Pe}} \left[\frac{\partial^2(\theta + \Delta\theta)}{\partial y^2} + \frac{\partial^2(\theta + \Delta\theta)}{\partial z^2} \right] \qquad (3.68)$$

Now, subtracting Equation 3.61 from Equation 3.68, we have the following sensitivity problem:

$$\frac{\partial(u\Delta\theta)}{\partial x} + \frac{\partial(v\Delta\theta)}{\partial y} = \frac{1}{\text{Pe}} \left(\frac{\partial^2(\Delta\theta)}{\partial y^2} + \frac{\partial^2(\Delta\theta)}{\partial z^2} \right) \qquad (3.69)$$

Similarly, in the boundary condition, Nu is replaced by Nu+ΔNu and θ by $\theta+\Delta\theta$; thus we have:

$$x = 0, \; \theta + \Delta\theta = 0 \qquad (3.70)$$

$$y = 0, \; \frac{\partial(\theta + \Delta\theta)}{\partial y} = -(\text{Nu} + \Delta\text{Nu}) \qquad (3.71)$$

$$y = d, \; \theta + \Delta\theta = 0 \qquad (3.72)$$

$$z = 0, \; \frac{\partial(\theta + \Delta\theta)}{\partial z} = 0 \qquad (3.73)$$

$$z = r, \; \frac{\partial(\theta + \Delta\theta)}{\partial z} = 0 \qquad (3.74)$$

Subtracting Equations 3.62, 3.63, 3.64, 3.65, 3.66 from Equations 3.70, 3.71, 3.72, 3.73, 3.74, respectively, we get the following boundary conditions for the sensitivity problem:

$$x = 0, \; \Delta\theta = 0 \qquad (3.75)$$

$$y = 0, \ \frac{\partial(\triangle\theta)}{\partial y} = -\triangle\mathrm{Nu} \tag{3.76}$$

$$y = d, \ \triangle\theta = 0 \tag{3.77}$$

$$z = 0, \ \frac{\partial(\triangle\theta)}{\partial z} = 0 \tag{3.78}$$

$$z = r, \ \frac{\partial(\triangle\theta)}{\partial z} = 0 \tag{3.79}$$

3.3.5 Adjoint Problem

Let, λ be the Lagrange multiplier that is associated with the constraint. We can write the functional

$$
\begin{aligned}
J = & \int_0^1 \int_0^d \int_0^r \left[(\theta_w - Y_w)^2 + w(\theta_m - Y_m)^2 \right] dx\,dy\,dz + \\
& \int_0^1 \int_0^d \int_0^r \lambda \left[\frac{1}{\mathrm{Pe}} \left(\frac{\partial^2\theta}{\partial y^2} + \frac{\partial^2\theta}{\partial z^2} \right) - \frac{\partial(u\theta)}{\partial x} - \frac{\partial(v\theta)}{\partial y} \right] dx\,dy\,dz
\end{aligned} \tag{3.80}
$$

In Equation 3.80, setting $\theta + \triangle\theta$ in place of θ and $J + \triangle J$ in place of J, we get

$$
\begin{aligned}
J + \triangle J = & \int_0^1 \int_0^d \int_0^r \left[(\theta + \triangle\theta - Y)^2 \delta(y) + w(\theta + \triangle\theta - Y)^2 \delta(y - y_1) \right] dx\,dy\,dz + \\
& \int_0^1 \int_0^d \int_0^r \frac{\lambda}{\mathrm{Pe}} \left[\frac{\partial^2(\theta + \triangle\theta)}{\partial y^2} + \frac{\partial^2(\theta + \triangle\theta)}{\partial z^2} \right] dx\,dy\,dz - \\
& \int_0^1 \int_0^d \int_0^r \lambda \left[\frac{\partial\{u(\theta + \triangle\theta)\}}{\partial x} + \frac{\partial\{v(\theta + \triangle\theta)\}}{\partial y} \right] dx\,dy\,dz
\end{aligned} \tag{3.81}
$$

where, $\delta(y - y_0)$ is the Dirac delta function centered around y_0

Subtracting Equation 3.80 from Equation 3.81 and neglecting the terms involving the squares of $\triangle\theta$, we get

$$
\begin{aligned}
\triangle J = & 2 \int_0^1 \int_0^d \int_0^r \triangle\theta \left[w(\theta - Y)\delta(y) + (\theta - Y)\delta(y - y_1) \right] dy\,dx\,dz + \\
& \int_0^1 \int_0^d \int_0^r \frac{\lambda}{\mathrm{Pe}} \left[\frac{\partial^2(\triangle\theta)}{\partial y^2} + \frac{\partial^2(\triangle\theta)}{\partial z^2} \right] dx\,dy\,dz - \\
& \int_0^1 \int_0^d \int_0^r \lambda \left[\frac{\partial\{u(\triangle\theta)\}}{\partial x} + \frac{\partial\{v(\triangle\theta)\}}{\partial y} \right] dx\,dy\,dz
\end{aligned} \tag{3.82}
$$

Using the boundary conditions from the sensitivity problem, we have

$$
\int_0^d \lambda \frac{\partial^2 (\triangle\theta)}{\partial y^2} dy = \left[\lambda \int \frac{\partial^2 (\triangle\theta)}{\partial y^2} dy - \int \left(\frac{\partial \lambda}{\partial y} \int \frac{\partial^2 (\triangle\theta)}{\partial y^2} dy \right) dy \right]_{y=0}^{y=d}
$$

$$
= \left[\lambda \frac{\partial (\triangle\theta)}{\partial y} \right]_{y=0}^{y=d} - \int_0^d \frac{\partial (\triangle\theta)}{\partial y} \frac{\partial \lambda}{\partial y} dy
$$

$$
= \left[\lambda \frac{\partial (\triangle\theta)}{\partial y} \right]_{y=0}^{y=d} - \left[\triangle\theta \frac{\partial \lambda}{\partial y} \right]_{y=0}^{y=d} + \int_0^d \frac{\partial^2 \lambda}{\partial y^2} (\triangle\theta) dy
$$

$$
= \left[\lambda \frac{\partial (\triangle\theta)}{\partial y} \right]_{y=0}^{y=d} + \left[\triangle\theta \frac{\partial \lambda}{\partial y} \right]_{y=0}^{y=d} + \int_0^d \frac{\partial^2 \lambda}{\partial y^2} (\triangle\theta) dy \quad (3.83)
$$

Therefore

$$
\int_0^1 \int_0^d \int_0^r \lambda \frac{\partial^2 (\triangle\theta)}{\partial y^2} dxdydz = \int_0^1 \int_0^r \left[\lambda \frac{\partial (\triangle\theta)}{\partial y} \right]_{y=0}^{y=d} dxdz +
$$

$$
\int_0^1 \int_0^r \left[\frac{\partial \lambda}{\partial y} \triangle\theta \right]_{y=0} dxdz +
$$

$$
\int_0^1 \int_0^d \int_0^r \triangle\theta \frac{\partial^2 \lambda}{\partial y^2} dxdydz \quad (3.84)
$$

Again

$$
\int_0^r \lambda \frac{\partial^2 (\triangle\theta)}{\partial z^2} dz = \left[\lambda \int \frac{\partial^2 (\triangle\theta)}{\partial z^2} dz - \int \left(\frac{\partial \lambda}{\partial z} \int \frac{\partial^2 (\triangle\theta)}{\partial z^2} dz \right) dz \right]_{z=0}^{z=r}
$$

$$
= \left[\lambda \frac{\partial (\triangle\theta)}{\partial z} \right]_{z=0}^{z=r} - \int_0^r \frac{\partial (\triangle\theta)}{\partial z} \frac{\partial \lambda}{\partial z} dz
$$

$$
= - \left[\triangle\theta \frac{\partial \lambda}{\partial z} \right]_{z=0}^{z=r} + \int_0^r \frac{\partial^2 \lambda}{\partial y^2} (\triangle\theta) dz \quad (3.85)
$$

Therefore

$$
\int_0^1 \int_0^d \int_0^r \lambda \frac{\partial^2 (\triangle\theta)}{\partial z^2} dxdydz = - \int_0^1 \int_0^d \left[\frac{\partial \lambda}{\partial y} \triangle\theta \right]_{z=0}^{z=r} dxdy +
$$

$$
\int_0^1 \int_0^d \int_0^r \triangle\theta \frac{\partial^2 \lambda}{\partial z^2} dxdydz \quad (3.86)
$$

Also

$$
\int_0^1 \lambda \frac{\partial \{u(\triangle\theta)\}}{\partial x} dx = \left[\lambda \int \frac{\partial \{u(\triangle\theta)\}}{\partial x} dx - \int \left(\frac{\partial \lambda}{\partial x} \int \frac{\partial \{u(\triangle\theta)\}}{\partial x} dx \right) dx \right]_{x=0}^{x=1}
$$

$$
= [\lambda u(\triangle\theta)]_{x=0}^{x=1} - \int_0^1 \frac{\partial \lambda}{\partial x} u(\triangle\theta) dx
$$

$$
= [\lambda u \triangle\theta]_{x=1} - \int_0^1 u \frac{\partial \lambda}{\partial x} (\triangle\theta) dx \quad (3.87)
$$

Therefore

$$\int_0^1 \int_0^d \int_0^r \lambda \frac{\partial\{u(\triangle\theta)\}}{\partial x} dx dy dz = \int_0^d \int_0^r [\lambda u \triangle\theta]_{x=1} dy dz -$$

$$\int_0^1 \int_0^d \int_0^r u \frac{\partial\lambda}{\partial x}(\triangle\theta) dx dy dz \quad (3.88)$$

Further

$$\int_0^d \lambda \frac{\partial\{v(\triangle\theta)\}}{\partial y} dy = \left[\lambda \int \frac{\partial\{v(\triangle\theta)\}}{\partial y} dy - \int \left(\frac{\partial\lambda}{\partial y} \int \frac{\partial\{v(\triangle\theta)\}}{\partial y} \right) dy \right]_{y=0}^{y=d}$$

$$= [\lambda v(\triangle\theta)]_{y=0}^{y=d} - \int_0^d \frac{\partial\lambda}{\partial y} v(\triangle\theta) dy$$

$$= - \int_0^1 v \frac{\partial\lambda}{\partial y}(\triangle\theta) dy \quad (3.89)$$

Therefore

$$\int_0^1 \int_0^d \int_0^r \lambda \frac{\partial\{v(\triangle\theta)\}}{\partial y} dx dy dz = - \int_0^1 \int_0^d \int_0^r v \frac{\partial\lambda}{\partial y}(\triangle\theta) dx dy dz \quad (3.90)$$

Combining Equations 3.82, 3.84, 3.86, 3.88, 3.90, we have

$$\triangle J = \int_0^1 \int_0^d \int_0^r \left[\frac{1}{\mathrm{Pe}} \left(\frac{\partial^2\lambda}{\partial y^2} + \frac{\partial^2\lambda}{\partial z^2} \right) + u \frac{\partial\lambda}{\partial x} + v \frac{\partial\lambda}{\partial y} \right] \triangle\theta dx dy dz +$$

$$2 \int_0^1 \int_0^d \int_0^r [w(\theta - Y)\delta(y) + (\theta - Y)\delta(y - y_1)] \triangle\theta dx dy dz +$$

$$\int_0^1 \int_0^r \triangle\theta \frac{1}{\mathrm{Pe}} \left[\frac{\partial\lambda}{\partial y} \right]_{y=0} dx dz + \frac{1}{\mathrm{Pe}} \int_0^1 \int_0^r \left[\lambda \frac{\partial(\triangle\theta)}{\partial y} \right]_{y=0}^{y=d} dx dz -$$

$$\int_0^d \int_0^r [\lambda u \triangle\theta]_{x=1} dy dz - \int_0^1 \int_0^d \frac{1}{\mathrm{Pe}} \left[\triangle\theta \frac{\partial\lambda}{\partial z} \right]_{z=0}^{z=r} dx dy \quad (3.91)$$

For $\triangle J \to 0$, the following adjoint equation and boundary conditions can be deduced,

$$\frac{1}{\mathrm{Pe}} \left(\frac{\partial^2\lambda}{\partial y^2} + \frac{\partial^2\lambda}{\partial z^2} \right) + \frac{\partial(u\lambda)}{\partial x} + \frac{\partial(v\lambda)}{\partial y} + 2(\theta - Y)\delta(y - y_1) = 0 \quad (3.92)$$

$$x = 1, \ \lambda = 0 \quad (3.93)$$

$$y = 0, \ \frac{\partial\lambda}{\partial y} = -2w\mathrm{Pe}(\theta_w - Y_w) \quad (3.94)$$

$$y = d, \ \lambda = 0 \quad (3.95)$$

$$z = 0, \ \frac{\partial\lambda}{\partial z} = 0 \quad (3.96)$$

$$z = r, \quad \frac{\partial \lambda}{\partial z} = 0 \tag{3.97}$$

Hence

$$\triangle J = -\frac{1}{\text{Pe}} \int_0^1 \int_0^r [\lambda(-\triangle Nu)]_{y=0} \, dx dz \tag{3.98}$$

From the definition of a gradient, we may write,

$$\triangle J = \int_0^1 \int_0^r J'(-\triangle \text{Nu}) dx dz \tag{3.99}$$

From Equations 3.98 and 3.99, we have the following expression for the gradient of the functional:

$$J' = \lim_{\triangle \text{Nu} \to 0} \frac{\triangle J}{\triangle \text{Nu}} = -\frac{\lambda(x,0,z)}{\text{Pe}} \tag{3.100}$$

3.3.6 Determination of Search Step Size.

If the value of the functional is J^k after the k-th iteration and it becomes J^{k+1} after temperatures are updated through a step size of β^k, the condition for the optimum step size will be given by

$$\frac{\partial J^{k+1}}{\partial \beta^k} = 0 \tag{3.101}$$

Recalling the expression of functional

$$J^k = \int_0^1 \int_0^d \int_0^r \left[w(\theta - Y)^2 \delta(y - y_1) + (\theta - Y)^\delta(y) \right] dx dy dz \tag{3.102}$$

we get

$$min_\beta J^k(-\triangle Nu)^k = min_\beta \int_0^1 \int_0^d \int_0^r \{w[\theta\{(-\triangle Nu)^k - \beta^k P^k\} - Y]^2 \delta(y - y_1)$$
$$+[\theta\{(-\triangle Nu)^k - \beta^k P^k\} - Y]^2 \delta(y)\} dx dy dz \tag{3.103}$$

Linearizing Equation 3.103 by Taylor's series expansion

$$J^{k+1}[(-\triangle Nu)^{k+1}] = w \int_0^1 \int_0^d \int_0^r \{\theta[(-\triangle Nu)^k - \beta^k \triangle\theta(P^k)] - Y\}^2 \delta(y - y_1) dx dy dz$$
$$+ \int_0^1 \int_0^d \int_0^r \{\theta[(-\triangle Nu)^k - \beta^k \triangle\theta(P^k)] - Y\}^2 \delta(y) dx dy dz$$
$$= \int_0^1 \int_0^d \int_0^r \{(\theta - Y) - \beta^k \triangle\theta\}^2 \{w\delta(y - y_1) + \delta(y)\} dx dy dz$$
$$\tag{3.104}$$

Therefore,

$$\frac{\partial J^{k+1}}{\partial \beta^k} = 2 \int_0^1 \int_0^d \int_0^r \triangle\theta(\theta - Y - \beta^k \triangle\theta)\{\delta(y - y_1) + w\delta(y)\}dxdydz \quad (3.105)$$

Using Equations 3.101 and 3.105, we have the following equation for the optimum step size,

$$\beta^k = \frac{\int_0^1 \int_0^d \int_0^r \triangle\theta(\theta - Y)\{\delta(y - y_1) + w\delta(y)\}dxdydz}{\int_0^1 \int_0^d \int_0^r (\triangle\theta)^2\{\delta(y - y_1) + w\delta(y)\}dxdydz} \quad (3.106)$$

3.3.7 Complete Inverse Algorithm.

The complete inverse algorithm for calculation the Nusselt number distribution over flat surface is summarized below:

1. Solve the continuity and momentum equations to get the two dimensional velocity field.

2. Filter the imperfect plate temperature data using Gram orthogonal polynomial filter.

3. Solve the three dimensional energy equation using the following boundary conditions:

$$x = 0, \ \theta = 0 \quad (3.107)$$

$$y = 0, \ \theta = \theta_w \quad (3.108)$$

$$y = d, \ \theta = 0 \quad (3.109)$$

$$z = 0, \ \frac{\partial\theta}{\partial z} = 0 \quad (3.110)$$

$$z = r, \ \frac{\partial\theta}{\partial z} = 0 \quad (3.111)$$

4. Get the values of local Nusselt numbers. Take an initial guess of Nusselt number based on the distribution obtained. Initialize $J = 0$

5. Solve the three dimensional energy equation using the following boundary conditions (with Nusselt number from step 4):

$$x = 0, \ \theta = 0 \quad (3.112)$$

$$y = 0, \; \frac{\partial \theta}{\partial y} = -\text{Nu} \qquad (3.113)$$

$$y = d, \; \theta = 0 \qquad (3.114)$$

$$z = 0, \; \frac{\partial \theta}{\partial z} = 0 \qquad (3.115)$$

$$z = r, \; \frac{\partial \theta}{\partial z} = 0 \qquad (3.116)$$

Find the temperatures at the plate as well as the plane of high quality data.

6. Compute the functional,

$$J = \int_0^1 \int_0^d \int_0^r \{(\theta_w - Y_w)^2 + w(\theta_m - Y_m)^2\} dx\, dy\, dz \qquad (3.117)$$

7. Check the stopping criterion

$$|J^k - J^{k-1}| < \epsilon \qquad (3.118)$$

where, ϵ is a predetermined real number, very close to zero.
If it is satisfied, stop iterations. Otherwise

8. Solve the adjoint problem

$$\frac{1}{\text{Pe}} \frac{\partial^2 \lambda}{\partial y^2} + \frac{\partial (u\lambda)}{\partial x} + \frac{\partial (v\lambda)}{\partial y} + 2(\theta - Y)\delta(y - y_1) = 0 \qquad (3.119)$$

with

$$x = 1, \; \lambda = 0 \qquad (3.120)$$

$$y = 0, \; \frac{\partial \lambda}{\partial y} = -2w\text{Pe}(\theta_w - Y_w) \qquad (3.121)$$

$$y = d, \; \lambda = 0 \qquad (3.122)$$

$$z = 0, \; \frac{\partial \lambda}{\partial z} = 0 \qquad (3.123)$$

$$z = r, \; \frac{\partial \lambda}{\partial z} = 0 \qquad (3.124)$$

9. Compute the gradient

$$J' = -\frac{\lambda(x, 0, z)}{\text{Pe}} \qquad (3.125)$$

10. Compute the descent direction

$$P^k = \gamma^k P^{k-1} + J'^k \qquad (3.126)$$

where

$$\text{for the first iteration } \gamma^k = 0 \qquad (3.127)$$

$$\text{otherwise } \gamma^k = \frac{\langle J^k - J^{k-1} | J^k \rangle}{\| J^{k-1} \|^2} \qquad (3.128)$$

11. Solve the sensitivity problem

$$\frac{\partial(u\triangle\theta)}{\partial x} + \frac{\partial(v\triangle\theta)}{\partial y} = \frac{1}{\text{Pe}} \left[\frac{\partial^2(\triangle\theta)}{\partial y^2} + \frac{\partial^2(\triangle\theta)}{\partial z^2} \right] \qquad (3.129)$$

with

$$x = 0, \ \triangle\theta = 0 \qquad (3.130)$$

$$y = 0, \ \frac{\partial(\triangle\theta)}{\partial y} = -\triangle\text{Nu} = P^k \qquad (3.131)$$

$$y = d, \ \triangle\theta = 0 \qquad (3.132)$$

$$z = 0, \ \frac{\partial(\triangle\theta)}{\partial z} = 0 \qquad (3.133)$$

$$z = r, \ \frac{\partial(\triangle\theta)}{\partial z} = 0 \qquad (3.134)$$

12. Compute the step size

$$\beta^k = \frac{\int_0^1 \int_0^r \triangle\theta(\theta - Y) \left[\sum_{j=1}^{mp} w_j \delta(y - y_j) + \delta(y) \right] dx dz}{\int_0^1 \int_0^r (\triangle\theta)^2 \left[\sum_{j=1}^{mp} w_j \delta(y - y_j) + \delta(y) \right] dx dz} \qquad (3.135)$$

where mp indicates number of measurement planes and w_j is the weight assigned to the data from the j-th plane of measurement.

13. Compute the new local Nusselt number

$$(-\text{Nu})^{k+1} = (-\text{Nu})^k - \beta^k P^k \qquad (3.136)$$

14. Go to 5 and continue till convergence.

3.4 Unsteady Three-Dimensional Temperature Field

The inverse estimation of the instantaneous Nusselt number distribution over a flat surface when the thermal field is three dimensional is presented in this section. The flow field is taken to be steady and two dimensional.

3.4.1 Direct Problem

The direct problem solves the following energy equation:

$$\frac{\partial \theta}{\partial t} + \frac{\partial (u\theta)}{\partial x} + \frac{\partial (v\theta)}{\partial y} = \frac{1}{\text{Pe}} \left(\frac{\partial^2 \theta}{\partial x^2} + \frac{\partial^2 \theta}{\partial y^2} + \frac{\partial^2 \theta}{\partial z^2} \right) \tag{3.137}$$

The initial and boundary conditions are:

$$t = 0, \ \theta = 0 \tag{3.138}$$

$$x = 0, \ \frac{\partial \theta}{\partial x} = 0 \tag{3.139}$$

$$x = 1, \ \theta = 0 \tag{3.140}$$

$$y = 0, \ \frac{\partial \theta}{\partial y} = -\text{Nu} \tag{3.141}$$

$$y = d, \ \theta = 0 \tag{3.142}$$

$$z = 0, \ \frac{\partial \theta}{\partial z} = 0 \tag{3.143}$$

$$z = r, \ \frac{\partial \theta}{\partial z} = 0 \tag{3.144}$$

where Nu represents the local Nusselt number.

3.4.2 Inverse Problem

The inverse problem is posed in the form of minimization of the following functional:

$$J = \int_0^{t_f} \int_0^1 \int_0^r \left[(\theta_w - Y_w)^2 + w(\theta_m - Y_m)^2 \right] dx\,dz\,dt \tag{3.145}$$

where θ_w and Y_w are the computed and measured temperatures at the wall, θ_m and Y_m are the computed and measured temperatures in the interior and w is the weight assigned to the high quality data.

3.4.3   Sensitivity Problem

The sensitivity problem determines the the dependence of the temperature on the local Nusselt numbers. To formulate the sensitivity problem, a perturbation of $\Delta\theta$ is given to θ and θ is replaced by $\theta + \Delta\theta$ in Equation 3.137 to yield

$$\frac{\partial(\theta + \Delta\theta)}{\partial t} + \frac{\partial[u(\theta + \Delta\theta)]}{\partial x} + \frac{\partial[v(\theta + \Delta\theta)]}{\partial y} = \frac{1}{\text{Pe}}\left[\frac{\partial^2(\theta + \Delta\theta)}{\partial x^2} + \frac{\partial^2(\theta + \Delta\theta)}{\partial y^2} + \frac{\partial^2(\theta + \Delta\theta)}{\partial z^2}\right] \qquad (3.146)$$

Now, subtracting equation(3.137) from equation(3.146), we have the following sensitivity problem

$$\frac{\partial(\Delta\theta)}{\partial t} + \frac{\partial(u\Delta\theta)}{\partial x} + \frac{\partial(v\Delta\theta)}{\partial y} = \frac{1}{\text{Pe}}\left[\frac{\partial^2(\Delta\theta)}{\partial x^2} + \frac{\partial^2(\Delta\theta)}{\partial y^2} + \frac{\partial^2(\Delta\theta)}{\partial z^2}\right] \qquad (3.147)$$

Similarly, in the initial and boundary condition, Nu is replaced by Nu+ΔNu and θ by $\theta + \Delta\theta$; thus we have:

$$t = 0, \ \theta + \Delta\theta = 0 \qquad (3.148)$$

$$x = 0, \ \theta + \Delta\theta = 0 \qquad (3.149)$$

$$x = 1, \ \frac{\partial(\theta + \Delta\theta)}{\partial y} = 0 \qquad (3.150)$$

$$y = 0, \ \frac{\partial(\theta + \Delta\theta)}{\partial y} = -(\text{Nu} + \Delta\text{Nu}) \qquad (3.151)$$

$$y = d, \ \theta + \Delta\theta = 0 \qquad (3.152)$$

$$z = 0, \ \frac{\partial(\theta + \Delta\theta)}{\partial z} = 0 \qquad (3.153)$$

$$z = r, \ \frac{\partial(\theta + \Delta\theta)}{\partial z} = 0 \qquad (3.154)$$

Subtracting Equations (3.148-3.154) from Equations (3.155-3.160) respectively, we get the following boundary conditions for the sensitivity problem:

$$t = 0, \ \Delta\theta = 0 \qquad (3.155)$$

$$x = 0, \ \Delta\theta = 0 \qquad (3.156)$$

$$x = 1, \ \frac{\Delta\theta}{x} = 0 \qquad (3.157)$$

$$y = 0, \quad \frac{\partial(\Delta\theta)}{\partial y} = -\Delta\mathrm{Nu} \qquad (3.158)$$

$$y = d, \quad \Delta\theta = 0 \qquad (3.159)$$

$$z = 0, \quad \frac{\partial(\Delta\theta)}{\partial z} = 0 \qquad (3.160)$$

$$z = r, \quad \frac{\partial(\Delta\theta)}{\partial z} = 0 \qquad (3.161)$$

3.4.4 Adjoint Problem

Let, λ be the Lagrange multiplier that is associated with the constraint. We can write the functional

$$J =$$
$$\int_0^{t_f} \int_0^1 \int_0^d \int_0^r \lambda \left[\frac{1}{\mathrm{Pe}} \left(\frac{\partial^2\theta}{\partial x^2} + \frac{\partial^2\theta}{\partial y^2} + \frac{\partial^2\theta}{\partial z^2} \right) - \frac{\partial(u\theta)}{\partial x} - \frac{\partial(v\theta)}{\partial y} - \frac{\partial\theta}{\partial t} \right] dxdydzdt$$
$$+ \int_0^{t_f} \int_0^1 \int_0^d \int_0^r \left[(\theta_w - Y_w)^2 + w(\theta_m - Y_m)^2 \right] dxdydzdt \qquad (3.162)$$

In Equation 3.162, setting $\theta + \Delta\theta$ in place of θ and $J + \Delta J$ in place of J, we have

$$J + \Delta J =$$
$$\int_0^{t_f} \int_0^1 \int_0^d \int_0^r \left[(\theta + \Delta\theta - Y)^2 \delta(y) + w(\theta + \Delta\theta - Y)^2 \delta(y - y_1) \right] dxdydzdt +$$
$$\int_0^{t_f} \int_0^1 \int_0^d \int_0^r \frac{\lambda}{\mathrm{Pe}} \left[\frac{\partial^2(\theta + \Delta\theta)}{\partial x^2} + \frac{\partial^2(\theta + \Delta\theta)}{\partial y^2} + \frac{\partial^2(\theta + \Delta\theta)}{\partial z^2} \right] dxdydzdt -$$
$$\int_0^{t_f} \int_0^1 \int_0^d \int_0^r \lambda \left[\frac{\partial\{u(\theta + \Delta\theta)\}}{\partial x} + \frac{\partial\{v(\theta + \Delta\theta)\}}{\partial y} + \frac{\partial(\theta + \Delta\theta)}{\partial t} \right] dxdydzdt$$
$$(3.163)$$

where, $\delta(y - y_0)$ is the Dirac delta function centered around y_0

Subtracting Equation 3.162 from Equation 3.163 and neglecting the terms involving the squares of $\Delta\theta$, we get

$$\Delta J = 2 \int_0^{t_f} \int_0^1 \int_0^d \int_0^r \Delta\theta \left[w(\theta - Y)\delta(y) + (\theta - Y)\delta(y - y_1) \right] dydxdzdt +$$
$$\int_0^{t_f} \int_0^1 \int_0^d \int_0^r \frac{\lambda}{\mathrm{Pe}} \left[\frac{\partial^2(\Delta\theta)}{\partial x^2} + \frac{\partial^2(\Delta\theta)}{\partial y^2} + \frac{\partial^2(\Delta\theta)}{\partial z^2} \right] dxdydzdt -$$
$$\int_0^{t_f} \int_0^1 \int_0^d \int_0^r \lambda \left[\frac{\partial\{u(\Delta\theta)\}}{\partial x} + \frac{\partial\{v(\Delta\theta)\}}{\partial y} + \frac{\partial(\Delta\theta)}{\partial t} \right] dxdydzdt$$
$$(3.164)$$

Using the boundary conditions from the sensitivity problem, we have

$$
\begin{aligned}
\int_0^1 \lambda \frac{\partial^2 (\triangle \theta)}{\partial x^2} dx &= \left[\lambda \int \frac{\partial^2 (\triangle \theta)}{\partial x^2} dx - \int \left(\frac{\partial \lambda}{\partial x} \int \frac{\partial^2 (\triangle \theta)}{\partial x^2} dx \right) dx \right]_{x=0}^{x=1} \\
&= \left[\lambda \frac{\partial (\triangle \theta)}{\partial x} \right]_{x=0}^{x=1} - \int_0^1 \frac{\partial (\triangle \theta)}{\partial x} \frac{\partial \lambda}{\partial x} dx \\
&= \left[\lambda \frac{\partial (\triangle \theta)}{\partial x} \right]_{x=0}^{x=1} - \left[\triangle \theta \frac{\partial \lambda}{\partial x} \right]_{x=0}^{x=1} + \int_0^1 \frac{\partial^2 \lambda}{\partial x^2} (\triangle \theta) dx \\
&= - \left[\lambda \frac{\partial (\triangle \theta)}{\partial x} \right]_{x=0} - \left[\triangle \theta \frac{\partial \lambda}{\partial x} \right]_{x=1} + \int_0^1 \frac{\partial^2 \lambda}{\partial x^2} (\triangle \theta) dx
\end{aligned}
$$

$$(3.165)$$

Therefore

$$
\begin{aligned}
\int_0^{t_f} \int_0^1 \int_0^d \int_0^r \lambda \frac{\partial^2 (\triangle \theta)}{\partial x^2} dx\, dy\, dz\, dt &= - \int_0^{t_f} \int_0^d \int_0^r \left[\lambda \frac{\partial (\triangle \theta)}{\partial x} \right]_{x=0} dy\, dz\, dt - \\
& \quad \int_0^{t_f} \int_0^d \int_0^r \left[\frac{\partial \lambda}{\partial x} \triangle \theta \right]_{x=1} dy\, dz\, dt + \\
& \quad \int_0^{t_f} \int_0^1 \int_0^d \int_0^r \triangle \theta \frac{\partial^2 \lambda}{\partial x^2} dx\, dy\, dz\, dt
\end{aligned}
$$

$$(3.166)$$

Again

$$
\begin{aligned}
\int_0^d \lambda \frac{\partial^2 (\triangle \theta)}{\partial y^2} dy &= \left[\lambda \int \frac{\partial^2 (\triangle \theta)}{\partial y^2} dy - \int \left(\frac{\partial \lambda}{\partial y} \int \frac{\partial^2 (\triangle \theta)}{\partial y^2} dy \right) dy \right]_{y=0}^{y=d} \\
&= \left[\lambda \frac{\partial (\triangle \theta)}{\partial y} \right]_{y=0}^{y=d} - \int_0^d \frac{\partial (\triangle \theta)}{\partial y} \frac{\partial \lambda}{\partial y} dy \\
&= \left[\lambda \frac{\partial (\triangle \theta)}{\partial y} \right]_{y=0}^{y=d} - \left[\triangle \theta \frac{\partial \lambda}{\partial y} \right]_{y=0}^{y=d} + \int_0^d \frac{\partial^2 \lambda}{\partial y^2} (\triangle \theta) dy \\
&= \left[\lambda \frac{\partial (\triangle \theta)}{\partial y} \right]_{y=0}^{y=d} + \left[\triangle \theta \frac{\partial \lambda}{\partial y} \right]_{y=0} + \int_0^d \frac{\partial^2 \lambda}{\partial y^2} (\triangle \theta) dy
\end{aligned}
$$

$$(3.167)$$

Therefore

$$\int_0^{t_f} \int_0^1 \int_0^d \int_0^r \lambda \frac{\partial^2(\triangle\theta)}{\partial y^2} dxdydzdt = \int_0^{t_f} \int_0^1 \int_0^r \left[\lambda\frac{\partial(\triangle\theta)}{\partial y}\right]_{y=0}^{y=d} dxdzdt +$$
$$\int_0^{t_f} \int_0^1 \int_0^r \left[\frac{\partial\lambda}{\partial y}\triangle\theta\right]_{y=0} dxdzdt +$$
$$\int_0^{t_f} \int_0^1 \int_0^d \int_0^r \triangle\theta\frac{\partial^2\lambda}{\partial y^2} dxdydzdt$$

$$(3.168)$$

Again

$$\int_0^r \lambda\frac{\partial^2(\triangle\theta)}{\partial z^2} dz = \left[\lambda\int\frac{\partial^2(\triangle\theta)}{\partial z^2}dz - \int\left(\frac{\partial\lambda}{\partial z}\int\frac{\partial^2(\triangle\theta)}{\partial z^2}dz\right)dz\right]_{z=0}^{z=r}$$
$$= \left[\lambda\frac{\partial(\triangle\theta)}{\partial z}\right]_{z=0}^{z=r} - \int_0^r\frac{\partial(\triangle\theta)}{\partial z}\frac{\partial\lambda}{\partial z}dz$$
$$= -\left[\triangle\theta\frac{\partial\lambda}{\partial z}\right]_{z=0}^{z=r} + \int_0^r\frac{\partial^2\lambda}{\partial y^2}(\triangle\theta)dz \qquad (3.169)$$

Therefore

$$\int_0^{t_f} \int_0^1 \int_0^d \int_0^r \lambda \frac{\partial^2(\triangle\theta)}{\partial z^2} dxdydzdt = -\int_0^{t_f} \int_0^1 \int_0^d \left[\frac{\partial\lambda}{\partial y}\triangle\theta\right]_{z=0}^{z=r} dxdydt +$$
$$\int_0^{t_f} \int_0^1 \int_0^d \int_0^r \triangle\theta\frac{\partial^2\lambda}{\partial z^2} dxdydzdt$$

$$(3.170)$$

Also

$$\int_0^1 \lambda\frac{\partial\{u(\triangle\theta)\}}{\partial x} dx = \left[\lambda\int\frac{\partial\{u(\triangle\theta)\}}{\partial x}dx - \int\left(\frac{\partial\lambda}{\partial x}\int\frac{\partial\{u(\triangle\theta)\}}{\partial x}\right)dx\right]_{x=0}^{x=1}$$
$$= \left[\lambda u(\triangle\theta)\right]_{x=0}^{x=1} - \int_0^1\frac{\partial\lambda}{\partial x}u(\triangle\theta)dx$$
$$= \left[\lambda u\triangle\theta\right]_{x=1} - \int_0^1 u\frac{\partial\lambda}{\partial x}(\triangle\theta)dx \qquad (3.171)$$

Therefore

$$\int_0^{t_f} \int_0^1 \int_0^d \int_0^r \lambda\frac{\partial\{u(\triangle\theta)\}}{\partial x} dxdydzdt = \int_0^{t_f} \int_0^d \int_0^r [\lambda u\triangle\theta]_{x=1} dydzdt -$$
$$\int_0^{t_f} \int_0^1 \int_0^d \int_0^r u\frac{\partial\lambda}{\partial x}(\triangle\theta)dxdydzdt$$

$$(3.172)$$

And

$$\int_0^d \lambda \frac{\partial \{v(\triangle\theta)\}}{\partial y} dy = \left[\lambda \int \frac{\partial \{v(\triangle\theta)\}}{\partial y} dy - \int \left(\frac{\partial \lambda}{\partial y} \int \frac{\partial \{v(\triangle\theta)\}}{\partial y} \right) dy \right]_{y=0}^{y=d}$$

$$= \left[\lambda v(\triangle\theta) \right]_{y=0}^{y=d} - \int_0^d \frac{\partial \lambda}{\partial y} v(\triangle\theta) dy$$

$$= -\int_0^1 v \frac{\partial \lambda}{\partial y}(\triangle\theta) dy \qquad (3.173)$$

Therefore

$$\int_0^{t_f} \int_0^1 \int_0^d \int_0^r \lambda \frac{\partial \{v(\triangle\theta)\}}{\partial y} dxdydzdt = -\int_0^{t_f} \int_0^1 \int_0^d \int_0^r v \frac{\partial \lambda}{\partial y}(\triangle\theta) dxdydzdt \qquad (3.174)$$

Further

$$\int_0^{t_f} \lambda \frac{\partial(\triangle\theta)}{\partial t} dt = \left[\lambda \int \frac{\partial(\triangle\theta)}{\partial t} dt - \int \frac{\partial \lambda}{\partial t} \triangle\theta dt \right]_{t=0}^{t=t_f}$$

$$= \left[\lambda\triangle\theta \right]_{t=0}^{t=t_f} - \int_0^{t_f} \triangle\theta \frac{\partial \lambda}{\partial t} dt$$

$$= \left[\lambda\triangle\theta \right]_{t=t_f} - \int_0^{t_f} \triangle\theta \frac{\partial \lambda}{\partial t} dt \qquad (3.175)$$

Therefore

$$\int_0^{t_f} \int_0^1 \int_0^d \int_0^r \lambda \frac{\partial(\triangle\theta)}{\partial t} dxdydzdt = \int_0^{t_f} \int_0^1 \int_0^d \int_0^r \left[\lambda\triangle\theta \right]_{t=t_f} dxdydzdt -$$

$$\int_0^{t_f} \int_0^1 \int_0^d \int_0^r \triangle\theta \frac{\partial \lambda}{\partial t} dxdydzdt \qquad (3.176)$$

Combining Equations 3.164 to 3.176, we have

$$\triangle J =$$

$$\int_0^{t_f} \int_0^1 \int_0^d \int_0^r \left[\frac{1}{\text{Pe}} \left(\frac{\partial^2 \lambda}{\partial x^2} + \frac{\partial^2 \lambda}{\partial y^2} + \frac{\partial^2 \lambda}{\partial z^2} \right) + u \frac{\partial \lambda}{\partial x} + v \frac{\partial \lambda}{\partial y} + \frac{\partial \lambda}{\partial t} \right] \triangle\theta dxdydzdt +$$

$$2 \int_0^{t_f} \int_0^1 \int_0^d \int_0^r \left[w(\theta - Y)\delta(y) + (\theta - Y)\delta(y - y_1) \right] \triangle\theta dxdydzdt -$$

$$\int_0^{t_f} \int_0^d \int_0^r \frac{1}{\text{Pe}} \left[\lambda \frac{\partial(\triangle\theta)}{\partial x} \right]_{x=0} dydzdt - \int_0^{t_f} \int_0^d \int_0^r \frac{1}{\text{Pe}} \left[\triangle\theta \frac{\partial \lambda}{\partial x} \right]_{x=1} dydzdt -$$

$$\int_0^{t_f} \int_0^1 \int_0^d \frac{1}{\text{Pe}} \left[\frac{\partial \lambda}{\partial y} \triangle\theta \right]_{z=0}^{z=r} dxdydt - \int_0^{t_f} \int_0^d \int_0^r \left[\lambda u \triangle\theta \right]_{x=1} dydzdt -$$

$$\int_0^1 \int_0^d \int_0^r \left[\lambda\triangle\theta \right]_{t=t_f} dxdydz \qquad (3.177)$$

For $\triangle J \to 0$, the following adjoint equation and boundary conditions can be deduced:

$$\frac{1}{\text{Pe}}\left(\frac{\partial^2 \lambda}{\partial x^2} + \frac{\partial^2 \lambda}{\partial y^2} + \frac{\partial^2 \lambda}{\partial z^2}\right) + \frac{\partial(u\lambda)}{\partial x} + \frac{\partial(v\lambda)}{\partial y} + \frac{\partial \lambda}{\partial t} + 2(\theta - Y)\delta(y - y_1) = 0 \quad (3.178)$$

$$t = t_f, \ \lambda = 0 \quad (3.179)$$

$$x = 0, \ \lambda = 0 \quad (3.180)$$

$$x = 1, \ \frac{\partial \lambda}{\partial x} + u\lambda\text{Pe} = 0 \quad (3.181)$$

$$y = 0, \ \frac{\partial \lambda}{\partial y} = -2w\text{Pe}(\theta_w - Y_w) \quad (3.182)$$

$$y = d, \ \lambda = 0 \quad (3.183)$$

$$z = 0, \ \frac{\partial \lambda}{\partial z} = 0 \quad (3.184)$$

$$z = r, \ \frac{\partial \lambda}{\partial z} = 0 \quad (3.185)$$

Hence

$$\triangle J = -\frac{1}{\text{Pe}}\int_0^{t_f}\int_0^1\int_0^r [\lambda(-\triangle Nu)]_{y=0}\, dxdzdt \quad (3.186)$$

From the definition of gradient, we may write,

$$\triangle J = \int_0^{t_f}\int_0^1\int_0^r J'(-\triangle Nu)dxdzdt \quad (3.187)$$

From Equations 3.186 and 3.187, we have the following expression for the gradient of the functional:

$$J' = \lim_{\triangle Nu \to 0}\frac{\triangle J}{\triangle(Nu)} = -\frac{\lambda(t, x, 0, z)}{\text{Pe}} \quad (3.188)$$

3.4.5   Determination of Search Step Size.

If the value of the functional is J^k after k-th iteration and it becomes J^{k+1} after temperatures are updated through a step size of β^k, the condition for the optimum step size will be given by

$$\frac{\partial J^{k+1}}{\partial \beta^k} = 0 \quad (3.189)$$

Recalling the expression of functional

$$J^k = \int_0^{t_f}\int_0^1\int_0^d\int_0^r \left[(\theta - Y)^2\delta(y - y_1) + w(\theta - Y)\delta(y)\right]dxdydzdt \quad (3.190)$$

Therefore,

$$min_\beta J^k(-\triangle Nu)^k = min_\beta \int_0^{t_f} \int_0^1 \int_0^d \int_0^r \{[\theta\{(-\triangle Nu)^k - \beta^k P^k\} - Y]^2 \delta(y - y_1)$$
$$+ w[\theta\{(-\triangle Nu)^k - \beta^k P^k\} - Y]^2 \delta(y)\} dx dy dz dt$$

$$(3.191)$$

linearizing by Taylor series expansion

$$J^{k+1}[(-\triangle Nu)^{k+1}] =$$
$$\int_0^{t_f} \int_0^1 \int_0^d \int_0^r \left[\theta[(-\triangle Nu)^k - \beta^k \triangle\theta(P^k)] - Y\right]^2 \delta(y - y_1) dx dy dz dt$$
$$+ w \int_0^{t_f} \int_0^1 \int_0^d \int_0^r \left[\theta[(-\triangle Nu)^k - \beta^k \triangle\theta(P^k)] - Y\right]^2 \delta(y) dx dy dz dt$$
$$= \int_0^{t_f} \int_0^1 \int_0^d \int_0^r \left[(\theta - Y) - \beta^k \triangle\theta\}^2 \{\delta(y - y_1) + w\delta(y)\right] dx dy dz dt$$

$$(3.192)$$

Therefore,

$$\frac{\partial J^{k+1}}{\partial \beta^k} = 2 \int_0^{t_f} \int_0^1 \int_0^d \int_0^r \triangle\theta(\theta - Y - \beta^k \triangle\theta)\{\delta(y - y_1) + w\delta(y)\} dx dy dz dt \quad (3.193)$$

Using Equations 3.189 and 3.193, we have the following equation for the optimum step size,

$$\beta^k = \frac{\int_0^{t_f} \int_0^1 \int_0^d \int_0^r \triangle\theta(\theta - Y) \left[\delta(y - y_1) + w\delta(y)\right] dx dy dz dt}{\int_0^{t_f} \int_0^1 \int_0^d \int_0^r (\triangle\theta)^2 \left[\delta(y - y_1) + w\delta(y)\right] dx dy dz dt} \quad (3.194)$$

3.4.6 Complete Inverse Algorithm.

The complete inverse algorithm for calculating the Nusselt number distribution over a ribbed surface is summarized below:

1. Solve the continuity and momentum equations to get the velocity field. .

2. Smooth imperfect plate temperature data using Gram orthogonal polynomial filter.

3. Solve energy equation using the following initial and boundary conditions:

$$t = 0, \ \theta = 0 \quad (3.195)$$

$$x = 0, \ \theta = 0 \tag{3.196}$$

$$x = 1, \ \frac{\partial \theta}{\partial x} = 0 \tag{3.197}$$

$$y = 0, \ \theta = \theta_w \tag{3.198}$$

$$y = d, \ \theta = 0 \tag{3.199}$$

$$z = 0, \ \frac{\partial \theta}{\partial z} = 0 \tag{3.200}$$

$$z = r, \ \frac{\partial \theta}{\partial z} = 0 \tag{3.201}$$

4. Get the values of local Nusselt numbers. Take an initial guess of Nusselt number to be same as that found at the end point of the domain. Initialize $J = 0$

5. Solve energy equation using the following initial and boundary conditions:

$$t = 0, \ \theta = 0 \tag{3.202}$$

$$x = 0, \ \theta = 0 \tag{3.203}$$

$$x = 1, \ \frac{\partial \theta}{\partial x} = 0 \tag{3.204}$$

$$y = 0, \ \frac{\partial \theta}{\partial y} = -\mathrm{Nu} \tag{3.205}$$

$$y = d, \ \theta = 0 \tag{3.206}$$

$$z = 0, \ \frac{\partial \theta}{\partial z} = 0 \tag{3.207}$$

$$z = r, \ \frac{\partial \theta}{\partial z} = 0 \tag{3.208}$$

Find out the temperatures at the plate and at the plane of measurement of redundant data.

6. Compute functional,

$$J = \int_0^{t_f} \int_0^1 \int_0^d \int_0^r \{(\theta_w - Y_w)^2 + w(\theta_m - Y_m)^2\} dx\,dy\,dz\,dt \tag{3.209}$$

7. Check the stopping criterion,

$$|J^k - J^{k-1}| < \epsilon \tag{3.210}$$

where, ϵ is a predetermined real number, very close to zero.

If it is satisfied, stop iterations. Otherwise:

8. Solve adjoint problem

$$\frac{1}{\text{Pe}}\left(\frac{\partial^2\lambda}{\partial x^2}+\frac{\partial^2\lambda}{\partial y^2}+\frac{\partial^2\lambda}{\partial z^2}\right)+\frac{\partial(u\lambda)}{\partial x}+\frac{\partial(v\lambda)}{\partial y}+\frac{\partial\lambda}{\partial t}+2(\theta-Y)\delta(y-y_1)=0$$

(3.211)

with

$$t=t_f,\ \lambda=0 \tag{3.212}$$

$$x=0,\ \lambda=0 \tag{3.213}$$

$$x=1,\ \frac{\partial\lambda}{\partial x}+u\lambda\text{Pe}=0 \tag{3.214}$$

$$y=0,\ \frac{\partial\lambda}{\partial y}=-2w\text{Pe}(\theta_w-Y_w) \tag{3.215}$$

$$y=d,\ \lambda=0 \tag{3.216}$$

$$z=0,\ \frac{\partial\lambda}{\partial z}=0 \tag{3.217}$$

$$z=r,\ \frac{\partial\lambda}{\partial z}=0 \tag{3.218}$$

9. Compute gradient

$$J'=-\frac{\lambda(t,x,0,z)}{\text{Pe}} \tag{3.219}$$

10. Compute the descent direction

$$P^k=\gamma^k P^{k-1}+J'^k \tag{3.220}$$

where

$$\text{for the first iteration } \gamma^k=0 \tag{3.221}$$

$$\text{otherwise } \gamma^k=\frac{\langle J^k-J^{k-1}|J^k\rangle}{\|J^{k-1}\|^2} \tag{3.222}$$

11. Solve the sensitivity problem

$$\frac{\partial(\Delta\theta)}{\partial t}+\frac{\partial(u\Delta\theta)}{\partial x}+\frac{\partial(v\Delta\theta)}{\partial y}=\frac{1}{\text{Pe}}\left[\frac{\partial^2(\Delta\theta)}{\partial x^2}+\frac{\partial^2(\Delta\theta)}{\partial y^2}+\frac{\partial^2(\Delta\theta)}{\partial z^2}\right] \tag{3.223}$$

with

$$t=0,\ \Delta\theta=0 \tag{3.224}$$

$$x=0,\ \Delta\theta=0 \tag{3.225}$$

$$x=1,\ \frac{\partial(\Delta\theta)}{\partial x}=0 \tag{3.226}$$

$$y = 0, \ \frac{\partial(\triangle\theta)}{\partial y} = -\triangle\text{Nu} = P^k \tag{3.227}$$

$$y = d, \ \triangle\theta = 0 \tag{3.228}$$

$$z = 0, \ \frac{\partial(\triangle\theta)}{\partial z} = 0 \tag{3.229}$$

$$z = r, \ \frac{\partial(\triangle\theta)}{\partial z} = 0 \tag{3.230}$$

12. Compute the step size

$$\beta^k = \frac{\int_0^{t_f} \int_0^1 \int_0^r \triangle\theta(\theta - Y) \left[\sum_{j=1}^{mp} w_j \delta(y - y_j) + \delta(y)\right] dxdzdt}{\int_0^{t_f} \int_0^1 \int_0^r (\triangle\theta)^2 \left[\sum_{j=1}^{mp} w_j \delta(y - y_j) + \delta(y)\right] dxdzdt} \tag{3.231}$$

where mp indicates number of measurement planes and w_j is the weight assigned to the data from the j-th plane of measurement.

13. Compute the new local Nusselt number

$$(-\text{Nu})^{k+1} = (-\text{Nu})^k - \beta^k P^k \tag{3.232}$$

14. Go to 5 and continue till convergence.

Chapter 4

Flow and Heat Transfer over a Surface with a Rib

The mathematical details of the inverse technique based on iterative regularization is explained in this chapter for flow and heat transfer over a ribbed plate. The basic algorithm is similar to Chapter 3. However, due to presence of rib, the boundary layer approximations are no longer valid here. The direct, adjoint and sensitivity problems need special treatment at the rib location.

The Figure 4.1 shows the single rib configuration that has been analyzed. The rib cross-section is rectangular and the cross-section does not change in the z direction. The flow field is taken to be steady two-dimensional, while unsteady two and three-dimensional temperature fields have been considered. The following assumptions have been employed throughout:

1. The fluid is Newtonian and incompressible.

2. The fluid properties are constant with respect to temperature.

3. The flow is laminar.

4. The velocity field is steady and two-dimensional.

5. The fluid inlet temperature is spatially uniform and temporally constant.

6. Viscous dissipation and mechanical work terms are negligibly small.

7. Forced convection is predominant; hence the momentum and energy equations are not coupled.
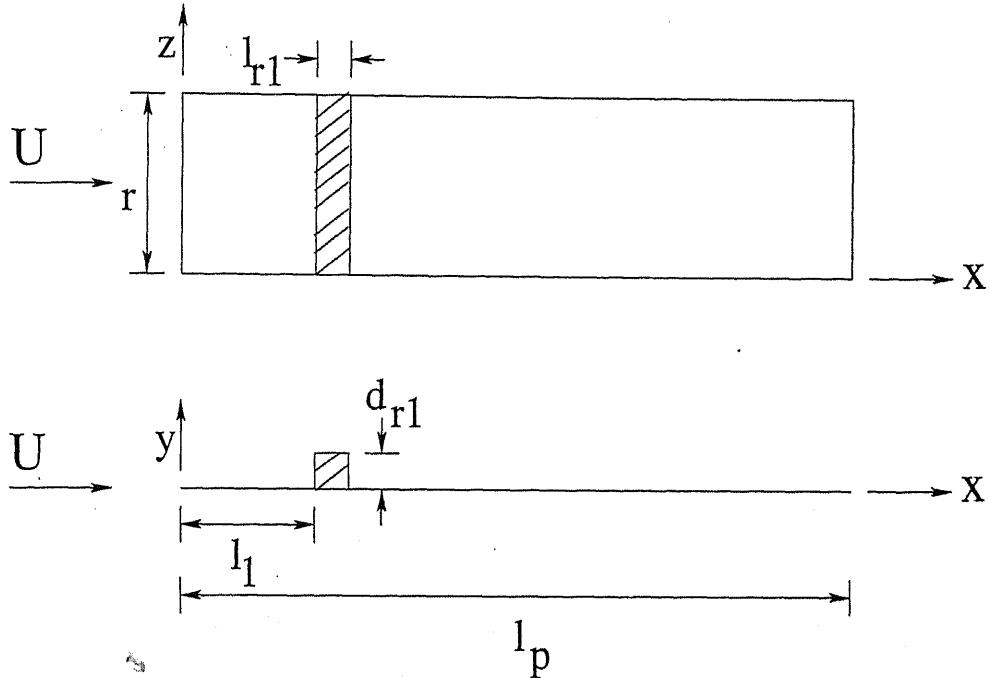
Figure 4.1: Plate with Single Rib

8. The flat plate temperature is temporally a constant.

9. Plate temperature data is available with some scatter whose characteristics are known; in addition, limited but high quality temperature data is available within the flow field.

For steady surface temperature case the algorithm consists of the following basic steps:

1. Smooth the given temperature data using Gram orthogonal polynomial filter through the seven point moving window averaging scheme.

2. Solve the continuity and momentum equations to find the velocity field.

3. Take an initial guess of local Nusselt number distribution over the plate.

4. Compute the temperature field using a guessed local Nusselt number as the boundary condition at the plate.

5. Compute the optimization functional.

6. If the value of the functional conforms to the stopping criteria, stop iterations and present the results.

7. Otherwise, solve the adjoint problem and find the gradient of the functional.

8. Find the search direction.

9. Solve the sensitivity problem and find the search step size.

10. Update the local Nusselt number values over the plate surface.

11. Return to 4 and continue.

4.1   Velocity Computation

The two-dimensional velocity field is computed by solving continuity and Navier-Stokes equations through the vorticity-stream function approach. The governing equations are:

$$\frac{\partial \omega}{\partial t} + \frac{\partial (u\omega)}{\partial x} + \frac{\partial (v\omega)}{\partial y} = \frac{1}{\mathrm{Re}} \left(\frac{\partial^2 \omega}{\partial x^2} + \frac{\partial^2 \omega}{\partial y^2} \right) \tag{4.1}$$

$$\nabla^2 \psi = -\omega \tag{4.2}$$

$$u = \frac{\partial \psi}{\partial y} \tag{4.3}$$

$$v = -\frac{\partial \psi}{\partial x} \tag{4.4}$$

The boundary conditions are:

$$x = 0, \ \omega = 0, \ \psi = y, \ u = 1, \ v = 0 \tag{4.5}$$

$$x = l_p, \ \frac{\partial \omega}{\partial x} = 0, \ \frac{\partial^2 \psi}{\partial x^2} = 0, \ \frac{\partial u}{\partial x} = 0, \ \frac{\partial v}{\partial x} = 0 \tag{4.6}$$

$$y = 0, \ \omega = -\nabla^2 \psi, \ \psi = 0, \ u = 0, \ v = 0 \tag{4.7}$$

$$y = h, \ \omega = -\nabla^2 \psi, \ \psi = y, \ u = 1 \tag{4.8}$$

$$x = l_1, \ \text{and} \ y \leq d_{r1}, \ \omega = -\nabla^2 \psi, \ \psi = 0, \ u = 0, \ v = 0 \tag{4.9}$$

$$x = l_1 + l_{r1}, \ \text{and} \ y \leq d_{r1}, \ \omega = -\nabla^2 \psi, \ \psi = 0, \ u = 0, \ v = 0 \tag{4.10}$$

$$x < l_1 + l_{r1}, \ \text{and} \ x > l_1, \ \text{and} \ y = d_{r1}, \ \omega = -\nabla^2 \psi, \ \psi = 0, \ u = 0, \ v = 0 \tag{4.11}$$

The rib is treated by the following condition:

$$x \leq l_1 + l_{r1}, \ \text{and} \ x \geq l_1, \ \text{and} \ y \leq d_{r1}, \ u = 0, \ v = 0, \ \psi = 0, \ \omega = 0 \tag{4.12}$$

4.2 Unsteady Two Dimensional Temperature Field

The inverse formulation for a two dimensional unsteady temperature field is described here. The flow field is considered steady.

4.2.1 Assumptions

1. Plate temperature is steady.

2. Plate temperature is varying with length only.

3. Temperature field is developing.

4.2.2 Direct Problem

The direct problem solves the following energy equation:

$$\frac{\partial \theta}{\partial t} + \frac{\partial (u\theta)}{\partial x} + \frac{\partial (v\theta)}{\partial y} = \frac{1}{\text{Pe}} \left(\frac{\partial^2 \theta}{\partial x^2} + \frac{\partial^2 \theta}{\partial y^2} \right) \tag{4.13}$$

The initial and boundary conditions are:

$$t = 0, \ \theta = 0 \tag{4.14}$$

$$x = 0, \ \frac{\partial \theta}{\partial x} = 0 \tag{4.15}$$

$$x = 1, \ \theta = 0 \tag{4.16}$$

$$y = 0, \ \frac{\partial \theta}{\partial y} = -\text{Nu} \tag{4.17}$$

$$y = d, \ \theta = 0 \tag{4.18}$$

where, Nu represents local Nusselt number values (initial guess or updated values after any iteration). The rib is treated by the following condition.

For $x \leq l_1 + l_{r1}$, and $x \geq l_1$, and $y \leq d_{r1}$
$$\frac{\partial \theta}{\partial t} = \frac{1}{\text{Pe}} \frac{\alpha_s}{\alpha_f} \left(\frac{\partial^2 \theta}{\partial x^2} + \frac{\partial^2 \theta}{\partial y^2} \right) \tag{4.19}$$

For $x = l_1$ or $x = l_1 + l_{r1}$, and $y \leq d_{r1}$, $k_s \left. \frac{\partial \theta}{\partial x} \right|_{\text{solid}} = k_f \left. \frac{\partial \theta}{\partial x} \right|_{\text{fluid}}$ (4.20)

For $x \geq l_1$ or $x \leq l_1 + l_{r1}$, and $y = d_{r1}$, $k_s \left. \frac{\partial \theta}{\partial y} \right|_{\text{solid}} = k_f \left. \frac{\partial \theta}{\partial y} \right|_{\text{fluid}}$ (4.21)

4.2.3   Inverse Problem

The inverse problem is posed in the form of minimization of the following functional:

$$J = \int_0^{t_f} \int_0^l \left[(\theta_w - Y_w)^2 + w(\theta_m - Y_m)^2 \right] dx dt \qquad (4.22)$$

where θ_w and Y_w are the computed and measured temperatures at the wall, θ_m and Y_m are the computed and measured temperatures in the interior and w is the weight assigned to the high quality data.

4.2.4   Sensitivity Problem

The sensitivity problem determines the the dependence of the temperature on the local Nusselt numbers. To formulate the sensitivity problem, a perturbation of $\Delta\theta$ is given to θ and θ is replaced by $\theta + \Delta\theta$ in Equation 4.13 to yield

$$\frac{\partial(\theta + \Delta\theta)}{\partial t} + \frac{\partial[u(\theta + \Delta\theta)]}{\partial x} + \frac{\partial[v(\theta + \Delta\theta)]}{\partial y} =$$
$$\frac{1}{\mathrm{Pe}} \left[\frac{\partial^2(\theta + \Delta\theta)}{\partial x^2} + \frac{\partial^2(\theta + \Delta\theta)}{\partial y^2} \right] \qquad (4.23)$$

Now, subtracting Equation 4.13 from Equation 4.23, we have the following sensitivity problem,

$$\frac{\partial(\Delta\theta)}{\partial t} + \frac{\partial(u\Delta\theta)}{\partial x} + \frac{\partial(v\Delta\theta)}{\partial y} = \frac{1}{\mathrm{Pe}} \left[\frac{\partial^2(\Delta\theta)}{\partial x^2} + \frac{\partial^2(\Delta\theta)}{\partial y^2} \right] \qquad (4.24)$$

Similarly, in the initial and boundary condition, Nu is replaced by Nu+ΔNu and θ by $\theta + \Delta\theta$; thus we have:

$$t = 0, \ \theta + \Delta\theta = 0 \qquad (4.25)$$

$$x = 0, \ \theta + \Delta\theta = 0 \qquad (4.26)$$

$$x = 1, \ \frac{\partial(\theta + \Delta\theta)}{\partial y} = 0 \qquad (4.27)$$

$$y = 0, \ \frac{\partial(\theta + \Delta\theta)}{\partial y} = -(\mathrm{Nu} + \Delta\mathrm{Nu}) \qquad (4.28)$$

$$y = d, \ \theta + \Delta\theta = 0 \qquad (4.29)$$

Now, subtracting Equations (4.14-4.18) from Equations (4.25-4.29) respectively, we have the following boundary conditions for the sensitivity problem

$$t = 0, \ \Delta\theta = 0 \qquad (4.30)$$

$$x = 0, \ \Delta\theta = 0 \tag{4.31}$$

$$x = 1, \ \frac{\Delta\theta}{x} = 0 \tag{4.32}$$

$$y = 0, \ \frac{\partial(\Delta\theta)}{\partial y} = -\Delta\mathrm{Nu} \tag{4.33}$$

$$y = d, \ \Delta\theta = 0 \tag{4.34}$$

The rib is treated by the following condition.

For $x \le l_1 + l_{r1}$, and $x \ge l_1$, and $y \le d_{r1}$
$$\frac{\partial(\Delta\theta)}{\partial t} = \frac{1}{\mathrm{Pe}}\frac{\alpha_s}{\alpha_f}\left(\frac{\partial^2(\Delta\theta)}{\partial x^2} + \frac{\partial^2(\Delta\theta)}{\partial y^2}\right) \tag{4.35}$$

For $x = l_1$ or $x = l_1 + l_{r1}$, and $y \le d_{r1}$, $k_s \left.\frac{\partial(\Delta\theta)}{\partial x}\right|_{\mathrm{solid}} = k_f \left.\frac{\partial(\Delta\theta)}{\partial x}\right|_{\mathrm{fluid}}$ (4.36)

For $x \ge l_1$ or $x \le l_1 + l_{r1}$, and $y = d_{r1}$, $k_s \left.\frac{\partial(\Delta\theta)}{\partial y}\right|_{\mathrm{solid}} = k_f \left.\frac{\partial(\Delta\theta)}{\partial y}\right|_{\mathrm{fluid}}$ (4.37)

4.2.5 Adjoint Problem

Let, λ be the Lagrange multiplier that is associated with the constraint. We can write the functional

$$
\begin{aligned}
J = & \int_0^{t_f}\int_0^l\int_0^d \left[(\theta_w - Y_w)^2 + w(\theta_m - Y_m)^2\right] dx\,dy\,dt + \\
& \int_0^{t_f}\int_0^l\int_0^d \lambda\left[\frac{1}{\mathrm{Pe}}\left(\frac{\partial^2\theta}{\partial x^2} + \frac{\partial^2\theta}{\partial y^2} + \frac{\partial^2\theta}{\partial z^2}\right) - \frac{\partial(u\theta)}{\partial x} - \frac{\partial(v\theta)}{\partial y} - \frac{\partial\theta}{\partial t}\right] dx\,dy\,dt
\end{aligned}
\tag{4.38}
$$

In Equation 4.38, setting $\theta + \Delta\theta$ in place of θ and $J + \Delta J$ in place of J, we have

$$
\begin{aligned}
J + \Delta J = & \\
& \int_0^{t_f}\int_0^l\int_0^d \left[(\theta + \Delta\theta - Y)^2\delta(y) + w(\theta + \Delta\theta - Y)^2\delta(y - y_1)\right] dx\,dy\,dt + \\
& \int_0^{t_f}\int_0^l\int_0^d \frac{\lambda}{\mathrm{Pe}}\left[\frac{\partial^2(\theta + \Delta\theta)}{\partial x^2} + \frac{\partial^2(\theta + \Delta\theta)}{\partial y^2}\right] dx\,dy\,dt - \\
& \int_0^{t_f}\int_0^l\int_0^d \lambda\left[\frac{\partial\{u(\theta + \Delta\theta)\}}{\partial x} + \frac{\partial\{v(\theta + \Delta\theta)\}}{\partial y} + \frac{\partial(\theta + \Delta\theta)}{\partial t}\right] dx\,dy\,dt
\end{aligned}
\tag{4.39}
$$

Subtracting Equation 4.38 from equation 4.39 and neglecting the terms involving squares of $\triangle\theta$, we have

$$
\begin{aligned}
\triangle J &= 2\int_0^{t_f}\int_0^1\int_0^d\int_0^r \triangle\theta\left[w(\theta-Y)\delta(y)+(\theta-Y)\delta(y-y_1)\right]dydxdzdt + \\
&\quad \int_0^{t_f}\int_0^l\int_0^d\int_0^r \frac{\lambda}{\text{Pe}}\left[\frac{\partial^2(\triangle\theta)}{\partial x^2}+\frac{\partial^2(\triangle\theta)}{\partial y^2}\right]dxdydt - \\
&\quad \int_0^{t_f}\int_0^l\int_0^d \lambda\left[\frac{\partial\{u(\triangle\theta)\}}{\partial x}+\frac{\partial\{v(\triangle\theta)\}}{\partial y}+\frac{\partial(\triangle\theta)}{\partial t}\right]dxdydt
\end{aligned}
$$

$$(4.40)$$

Using the boundary conditions from the sensitivity problem, we get

$$
\begin{aligned}
\int_0^l \lambda\frac{\partial^2(\triangle\theta)}{\partial x^2}dx &= \left[\lambda\int\frac{\partial^2(\triangle\theta)}{\partial x^2}dx-\int\left(\frac{\partial\lambda}{\partial x}\int\frac{\partial^2(\triangle\theta)}{\partial x^2}dx\right)dx\right]_{x=0}^{x=l} \\
&= \left[\lambda\frac{\partial(\triangle\theta)}{\partial x}\right]_{x=0}^{x=l}-\int_0^l\frac{\partial(\triangle\theta)}{\partial x}\frac{\partial\lambda}{\partial x}dx \\
&= \left[\lambda\frac{\partial(\triangle\theta)}{\partial x}\right]_{x=0}^{x=l}-\left[\triangle\theta\frac{\partial\lambda}{\partial x}\right]_{x=0}^{x=l}+\int_0^l\frac{\partial^2\lambda}{\partial x^2}(\triangle\theta)dx \\
&= -\left[\lambda\frac{\partial(\triangle\theta)}{\partial x}\right]_{x=0}-\left[\triangle\theta\frac{\partial\lambda}{\partial x}\right]_{x=l}+\int_0^1\frac{\partial^2\lambda}{\partial x^2}(\triangle\theta)dx
\end{aligned}
$$

$$(4.41)$$

Therefore

$$
\begin{aligned}
\int_0^{t_f}\int_0^l\int_0^d\lambda\frac{\partial^2(\triangle\theta)}{\partial x^2}dxdydt &= -\int_0^{t_f}\int_0^d\left[\lambda\frac{\partial(\triangle\theta)}{\partial x}\right]_{x=0}dydt - \\
&\quad \int_0^{t_f}\int_0^d\left[\frac{\partial\lambda}{\partial x}\triangle\theta\right]_{x=l}dydt + \\
&\quad \int_0^{t_f}\int_0^l\int_0^d\triangle\theta\frac{\partial^2\lambda}{\partial x^2}dxdydt
\end{aligned}
$$

$$(4.42)$$

Again

$$
\begin{aligned}
\int_0^d \lambda \frac{\partial^2(\triangle\theta)}{\partial y^2}dy &= \left[\lambda\int\frac{\partial^2(\triangle\theta)}{\partial y^2}dy - \int\left(\frac{\partial\lambda}{\partial y}\int\frac{\partial^2(\triangle\theta)}{\partial y^2}dy\right)dy\right]_{y=0}^{y=d} \\
&= \left[\lambda\frac{\partial(\triangle\theta)}{\partial y}\right]_{y=0}^{y=d} - \int_0^d\frac{\partial(\triangle\theta)}{\partial y}\frac{\partial\lambda}{\partial y}dy \\
&= \left[\lambda\frac{\partial(\triangle\theta)}{\partial y}\right]_{y=0}^{y=d} - \left[\triangle\theta\frac{\partial\lambda}{\partial y}\right]_{y=0}^{y=d} + \int_0^d\frac{\partial^2\lambda}{\partial y^2}(\triangle\theta)dy \\
&= \left[\lambda\frac{\partial(\triangle\theta)}{\partial y}\right]_{y=0}^{y=d} + \left[\triangle\theta\frac{\partial\lambda}{\partial y}\right]_{y=0} + \int_0^d\frac{\partial^2\lambda}{\partial y^2}(\triangle\theta)dy
\end{aligned}
$$

(4.43)

Therefore

$$
\begin{aligned}
\int_0^{t_f}\int_0^l\int_0^d\lambda\frac{\partial^2(\triangle\theta)}{\partial y^2}dxdydt &= \int_0^{t_f}\int_0^l\int_0^r\left[\lambda\frac{\partial(\triangle\theta)}{\partial y}\right]_{y=0}^{y=d}dxdt + \\
&\quad \int_0^{t_f}\int_0^l\left[\frac{\partial\lambda}{\partial y}\triangle\theta\right]_{y=0}dxdt + \\
&\quad \int_0^{t_f}\int_0^l\int_0^d\triangle\theta\frac{\partial^2\lambda}{\partial y^2}dxdydt
\end{aligned}
$$

(4.44)

Also

$$
\begin{aligned}
\int_0^l\lambda\frac{\partial\{u(\triangle\theta)\}}{\partial x}dx &= \left[\lambda\int\frac{\partial\{u(\triangle\theta)\}}{\partial x}dx - \int\left(\frac{\partial\lambda}{\partial x}\int\frac{\partial\{u(\triangle\theta)\}}{\partial x}\right)dx\right]_{x=0}^{x=l} \\
&= [\lambda u(\triangle\theta)]_{x=0}^{x=l} - \int_0^1\frac{\partial\lambda}{\partial x}u(\triangle\theta)dx \\
&= [\lambda u\triangle\theta]_{x=l} - \int_0^1 u\frac{\partial\lambda}{\partial x}(\triangle\theta)dx
\end{aligned}
$$

(4.45)

Therefore

$$
\begin{aligned}
\int_0^{t_f}\int_0^l\int_0^d\lambda\frac{\partial\{u(\triangle\theta)\}}{\partial x}dxdydt &= \int_0^{t_f}\int_0^d[\lambda u\triangle\theta]_{x=l}dydt - \\
&\quad \int_0^{t_f}\int_0^l\int_0^d u\frac{\partial\lambda}{\partial x}(\triangle\theta)dxdydt
\end{aligned}
$$

(4.46)

Again

$$\int_0^d \lambda \frac{\partial\{v(\triangle\theta)\}}{\partial y} dy = \left[\lambda \int \frac{\partial\{v(\triangle\theta)\}}{\partial y} dy - \int \left(\frac{\partial\lambda}{\partial y} \int \frac{\partial\{v(\triangle\theta)\}}{\partial y}\right) dy\right]_{y=0}^{y=d}$$

$$= [\lambda v(\triangle\theta)]_{y=0}^{y=d} - \int_0^d \frac{\partial\lambda}{\partial y} v(\triangle\theta) dy$$

$$= -\int_0^1 v\frac{\partial\lambda}{\partial y}(\triangle\theta) dy \qquad (4.47)$$

Therefore

$$\int_0^{t_f} \int_0^l \int_0^d \lambda \frac{\partial\{v(\triangle\theta)\}}{\partial y} dxdydt = -\int_0^{t_f} \int_0^l \int_0^d v\frac{\partial\lambda}{\partial y}(\triangle\theta) dxdydt \qquad (4.48)$$

Further

$$\int_0^{t_f} \lambda \frac{\partial(\triangle\theta)}{\partial t} dt = \left[\lambda \int \frac{\partial(\triangle\theta)}{\partial t} dt - \int \frac{\partial\lambda}{\partial t}\triangle\theta dt\right]_{t=0}^{t=t_f}$$

$$= [\lambda\triangle\theta]_{t=0}^{t=t_f} - \int_0^{t_f} \triangle\theta\frac{\partial\lambda}{\partial t} dt$$

$$= [\lambda\triangle\theta]_{t=t_f} - \int_0^{t_f} \triangle\theta\frac{\partial\lambda}{\partial t} dt \qquad (4.49)$$

Therefore

$$\int_0^{t_f} \int_0^l \int_0^d \lambda \frac{\partial(\triangle\theta)}{\partial t} dxdydt = \int_0^{t_f} \int_0^l \int_0^d [\lambda\triangle\theta]_{t=t_f} dxdydt -$$

$$\int_0^{t_f} \int_0^l \int_0^d \triangle\theta\frac{\partial\lambda}{\partial t} dxdydt \qquad (4.50)$$

Now combining Equations 4.40 to 4.50, we have

$$\triangle J =$$

$$\int_0^{t_f} \int_0^l \int_0^d \left[\frac{1}{Pe}\left(\frac{\partial^2\lambda}{\partial x^2} + \frac{\partial^2\lambda}{\partial y^2}\right) + u\frac{\partial\lambda}{\partial x} + v\frac{\partial\lambda}{\partial y} + \frac{\partial\lambda}{\partial t}\right]\triangle\theta dxdydt +$$

$$2\int_0^{t_f} \int_0^l \int_0^d [w(\theta - Y)\delta(y) + (\theta - Y)\delta(y - y_1)]\triangle\theta dxdydt -$$

$$\int_0^{t_f} \int_0^d \frac{1}{Pe}\left[\lambda\frac{\partial(\triangle\theta)}{\partial x}\right]_{x=0} dydt - \int_0^{t_f} \int_0^d \frac{1}{Pe}\left[\triangle\theta\frac{\partial\lambda}{\partial x}\right]_{x=l} dydt -$$

$$\int_0^{t_f} \int_0^d [\lambda u\triangle\theta]_{x=l} dydt - \int_0^l \int_0^d [\lambda\triangle\theta]_{t=t_f} dxdy \qquad (4.51)$$

For $\triangle J \to 0$, the following adjoint equation and final boundary conditions can be deduced

$$\frac{1}{Pe}\left(\frac{\partial^2\lambda}{\partial x^2} + \frac{\partial^2\lambda}{\partial y^2}\right) + \frac{\partial(u\lambda)}{\partial x} + \frac{\partial(v\lambda)}{\partial y} + \frac{\partial\lambda}{\partial t} + 2(\theta - Y)\delta(y - y_1) = 0 \qquad (4.52)$$

$$t = t_f, \ \lambda = 0 \tag{4.53}$$

$$x = 0, \ \lambda = 0 \tag{4.54}$$

$$x = 1, \ \frac{\partial \lambda}{\partial x} + u\lambda \text{Pe} = 0 \tag{4.55}$$

$$y = 0, \ \frac{\partial \lambda}{\partial y} = -2w\text{Pe}(\theta_w - Y_w) \tag{4.56}$$

$$y = d, \ \lambda = 0 \tag{4.57}$$

The rib is treated by the following condition.

For $x \leq l_1 + l_{r1}$, and $x \geq l_1$, and $y \leq d_{r1}$
$$\frac{\partial \lambda}{\partial t} = -\frac{1}{\text{Pe}}\frac{\alpha_s}{\alpha_f}\left(\frac{\partial^2 \lambda}{\partial x^2} + \frac{\partial^2 \lambda}{\partial y^2}\right) \tag{4.58}$$

For $x = l_1$ or $x = l_1 + l_{r1}$, and $y \leq d_{r1}$, $k_s \left.\frac{\partial \lambda}{\partial x}\right|_{\text{solid}} = k_f \left.\frac{\partial \lambda}{\partial x}\right|_{\text{fluid}} \tag{4.59}$

For $x \geq l_1$ or $x \leq l_1 + l_{r1}$, and $y = d_{r1}$, $k_s \left.\frac{\partial \lambda}{\partial y}\right|_{\text{solid}} = k_f \left.\frac{\partial \lambda}{\partial y}\right|_{\text{fluid}} \tag{4.60}$

Since
$$\triangle J = -\frac{1}{\text{Pe}}\int_0^{t_f}\int_0^l [\lambda(-\triangle Nu)]_{y=0}\, dxdt \tag{4.61}$$

and the definition of gradient

$$\triangle J = \int_0^{t_f}\int_0^l J'(-\triangle \text{Nu})dxdt \tag{4.62}$$

From Equations 4.61 and 4.62, we have the following expression for the gradient of the functional:

$$J' = \lim_{\triangle \text{Nu} \to 0} \frac{\triangle J}{\triangle \text{Nu}} = -\frac{\lambda(t,x,0)}{\text{Pe}} \tag{4.63}$$

4.2.6 Determination of Search Step Size.

If the value of the functional is J^k after k-th iteration and it becomes J^{k+1} after temperatures are updated through a step size of β^k, the condition for the optimum step size will be given by
$$\frac{\partial J^{k+1}}{\partial \beta^k} = 0 \tag{4.64}$$

Recalling the expression of functional

$$J^k = \int_0^{t_f}\int_0^l\int_0^d \left[(\theta - Y)^2\delta(y - y_1) + w(\theta - Y)\delta(y)\right] dxdydt \tag{4.65}$$

Therefore

$$
min_\beta J^k(-\triangle Nu)^k = min_\beta \int_0^{t_f}\int_0^l\int_0^d \{[\theta\{(-\triangle Nu)^k - \beta^k P^k\} - Y]^2\delta(y - y_1)
$$
$$
+ w[\theta\{(-\triangle Nu)^k - \beta^k P^k\} - Y]^2\delta(y)\}dxdydt
$$

(4.66)

linearizing by Taylor series expansion

$$
J^{k+1}[(-\triangle Nu)^{k+1}] =
$$
$$
\int_0^{t_f}\int_0^l\int_0^d \left[w\theta[(-\triangle Nu)^k - \beta^k\triangle\theta(P^k)] - Y\right]^2\delta(y - y_1)dxdydt
$$
$$
+ \int_0^{t_f}\int_0^l\int_0^d \left[\theta[(-\triangle Nu)^k - \beta^k\triangle\theta(P^k)] - Y\right]^2\delta(y)dxdydt
$$
$$
= \int_0^{t_f}\int_0^l\int_0^d \left[w(\theta - Y) - \beta^k\triangle\theta\right]^2\{\delta(y - y_1) + \delta(y)]dxdydt
$$

(4.67)

Therefore

$$
\frac{\partial J^{k+1}}{\partial\beta^k} = 2\int_0^{t_f}\int_0^l\int_0^d \triangle\theta(\theta - Y - \beta^k\triangle\theta)\{w\delta(y - y_1) + \delta(y)\}dxdydt \quad (4.68)
$$

Using Equations 4.68 and 4.69, we have the following equation for the optimum step size

$$
\beta^k = \frac{\int_0^{t_f}\int_0^l\int_0^d \triangle\theta(\theta - Y)\left[w\delta(y - y_1) + \delta(y)\right]dxdydt}{\int_0^{t_f}\int_0^l\int_0^d (\triangle\theta)^2\left[w\delta(y - y_1) + \delta(y)\right]dxdydt}
$$

(4.69)

4.2.7 Complete Inverse Algorithm.

The complete inverse algorithm for calculating the Nusselt number distribution over a ribbed surface is summarized below:

1. Solve the continuity and momentum equations to get the two dimensional velocity field.

2. Filter the imperfect temperature data using Gram orthogonal polynomial filter.

3. Solve the three dimensional energy equation using the following initial and boundary conditions:

$$
t = 0, \ \theta = 0 \qquad (4.70)
$$

$$x = 0, \ \theta = 0 \tag{4.71}$$

$$x = 1, \ \frac{\partial \theta}{\partial x} = 0 \tag{4.72}$$

$$y = 0, \ \theta = \theta_w \tag{4.73}$$

$$y = d, \ \theta = 0 \tag{4.74}$$

The rib is treated by the following condition.

$$x \leq l_1 + l_{r1}, \ \text{and} \ x \geq l_1, \ \text{and} \ y \leq d_{r1}, \ u = 0, \ v = 0 \tag{4.75}$$

4. Get the values of local Nusselt numbers. Take an initial guess local Nusselt number. Initialize $J = 0$

5. Solve the two dimensional energy equation using the following initial and boundary conditions (with Nusselt number from step 4):

$$t = 0, \ \theta = 0 \tag{4.76}$$

$$x = 0, \ \theta = 0 \tag{4.77}$$

$$x = 1, \ \frac{\partial \theta}{\partial x} = 0 \tag{4.78}$$

$$y = 0, \ \frac{\partial \theta}{\partial y} = -\text{Nu} \tag{4.79}$$

$$y = d, \ \theta = 0 \tag{4.80}$$

The rib is treated by the following condition.

$$x \leq l_1 + l_{r1}, \ \text{and} \ x \geq l_1, \ \text{and} \ y \leq d_{r1}, \ u = 0, \ v = 0 \tag{4.81}$$

Find the temperatures at the plate as well as the plane of high quality data.

6. Compute the functional

$$J = \int_0^{t_f} \int_0^l \int_0^d \{(\theta_w - Y_w)^2 + w(\theta_m - Y_m)^2\} dx \, dy \, dt \tag{4.82}$$

7. Check the stopping criterion,

$$|J^k - J^{k-1}| < \epsilon \tag{4.83}$$

where, ϵ is a predetermined real number, very close to zero.

If it is satisfied, stop iterations. Otherwise

8. Solve the adjoint problem

$$\frac{1}{\mathrm{Pe}}\left(\frac{\partial^2 \lambda}{\partial x^2} + \frac{\partial^2 \lambda}{\partial y^2}\right) + \frac{\partial(u\lambda)}{\partial x} + \frac{\partial(v\lambda)}{\partial y} + \frac{\partial \lambda}{\partial t} + 2(\theta - Y)\delta(y - y_1) = 0 \quad (4.84)$$

with

$$t = t_f, \ \lambda = 0 \tag{4.85}$$

$$x = 0, \ \lambda = 0 \tag{4.86}$$

$$x = 1, \ \frac{\partial \lambda}{\partial x} + u\lambda\mathrm{Pe} = 0 \tag{4.87}$$

$$y = 0, \ \frac{\partial \lambda}{\partial y} = -2w\mathrm{Pe}(\theta_w - Y_w) \tag{4.88}$$

$$y = d, \ \lambda = 0 \tag{4.89}$$

The rib is treated by the following condition.

$$x \leq l_1 + l_{r1}, \text{ and } x \geq l_1, \text{ and } y \leq d_{r1}, \ u = 0, \ v = 0 \tag{4.90}$$

9. Compute the gradient

$$J' = -\frac{\lambda(t, x, 0)}{\mathrm{Pe}} \tag{4.91}$$

10. Compute the descent direction

$$P^k = \gamma^k P^{k-1} + J'^k \tag{4.92}$$

where

$$\text{for the first iteration } \gamma^k = 0 \tag{4.93}$$

$$\text{otherwise } \gamma^k = \frac{\langle J^k - J^{k-1}|J^k\rangle}{\|J^{k-1}\|^2} \tag{4.94}$$

11. Solve the sensitivity problem

$$\frac{\partial(\triangle\theta)}{\partial t} + \frac{\partial(u\triangle\theta)}{\partial x} + \frac{\partial(v\triangle\theta)}{\partial y} = \frac{1}{\mathrm{Pe}}\left[\frac{\partial^2(\triangle\theta)}{\partial x^2} + \frac{\partial^2(\triangle\theta)}{\partial y^2}\right] \tag{4.95}$$

with

$$t = 0, \ \triangle\theta = 0 \tag{4.96}$$

$$x = 0, \ \triangle\theta = 0 \tag{4.97}$$

$$x = 1, \ \frac{\partial(\triangle\theta)}{\partial x} = 0 \tag{4.98}$$

$$y = 0, \ \frac{\partial(\triangle\theta)}{\partial y} = -\triangle\mathrm{Nu} = P^k \tag{4.99}$$

$$y = d, \ \triangle\theta = 0 \tag{4.100}$$

12. Compute the step size

$$\beta^k = \frac{\int_0^{t_f} \int_0^1 \triangle\theta(\theta - Y) \left[\sum_{j=1}^{mp} w_j \delta(y - y_j) + \delta(y)\right] dx dt}{\int_0^{t_f} \int_0^1 (\triangle\theta)^2 \left[\sum_{j=1}^{mp} w_j \delta(y - y_j) + \delta(y)\right] dx dz dt} \tag{4.101}$$

where mp indicates number of measurement planes and w_j is the weight assigned to the data from the j-th plane of measurement.

13. Compute the new local Nusselt number

$$(-\mathrm{Nu})^{k+1} = (-\mathrm{Nu})^k - \beta^k P^k \tag{4.102}$$

14. Go to 5 and continue till convergence.

4.3 Unsteady Three Dimensional Temperature Field

The inverse estimation of the instantaneous Nusselt number distribution over a flat surface when the thermal field is three dimensional is presented in this section. The flow field is taken to be steady and two dimensional.

4.3.1 Direct Problem

The direct problem solves the following energy equation:

$$\frac{\partial\theta}{\partial t} + \frac{\partial(u\theta)}{\partial x} + \frac{\partial(v\theta)}{\partial y} = \frac{1}{\mathrm{Pe}} \left(\frac{\partial^2\theta}{\partial x^2} + \frac{\partial^2\theta}{\partial y^2} + \frac{\partial^2\theta}{\partial z^2}\right) \tag{4.103}$$

The initial and boundary conditions are:

$$t = 0, \ \theta = 0 \tag{4.104}$$

$$x = 0, \ \frac{\partial\theta}{\partial x} = 0 \tag{4.105}$$

$$x = 1, \ \theta = 0 \tag{4.106}$$

$$y = 0, \ \frac{\partial\theta}{\partial y} = -\mathrm{Nu} \tag{4.107}$$

$$y = d, \ \theta = 0 \tag{4.108}$$

$$z = 0, \ \frac{\partial\theta}{\partial z} = 0 \tag{4.109}$$

$$z = r, \ \frac{\partial \theta}{\partial z} = 0 \qquad (4.110)$$

where, Nu is the local Nusselt number. The rib is treated by the following condition.

For $x \leq l_1 + l_{r1}$, and $x \geq l_1$, and $y \leq d_{r1}$

$$\frac{\partial \theta}{\partial t} = \frac{1}{\text{Pe}} \frac{\alpha_s}{\alpha_f} \left(\frac{\partial^2 \theta}{\partial x^2} + \frac{\partial^2 \theta}{\partial y^2} + \frac{\partial^2 \theta}{\partial z^2} \right) \qquad (4.111)$$

For $x = l_1$ or $x = l_1 + l_{r1}$, and $y \leq d_{r1}$, $k_s \left. \frac{\partial \theta}{\partial x} \right|_{\text{solid}} = k_f \left. \frac{\partial \theta}{\partial x} \right|_{\text{fluid}}$ \qquad (4.112)

For $x \geq l_1$ or $x \leq l_1 + l_{r1}$, and $y = d_{r1}$, $k_s \left. \frac{\partial \theta}{\partial y} \right|_{\text{solid}} = k_f \left. \frac{\partial \theta}{\partial y} \right|_{\text{fluid}}$ \qquad (4.113)

4.3.2 Inverse Problem

The inverse problem is posed in the form of minimization of the following functional:

$$J = \int_0^{t_f} \int_0^1 \int_0^r \left[(\theta_w - Y_w)^2 + w(\theta_m - Y_m)^2 \right] dx\, dz\, dt \qquad (4.114)$$

where θ_w and Y_w are the computed and measured temperatures at the wall, θ_m and Y_m are the computed and measured temperatures in the interior and w is the weight assigned to the high quality data.

4.3.3 Sensitivity Problem

Sensitivity problem determines the the dependence of the temperature on the unknown local Nusselt numbers. To formulate the sensitivity problem, a perturbation of $\Delta \theta$ is given to θ and θ is replaced by $\theta + \Delta \theta$ in Equation 4.103 to yield

$$\frac{\partial(\theta + \Delta\theta)}{\partial t} + \frac{\partial[u(\theta + \Delta\theta)]}{\partial x} + \frac{\partial[v(\theta + \Delta\theta)]}{\partial y} =$$
$$\frac{1}{\text{Pe}} \left[\frac{\partial^2(\theta + \Delta\theta)}{\partial x^2} + \frac{\partial^2(\theta + \Delta\theta)}{\partial y^2} + \frac{\partial^2(\theta + \Delta\theta)}{\partial z^2} \right] \qquad (4.115)$$

Now, subtracting Equation 4.103 from Equation 4.115, we have the following sensitivity problem,

$$\frac{\partial(\Delta\theta)}{\partial t} + \frac{\partial(u\Delta\theta)}{\partial x} + \frac{\partial(v\Delta\theta)}{\partial y} = \frac{1}{\text{Pe}} \left[\frac{\partial^2(\Delta\theta)}{\partial x^2} + \frac{\partial^2(\Delta\theta)}{\partial y^2} + \frac{\partial^2(\Delta\theta)}{\partial z^2} \right] \qquad (4.116)$$

In the initial and boundary conditions, Nu is replaced by Nu+ΔNu and θ by $\theta + \Delta\theta$; thus we have:

$$t = 0, \ \theta + \Delta\theta = 0 \tag{4.117}$$

$$x = 0, \ \theta + \Delta\theta = 0 \tag{4.118}$$

$$x = 1, \ \frac{\partial(\theta + \Delta\theta)}{\partial y} = 0 \tag{4.119}$$

$$y = 0, \ \frac{\partial(\theta + \Delta\theta)}{\partial y} = -(\text{Nu} + \Delta\text{Nu}) \tag{4.120}$$

$$y = d, \ \theta + \Delta\theta = 0 \tag{4.121}$$

$$z = 0, \ \frac{\partial(\theta + \Delta\theta)}{\partial z} = 0 \tag{4.122}$$

$$z = r, \ \frac{\partial(\theta + \Delta\theta)}{\partial z} = 0 \tag{4.123}$$

Now, subtracting Equations (4.104-4.110) from Equations (4.117-4.123) respectively, we have the following boundary conditions for the sensitivity problem

$$t = 0, \ \Delta\theta = 0 \tag{4.124}$$

$$x = 0, \ \Delta\theta = 0 \tag{4.125}$$

$$x = 1, \ \frac{\Delta\theta}{x} = 0 \tag{4.126}$$

$$y = 0, \ \frac{\partial(\Delta\theta)}{\partial y} = -\Delta\text{Nu} \tag{4.127}$$

$$y = d, \ \Delta\theta = 0 \tag{4.128}$$

$$z = 0, \ \frac{\partial(\Delta\theta)}{\partial z} = 0 \tag{4.129}$$

$$z = r, \ \frac{\partial(\Delta\theta)}{\partial z} = 0 \tag{4.130}$$

The rib is treated by the following condition.

For $x \leq l_1 + l_{r1}$, and $x \geq l_1$, and $y \leq d_{r1}$
$$\frac{\partial(\Delta\theta)}{\partial t} = \frac{1}{\text{Pe}}\frac{\alpha_s}{\alpha_f}\left(\frac{\partial^2(\Delta\theta)}{\partial x^2} + \frac{\partial^2(\Delta\theta)}{\partial y^2} + \frac{\partial^2(\Delta\theta)}{\partial z^2}\right) \tag{4.131}$$

For $x = l_1$ or $x = l_1 + l_{r1}$, and $y \leq d_{r1}$, $k_s \left.\frac{\partial(\Delta\theta)}{\partial x}\right|_{\text{solid}} = k_f \left.\frac{\partial(\Delta\theta)}{\partial x}\right|_{\text{fluid}}$
$$\tag{4.132}$$

For $x \geq l_1$ or $x \leq l_1 + l_{r1}$, and $y = d_{r1}$, $k_s \left.\frac{\partial(\Delta\theta)}{\partial y}\right|_{\text{solid}} = k_f \left.\frac{\partial(\Delta\theta)}{\partial y}\right|_{\text{fluid}}$
$$\tag{4.133}$$

4.3.4 Adjoint Problem

Let, λ be the Lagrange multiplier that is associated with the constraint. We can write the functional

$$
\begin{aligned}
J \;=\; & \int_0^{t_f}\int_0^1\int_0^d\int_0^r \left[(\theta_w - Y_w)^2 + w(\theta_m - Y_m)^2\right] dx\,dy\,dz\,dt\; + \\
& \int_0^{t_f}\int_0^1\int_0^d\int_0^r \lambda \left[\frac{1}{\mathrm{Pe}}\left(\frac{\partial^2\theta}{\partial x^2} + \frac{\partial^2\theta}{\partial y^2} + \frac{\partial^2\theta}{\partial z^2}\right) - \frac{\partial(u\theta)}{\partial x} - \frac{\partial(v\theta)}{\partial y} - \frac{\partial\theta}{\partial t}\right] dx\,dy\,dz\,dt
\end{aligned}
\tag{4.134}
$$

In Equation 4.134, setting $\theta + \triangle\theta$ in place of θ and $J + \triangle J$ in place of J, we have

$$
\begin{aligned}
J + \triangle J =& \\
& \int_0^{t_f}\int_0^1\int_0^d\int_0^r \left[(\theta + \triangle\theta - Y)^2\delta(y) + w(\theta + \triangle\theta - Y)^2\delta(y - y_1)\right] dx\,dy\,dz\,dt\; + \\
& \int_0^{t_f}\int_0^1\int_0^d\int_0^r \frac{\lambda}{\mathrm{Pe}}\left[\frac{\partial^2(\theta + \triangle\theta)}{\partial x^2} + \frac{\partial^2(\theta + \triangle\theta)}{\partial y^2} + \frac{\partial^2(\theta + \triangle\theta)}{\partial z^2}\right] dx\,dy\,dz\,dt\; - \\
& \int_0^{t_f}\int_0^1\int_0^d\int_0^r \lambda\left[\frac{\partial\{u(\theta + \triangle\theta)\}}{\partial x} + \frac{\partial\{v(\theta + \triangle\theta)\}}{\partial y} + \frac{\partial(\theta + \triangle\theta)}{\partial t}\right] dx\,dy\,dz\,dt
\end{aligned}
\tag{4.135}
$$

where, $\delta(y - y_0)$ is the Dirac delta function centered around y_0

Subtracting Equation 4.134 from Equation 4.135 and neglecting the terms involving squares of $\triangle\theta$, we have

$$
\begin{aligned}
\triangle J \;=\; & 2\int_0^{t_f}\int_0^1\int_0^d\int_0^r \triangle\theta\left[w(\theta - Y)\delta(y) + (\theta - Y)\delta(y - y_1)\right] dy\,dx\,dz\,dt\; + \\
& \int_0^{t_f}\int_0^1\int_0^d\int_0^r \frac{\lambda}{\mathrm{Pe}}\left[\frac{\partial^2(\triangle\theta)}{\partial x^2} + \frac{\partial^2(\triangle\theta)}{\partial y^2} + \frac{\partial^2(\triangle\theta)}{\partial z^2}\right] dx\,dy\,dz\,dt\; - \\
& \int_0^{t_f}\int_0^1\int_0^d\int_0^r \lambda\left[\frac{\partial\{u(\triangle\theta)\}}{\partial x} + \frac{\partial\{v(\triangle\theta)\}}{\partial y} + \frac{\partial(\triangle\theta)}{\partial t}\right] dx\,dy\,dz\,dt
\end{aligned}
\tag{4.136}
$$

Using the boundary conditions from the sensitivity problem, we get

$$\int_0^1 \lambda \frac{\partial^2 (\triangle \theta)}{\partial x^2} dx = \left[\lambda \int \frac{\partial^2 (\triangle \theta)}{\partial x^2} dx - \int \left(\frac{\partial \lambda}{\partial x} \int \frac{\partial^2 (\triangle \theta)}{\partial x^2} dx \right) dx \right]_{x=0}^{x=1}$$

$$= \left[\lambda \frac{\partial (\triangle \theta)}{\partial x} \right]_{x=0}^{x=1} - \int_0^1 \frac{\partial (\triangle \theta)}{\partial x} \frac{\partial \lambda}{\partial x} dx$$

$$= \left[\lambda \frac{\partial (\triangle \theta)}{\partial x} \right]_{x=0}^{x=1} - \left[\triangle \theta \frac{\partial \lambda}{\partial x} \right]_{x=0}^{x=1} + \int_0^1 \frac{\partial^2 \lambda}{\partial x^2} (\triangle \theta) dx$$

$$= - \left[\lambda \frac{\partial (\triangle \theta)}{\partial x} \right]_{x=0} - \left[\triangle \theta \frac{\partial \lambda}{\partial x} \right]_{x=1} + \int_0^1 \frac{\partial^2 \lambda}{\partial x^2} (\triangle \theta) dx$$

$$(4.137)$$

Further

$$\int_0^{t_f} \int_0^1 \int_0^d \int_0^r \lambda \frac{\partial^2 (\triangle \theta)}{\partial x^2} dx dy dz dt \approx - \int_0^{t_f} \int_0^d \int_0^r \left[\lambda \frac{\partial (\triangle \theta)}{\partial x} \right]_{x=0} dy dz dt -$$

$$\int_0^{t_f} \int_0^d \int_0^r \left[\frac{\partial \lambda}{\partial x} \triangle \theta \right]_{x=1} dy dz dt +$$

$$\int_0^{t_f} \int_0^1 \int_0^d \int_0^r \triangle \theta \frac{\partial^2 \lambda}{\partial x^2} dx dy dz dt$$

$$(4.138)$$

Again

$$\int_0^d \lambda \frac{\partial^2 (\triangle \theta)}{\partial y^2} dy = \left[\lambda \int \frac{\partial^2 (\triangle \theta)}{\partial y^2} dy - \int \left(\frac{\partial \lambda}{\partial y} \int \frac{\partial^2 (\triangle \theta)}{\partial y^2} dy \right) dy \right]_{y=0}^{y=d}$$

$$= \left[\lambda \frac{\partial (\triangle \theta)}{\partial y} \right]_{y=0}^{y=d} - \int_0^d \frac{\partial (\triangle \theta)}{\partial y} \frac{\partial \lambda}{\partial y} dy$$

$$= \left[\lambda \frac{\partial (\triangle \theta)}{\partial y} \right]_{y=0}^{y=d} - \left[\triangle \theta \frac{\partial \lambda}{\partial y} \right]_{y=0}^{y=d} + \int_0^d \frac{\partial^2 \lambda}{\partial y^2} (\triangle \theta) dy$$

$$= \left[\lambda \frac{\partial (\triangle \theta)}{\partial y} \right]_{y=0}^{y=d} + \left[\triangle \theta \frac{\partial \lambda}{\partial y} \right]_{y=0} + \int_0^d \frac{\partial^2 \lambda}{\partial y^2} (\triangle \theta) dy$$

$$(4.139)$$

Therefore

$$\int_0^{t_f} \int_0^1 \int_0^d \int_0^r \lambda \frac{\partial^2(\triangle\theta)}{\partial y^2} dx dy dz dt = \int_0^{t_f} \int_0^1 \int_0^r \left[\lambda \frac{\partial(\triangle\theta)}{\partial y}\right]_{y=0}^{y=d} dx dz dt +$$

$$\int_0^{t_f} \int_0^1 \int_0^r \left[\frac{\partial\lambda}{\partial y}\triangle\theta\right]_{y=0} dx dz dt +$$

$$\int_0^{t_f} \int_0^1 \int_0^d \int_0^r \triangle\theta \frac{\partial^2\lambda}{\partial y^2} dx dy dz dt$$

$$(4.140)$$

Again

$$\int_0^r \lambda \frac{\partial^2(\triangle\theta)}{\partial z^2} dz = \left[\lambda \int \frac{\partial^2(\triangle\theta)}{\partial z^2} dz - \int \left(\frac{\partial\lambda}{\partial z} \int \frac{\partial^2(\triangle\theta)}{\partial z^2} dz\right) dz\right]_{z=0}^{z=r}$$

$$= \left[\lambda \frac{\partial(\triangle\theta)}{\partial z}\right]_{z=0}^{z=r} - \int_0^r \frac{\partial(\triangle\theta)}{\partial z} \frac{\partial\lambda}{\partial z} dz$$

$$= -\left[\triangle\theta \frac{\partial\lambda}{\partial z}\right]_{z=0}^{z=r} + \int_0^r \frac{\partial^2\lambda}{\partial y^2}(\triangle\theta) dz \qquad (4.141)$$

Therefore

$$\int_0^{t_f} \int_0^1 \int_0^d \int_0^r \lambda \frac{\partial^2(\triangle\theta)}{\partial z^2} dx dy dz dt = -\int_0^{t_f} \int_0^1 \int_0^d \left[\frac{\partial\lambda}{\partial y}\triangle\theta\right]_{z=0}^{z=r} dx dy dt +$$

$$\int_0^{t_f} \int_0^1 \int_0^d \int_0^r \triangle\theta \frac{\partial^2\lambda}{\partial z^2} dx dy dz dt$$

$$(4.142)$$

Also

$$\int_0^1 \lambda \frac{\partial\{u(\triangle\theta)\}}{\partial x} dx = \left[\lambda \int \frac{\partial\{u(\triangle\theta)\}}{\partial x} dx - \int \left(\frac{\partial\lambda}{\partial x} \int \frac{\partial\{u(\triangle\theta)\}}{\partial x}\right) dx\right]_{x=0}^{x=1}$$

$$= [\lambda u(\triangle\theta)]_{x=0}^{x=1} - \int_0^1 \frac{\partial\lambda}{\partial x} u(\triangle\theta) dx$$

$$= [\lambda u\triangle\theta]_{x=1} - \int_0^1 u\frac{\partial\lambda}{\partial x}(\triangle\theta) dx \qquad (4.143)$$

Therefore,

$$\int_0^{t_f} \int_0^1 \int_0^d \int_0^r \lambda \frac{\partial\{u(\triangle\theta)\}}{\partial x} dx dy dz dt = \int_0^{t_f} \int_0^d \int_0^r [\lambda u\triangle\theta]_{x=1} dy dz dt -$$

$$\int_0^{t_f} \int_0^1 \int_0^d \int_0^r u\frac{\partial\lambda}{\partial x}(\triangle\theta) dx dy dz dt$$

$$(4.144)$$

And

$$\int_0^d \lambda \frac{\partial\{v(\triangle\theta)\}}{\partial y}dy = \left[\lambda\int\frac{\partial\{v(\triangle\theta)\}}{\partial y}dy - \int\left(\frac{\partial\lambda}{\partial y}\int\frac{\partial\{v(\triangle\theta)\}}{\partial y}\right)dy\right]_{y=0}^{y=d}$$

$$= [\lambda v(\triangle\theta)]_{y=0}^{y=d} - \int_0^d \frac{\partial\lambda}{\partial y}v(\triangle\theta)dy$$

$$= -\int_0^1 v\frac{\partial\lambda}{\partial y}(\triangle\theta)dy \qquad (4.145)$$

Therefore

$$\int_0^{t_f}\int_0^1\int_0^d\int_0^r \lambda\frac{\partial\{v(\triangle\theta)\}}{\partial y}dxdydzdt = -\int_0^{t_f}\int_0^1\int_0^d\int_0^r v\frac{\partial\lambda}{\partial y}(\triangle\theta)dxdydzdt$$

$$(4.146)$$

And

$$\int_0^{t_f} \lambda\frac{\partial(\triangle\theta)}{\partial t}dt = \left[\lambda\int\frac{\partial(\triangle\theta)}{\partial t}dt - \int\frac{\partial\lambda}{\partial t}\triangle\theta dt\right]_{t=0}^{t=t_f}$$

$$= [\lambda\triangle\theta]_{t=0}^{t=t_f} - \int_0^{t_f} \triangle\theta\frac{\partial\lambda}{\partial t}dt$$

$$= [\lambda\triangle\theta]_{t=t_f} - \int_0^{t_f} \triangle\theta\frac{\partial\lambda}{\partial t}dt \qquad (4.147)$$

Therefore

$$\int_0^{t_f}\int_0^1\int_0^d\int_0^r \lambda\frac{\partial(\triangle\theta)}{\partial t}dxdydzdt = \int_0^{t_f}\int_0^1\int_0^d\int_0^r [\lambda\triangle\theta]_{t=t_f}dxdydzdt -$$

$$\int_0^{t_f}\int_0^1\int_0^d\int_0^r \triangle\theta\frac{\partial\lambda}{\partial t}dxdydzdt \quad (4.148)$$

Now combining Equations 4.136 to 4.148, we have

$$\triangle J =$$

$$\int_0^{t_f}\int_0^1\int_0^d\int_0^r \left[\frac{1}{Pe}\left(\frac{\partial^2\lambda}{\partial x^2}+\frac{\partial^2\lambda}{\partial y^2}+\frac{\partial^2\lambda}{\partial z^2}\right)+u\frac{\partial\lambda}{\partial x}+v\frac{\partial\lambda}{\partial y}+\frac{\partial\lambda}{\partial t}\right]\triangle\theta dxdydzdt +$$

$$2\int_0^{t_f}\int_0^1\int_0^d\int_0^r [w(\theta-Y)\delta(y)+(\theta-Y)\delta(y-y_1)]\triangle\theta dxdydzdt -$$

$$\int_0^{t_f}\int_0^d\int_0^r \frac{1}{Pe}\left[\lambda\frac{\partial(\triangle\theta)}{\partial x}\right]_{x=0}dydzdt - \int_0^{t_f}\int_0^d\int_0^r \frac{1}{Pe}\left[\triangle\theta\frac{\partial\lambda}{\partial x}\right]_{x=1}dydzdt -$$

$$\int_0^{t_f}\int_0^1\int_0^d \frac{1}{Pe}\left[\frac{\partial\lambda}{\partial y}\triangle\theta\right]_{z=0}^{z=r}dxdydt - \int_0^{t_f}\int_0^d\int_0^r [\lambda u\triangle\theta]_{x=1}dydzdt -$$

$$\int_0^1\int_0^d\int_0^r [\lambda\triangle\theta]_{t=t_f}dxdydz \qquad (4.149)$$

For $\triangle J \to 0$, the following adjoint equation and final boundary conditions are deduced

$$\frac{1}{\text{Pe}}\left(\frac{\partial^2 \lambda}{\partial x^2} + \frac{\partial^2 \lambda}{\partial y^2} + \frac{\partial^2 \lambda}{\partial z^2}\right) + \frac{\partial(u\lambda)}{\partial x} + \frac{\partial(v\lambda)}{\partial y} + \frac{\partial \lambda}{\partial t} + 2(\theta - Y)\delta(y - y_1) = 0 \quad (4.150)$$

$$t = t_f, \ \lambda = 0 \quad (4.151)$$

$$x = 0, \ \lambda = 0 \quad (4.152)$$

$$x = 1, \ \frac{\partial \lambda}{\partial x} + u\lambda\text{Pe} = 0 \quad (4.153)$$

$$y = 0, \ \frac{\partial \lambda}{\partial y} = -2w\text{Pe}(\theta_w - Y_w) \quad (4.154)$$

$$y = d, \ \lambda = 0 \quad (4.155)$$

$$z = 0, \ \frac{\partial \lambda}{\partial z} = 0 \quad (4.156)$$

$$z = r, \ \frac{\partial \lambda}{\partial z} = 0 \quad (4.157)$$

The rib is treated by the following condition.

For $x \leq l_1 + l_{r1}$, and $x \geq l_1$, and $y \leq d_{r1}$
$$\frac{\partial \lambda}{\partial t} = -\frac{1}{\text{Pe}}\frac{\alpha_s}{\alpha_f}\left(\frac{\partial^2 \lambda}{\partial x^2} + \frac{\partial^2 \lambda}{\partial y^2} + \frac{\partial^2 \lambda}{\partial z^2}\right) \quad (4.158)$$

For $x = l_1$ or $x = l_1 + l_{r1}$, and $y \leq d_{r1}$, $k_s \left.\frac{\partial \lambda}{\partial x}\right|_{\text{solid}} = k_f \left.\frac{\partial \lambda}{\partial x}\right|_{\text{fluid}}$ \quad (4.159)

For $x \geq l_1$ or $x \leq l_1 + l_{r1}$, and $y = d_{r1}$, $k_s \left.\frac{\partial \lambda}{\partial y}\right|_{\text{solid}} = k_f \left.\frac{\partial \lambda}{\partial y}\right|_{\text{fluid}}$ \quad (4.160)

Since
$$\triangle J = -\frac{1}{\text{Pe}}\int_0^{t_f}\int_0^1\int_0^r [\lambda(-\triangle Nu)]_{y=0} \, dxdzdt \quad (4.161)$$

and the definition of a gradient

$$\triangle J = \int_0^{t_f}\int_0^1\int_0^r J'(-\triangle\text{Nu})dxdzdt \quad (4.162)$$

From Equations 4.161 and 4.162, we have the following expression for the gradient of the functional:

$$J' = \lim_{\triangle\text{Nu}\to 0}\frac{\triangle J}{\triangle\text{Nu}} = -\frac{\lambda(t, x, 0, z)}{\text{Pe}} \quad (4.163)$$

4.3.5   Determination of Search Step Size.

If the value of the functional is J^k after k-th iteration and it becomes J^{k+1} after temperatures are updated through a step size of β^k, the condition for the optimum step size will be given by

$$\frac{\partial J^{k+1}}{\partial \beta^k} = 0 \tag{4.164}$$

Recalling the expression of functional

$$J^k = \int_0^{t_f} \int_0^1 \int_0^d \int_0^r \left[w(\theta - Y)^2 \delta(y - y_1) + (\theta - Y)\delta(y) \right] dx\,dy\,dz\,dt \tag{4.165}$$

Therefore

$$
\begin{aligned}
min_\beta J^k (-\triangle Nu)^k &= min_\beta \int_0^{t_f} \int_0^1 \int_0^d \int_0^r \{ [\theta\{(-\triangle Nu)^k - \beta^k P^k\} - Y]^2 \delta(y - y_1) \\
&\quad + w[\theta\{(-\triangle Nu)^k - \beta^k P^k\} - Y]^2 \delta(y) \} dx\,dy\,dz\,dt
\end{aligned}
$$

$$\tag{4.166}$$

linearizing by Taylor's series expansion

$$
\begin{aligned}
J^{k+1}[(-\triangle Nu)^{k+1}] &= \\
&\int_0^{t_f} \int_0^1 \int_0^d \int_0^r \left[\theta[(-\triangle Nu)^k - \beta^k \triangle\theta(P^k)] - Y \right]^2 \delta(y - y_1) dx\,dy\,dz\,dt \\
&+ w \int_0^{t_f} \int_0^1 \int_0^d \int_0^r \left[\theta[(-\triangle Nu)^k - \beta^k \triangle\theta(P^k)] - Y \right]^2 \delta(y) dx\,dy\,dz\,dt \\
&= \int_0^{t_f} \int_0^1 \int_0^d \int_0^r \left[(\theta - Y) - \beta^k \triangle\theta \}^2 \{ \delta(y - y_1) + w\delta(y) \right] dx\,dy\,dz\,dt
\end{aligned}
$$

$$\tag{4.167}$$

Therefore

$$\frac{\partial J^{k+1}}{\partial \beta^k} = 2 \int_0^{t_f} \int_0^1 \int_0^d \int_0^r \triangle\theta(\theta - Y - \beta^k \triangle\theta)\{\delta(y-y_1) + w\delta(y)\} dx\,dy\,dz\,dt \tag{4.168}$$

Using Equations 4.164 and 4.167, we have the following equation for the optimum step size

$$\beta^k = \frac{\int_0^{t_f} \int_0^1 \int_0^d \int_0^r \triangle\theta(\theta - Y) \left[\delta(y - y_1) + w\delta(y) \right] dx\,dy\,dz\,dt}{\int_0^{t_f} \int_0^1 \int_0^d \int_0^r (\triangle\theta)^2 \left[\delta(y - y_1) + w\delta(y) \right] dx\,dy\,dz\,dt} \tag{4.169}$$

4.3.6   Complete Inverse Algorithm.

The complete inverse algorithm for calculation the Nusselt number distribution over flat surface is summarized below:

1. Solve continuity and momentum equations to get the velocity field.

2. Smooth imperfect plate temperature data using Gram orthogonal polynomial filter.

3. Solve energy equation using the following initial and boundary conditions:

$$t = 0, \ \theta = 0 \tag{4.170}$$

$$x = 0, \ \theta = 0 \tag{4.171}$$

$$x = 1, \ \frac{\partial \theta}{\partial x} = 0 \tag{4.172}$$

$$y = 0, \ \theta = \theta_w \tag{4.173}$$

$$y = d, \ \theta = 0 \tag{4.174}$$

$$z = 0, \ \frac{\partial \theta}{\partial z} = 0 \tag{4.175}$$

$$z = r, \ \frac{\partial \theta}{\partial z} = 0 \tag{4.176}$$

The rib is treated by the following condition.

$$x \leq l_1 + l_{r1}, \ \text{and} \ x \geq l_1, \ \text{and} \ y \leq d_{r1}, \ u = 0, \ v = 0 \tag{4.177}$$

4. Get the values of local Nusselt numbers. Take an initial guess of Nusselt number to be same as that found at the end point of the domain. Initialize $J = 0$

5. Solve energy equation using the following initial and boundary conditions (with Nusselt number from step 4):

$$t = 0, \ \theta = 0 \tag{4.178}$$

$$x = 0, \ \theta = 0 \tag{4.179}$$

$$x = 1, \ \frac{\partial \theta}{\partial x} = 0 \tag{4.180}$$

$$y = 0, \ \frac{\partial \theta}{\partial y} = -\mathrm{Nu} \tag{4.181}$$

$$y = d, \ \theta = 0 \tag{4.182}$$

$$z = 0, \ \frac{\partial \theta}{\partial z} = 0 \tag{4.183}$$

$$z = r, \ \frac{\partial \theta}{\partial z} = 0 \tag{4.184}$$

The rib is treated by the following condition.

$$x \leq l_1 + l_{r1}, \ \text{and} \ x \geq l_1, \ \text{and} \ y \leq d_{r1}, \ u = 0, \ v = 0 \tag{4.185}$$

Find out the temperatures at the plate as well as the plane of measurement of redundant data.

6. Compute the functional,

$$J = \int_0^{t_f} \int_0^1 \int_0^d \int_0^r \{(\theta_w - Y_w)^2 + w(\theta_m - Y_m)^2\} dx \, dy \, dz \, dt \tag{4.186}$$

7. Check the stopping criterion,

$$|J^k - J^{k-1}| < \epsilon \tag{4.187}$$

where, ϵ is a predetermined real number, very close to zero.

If it is satisfied, stop iterations. Otherwise,

8. Solve the adjoint problem

$$\frac{1}{\mathrm{Pe}} \left(\frac{\partial^2 \lambda}{\partial x^2} + \frac{\partial^2 \lambda}{\partial y^2} + \frac{\partial^2 \lambda}{\partial z^2} \right) + \frac{\partial (u\lambda)}{\partial x} + \frac{\partial (v\lambda)}{\partial y} + \frac{\partial \lambda}{\partial t} + 2(\theta - Y)\delta(y - y_1) = 0 \tag{4.188}$$

$$t = t_f, \ \lambda = 0 \tag{4.189}$$

$$x = 0, \ \lambda = 0 \tag{4.190}$$

$$x = 1, \ \frac{\partial \lambda}{\partial x} + u\lambda \mathrm{Pe} = 0 \tag{4.191}$$

$$y = 0, \ \frac{\partial \lambda}{\partial y} = -2w\mathrm{Pe}(\theta_w - Y_w) \tag{4.192}$$

$$y = d, \ \lambda = 0 \tag{4.193}$$

$$z = 0, \ \frac{\partial \lambda}{\partial z} = 0 \tag{4.194}$$

$$z = r, \ \frac{\partial \lambda}{\partial z} = 0 \tag{4.195}$$

The rib is treated by the following condition.

$$x \leq l_1 + l_{r1}, \ \text{and} \ x \geq l_1, \ \text{and} \ y \leq d_{r1}, \ u = 0, \ v = 0 \tag{4.196}$$

9. Compute the gradient

$$J' = -\frac{\lambda(t, x, 0, z)}{\text{Pe}} \tag{4.197}$$

10. Compute the descent direction

$$P^k = \gamma^k P^{k-1} + J'^k \tag{4.198}$$

where

$$\text{for first iteration } \gamma^k = 0 \tag{4.199}$$

$$\text{otherwise } \gamma^k = \frac{\langle J^k - J^{k-1} | J^k \rangle}{\|J^{k-1}\|^2} \tag{4.200}$$

11. Solve the sensitivity problem

$$\frac{\partial(\triangle\theta)}{\partial t} + \frac{\partial(u\triangle\theta)}{\partial x} + \frac{\partial(v\triangle\theta)}{\partial y} = \frac{1}{\text{Pe}} \left[\frac{\partial^2(\triangle\theta)}{\partial x^2} + \frac{\partial^2(\triangle\theta)}{\partial y^2} + \frac{\partial^2(\triangle\theta)}{\partial z^2} \right] \tag{4.201}$$

with the following initial and boundary conditions:

$$t = 0, \ \triangle\theta = 0 \tag{4.202}$$

$$x = 0, \ \triangle\theta = 0 \tag{4.203}$$

$$x = 1, \ \frac{\partial(\triangle\theta)}{\partial x} = 0 \tag{4.204}$$

$$y = 0, \ \frac{\partial(\triangle\theta)}{\partial y} = -\triangle\text{Nu} = P^k \tag{4.205}$$

$$y = d, \ \triangle\theta = 0 \tag{4.206}$$

$$z = 0, \ \frac{\partial(\triangle\theta)}{\partial z} = 0 \tag{4.207}$$

$$z = r, \ \frac{\partial(\triangle\theta)}{\partial z} = 0 \tag{4.208}$$

12. Compute the step size

$$\beta^k = \frac{\int_0^{t_f} \int_0^l \int_0^r \triangle\theta(\theta - Y) \left[\sum_{j=1}^{mp} w_j \delta(y - y_j) + \delta(y)\right] dx dz dt}{\int_0^{t_f} \int_0^1 \int_0^r (\triangle\theta)^2 \left[\sum_{j=1}^{mp} w_j \delta(y - y_j) + \delta(y)\right] dx dz dt} \tag{4.209}$$

where mp indicates number of measurement planes and w_j is the weight assigned to the data from the j-th plane of measurement.

13. Compute new local Nusselt number

$$(-\text{Nu})^{k+1} = (-\text{Nu})^k - \beta^k P^k \tag{4.210}$$

14. Go to 5 and continue till convergence.

4.4 Transient Plate Temperature Problem

The inverse formulation for an transient surface temperature is studied here. Both the velocity and temperature fields are two dimensional. No additional interior measurement is considered.

4.4.1 Assumptions

1. Temperature field is two dimensional, i.e., plate temperature is varying with length only.

2. Plate temperature is unsteady.

3. The local Nusselt number distribution is not varying with time.

The local Nusselt Number is defined as

$$\text{Nu}(x) = -\frac{1}{\theta} \frac{\partial\theta}{\partial y}\bigg|_{y=0} \tag{4.211}$$

4.4.2 Direct Problem

The direct problem solves the following energy equation:

$$\frac{\partial\theta}{\partial t} + \frac{\partial(u\theta)}{\partial x} + \frac{\partial(v\theta)}{\partial y} = \frac{1}{\text{Pe}} \left(\frac{\partial^2\theta}{\partial x^2} + \frac{\partial^2\theta}{\partial y^2}\right) \tag{4.212}$$

The initial and boundary conditions are:

$$t = 0, \ \theta = 0 \tag{4.213}$$

$$x = 0, \ \frac{\partial \theta}{\partial x} = 0 \tag{4.214}$$

$$x = 1, \ \theta = 0 \tag{4.215}$$

$$y = 0, \ \frac{\partial \theta}{\partial y} = -\theta \mathrm{Nu} \tag{4.216}$$

$$y = d, \ \theta = 0 \tag{4.217}$$

where, Nu represents local Nusselt number. The rib is treated by the following condition.

For $x \leq l_1 + l_{r1}$, and $x \geq l_1$, and $y \leq d_{r1}$

$$\frac{\partial \theta}{\partial t} = \frac{1}{\mathrm{Pe}} \frac{\alpha_s}{\alpha_f} \left(\frac{\partial^2 \theta}{\partial x^2} + \frac{\partial^2 \theta}{\partial y^2} \right) \tag{4.218}$$

For $x = l_1$ or $x = l_1 + l_{r1}$, and $y \leq d_{r1}$, $\left. k_s \frac{\partial \theta}{\partial x} \right|_{\text{solid}} = \left. k_f \frac{\partial \theta}{\partial x} \right|_{\text{fluid}}$ (4.219)

For $x \geq l_1$ or $x \leq l_1 + l_{r1}$, and $y = d_{r1}$, $\left. k_s \frac{\partial \theta}{\partial y} \right|_{\text{solid}} = \left. k_f \frac{\partial \theta}{\partial y} \right|_{\text{fluid}}$ (4.220)

4.4.3 Inverse Problem

The inverse problem is posed in the form of minimization of the following functional:

$$J = \int_0^{t_f} \int_0^l \int_0^d \left[(\theta - Y)^2 \right] \delta(y) dx dy dt \tag{4.221}$$

where θ and Y are the computed and measured temperatures and δ is the Dirac delta function.

4.4.4 Sensitivity Problem

Sensitivity problem determines the dependence of the temperature on the unknown local Nusselt numbers. To formulate the sensitivity problem, a perturbation of $\Delta\theta$ is given to θ and θ is replaced by $\theta + \Delta\theta$ in Equation 4.212 to yield

$$\frac{\partial(\theta + \Delta\theta)}{\partial t} + \frac{\partial[u(\theta + \Delta\theta)]}{\partial x} + \frac{\partial[v(\theta + \Delta\theta)]}{\partial y} = \frac{1}{\mathrm{Pe}} \left[\frac{\partial^2(\theta + \Delta\theta)}{\partial x^2} + \frac{\partial^2(\theta + \Delta\theta)}{\partial y^2} \right] \tag{4.222}$$

Now, subtracting equation(4.212) from equation(4.222), we have the following sensitivity problem,

$$\frac{\partial(\Delta\theta)}{\partial t} + \frac{\partial(u\Delta\theta)}{\partial x} + \frac{\partial(v\Delta\theta)}{\partial y} = \frac{1}{\text{Pe}}\left[\frac{\partial^2(\Delta\theta)}{\partial x^2} + \frac{\partial^2(\Delta\theta)}{\partial y^2}\right] \quad (4.223)$$

In the initial and boundary conditions, Nu is replaced by Nu+ΔNu and θ by $\theta + \Delta\theta$, we have:

$$t = 0, \ \theta + \Delta\theta = 0 \quad (4.224)$$

$$x = 0, \ \theta + \Delta\theta = 0 \quad (4.225)$$

$$x = 1, \ \frac{\partial(\theta + \Delta\theta)}{\partial y} = 0 \quad (4.226)$$

$$y = 0, \ \frac{\partial(\theta + \Delta\theta)}{\partial y} = -(\text{Nu} + \Delta\text{Nu})(\theta + \Delta\theta) \quad (4.227)$$

$$y = d, \ \theta + \Delta\theta = 0 \quad (4.228)$$

Now, subtracting Equations (4.213-4.217) from Equations (4.224-4.228) respectively, we get the following boundary conditions for the sensitivity problem:

$$t = 0, \ \Delta\theta = 0 \quad (4.229)$$

$$x = 0, \ \Delta\theta = 0 \quad (4.230)$$

$$x = 1, \ \frac{\partial(\Delta\theta)}{\partial x} = 0 \quad (4.231)$$

$$y = 0, \ \frac{\partial(\Delta\theta)}{\partial y} = -\theta\Delta\text{Nu} - \text{Nu}\Delta\theta \quad (4.232)$$

$$y = d, \ \Delta\theta = 0 \quad (4.233)$$

The rib is treated by the following condition.

For $x \leq l_1 + l_{r1}$, and $x \geq l_1$, and $y \leq d_{r1}$
$$\frac{\partial(\Delta\theta)}{\partial t} = \frac{1}{\text{Pe}}\frac{\alpha_s}{\alpha_f}\left[\frac{\partial^2(\Delta\theta)}{\partial x^2} + \frac{\partial^2(\Delta\theta)}{\partial y^2}\right] \quad (4.234)$$

For $x = l_1$ or $x = l_1 + l_{r1}$, and $y \leq d_{r1}$, $k_s \left.\frac{\partial(\Delta\theta)}{\partial x}\right|_{\text{solid}} = k_f \left.\frac{\partial(\Delta\theta)}{\partial x}\right|_{\text{fluid}}$ (4.235)

For $x \geq l_1$ or $x \leq l_1 + l_{r1}$, and $y = d_{r1}$, $k_s \left.\frac{\partial(\Delta\theta)}{\partial y}\right|_{\text{solid}} = k_f \left.\frac{\partial(\Delta\theta)}{\partial y}\right|_{\text{fluid}}$ (4.236)

4.4.5 Adjoint Problem

Let, λ be the Lagrange multiplier that is associated with the constraint. We can write the functional.

$$J = \int_0^{t_f} \int_0^l \int_0^d (\theta - Y)^2 \delta(y) dx dy dt +$$
$$\int_0^{t_f} \int_0^l \int_0^d \lambda \left[\frac{1}{\text{Pe}} \left(\frac{\partial^2 \theta}{\partial x^2} + \frac{\partial^2 \theta}{\partial y^2} \right) - \frac{\partial(u\theta)}{\partial x} - \frac{\partial(v\theta)}{\partial y} - \frac{\partial \theta}{\partial t} \right] dx dy dt$$

(4.237)

In Equation 4.237, setting $\theta + \triangle\theta$ in place of θ and $J + \triangle J$ in place of J, we have

$$J + \triangle J = \int_0^{t_f} \int_0^l \int_0^d (\theta + \triangle\theta - Y)^2 \delta(y) dx dy dt +$$
$$\int_0^{t_f} \int_0^l \int_0^d \frac{\lambda}{\text{Pe}} \left[\frac{\partial^2(\theta + \triangle\theta)}{\partial x^2} + \frac{\partial^2(\theta + \triangle\theta)}{\partial y^2} \right] dx dy dt -$$
$$\int_0^{t_f} \int_0^l \int_0^d \lambda \left[\frac{\partial\{u(\theta + \triangle\theta)\}}{\partial x} + \frac{\partial\{v(\theta + \triangle\theta)\}}{\partial y} + \frac{\partial(\theta + \triangle\theta)}{\partial t} \right] dx dy dt$$

(4.238)

Subtracting Equation 4.237 from Equation 4.238 and neglecting the terms involving squares of $\triangle\theta$, we have

$$\triangle J = 2 \int_0^{t_f} \int_0^l \int_0^d \triangle\theta(\theta - Y)\delta(y) dx dy dt +$$
$$\int_0^{t_f} \int_0^1 \int_0^d \frac{\lambda}{\text{Pe}} \left[\frac{\partial^2(\triangle\theta)}{\partial x^2} + \frac{\partial^2(\triangle\theta)}{\partial y^2} \right] dx dy dt -$$
$$\int_0^{t_f} \int_0^1 \int_0^d \lambda \left[\frac{\partial\{u(\triangle\theta)\}}{\partial x} + \frac{\partial\{v(\triangle\theta)\}}{\partial y} + \frac{\partial(\triangle\theta)}{\partial t} \right] dx dy dt \quad (4.239)$$

Using the boundary conditions from the sensitivity problem, we get

$$\int_0^l \lambda \frac{\partial^2(\triangle\theta)}{\partial x^2} dx = \left[\lambda \int \frac{\partial^2(\triangle\theta)}{\partial x^2} dx - \int \left(\frac{\partial\lambda}{\partial x} \int \frac{\partial^2(\triangle\theta)}{\partial x^2} dx \right) dx \right]_{x=0}^{x=l}$$
$$= \left[\lambda \frac{\partial(\triangle\theta)}{\partial x} \right]_{x=0}^{x=l} - \int_0^l \frac{\partial(\triangle\theta)}{\partial x} \frac{\partial\lambda}{\partial x} dx$$
$$= \left[\lambda \frac{\partial(\triangle\theta)}{\partial x} \right]_{x=0}^{x=l} - \left[\triangle\theta \frac{\partial\lambda}{\partial x} \right]_{x=0}^{x=l} + \int_0^l \frac{\partial^2\lambda}{\partial x^2}(\triangle\theta) dx$$
$$= - \left[\lambda \frac{\partial(\triangle\theta)}{\partial x} \right]_{x=0} - \left[\triangle\theta \frac{\partial\lambda}{\partial x} \right]_{x=l} + \int_0^l \frac{\partial^2\lambda}{\partial x^2}(\triangle\theta) dx$$

(4.240)

Further

$$
\int_0^{t_f} \int_0^l \int_0^d \lambda \frac{\partial^2 (\triangle\theta)}{\partial x^2} dxdydt = -\int_0^{t_f} \int_0^d \int_0^r \left[\lambda \frac{\partial(\triangle\theta)}{\partial x} \right]_{x=0} dydt -
$$
$$
\int_0^{t_f} \int_0^d \left[\frac{\partial \lambda}{\partial x} \triangle\theta \right]_{x=1} dydt +
$$
$$
\int_0^{t_f} \int_0^1 \int_0^d \triangle\theta \frac{\partial^2 \lambda}{\partial x^2} dxdydt \qquad (4.241)
$$

Again

$$
\int_0^d \lambda \frac{\partial^2 (\triangle\theta)}{\partial y^2} dy = \left[\lambda \int \frac{\partial^2(\triangle\theta)}{\partial y^2} dy - \int \left(\frac{\partial \lambda}{\partial y} \int \frac{\partial^2(\triangle\theta)}{\partial y^2} dy \right) dy \right]_{y=0}^{y=d}
$$
$$
= \left[\lambda \frac{\partial(\triangle\theta)}{\partial y} \right]_{y=0}^{y=d} - \int_0^d \frac{\partial(\triangle\theta)}{\partial y} \frac{\partial \lambda}{\partial y} dy
$$
$$
= \left[\lambda \frac{\partial(\triangle\theta)}{\partial y} \right]_{y=0}^{y=d} - \left[\triangle\theta \frac{\partial \lambda}{\partial y} \right]_{y=0}^{y=d} + \int_0^d \frac{\partial^2 \lambda}{\partial y^2} (\triangle\theta) dy
$$
$$
= \left[\lambda \frac{\partial(\triangle\theta)}{\partial y} \right]_{y=0}^{y=d} + \left[\triangle\theta \frac{\partial \lambda}{\partial y} \right]_{y=0} + \int_0^d \frac{\partial^2 \lambda}{\partial y^2} (\triangle\theta) dy
$$
$$
\qquad (4.242)
$$

Therefore

$$
\int_0^{t_f} \int_0^l \int_0^d \lambda \frac{\partial^2 (\triangle\theta)}{\partial y^2} dxdydt = \int_0^{t_f} \int_0^l \left[\lambda \frac{\partial(\triangle\theta)}{\partial y} \right]_{y=0}^{y=d} dxdt +
$$
$$
\int_0^{t_f} \int_0^l \left[\frac{\partial \lambda}{\partial y} \triangle\theta \right]_{y=0} dxdt +
$$
$$
\int_0^{t_f} \int_0^l \int_0^d \triangle\theta \frac{\partial^2 \lambda}{\partial y^2} dxdydt \qquad (4\!:\!243)
$$

Also

$$
\int_0^l \lambda \frac{\partial \{u(\triangle\theta)\}}{\partial x} dx = \left[\lambda \int \frac{\partial\{u(\triangle\theta)\}}{\partial x} dx - \int \left(\frac{\partial \lambda}{\partial x} \int \frac{\partial\{u(\triangle\theta)\}}{\partial x} \right) dx \right]_{x=0}^{x=l}
$$
$$
= [\lambda u(\triangle\theta)]_{x=0}^{x=l} - \int_0^l \frac{\partial \lambda}{\partial x} u(\triangle\theta) dx
$$
$$
= [\lambda u \triangle\theta]_{x=l} - \int_0^l u \frac{\partial \lambda}{\partial x} (\triangle\theta) dx \qquad (4.244)
$$

Therefore

$$
\int_0^{t_f} \int_0^1 \int_0^d \lambda \frac{\partial \{u(\triangle\theta)\}}{\partial x} dxdydt = \int_0^{t_f} \int_0^d [\lambda u \triangle\theta]_{x=1} dydt -
$$
$$
\int_0^{t_f} \int_0^1 \int_0^d u \frac{\partial \lambda}{\partial x} (\triangle\theta) dxdydt \quad (4.245)
$$

And

$$
\begin{aligned}
\int_0^d \lambda \frac{\partial\{v(\triangle\theta)\}}{\partial y} dy &= \left[\lambda \int \frac{\partial\{v(\triangle\theta)\}}{\partial y} dy - \int \left(\frac{\partial\lambda}{\partial y} \int \frac{\partial\{v(\triangle\theta)\}}{\partial y} \right) dy \right]_{y=0}^{y=d} \\
&= [\lambda v(\triangle\theta)]_{y=0}^{y=d} - \int_0^d \frac{\partial\lambda}{\partial y} v(\triangle\theta) dy \\
&= [\lambda v(\triangle\theta)]_{y=d} - \int_0^d v \frac{\partial\lambda}{\partial y}(\triangle\theta) dy \qquad (4.246)
\end{aligned}
$$

Therefore

$$
\begin{aligned}
\int_0^{t_f}\int_0^l\int_0^d \lambda \frac{\partial\{v(\triangle\theta)\}}{\partial y} dxdydt &= -\int_0^{t_f}\int_0^l\int_0^d v\frac{\partial\lambda}{\partial y}(\triangle\theta) dxdydt \\
&\quad + \int_0^{t_f}\int_0^l [\lambda v(\triangle\theta)]_{y=d}\, dxdt \qquad (4.247)
\end{aligned}
$$

And

$$
\begin{aligned}
\int_0^{t_f} \lambda \frac{\partial(\triangle\theta)}{\partial t} dt &= \left[\lambda \int \frac{\partial(\triangle\theta)}{\partial t} dt - \int \frac{\partial\lambda}{\partial t} \triangle\theta dt \right]_{t=0}^{t=t_f} \\
&= [\lambda\triangle\theta]_{t=0}^{t=t_f} - \int_0^{t_f} \triangle\theta \frac{\partial\lambda}{\partial t} dt \\
&= [\lambda\triangle\theta]_{t=t_f} - \int_0^{t_f} \triangle\theta \frac{\partial\lambda}{\partial t} dt \qquad (4.248)
\end{aligned}
$$

Further

$$
\begin{aligned}
\int_0^{t_f}\int_0^l\int_0^d \lambda \frac{\partial(\triangle\theta)}{\partial t} dxdydt &= \int_0^{t_f}\int_0^l\int_0^d [\lambda\triangle\theta]_{t=t_f}\, dxdydt - \\
&\quad \int_0^{t_f}\int_0^1\int_0^d \triangle\theta\frac{\partial\lambda}{\partial t} dxdydt \qquad (4.249)
\end{aligned}
$$

Now combining Equations 4.239-4.249, we have

$$
\begin{aligned}
\triangle J &= \int_0^{t_f}\int_0^l\int_0^d \left[\frac{1}{Pe}\left(\frac{\partial^2\lambda}{\partial x^2} + \frac{\partial^2\lambda}{\partial y^2} \right) + u\frac{\partial\lambda}{\partial x} + v\frac{\partial\lambda}{\partial y} + \frac{\partial\lambda}{\partial t} \right] \triangle\theta dxdydt + \\
&\quad 2\int_0^{t_f}\int_0^1\int_0^d (\theta - Y)\delta(y)\triangle\theta dxdydt - \int_0^l\int_0^d [\lambda\triangle\theta]_{t=t_f}\, dxdt - \\
&\quad \int_0^{t_f}\int_0^d \frac{1}{Pe}\left[\lambda\frac{\partial(\triangle\theta)}{\partial x} \right]_{x=0} dydt - \int_0^{t_f}\int_0^d \frac{1}{Pe}\left[\triangle\theta\frac{\partial\lambda}{\partial x} \right]_{x=l} dydt - \\
&\quad \int_0^{t_f}\int_0^d [\lambda u\triangle\theta]_{x=l}\, dydt - \int_0^{t_f}\int_0^l [\lambda v(\triangle\theta)]_{y=d}\, dxdt + \\
&\quad \int_0^{t_f}\int_0^l \frac{1}{Pe}\left[\lambda\frac{\partial(\triangle\theta)}{\partial y} \right]_{y=0}^{y=d} dxdt + \int_0^{t_f}\int_0^l \frac{1}{Pe}\left[\frac{\partial\lambda}{\partial y}\triangle\theta \right]_{y=0} dxdt \qquad (4.250)
\end{aligned}
$$

For $\triangle J \to 0$, the following adjoint equation and final boundary conditions are deduced:

$$\frac{1}{\text{Pe}}\left(\frac{\partial^2 \lambda}{\partial x^2} + \frac{\partial^2 \lambda}{\partial y^2}\right) + \frac{\partial(u\lambda)}{\partial x} + \frac{\partial(v\lambda)}{\partial y} + \frac{\partial \lambda}{\partial t} = 0 \tag{4.251}$$

$$t = t_f, \ \lambda = 0 \tag{4.252}$$

$$x = 0, \ \lambda = 0 \tag{4.253}$$

$$x = l, \ \frac{\partial \lambda}{\partial x} + u\lambda\text{Pe} = 0 \tag{4.254}$$

$$y = 0, \ \frac{\partial \lambda}{\partial y} + \lambda\text{Nu} + 2\text{Pe}(\theta - Y) = 0 \tag{4.255}$$

$$y = d, \ \lambda = 0 \tag{4.256}$$

The rib is treated by the following condition.

For $x \leq l_1 + l_{r1}$, and $x \geq l_1$, and $y \leq d_{r1}$

$$\frac{\partial \lambda}{\partial t} = -\frac{1}{\text{Pe}}\frac{\alpha_s}{\alpha_f}\left(\frac{\partial^2 \lambda}{\partial x^2} + \frac{\partial^2 \lambda}{\partial y^2}\right) \tag{4.257}$$

For $x = l_1$ or $x = l_1 + l_{r1}$, and $y \leq d_{r1}$, $k_s \left.\frac{\partial \lambda}{\partial x}\right|_{\text{solid}} = k_f \left.\frac{\partial \lambda}{\partial x}\right|_{\text{fluid}} \tag{4.258}$

For $x \geq l_1$ or $x \leq l_1 + l_{r1}$, and $y = d_{r1}$, $k_s \left.\frac{\partial \lambda}{\partial y}\right|_{\text{solid}} = k_f \left.\frac{\partial \lambda}{\partial y}\right|_{\text{fluid}} \tag{4.259}$

Since

$$\triangle J = \frac{1}{\text{Pe}}\int_0^{t_f}\int_0^1 [\lambda\theta(\triangle\text{Nu})]_{y=0}\, dxdt \tag{4.260}$$

and the definition of a gradient

$$\triangle J = \int_0^{t_f}\int_0^1 J'(\triangle\text{Nu})dxdt \tag{4.261}$$

From Equations 4.260 and 4.261, we have the following expression for the gradient of the functional:

$$J'(x) = \lim_{\triangle\text{Nu}\to 0}\frac{\triangle J}{\triangle\text{Nu}} = \int_0^{t_f}\left[\frac{\lambda\theta}{\text{Pe}}\right]_{y=0} dt \tag{4.262}$$

4.4.6   Determination of Search Step Size

If the value of the functional is J^k after k-th iteration and it becomes J^{k+1} after temperatures are updated through a step size of β^k, the condition for the optimum step size will be given by

$$\frac{\partial J^{k+1}}{\partial \beta^k} = 0 \qquad (4.263)$$

Recalling the expression of functional

$$J^k = \int_0^{t_f} \int_0^l \int_0^d \left[(\theta - Y)^2 \delta(y) \right] dx\, dy\, dt \qquad (4.264)$$

Therefore

$$min_\beta J^k (-\triangle Nu)^k \;=\; min_\beta \int_0^{t_f} \int_0^l \int_0^d [\theta\{ (-\triangle Nu)^k - \beta^k P^k \} - Y]^2 \delta(y) dx\, dy\, dt \qquad (4.265)$$

linearizing by Taylor series expansion

$$J^{k+1} [(-\triangle Nu)^{k+1}] = \int_0^{t_f} \int_0^l \int_0^d \left[\theta[(-\triangle Nu)^k - \beta^k \triangle\theta(P^k)] - Y \right]^2 \delta(y) dx\, dy\, dt \qquad (4.266)$$

Therefore

$$\frac{\partial J^{k+1}}{\partial \beta^k} = 2 \int_0^{t_f} \int_0^l \int_0^d \triangle\theta(\theta - Y - \beta^k \triangle\theta)\delta(y) dx\, dy\, dt \qquad (4.267)$$

Using Equations 4.263 and 4.267, we have the following equation for the optimum step size

$$\beta^k = \frac{\int_0^{t_f} \int_0^l \int_0^d \triangle\theta(\theta - Y)\delta(y) dx\, dy\, dt}{\int_0^{t_f} \int_0^l \int_0^d (\triangle\theta)^2 \delta(y) dx\, dy\, dt} \qquad (4.268)$$

4.4.7   Stopping Criterion

The additional measurement approach [Section 2.5.2] is considered as the stopping criterion. An additional functional J_1 is constructed with extra temperature data that is known to have small errors. The iteration stops when J_1 starts to increase.

4.4.8   Complete Algorithm

1. Solve continuity and momentum equations to get the velocity field.

2. Take an initial guess of Nusselt number. Initialize $J = 0$

3. Solve energy equation using the following initial and boundary conditions:

$$t = 0, \ \theta = 0 \tag{4.269}$$

$$x = 0, \ \theta = 0 \tag{4.270}$$

$$x = 1, \ \frac{\partial \theta}{\partial x} = 0 \tag{4.271}$$

$$y = 0, \ \frac{\partial \theta}{\partial y} = -\text{Nu}\theta \tag{4.272}$$

$$y = d, \ \theta = 0 \tag{4.273}$$

The rib is treated by the following condition.

$$x \leq l_1 + l_{r1}, \ \text{and} \ x \geq l_1, \ \text{and} \ y \leq d_{r1}, \ u = 0, \ v = 0 \tag{4.274}$$

Find out the temperatures at the plate.

4. Compute functional,

$$J = \int_0^{t_f} \int_0^l \int_0^d \left[(\theta - Y)^2 \right] \delta(y) dx dy dt \tag{4.275}$$

5. Check stopping criterion

$$J_1{}^k > J_1{}^{k-1} \tag{4.276}$$

where, ϵ is a predetermined real number, very close to zero.
If it is satisfied, stop iterations. Otherwise,

6. Solve adjoint problem

$$\frac{1}{\text{Pe}} \left(\frac{\partial^2 \lambda}{\partial x^2} + \frac{\partial^2 \lambda}{\partial y^2} \right) + \frac{\partial(u\lambda)}{\partial x} + \frac{\partial(v\lambda)}{\partial y} + \frac{\partial \lambda}{\partial t} = 0 \tag{4.277}$$

$$t = t_f, \ \lambda = 0 \tag{4.278}$$

$$x = 0, \ \lambda = 0 \tag{4.279}$$

$$x = l, \ \frac{\partial \lambda}{\partial x} + u\lambda \text{Pe} = 0 \tag{4.280}$$

$$y = 0, \ \frac{\partial \lambda}{\partial y} + \lambda \text{Nu} + 2\text{Pe}(\theta - Y) \tag{4.281}$$

$$y = d, \ \lambda = 0 \tag{4.282}$$

The rib is treated by the following condition.

$$x \leq l_1 + l_{r1}, \ \text{and} \ x \geq l_1, \ \text{and} \ y \leq d_{r1}, \ u = 0, \ v = 0 \tag{4.283}$$

7. Compute the gradient

$$J' = \int_0^{t_f} \left[\frac{\lambda \theta}{\text{Pe}} \right]_{y=0} dt \qquad (4.284)$$

8. Compute the descent direction

$$P^k = \gamma^k P^{k-1} + J'^k \qquad (4.285)$$

where

$$\text{for first iteration } \gamma^k = 0 \qquad (4.286)$$

$$\text{otherwise } \gamma^k = \frac{\langle J^k - J^{k-1} | J^k \rangle}{\| J^{k-1} \|^2} \qquad (4.287)$$

9. Solve the sensitivity problem

$$\frac{\partial (\triangle \theta)}{\partial t} + \frac{\partial (u \triangle \theta)}{\partial x} + \frac{\partial (v \triangle \theta)}{\partial y} = \frac{1}{\text{Pe}} \left[\frac{\partial^2 (\triangle \theta)}{\partial x^2} + \frac{\partial^2 (\triangle \theta)}{\partial y^2} \right] \qquad (4.288)$$

with the following initial and boundary conditions:

$$t = 0, \ \triangle \theta = 0 \qquad (4.289)$$

$$x = 0, \ \triangle \theta = 0 \qquad (4.290)$$

$$x = l, \ \frac{\partial (\triangle \theta)}{\partial x} = 0 \qquad (4.291)$$

$$y = 0, \ \frac{\partial (\triangle \theta)}{\partial y} + \triangle \theta \text{Nu} = -\triangle \text{Nu} \theta = P^k \theta \qquad (4.292)$$

$$y = d, \ \triangle \theta = 0 \qquad (4.293)$$

10. Compute the step size

$$\beta^k = \frac{\int_0^{t_f} \int_0^l \int_0^d \triangle \theta (\theta - Y) \delta(y) dx dy dt}{\int_0^{t_f} \int_0^l \int_0^d (\triangle \theta)^2 \delta(y) dx dy dt} \qquad (4.294)$$

11. Compute the new local Nusselt number

$$(-\text{Nu})^{k+1} = (-\text{Nu})^k - \beta^k P^k \qquad (4.295)$$

12. Go to 3 and continue till convergence.

Chapter 5

Apparatus and Instrumentation

The present study is concerned with the measurement of heat transfer coefficient and the Nusselt number a heated surface of a rectangular duct exposed to a flow field. Figure 5.1 shows the sketch of the experimental setup used in this work. It is identical to the one used by Singh [2002]. The experimental facility comprises of a flow circuit(wind tunnel), the heating section, traverse mechanism and an image processing system. Hot wire anemometry (HWA) and resistance thermometry (RTD) have been utilized for velocity and temperature measurements adjacent to the surface carrying the rib. Local temperature of the plate has been measured using K-type thermocouples connected to a National Instrument data acquisition card (NI 4351). Wall temperature distributions has also been recorded with liquid crystal sheets, exposed to two 150W tungsten-halogen lamps. The lamps provides an excellent color rendering even in the long run, a reasonable high efficiency, high luminance and compact size, as described by de Boer and Fischer [1981].

5.1   Wind Tunnel

The wind tunnel is of the open loop type which operates with the fan in the suction mode. The ambient air flow is sucked from the temperature controlled room into the test section through a flow straightener and five screens in the settling chamber and a 3:1 contraction cone. Air flows through the bell-shaped contraction cone, the heated section, the unheated length of the duct and is then exhausted by a centrifugal fan that is run by a 3-phase motor. The speed of the blower is controlled by a speed controller (Victor G1000) supplied by Kirloskar Electric Co., India. The settling chamber is 1950 mm long and has a rectangular
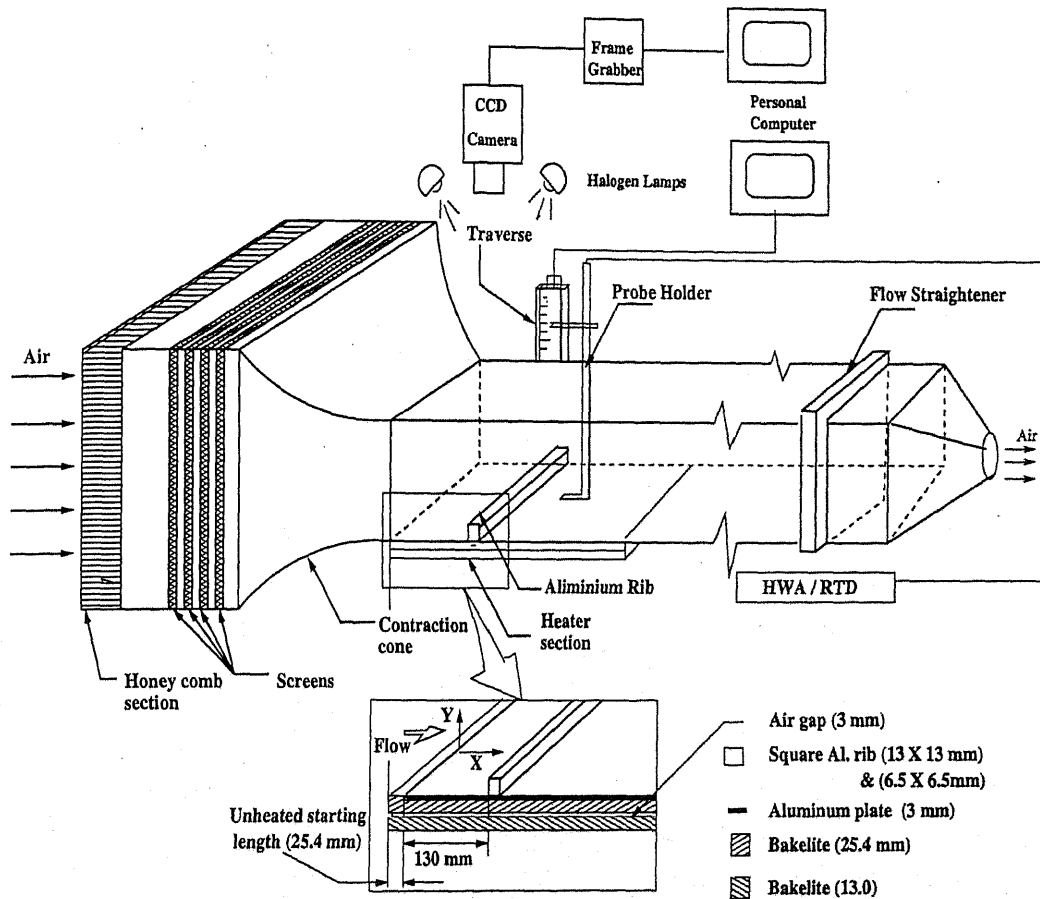
Figure 5.1: Schematic drawing of flow system, coordinate system and instrumentation.

cross section of 500 mm by 1000 mm. The test channel is 3300 mm long with an aspect ratio of 1.8:1, (160 mm × 298 mm in the vertical plane). The test channel is made of perspex sheet of 12 mm thickness. Velocities in the range 0.3-4 m/s are presently realizable in the tunnel. The turbulence intensity in the incoming flow was found to be less than 0.5%.

5.2   Heating Section

The heating section is an assembly of an aluminum plate, Bakelite sheets, and a stainless steel foil.

The heating section is situated just at the entrance of test duct. The test plate is 730 mm long and is located flush with the bottom wall. It serves as the heat

transfer surface, both as smooth and one roughened by a rib, while the top and two vertical walls are smooth and thermally insulated. Downstream of the test duct is an unheated section made of perspex with the same cross section. The heat transfer surface is constructed using a single aluminum plate (680 mm × 298 mm × 3 mm). There are six stainless stainless steel foils of dimension 690 mm × 47 mm × 0.045 mm that are cemented on to the 25 mm thick Bakelite sheet. These foils are electrically connected in series and finally connected to a DC source for power supply. To prevent the aluminum plate from electrical contact the upper surface of the stainless steel foil is coated with varnish. A 2 mm mica sheet is placed between the Bakelite and aluminum plate for thermal insulation. The surface of the aluminum plate is highly polished to minimize thermal emission, and hence the radiative losses. In addition, to minimize the conductive heat losses, the lower surface of the Bakelite board is insulated using a 13 mm thick of Bakelite with a 2 mm thick air gap between them.

The heat transfer surface is also instrumented with thirteen calibrated thermocouples of the chromel-alumel type. The thermocouples are located inside the heated surface with omega-bond 101 epoxy. Twelve thermocouples are distributed along the center-line of the heated plate for wall temperature measurement. In order to check the span-wise temperature uniformity, surface temperature along the lateral of the heated plate is also instrumented with one thermocouple. To maintain a smooth flow surface, the thermocouple beads are attached to the underside of the aluminum plate fed through the opening made in the two Bakelite sheets and mica. To measure the conduction losses on the underside there are two thermocouple are mounted on the two sides of the upper Bakelite sheet. There are two more thermocouples mounted at the two sides of the lower Bakelite sheet. The four thermocouples fall on one line. This arrangement is repeated at a second location in the downstream.

5.3   Hot-Wire Anemometry

The hot-wire anemometer is an example of an intrusive technique whose application for measuring turbulent flow has far outstripped other instruments. The hot-wire is basically a thermal transducer and responds primarily to the velocity magnitude and is based on the principle of heat transfer. This sensor is small in

size and coupled with a feedback circuit, it has a very high frequency response. The DANTEC model 56 C 17 CTA has been used in the present study. The main unit 56 C 17 CTA delivers the servo-voltage as the output of the instrument. This voltage is a measure of the fluid velocity. The feedback circuit of the CTA plays an important role in improving the frequency response of the hot-wire from about 100Hz to 10KHz.

The 56 C 01 CTA contains a function switch with three modes for operation, namely TEMP, STD.BY and FLOW. In TEMP position the resistance of the connected probe can be measured in terms of a current supplied to it. In STD.BY position no current flows through the bridge. In FLOW setting the CTA starts operating with the function of the servo amplifier. A setting named BRIDGE ADJ enables the adjustment of bridge balance for measurement of probe resistance and setting of the desired overheat resistance. In addition, BRIDGE ADJ has a switch pair for coarser adjustment of overheat resistance and a screw for fine adjustment. Resistance settings ranging from 0-30 Ω in steps of 0.001Ω are possible. This adjustment is crucial for adjusting the overheat resistance for the calibration procedure. The CTA in TEMP mode produces a voltage proportional to the resistance of wire. The Calibration of this voltage against a known temperature can be used to measure the instantaneous temperature of the probe. The mean value unit 56 N 22 is a 5.5 digit display voltmeter. The primary purpose of this module is to measure the DC component of the output signal from 56 C 17 CTA. This module has 100 μvolt resolution, 1-1000 second integration time and 14 switch selectable inputs.

The accuracy of hot-wire measurements is affected by the accuracy of the calibration procedure that of the procedure that is used to solve the nonlinear simultaneous equation. Calibration of a hot-wire probe involves two major steps, namely data generation and curve fitting. Calibration data is generated by measuring the output of the anemometer when the probe is subjected to flow with known velocity. In the present study, calibration has been performed in the test cell itself due to its high quality uniform inflow.

5.4   Resistance Thermometry

DANTEC Platinum coated tungsten wire ($\alpha_{20} = 0.36/^\circ C$) probe (P11) has been utilized as a temperature measuring device. The resistance of the wire of the probe at $20^\circ C$ has been determined by a 5.5 digit display HP 3457A multimeter against the precalibrated thermister TBX-68T mounted on the terminal block of the National Instrument's data acquisition card (NI 4351). The HP 3457A has a reading and program storage module and is available of making unsteady measurements. The HP 3457A's math operations manipulate or modify a measured reading before it is displayed; in addition the STAT operation evaluates mean and standard deviation. HP 3457A is programmed for converting the resistance in terms of the operating wire temperature. The temperature of the fluid flow is measured by using the relation:

$$R(T_{sensor}) = R_{20} + \alpha_{20} R_{20}(T_{sensor} - T_{20}) \tag{5.1}$$

The RTD probe is attached with a computer controlled traverse mechanism for accurate positioning.

5.5   Liquid Crystal Thermography (LCT)

The liquid crystal technology is one of the important inventions of the twentieth century that has found many applications as a visualization tool today. Liquid crystals change their color on applications of external stimulus, for example temperature and shear stress distributions and thus act as a measure of their change.

Liquid crystal is a unique substance, which exists between the solid and the isotropic-liquid phase of some organic compounds. It scatters incident light very selectively. The lowest temperature where liquid crystals scatters visible light is called the event temperature. At a temperature below the liquid crystal's event temperature, the liquid crystal will be in the solid state and will appear transparent. The clearing point temperature is the temperature at which the liquid crystal ceases to reflect visible light. When the temperature exceeds the clearing temperature point, the liquid crystal will enter the pure liquid state and appear transparent. The color output in liquid crystals is reversible and reproducible.

5.5.1 Forms of Liquid Crystals

Liquid crystals are commonly categorized based on their molecular morphology and optical properties, e.g. smectic, nematic, and cholesteric. Cholestric LCs, so named because the first of this type were derived from cholesterol, are capable of displaying a range of visible colors and are thus classified as thermochromic. However non-sterol based thermochromic LCs have also been developed, and are termed chiral-nematic, in reference to their molecular arrangement.

The nematic structure comes about when long range inter-molecular forces cause molecules to align relative to one another in planes. These planes are determined by the local solid boundaries and the direction of alignment of molecules within a plane is called director. Direction of this director changes on the application of mechanical or electrical deformation. The cholesteric materials form a similar structure. However, due to the shape of the molecules, the director of adjacent planes are rotated through certain angle and thus forming a helix of a certain pitch. The pitch of the helix changes depending upon the temperature of the liquid crystal. For the liquid crystal cholesteric materials considered for temperature sensing purpose, It is necessary that the pitch of the helix represented by the director is of the order of the wavelength of the visible light.

5.5.2 TLC Surface Coating

The most common means of applying thermochromic liquid crystals to a surface is by using micro-encapsulated form of the material. The tiny spherical capsules (20μm in diameter) are glued to the test surface using an adhesive. Care is taken to ensure that the surface is fully dry before the mixture of crystal and binder mixture is applied. A thin (20μ mm thick) coating is best developed by spraying many thick coats, with interim drying using an air heater. It is also worth noting that thin plastic sheets are available from suppliers and these often display a very clear color display. TLCs are available in different bandwidths, which defines the temperature range in which it actively reflects visible light. In the present work the commercially available thin plastic sheet of TLC (Hallcrest, Inc.;R35C5W) is pasted on the heating surface. This means the activation of the red color of this particular TLC begins at 35°C and the bandwidth is 5 degrees. The advantage of a precoated sheet are convenience and quality of color but these must be set

against possible difficulties in wrapping the sheet over complex surfaces with compound curvature. This is not the case for the present work.

5.5.3   Response Time

During the transient heat transfer experiment, the accuracy of the measured temperature depends on the rate at which the liquid crystal's optical properties respond to the change in the surface temperature. Ireland and Jones [1987] measured the response of nematic type LC material and they were able to quantify the lag in the optical signals at rate of increase of surface temperature as high as 2000 °C/sec. Experiments showed that the delay between the time at which the surface reached a steady state color display temperature and the occurrence of the color display was no more than a few milliseconds (typically 3 to 10 milliseconds). In fact, the time taken for any point within the liquid crystal layer to achieve the heated surface temperature is a function of the distance from the surface, the layer thickness and the film diffusivity.

5.5.4   Range of Application and Limitation

Although the TLCs offer an excellent way of measurement of full surface temperatures there are always some constraints on their use.

Temperature Range

Encapsulated liquid crystal materials are available in the temperature range -30 to 115 °C. The temperature range over which a material is optically active (the color play) can also be selected. The narrowest color range is 1.0 °C and the widest is about 20 °C. Wide-band crystals typically have bandwidths between 5°C and 20°C. They are useful when an object has large temperature variations. Practical applications of wide-band crystals include investigation of the surface temperature distribution on gas turbine blades or characterizing the temperature distribution on electronic components.

Pressure Range

Encapsulated TLCs are insensitive to pressure. They are tested up to 133 bar without any appreciable change in its behavior.

Speed of response

As discussed earlier, the optical response time of TLCs are in the range of few milliseconds e.g. for chiral-nematic it is around 3 msec.

Chemical Contamination

TLCs are complex organic compounds that are particularly susceptible to attack from organic solvents. In addition, UV (ultraviolet) light can destroy the color display, so care must be taken to minimize exposure to UV light.

Maximum Heat Flux

As a rule-of -thumb, a value for maximum heat flux of 2×10^4 KW/m^2 can be taken. The conductivity of the liquid crystal layer is typically 0.2 W/mK and hence the above heat flux gives a 2°C temperature drop across a 20 μm layer.

5.5.5 Image Processing

In a transient experiment, any site on the TLC surface will change color as the surface passes through optically active temperature range. This permits either color processing or intensity based (black and white) processing of the image of the surface optical response.

The standard color television practice of representing color by R, G and B tristimulus signals, red, green and blue, is used in color analysis. The tristimulus signals can be thought of as outputs from three camera detectors each with its optically sensitive range centered on a different wavelength in the visible spectrum. The intensity signals is made up of the sum of the R, G, and B signals. The R, G, and B signals are changed to H, S, and I (namely hue, saturation and intensity) form, which is less sensitive to the variations in strength of illumination. The derived signals hue and saturation are both independent of intensity and are produced using look-up tables in commercially available color frame grabbers. Hue depends on the ratio of RGB signals and its use has found favor in TLC work since its value normally increases monotonically with temperature. Hue physically represents the dominant wavelength of the light being displayed by the LCs. It is determined by establishing the angle between the orthogonal red, green, and blue components in RGB space.

Various techniques have been employed to calculate hue from the RGB components of the digitized images. The hue is calculated as (Ireland and Jones, 1987):

$$\cos(\mathrm{H}) = \frac{2R - G - B}{\{6[R-I)^2 + (G-I)^2 + (B-I)^2]\}^{0.5}} \tag{5.2}$$

where I is defined as:

$$I = \frac{R + G + B}{3} \tag{5.3}$$

The value of hue varies from 0 to 180°. The highest value of hue corresponds to perfect blue while the lowest is red.

5.5.6 True Color Image Processing System

The image acquisition and processing system used in the present investigation consists of a high resolution 768 (horizontal) × 574 (vertical) pixels CCD video camera (SONY XC-003P) with 16 mm focal length lens (VCL-16WM), a 24-bit color frame grabber board (Imaging Technology) and a high speed PC. These systems store the appropriate intensities of red, green, and blue needed to produce a corresponding matched color response at each point in an image. The frame grabber can be programmed for color analysis using base level C-programs. Several software programs are commercially available to analyze images. The software is capable of acquiring, freezing, sequential grabbing of images with specific functions such as determination of red, green, blue values and also the corresponding hue distribution. The current 24-bit true color image processing board from Imaging Technology, USA is programmed for the aforementioned color analysis using base level C-programs.

5.6 Uncertainty and Measurement Errors

Possible sources of errors in the experimental data are: (a) fluctuations in the supply voltage of the D.C. power source, (b) the positional accuracy in locating the probe, (c) errors in calibration data, (d) inadequate compensation for room temperature, (e) inadequate signal length and sampling rate, (f) drift in electronics and (g) non-uniformity in illumination on the liquid crystals. Most of the experiments have been conducted several times and the repeatability of the

results presented have been confirmed. The local Nusselt number and average Nusselt number were found to be in good agreement with published correlations and energy balance check [Tariq *et al.*, in press].

Chapter 6

Data Reduction

Data reduction for velocity, temperature and the local Nusselt number is discussed in the present chapter

6.1 Velocity Data Reduction

One dimensional velocity data was collected using a hot-wire anemometer. A single wire probe was used for this purpose. The data obtained was not in terms of velocity but it was in terms of voltage which is required in excess to maintained the wire at its original temperature. There is a unique relationship between this voltage and velocity, and the relationship must be obtained by proper calibration.

6.1.1 Hot-wire Calibration

Calibration of a hot-wire probe involves two steps, namely data-generation and curve-fitting.

Data-Generation

Calibration data is generated by measuring the output of the wire when it is subjected to a fluid with a known velocity. Specially designed apparatus is normally used to generate high quality flow with uniform velocity, temperature and very low turbulence level. Hot-wire to be calibrated is kept firmly in the calibration apparatus such that the direction of velocity is normal to the wire. The flow should be steady. The voltage output of the wire is noted at zero velocity and at higher fluid velocities. The calibration data should be repeatable with very low scatter.

In the present study, calibration has been performed in the wind tunnel itself due to its high quality. The maximum turbulence level is 0.5% in the upstream section of the apparatus.

Isothermal Calibration of Hot-wire

DANTEC hot-wire equipment uses a linearizer card (56 N 21) which produces a voltage signal linearly proportional to flow velocity. The mathematical curve used by this card is given below.

$$y = 10^{A+Bx+Ey} + Cx + D \tag{6.1}$$

Here A, B, C, D and E are constants. Normally constants are selected to give a fluid velocity equal to 10m/sec for a wire output of 10 V. Here y is the linearizer output equal to normalized velocity of fluid defined as

$$y = 10 \times \frac{U}{U_{max}} \tag{6.2}$$

and x is normalized voltage defined as,

$$x = 10 \times \left[\frac{V - V_0}{V_{max} - V_0} \right] \tag{6.3}$$

where V_0 is the output of the wire measured at zero velocity of fluid and V_{max} is the measured voltage at the maximum fluid velocity U_{max}.

The constants A, B, C, D and E are obtained by means of an iterative least square error approach. For any calibration point (x_i, y_i) Equation 6.1 will produce an error ϕ_i given by

$$\phi_i = y_i - \left[10^{A+Bx_i+Ey_i} + Cx_i + D \right]. \tag{6.4}$$

The least square approach requires the sum of errors at all calibration points to be minimum, i.e.

$$\Phi = \sum_{i=1}^{n} \phi_i = \sum_{i=1}^{n} \left\{ y_i - \left[10^{A+Bx_i+Ey_i} + Cx_i + D \right] \right\}^2 \tag{6.5}$$

$$\text{and} \qquad \frac{\partial \Phi}{\partial A} = \frac{\partial \Phi}{\partial B} = \frac{\partial \Phi}{\partial C} = \frac{\partial \Phi}{\partial D} = \frac{\partial \Phi}{\partial E} = 0. \tag{6.6}$$

Let I be any of the parameters A, B, C, D or E, then

$$\frac{\partial \Phi}{\partial I} = 2 \sum_{i=1}^{n} \phi_i \frac{\partial \phi_i}{\partial I} = 0 \tag{6.7}$$

Hence A, B, C, D and E can be calculated using the above system of equation.

6.2   Temperature Data Reduction

Temperature data was collected by RTD for which the resistance is determined by a precalibrated thermistor. The HP 3457A multimeter was used for the display of the resistance of probe wire. It was programed for converting the operating resistance of the probe wire into the corresponding temperature. MATH and STAT operations were utilized for the purpose of conversion.

6.3   Liquid Crystal Thermography

Thermocromic liquid crystals were spread uniformly on the test surface and after the rib. The liquid crystal experiment was performed in two phases.

1. Calibration test to relate color with temperature.

2. Transient test with two different Reynolds numbers to capture the colour images in a time sequence, around the rib.

6.3.1   Calibration Test

Prior to the unsteady temperature measurement over the test surface, the method of color expression was defined and the relationship between the color and temperature of the liquid crystal was assessed in a calibration test. Although the colors of the liquid crystals are observed in terms of color components RGB, the R, G and B-data has not been used to calibrate the sheet. Instead, the RGB color space is transformed to the hue-intensity-saturation space, because the hue value is a monotonic function of the dominant wavelength reflected by the crystals. It is therefore best suited for a unique color-to temperature relation. A perfectly lighted surface showed uniform background intensity of the color over the entire test surface. The background intensity determines the clarity of the picture seen by the camera.

The test surface was heated to a temperature of nearly 43°C. The reading of one thermocouple was monitored continuously by a PC connected through a data acquisition card. Then the heater power supply was cut off. The calibration test was done under the no flow condition. The plate started to cool owing to natural convection and images were captured at every 0.2°C temperature interval.

Images were captured until the color of the surface became red. Assuming that temperature is same within a small area, 45×45 pixels were selected in the image around the location where the thermocouple was placed. These images were processed in the PC to get HSI values from RGB values separately for those particular pixels. The HSI values were averaged to get a single hue, saturation and intensity value appropriate for the temperature. With appropriate curve fitting a plot was obtained between hue and temperature. Figure 6.1 shows the calibration curve which was derived from the transient experiment. It can be observed that intensity is almost constant for the entire range of temperature. Figures 6.3 and 6.4 show RGB and HSI plots in present calibration.
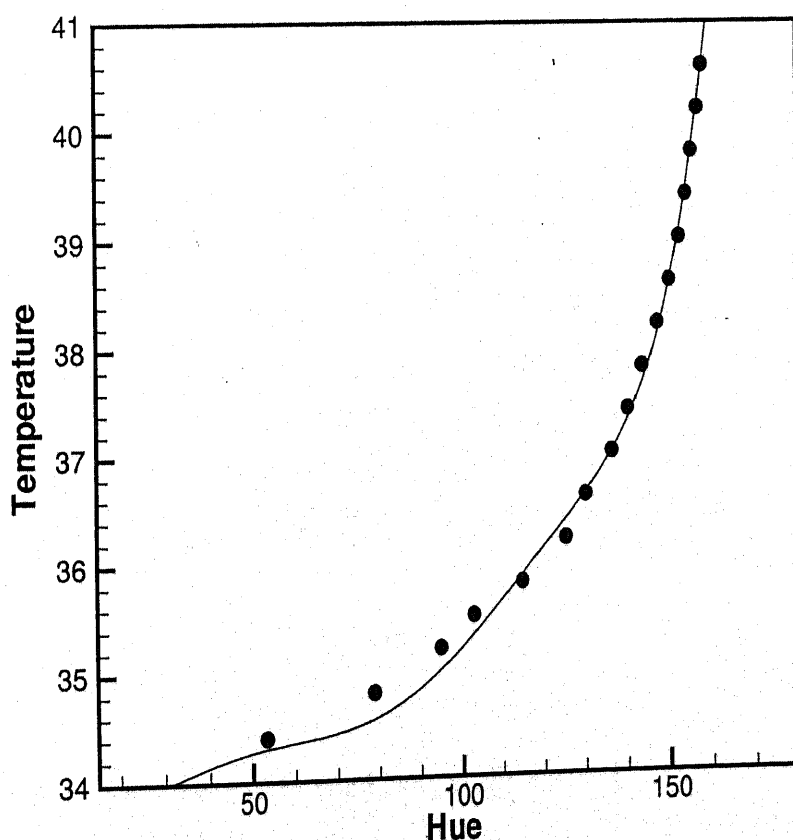
Figure 6.1: Calibration chart of the liquid crystal used in the present work.

Using hue from the HSI space reduces possible sources of uncertainty, such

as the brightness of the light source [Farina *et al.*, 1994] The hue is observed to have a monotonic change with temperature and also remains independent of the local illumination strength. The variance of hue with temperature is found to be small and constant, characterizing the uniform distribution of color over the chosen pixels.

6.3.2 Transient Test

The transient heat transfer method offers a significant advantage of yielding the local heat transfer coefficient over the complete test surface in a single experiment. The technique involves heating of the test plate to a certain temperature. The flow is then turned on. The lighting arrangement and the camera position are kept identical to that of the calibration test. After the plate reaches a particular temperature, the heater power supply is cut off while the flow continues to cool the surface. Due to forced convection the plate stars to cool. Images are then captured at 2 seconds time intervals. This experiment was carried out for two Reynolds numbers, namely 160 and 260. Here, the Reynolds number is based on rib height. Using the calibration curve, temperatures at different points over the surface were evaluated.

During the transient heat transfer experiment each pixel location will reach a prescribed temperature at different times, depending upon the local heat transfer coefficient. The transient temperature distribution can be used for evaluation of the local heat transfer coefficient by assuming the test surface as a semi-infinite solid. For a semi-infinite solid, the one dimensional transient conduction equation is:

$$\frac{\partial T}{\partial t} = \alpha \frac{\partial^2 T}{\partial y^2} \tag{6.8}$$

Using a convective boundary condition at the surface,

$$-k(\frac{\partial T}{\partial y})|_{y=0} = h[T(y=0,t) - T_\infty] \tag{6.9}$$

where T_∞ is the free-stream temperature (or the local bulk mean temperature (T_{bm}) in the case of a duct) and $T(t)$ is the temperature of the surface at any

time t. Assuming T_∞ or T_{bm} to be constant, a semi-infinite wall with constant properties, and a uniform initial temperature of T_{wi}, the solution for the temperature at the surface ($y = 0$) is

$$\frac{T_{wi} - T(t)}{T_{wi} - T_\infty} = 1 - \exp\left(\frac{h^2 \alpha t}{k^2}\right) \operatorname{erfc}\left(\frac{h\sqrt{\alpha t}}{k}\right) \qquad (6.10)$$

or

$$\frac{T(t) - T_\infty}{T_{wi} - T_\infty} = \exp(\gamma^2) \operatorname{erfc}(\gamma) \qquad (6.11)$$

where the parameter γ is defined as

$$\gamma = \frac{h\sqrt{t}}{\sqrt{\rho c k}} \qquad (6.12)$$

The only unknown in the Equation 6.12 is h, which is determined by a least squares fit through the experimental data in a prescribed total time span Δt. It was observed that the changes in temperature with time at any particular pixel starts diverging from the theoretical profile based on the semi-infinite solid assumption. So, the total time span (Δt) for which the curve fitting is done, plays an important role. If Δt is very high, then at some pixels, where heat transfer rate is very high, would reach to a temperature which is beyond the color display range of the liquid crystal. At the same time, some other pixels where heat transfer is low, would reach to a condition where experimental temperature gradient starts diverging from theoretical curve. At these pixels the predicted heat transfer coefficient would be comparatively higher than the actual. Hence, the pixels with higher heat transfer rate give the estimate of the total time span (Δt), for which the curve fitting should be done at each pixel.

Validity of Semi-infinite Solid Assumption

The validity of the semi-infinite solid assumption is verified from the transient temperature measurement of the thermocouples located at the top and bottom of the bakelite plate and its thickness. The assumption of a semi-infinite solid is valid only if the specimen is made from a material with a low thermal diffusivity
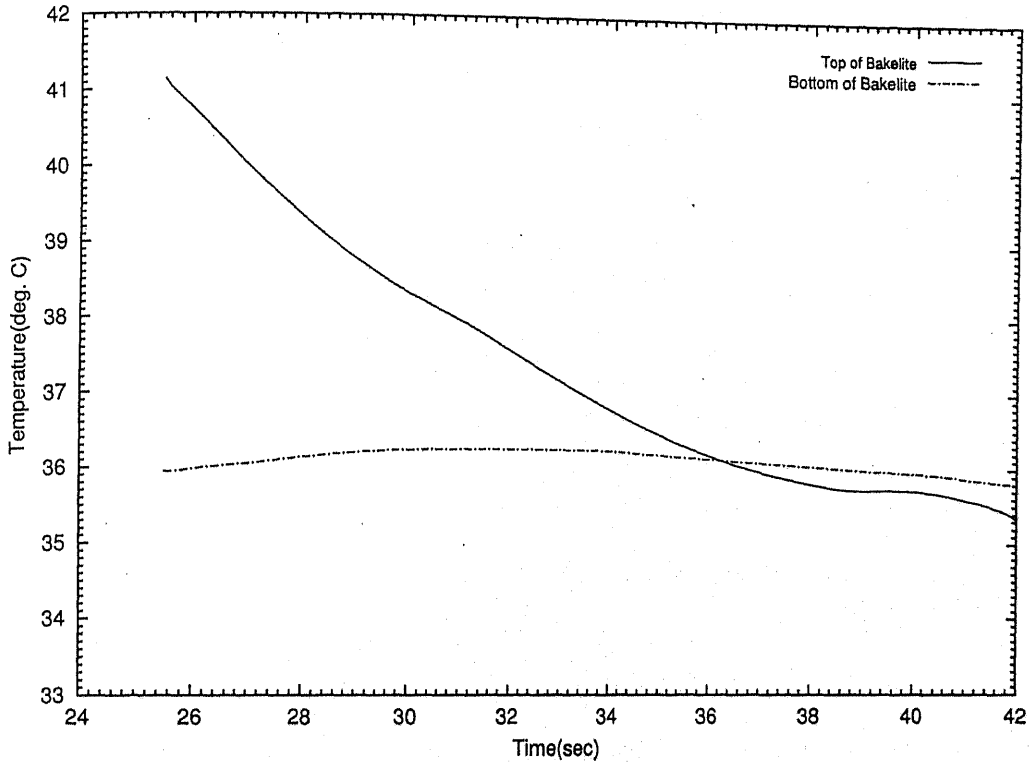
Figure 6.2: Verification of semi-infinite solid assumption with temperature measurement at different locations of the plate

and chosen to be sufficiently thick. Chan *et al.* [2001] suggested a criterion for the minimum thickness of the material (y), as:

$$y > 4\sqrt{\alpha\Delta t} \qquad\qquad (6.13)$$

In the present work, bakelite is assumed to be the semi-infinite solid for which the thermal diffusivity is very low. The required thickness for the plate for even 150 seconds of experimentation would be 16.54 mm. Since the thickness of the upper bakelite plate is more than 25 mm, the above condition (Equation 6.13) is fully satisfied. Temperature variation of the thermocouples placed at the top and bottom surface of the bakelite plate are shown in Figure 6.2. It can be observed that the temperature of the lower surface of the Bakelite is unchanged while the temperature of the top surface decreases with time. This observation confirms the validity of semi-infinite solid assumption.

The other assumption in the present study is that conductivity of the aluminum plate is very high and thickness is very small, so that the temperature gradient in the aluminum plate is equal to the temperature gradient of the upper

surface of the bakelite sheet.

6.3.3   Inverse Approach for Nusselt Number Estimation

An inverse forced convection formulation for transient heat transfer has been discussed in Section 4.4. This approach has been adopted in the present work to obtain local Nusselt number from unsteady measurements of the plate temperature. The calculation proceeds with the following assumptions:

1. The velocity and the temperature fields are two dimensional.

2. The flow field is steady.

3. As the rib height to channel height ratio is quite small, being equal to 1/24, the free slip boundary condition has been applied in the far field of the rib. This assumption has been validated by suitable numerical experiments.

4. Constancy of the local Nusselt number with time has been assumed. This is equivalent to requiring that the thermal field is fully evolved in time. In other words, the temperature in the fluid medium fall continuously with time during the cooling of the plate. The cooling rates are thus taken to be dependent only on the heat transfer coefficient.

5. The effects of free convection and radiation are neglected.
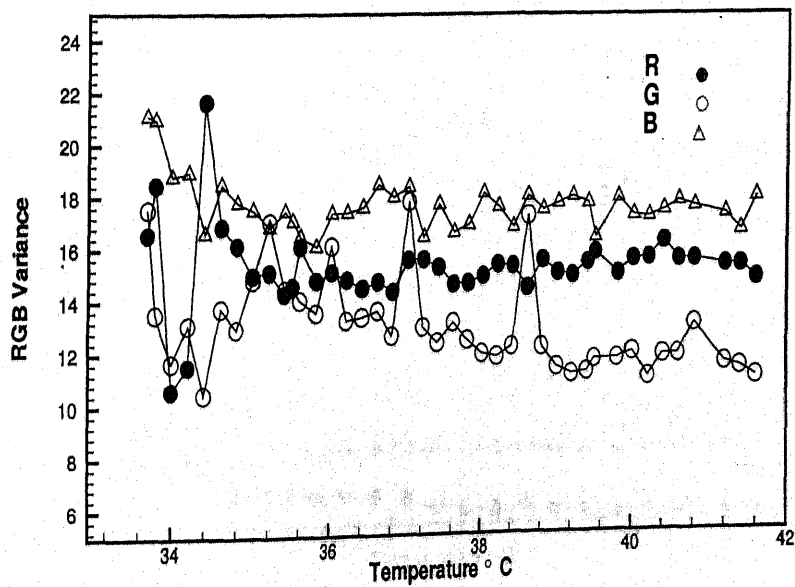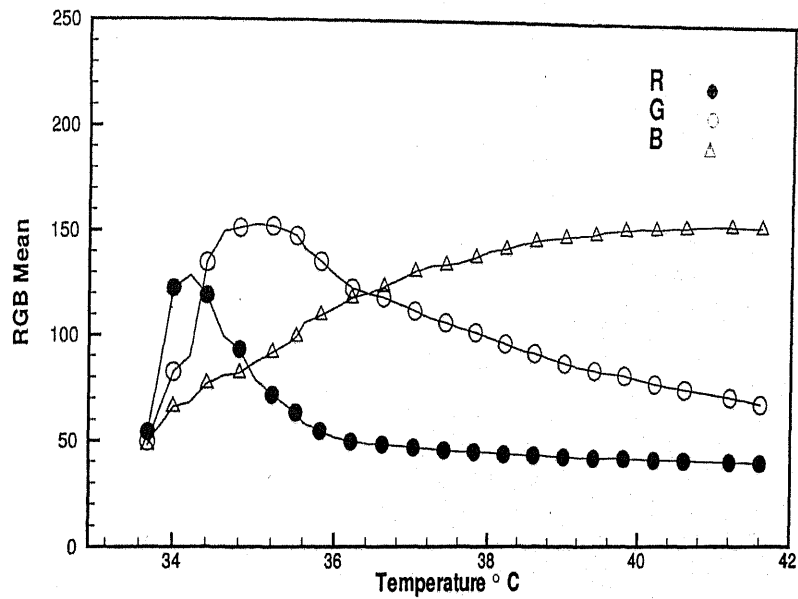
Figure 6.3: RGB variation with temperature during LCT calibration.
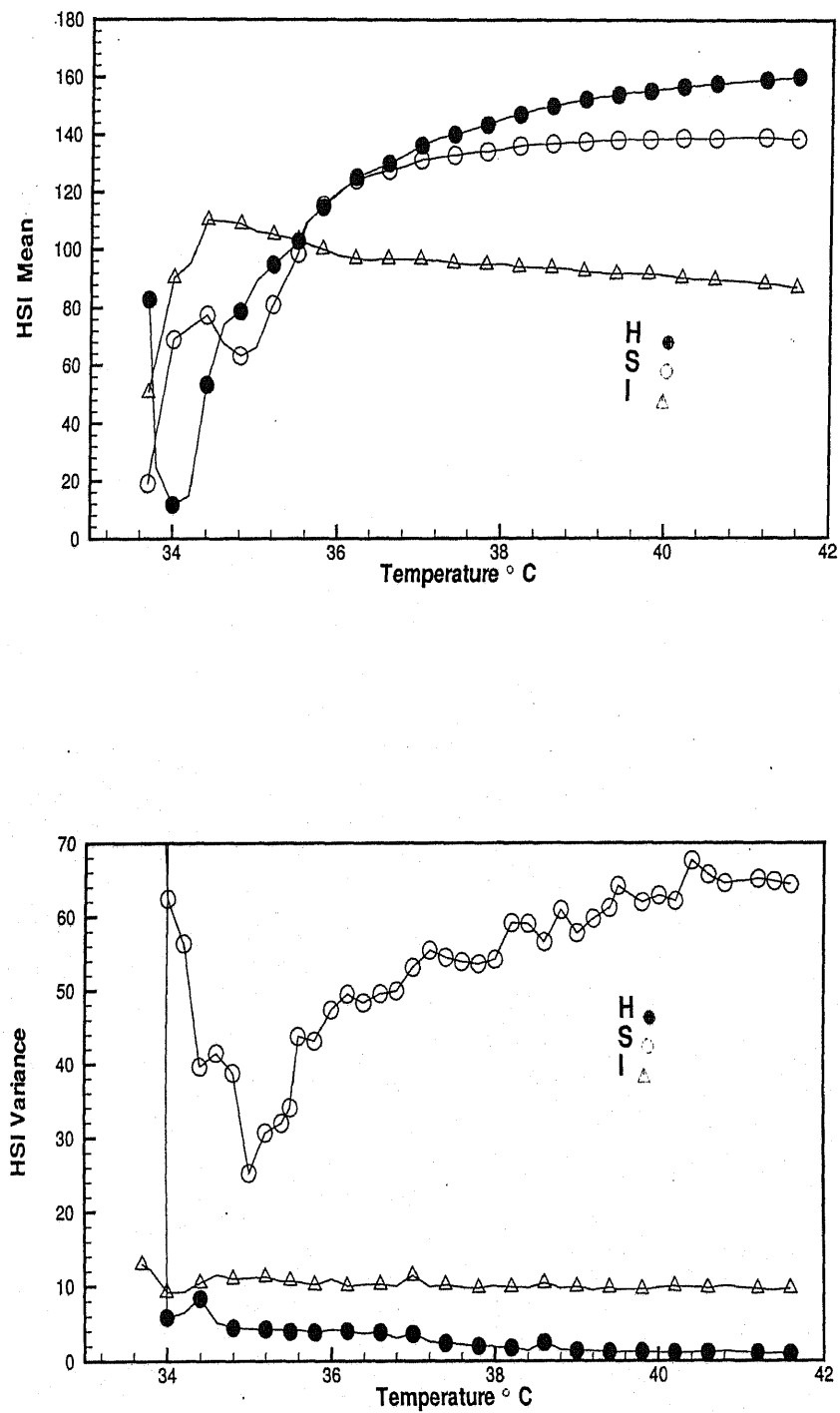
Figure 6.4: HSI variation with temperature during LCT calibration.

Chapter 7

Convective Heat Transfer from a Flat Plate

This chapter presents the outcome of applying the inverse technique to predict the local Nusselt number for flow over a flat surface. Three different solvers[1] are used namely, (1) steady two dimensional parabolic, (2) steady three dimensional parabolic and (3) unsteady three dimensional elliptic. Detailed formulations are furnished in Chapter 3 and the numerical issues are discussed in Appendices A and B. The goal of the simulation is to asses the capability of the inverse procedure to accommodate noise in the measured data and its ability to use additional (though limited) use high quality data. Study proceeds along the following steps:

1. Solve direct problem assuming a meaningful plate temperature distribution. The plate temperature is steady but may vary with position over the plate. This step will generate interior fluid temperature field and the local Nusselt number variation over the surface. The solution of this problem is termed as *exact solution*.

2. Select interior temperature on certain planes for inclusion in the functional.

3. Perturb the plate temperature and the interior temperatures of step 2 with zero mean Gaussian noise (Appendix C). Thus each perturbed temperature fall in the range

$$\theta|_{\text{perturbed}} = \theta|_{\text{exact}} \pm \Gamma\sigma \tag{7.1}$$

---

[1]The solvers refer to the numerical algorithm for solving the direct problem embedded in the inverse technique.

where σ is the standard deviation of the Gaussian distribution. Γ indicates the confidence interval. For present analysis a 99% confidence interval is maintained by keeping $-2.576 < \Gamma < 2.576$. It is expected in practice that the standard deviation of the interior temperature is much smaller than that of the surface temperature.

4. Filter the plate and interior point temperatures by Gram orthogonal polynomial smoothing.

5. Solve the complete inverse problem to estimate the local Nusselt number distribution.

6. Compare the Nusselt number distribution with the exact solution of step 1.

Sensitivity analysis is presented in all cases to authenticate the behavior of the inverse algorithm. The sensitivity coefficient at any point of the domain defined as the absolute change in the temperature for a unit change in local Nusselt number. Values of the sensitivity coefficients are obtained from the numerical solution of the sensitivity equation. While the absolute values of sensitivity carries little physical interest, they reflect the relative influence of the wall boundary condition over the field data.

7.1 Two Dimensional Steady Parabolic Solver

The two dimensional parabolic problem is less complex and computationally less intensive. Hence it permits numerical experimentation with this formulation.

The effectiveness of inverse approach in local Nusselt number estimation is shown in Figures 7.1, 7.2 and 7.3. The inverse solution has been compared with the direct solution given by filtered data as well as the exact solution. The quality of inverse estimation shown here is quite superior to simple filtering.

In the present work it is observed that the success of any inverse algorithm depends upon sensitivity, quantity and the noise level in the input data. These factors are studied and discussed below.

7.1.1   Sensitivity Study

It is to be realized that for the present problem the boundary information is contained only in the vicinity of the plate. Figure 7.4 shows the results of the sensitivity study. The maximum value of sensitivity occurs at the plate for a Reynolds number of 500, while the minimum value is zero. All the data has been normalized between these two values. The high sensitivity zone is observed to become smaller with an increase in the Reynolds number. This clearly conforms to the physical nature of the problem. The thickness of the zone which contains the boundary information, i.e. the thermal boundary layer thickness, becomes smaller with the increase of Reynolds number[2]. This is one of the major constraints in the design of an experiment in which additional data is recorded.

As the measurement plane shifts from the surface, the quality of inverse estimation degrades. This is shown in Figure 7.5. This effect is studied by the noise free inputs from five different measurement planes. At each plane all temperatures are assumed to be known but the surface temperature information is not included. At higher Reynolds number it is observed that their is no improvement in the initial guess if the plane is placed beyond a critical distance. The sensitivity coefficients at this planes are found to be zero. These observations are self-consistent.

7.1.2   Effect of Noise Level and Grid Fineness

As the scatter in the data poses the primary constraint, any inverse analysis is considered incomplete if it does not account for it. In the present study we have considered two different error levels in data. The plate temperature is known at all points but with substantial errors, while a smaller amount of high quality interior temperatures are available.

While very few noise-free interior data points can absorb a substantial noise in the plate temperature, a small noise in the interior data can degrade the solution to a large extent. These observations are presented in Figures 7.6 and 7.7. These trends confirm the ill-posedness of the inverse problem. During the study of scatter in plate temperature, it is assumed that 20% error-free data is available. The effect of interior data error has been studied when the surface data is not

---

[2]Prandtl number is constant here

available.

The negative effect of interior data error increases with Reynolds number. This fact can be explained from the sensitivity study (Figure 7.4). It shows that the sensitivity coefficient at any plane decreases with Reynolds number. For higher Reynolds numbers, the data quality deteriorates by both low sensitivity and scatter in the interior point temperature.

The effect of data error are more critically examined by varying the amount and sensitivity of data. Figure 7.8 shows that diminishing the data quantity, data sensitivity and increasing data error, are all detrimental to the final solution. But their interdependence is quite subtle Figure 7.9 shows that a higher amount of data might not always be a guarantee of an improved solution, especially if the data error is substantially high. In fact, in some cases a lower amount of data can generate a better solution. With the increase of the number data points, noise as well as information are absorbed in the predicted solution. Which of these two will ultimately dominate is problem-specific. Higher scatter in input data from a higher sensitivity region may deteriorate the solution further.

Unlike the direct problem, the solution of the inverse problem may not always tend to exact solution with the improvement in grid fineness, particularly if the data contains substantial scatter. This behavior is shown in Figure 7.9. Here the solutions have been derived on two different grids. In the finer grid, the number of additional data points is varied. It is observed that the solution On the finer grid with larger amount of data leads to a poor solution. Conversely the solution quality improves with a reduced number of data.

With the improvement in grid fineness, the change of the computed variables (i. e., temperature, in this case) decreases in between two consecutive grid points. If the standard deviation of data error becomes greater than the change in temperature in consecutive grid points, the inverse algorithm receives misinformation, causing degradation in accuracy. This phenomenon poses a great restriction on fix the optimum number of grid points for the inverse solution.

7.1.3   Studies on Initial Guess and Uniqueness

An effective optimization algorithm is expected to eliminate the remnants of initial guess from the final solution. However, this is not always true for inverse

problems, as the property of uniqueness may not be strictly applicable here. Figure 7.11 confirms this observation. If the experimental data exactly satisfies the energy equation, the final value of the functional would be zero; otherwise it will converge to a non zero positive value. If the amount of input data is very less, it can always be fit into the energy equation to produce an almost zero functional. If the data amount is large, the functional can be brought to a near zero value only when the data is exact. For a large amount of noisy data, irrespective of the boundary condition, it is to be expected that the solution will not conform point-wise to the energy equation.

7.1.4   Studies on Stopping Criteria

In the present study several stopping criteria have been employed. A comparative study is shown in Figure 7.12. If only one level of data scatter is assumed, all the criteria have shown similar performance. For two different scatter levels discrepancy principle is not applicable. It is realized that as the scatter level mismatch increases data smoothing produces better solution than the additional data criterion.
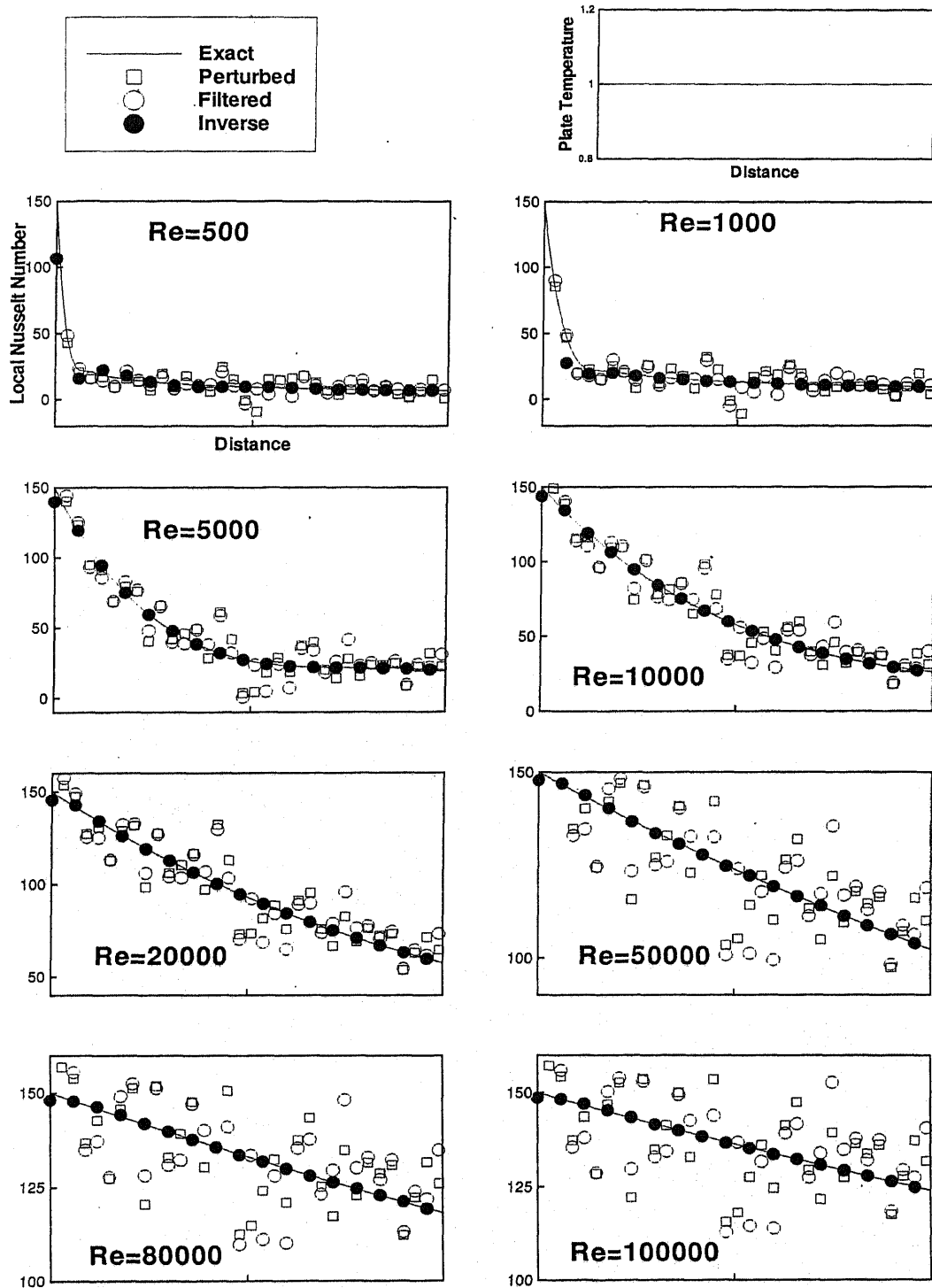
Figure 7.1: Comparison of inverse and direct solution with perturbed and filtered data. Scatter in plate temperature is σ=0.2. Scatter in interior temperature is σ=0.0001. Only 50% interior temperatures are available at $y = 0.01$. Velocity and temperature have been obtained from a parabolic formulation.
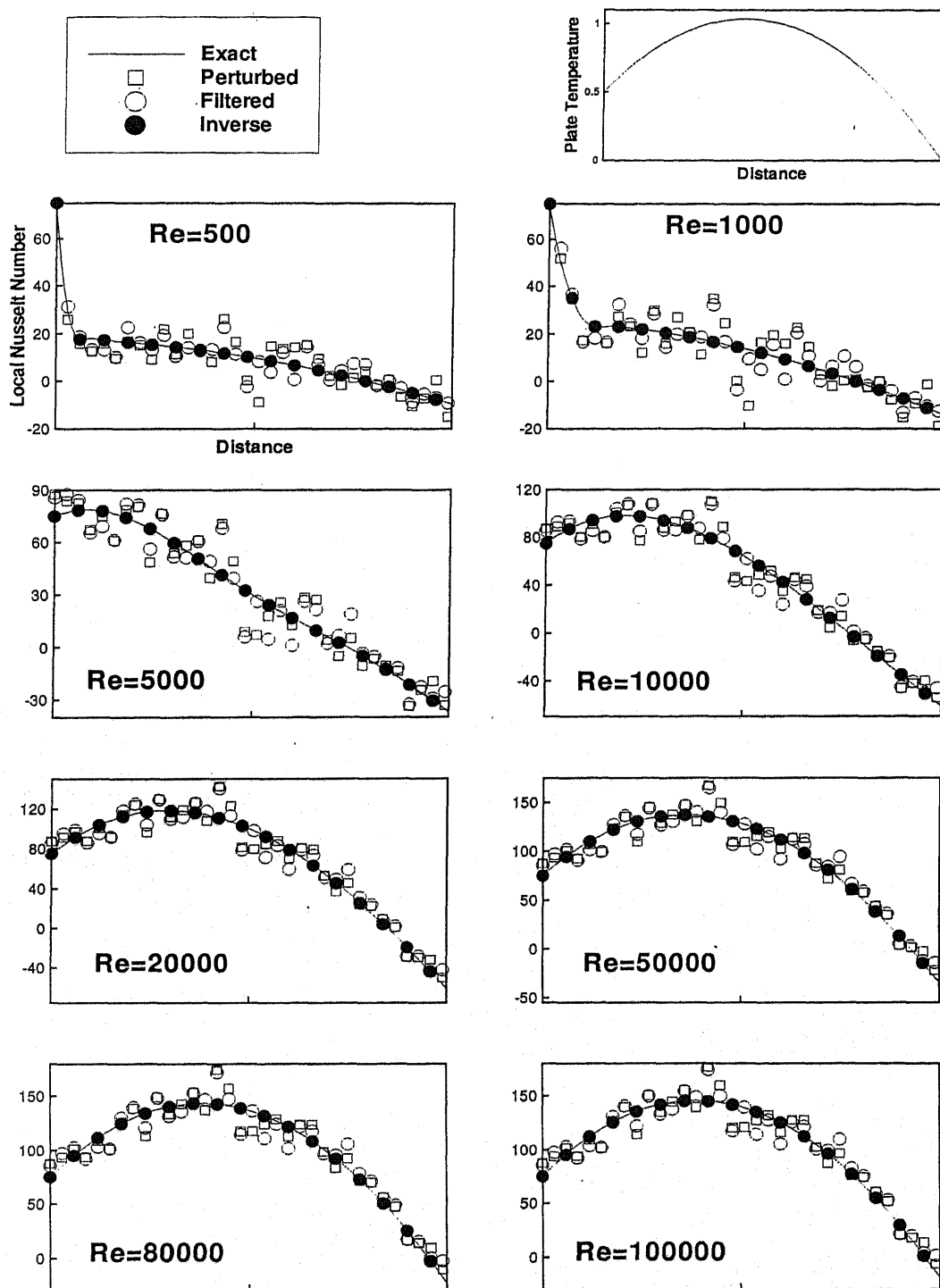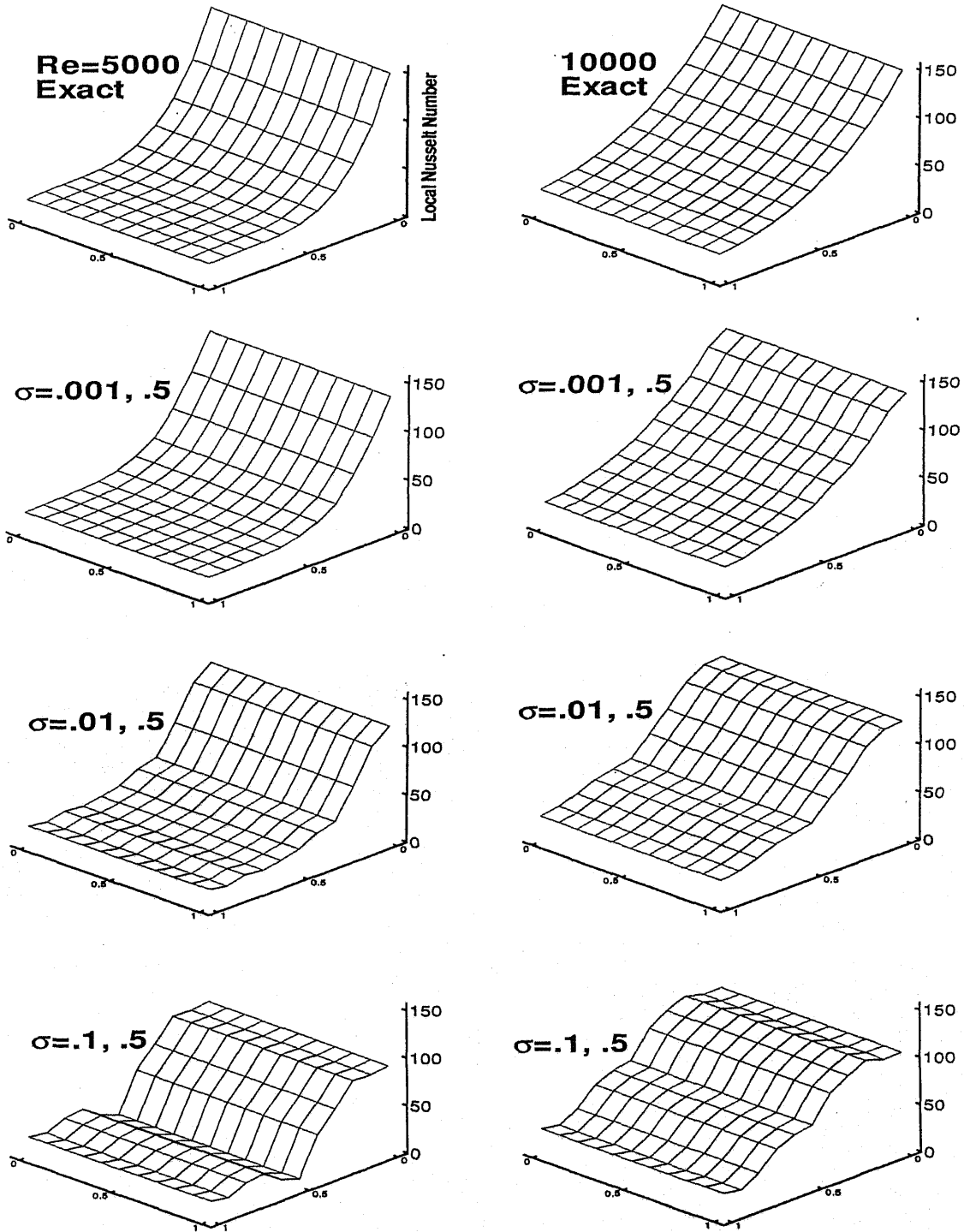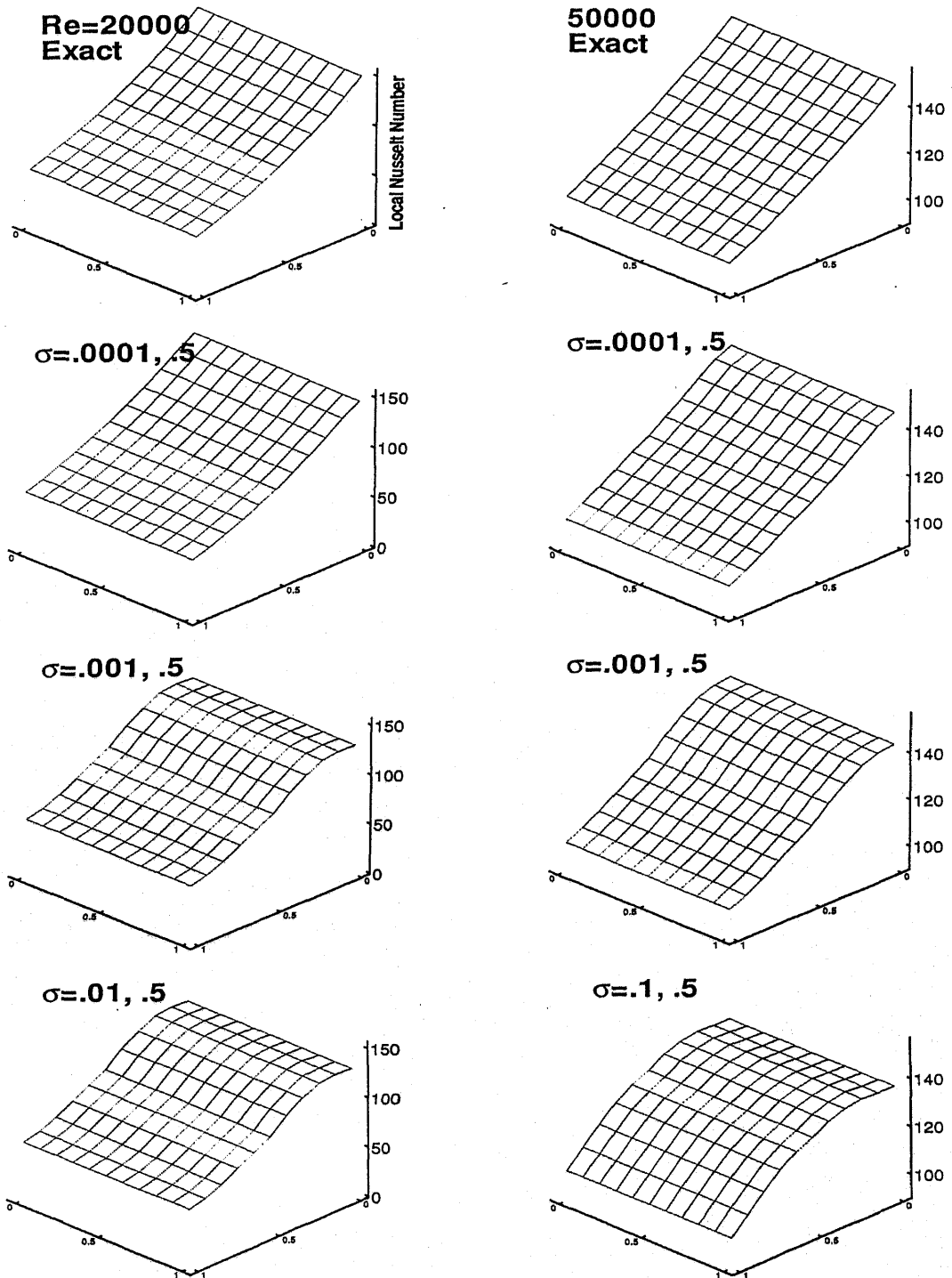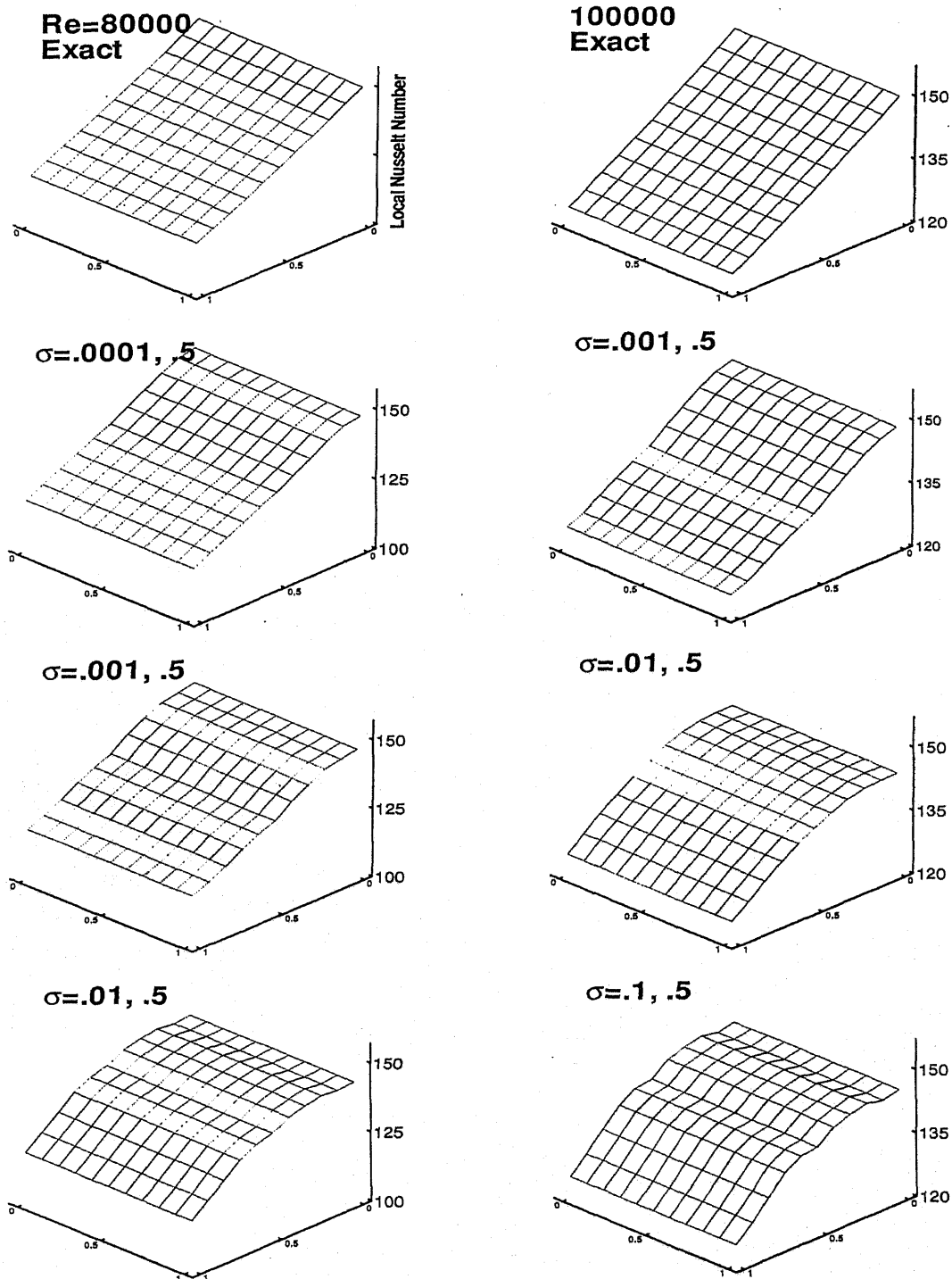
Figure 7.2: Comparison of inverse and direct solution with perturbed and filtered data. Scatter in plate temperature is σ=0.2. Scatter in interior temperature is σ=0.0001. Only 50% interior temperatures are available at $y = 0.01$. Velocity and temperature have been obtained from a parabolic formulation.
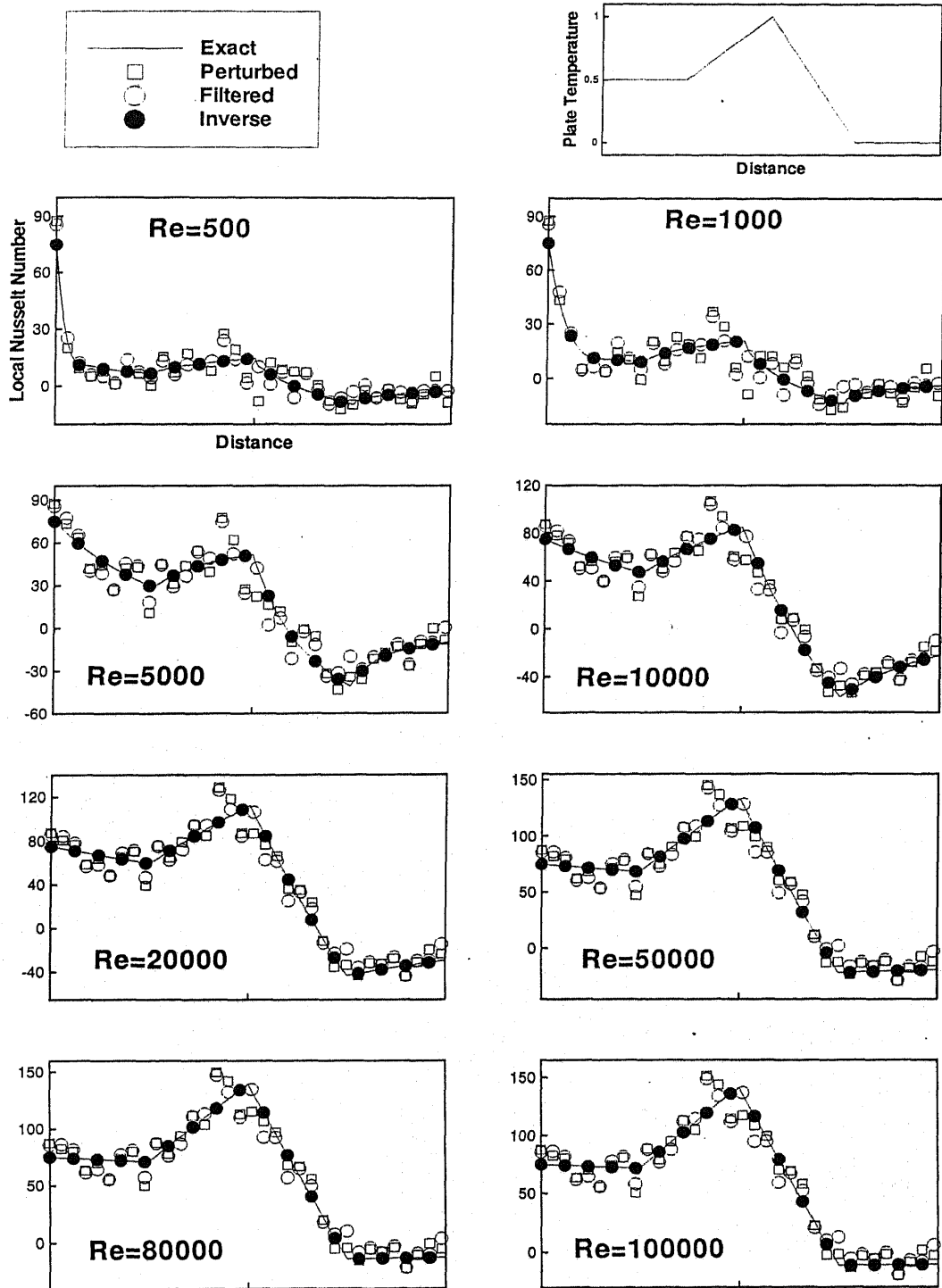
Figure 7.3: Comparison of inverse and direct solution with perturbed and filtered data. Scatter in plate temperature is σ=0.2. Scatter in interior temperature is σ=0.0001. Only 50% interior temperatures are available at $y = 0.01$. Velocity and temperature have been obtained from a parabolic formulation.
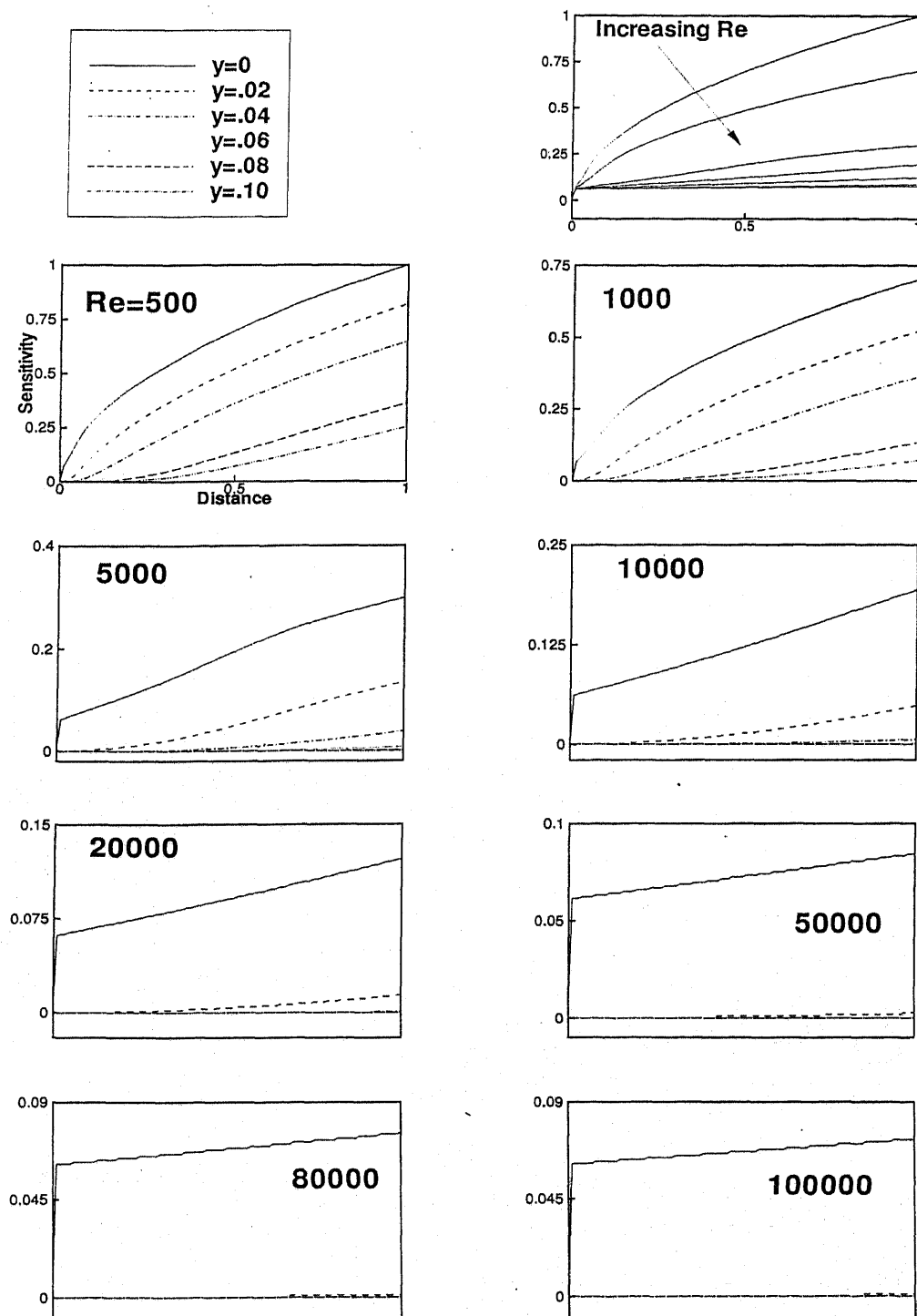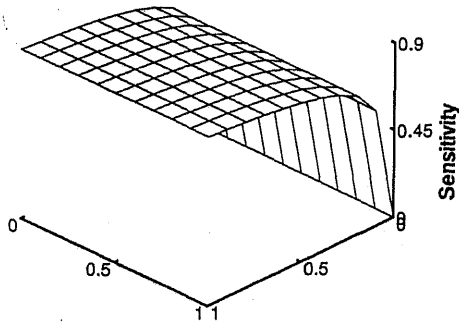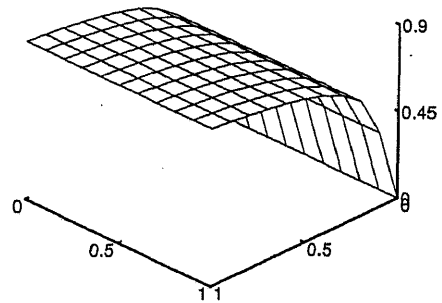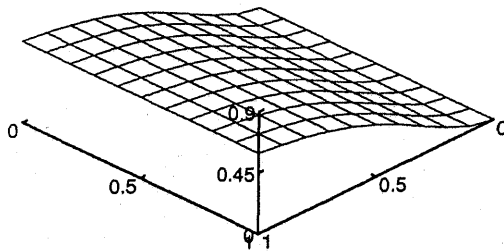
Figure 7.4: Variation of sensitivity coefficient with distance from the plate at different Reynolds numbers. (a) Variation of sensitivity at a given plane with Reynolds numbers.
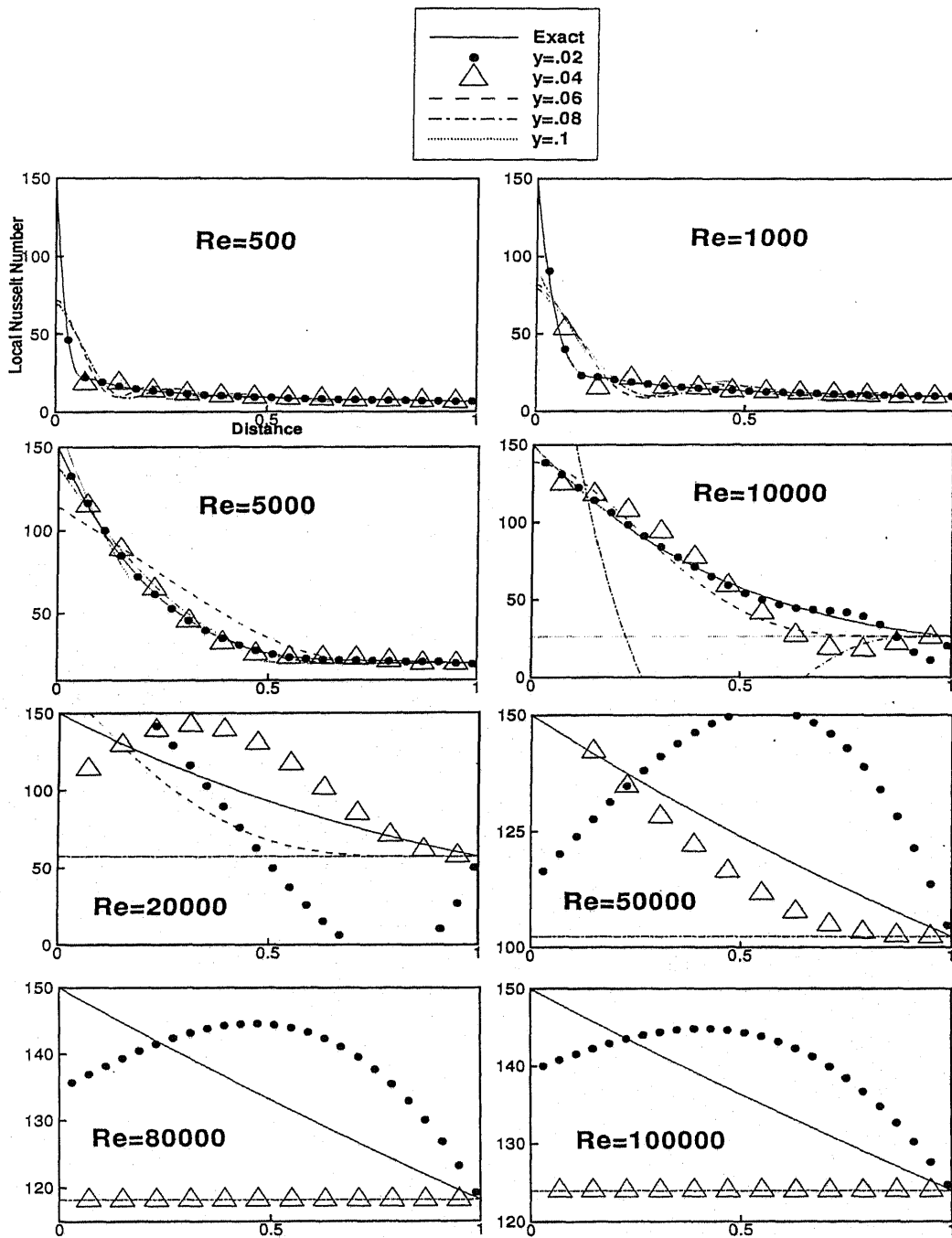
Figure 7.5: Effect of the choice of the additional high quality data on inverse estimation. This data lies on the plane $y=$ constant.
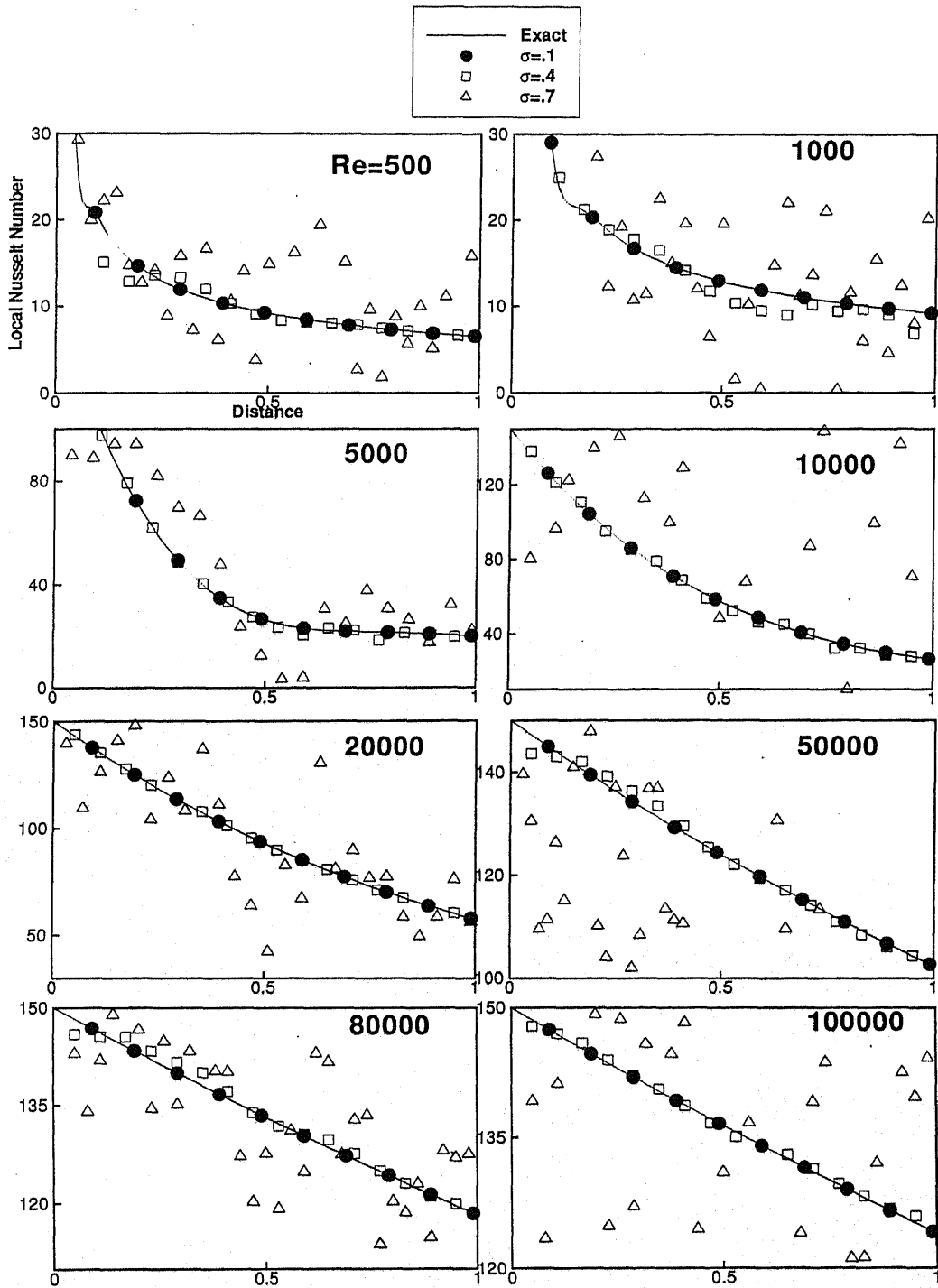
Figure 7.6: Effect of scatter in plate temperature data on the inverse solution.
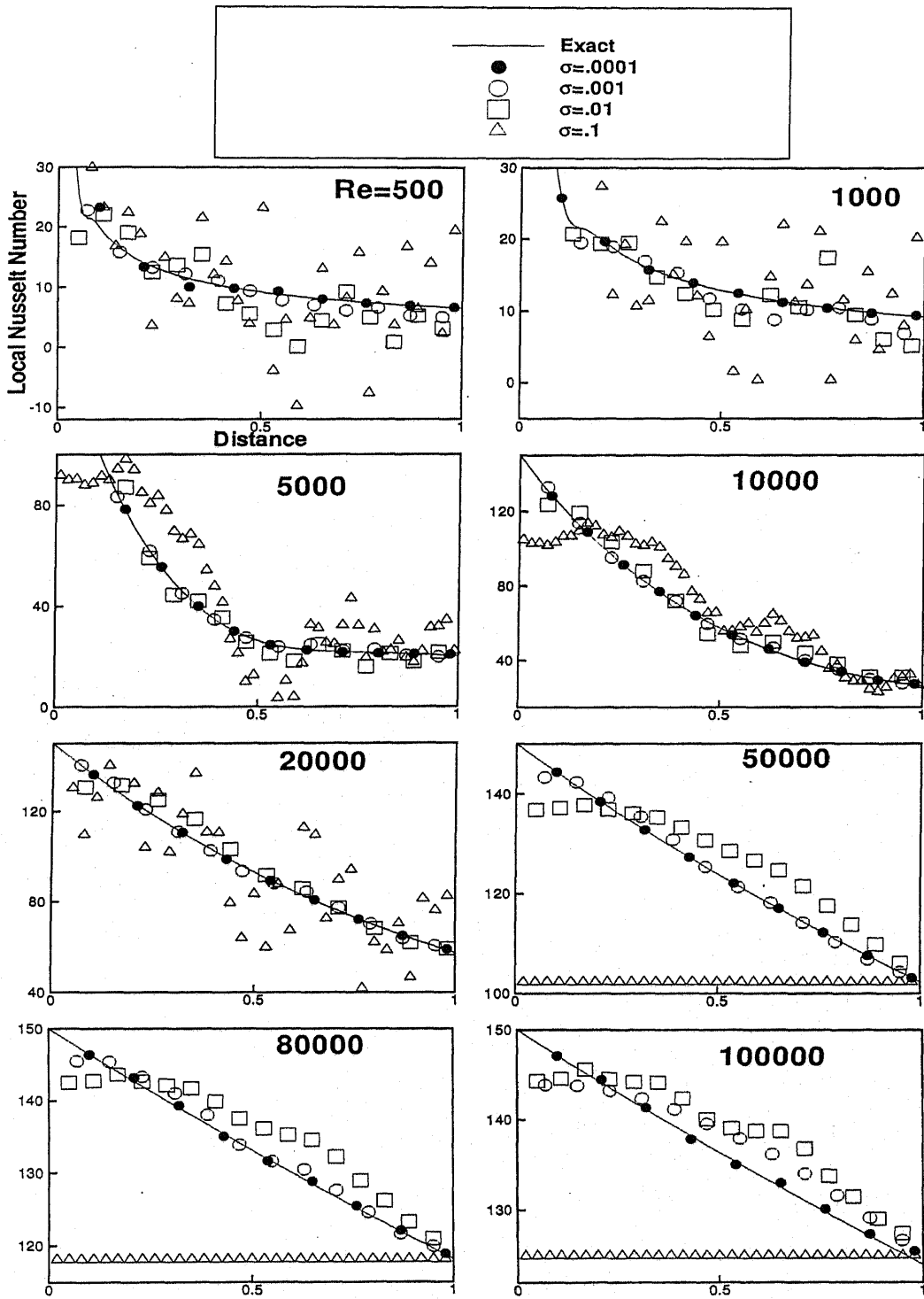
Figure 7.7: Effect of scatter in interior temperature data on the inverse solution.
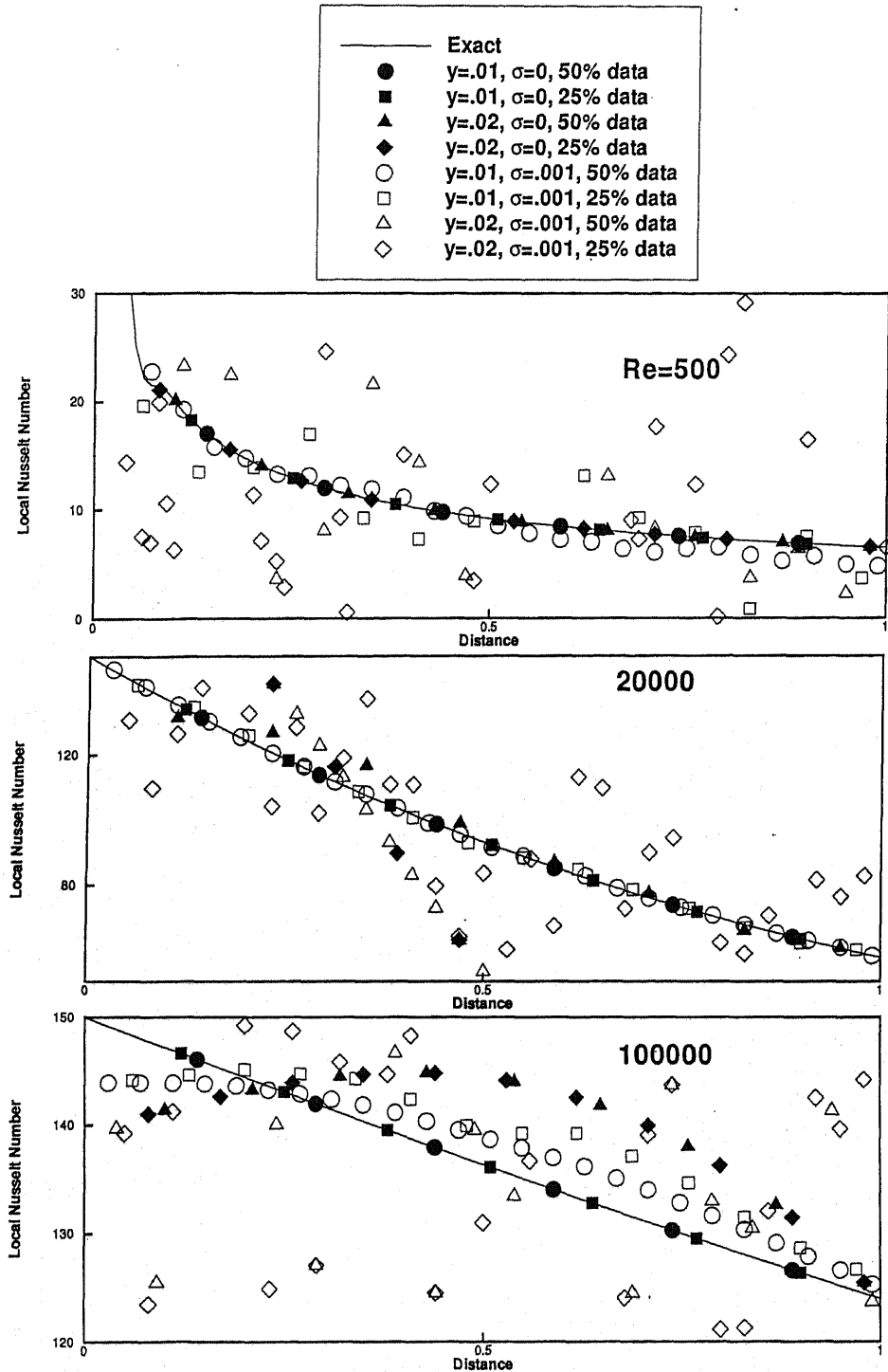
Figure 7.8: Effect of the quality (standard deviation), quantity and sensitivity of interior data on the inverse solution.
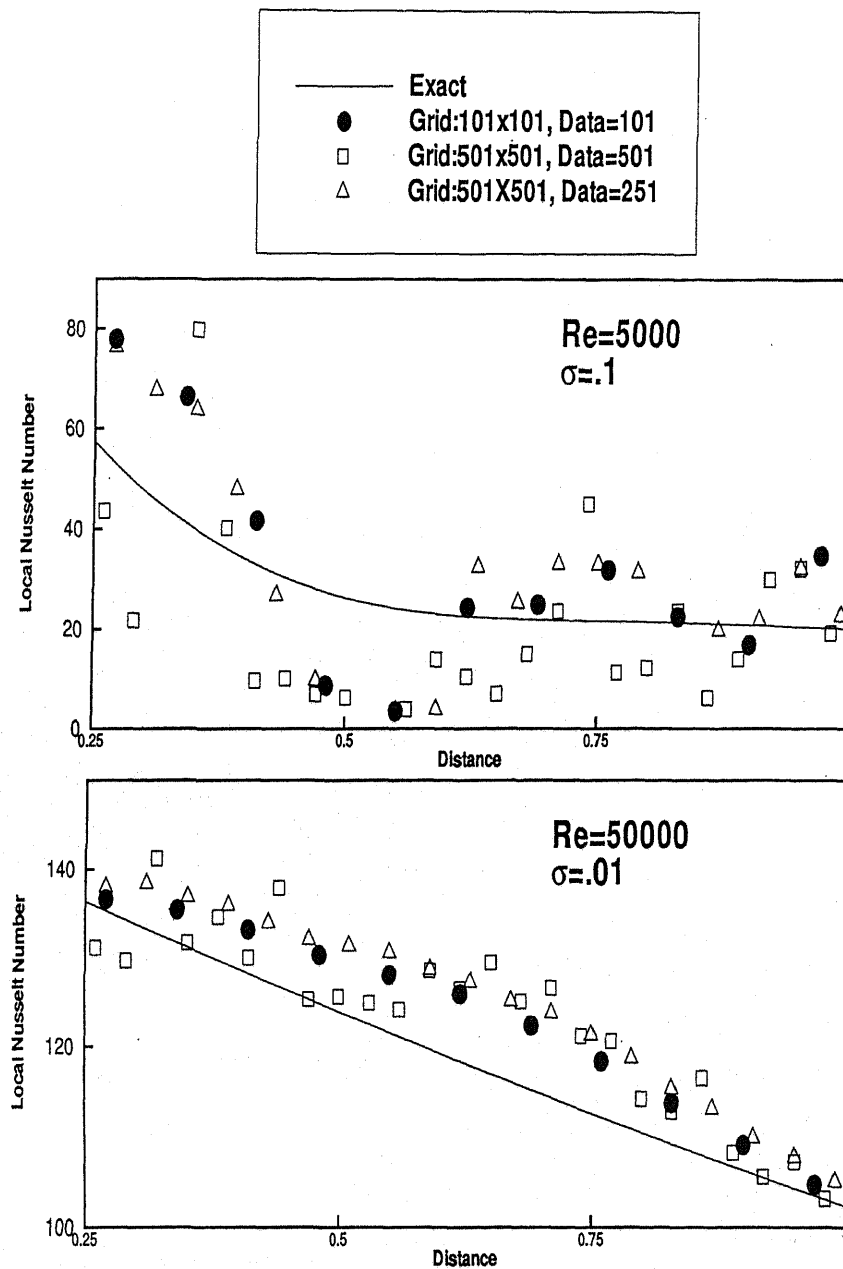
Figure 7.9: Effect of grid refinement on inverse estimation of the local Nusselt number.
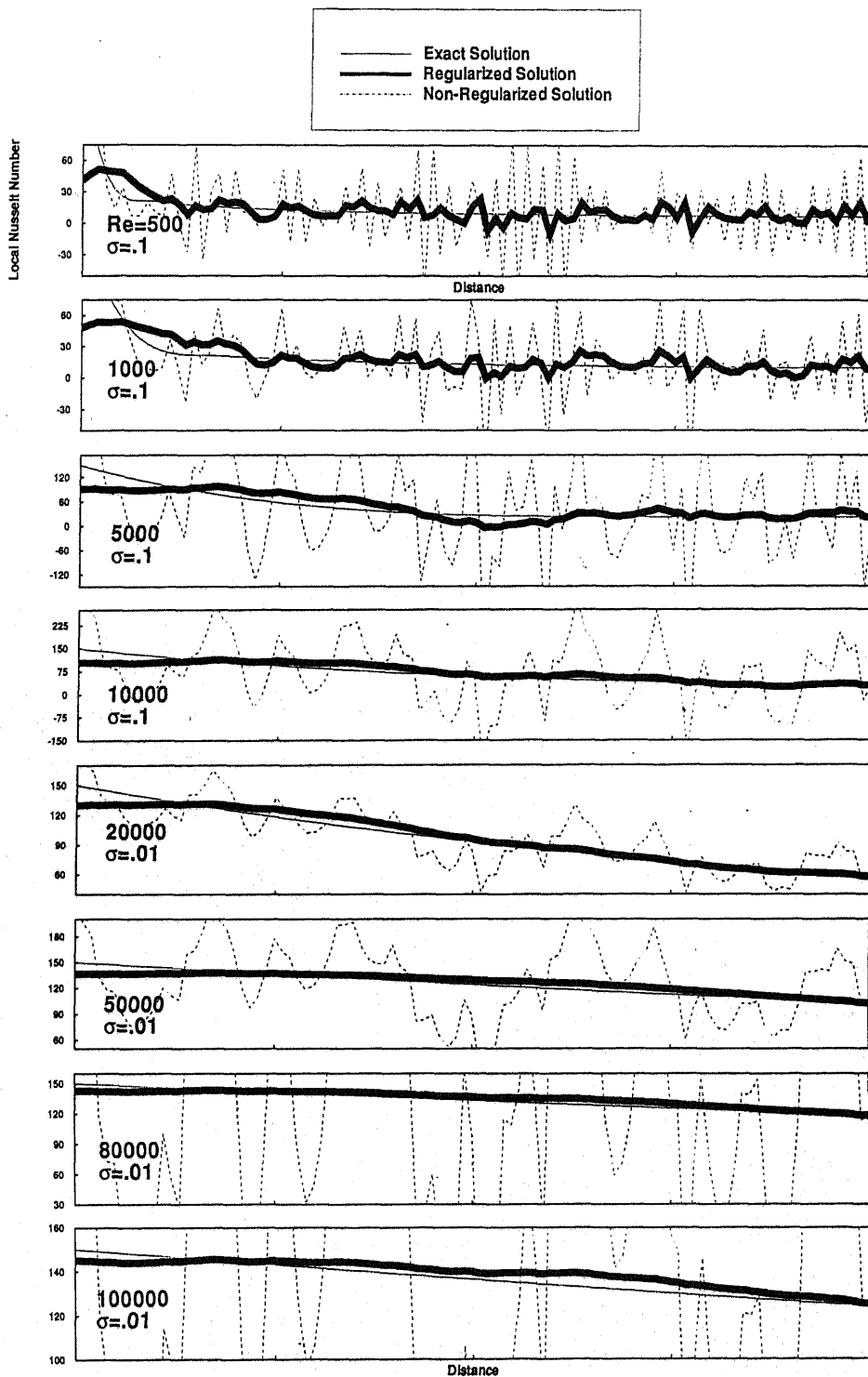
Figure 7.10: Comparison of regularized and non-regularized inverse solutions.
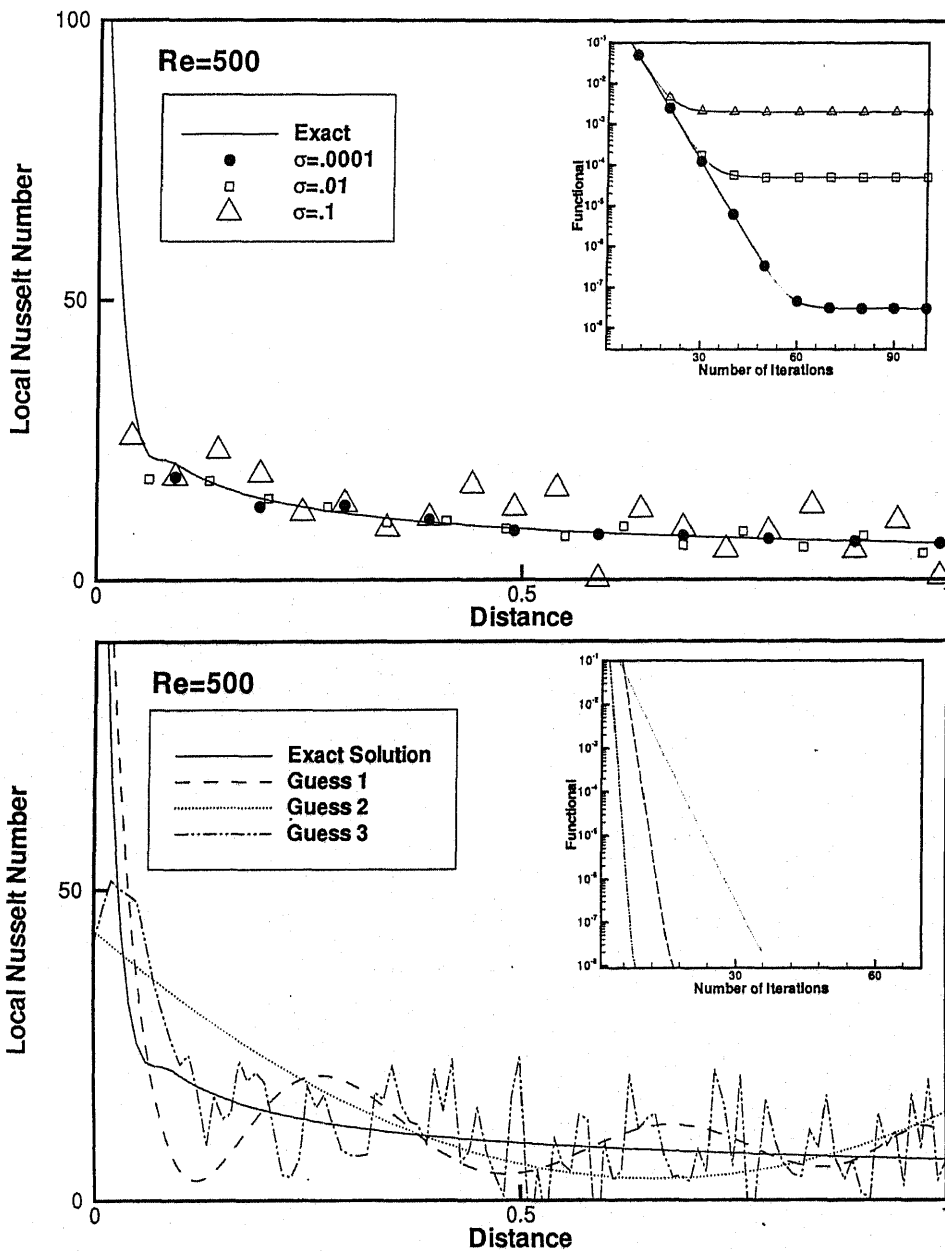
Figure 7.11: Effect of initial guess on the inverse solution of local Nusselt number.
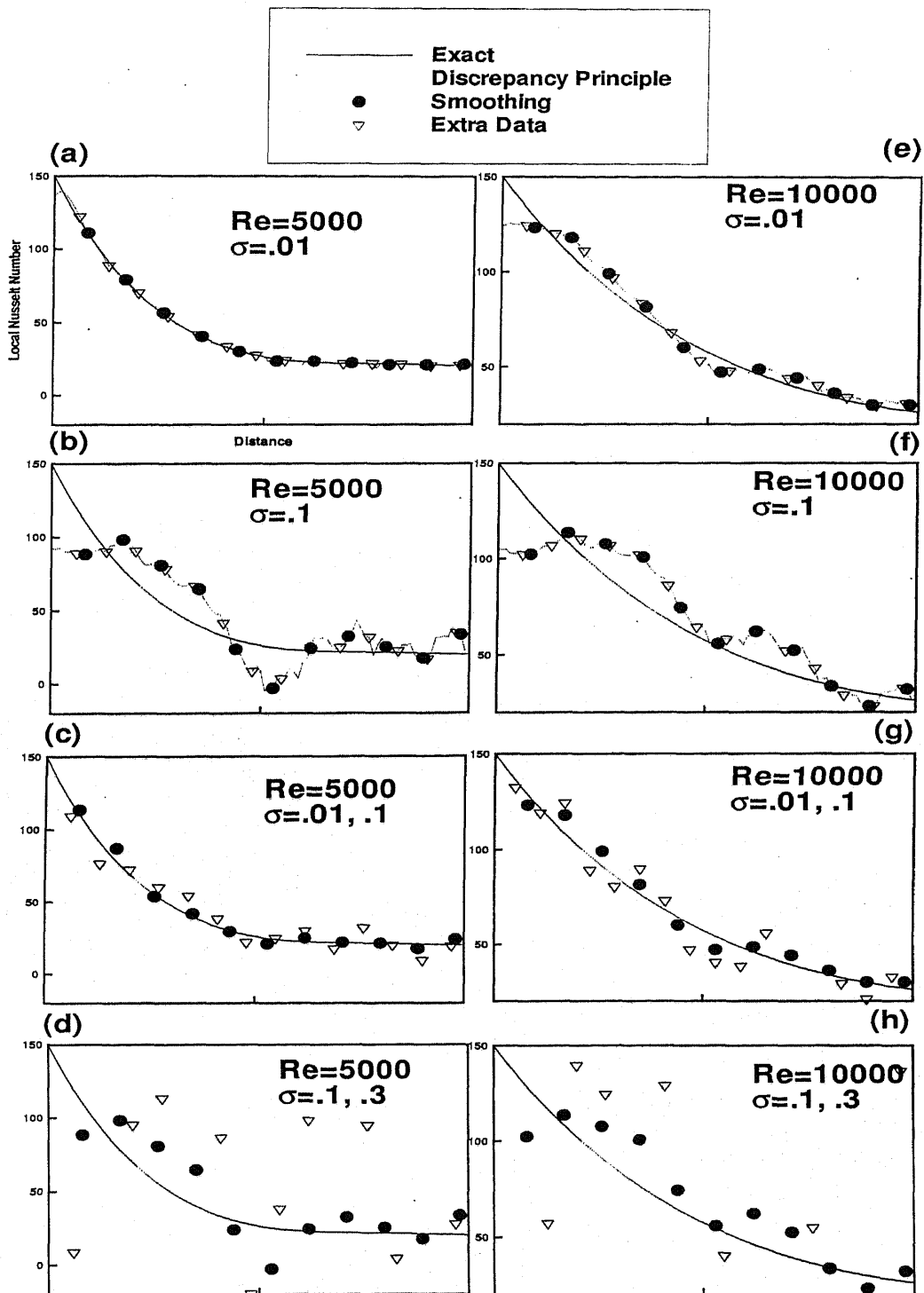
Figure 7.12: Effect of stopping criteria on the inverse solution of local Nusselt number.

7.2   Three Dimensional Steady Parabolic Solver

The effectiveness of the inverse formulation is revealed for three dimensional geometries in Figures 7.13 - 7.16. The sensitivity analysis has also been carried out and presented in Figures 7.17 - 7.19.

These figures clearly show that the inverse formulation presented here is capable of generating meaningful results for the three dimensional thermal field. Specific observations are:

1. Reasonable solutions have been achieved upto 10% scatter in interior data.

2. For noise level and measurement plane remaining same, inverse estimation quality degrades with the increase in Reynolds number.

3. The sensitivity analysis complies with the inverse estimations.
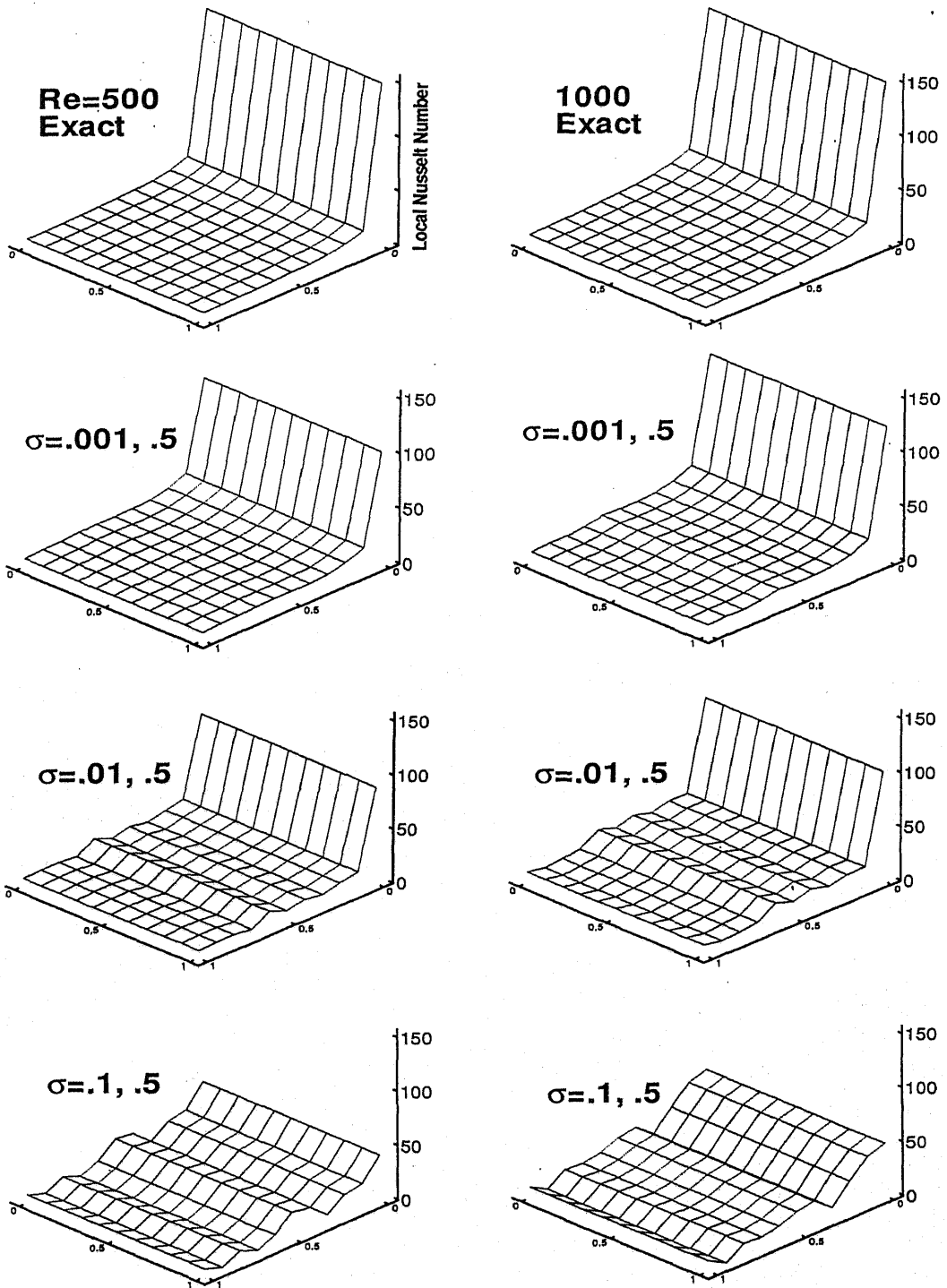
Figure 7.13: Comparison of inverse and direct solution. Scatter in plate temperature is $\sigma=0.5$. Scatter in interior temperature varies from $\sigma=0.001$ to $\sigma=0.1$. Only 50% interior temperatures are available at $y = 0.01$. Velocity and temperature have been obtained from a parabolic formulation. Velocity field is two dimensional.

Figure 7.14: Comparison of inverse and direct solution. Scatter in plate temperature is $\sigma=0.5$. Scatter in interior temperature varies from $\sigma=0.001$ to $\sigma=0.1$. Only 50% interior temperatures are available at $y=0.01$. Velocity and temperature have been obtained from a parabolic formulation. Velocity field is two dimensional.

Figure 7.15: Comparison of inverse and direct solution. Scatter in plate temperature is $\sigma=0.5$. Scatter in interior temperature varies from $\sigma=0.001$ to $\sigma=0.1$. Only 50% interior temperatures are available at $y = 0.01$. Velocity and temperature have been obtained from a parabolic formulation. Velocity field is two dimensional.

Figure 7.16: Comparison of inverse and direct solution. Scatter in plate temperature is $\sigma = 0.5$. Scatter in interior temperature varies from $\sigma = 0.001$ to $\sigma = 0.1$. Only 50% interior temperatures are available at $y = 0.01$. Velocity and temperature have been obtained from a parabolic formulation. Velocity field is two dimensional.
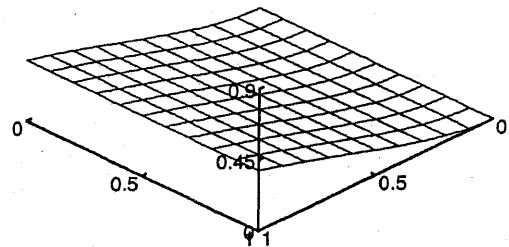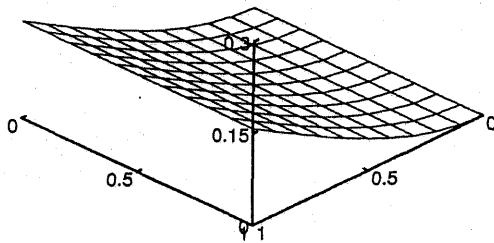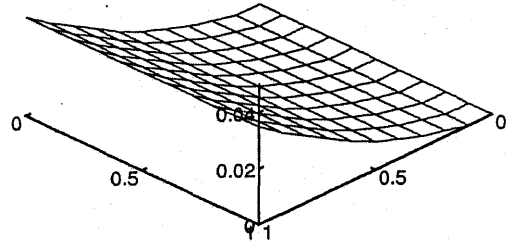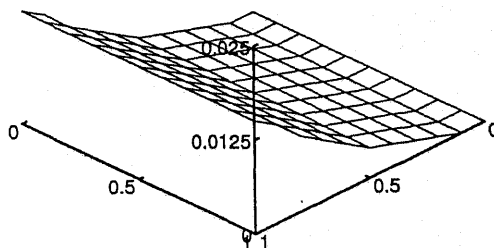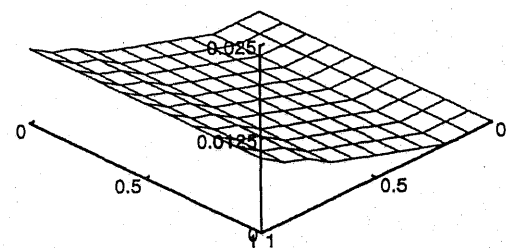
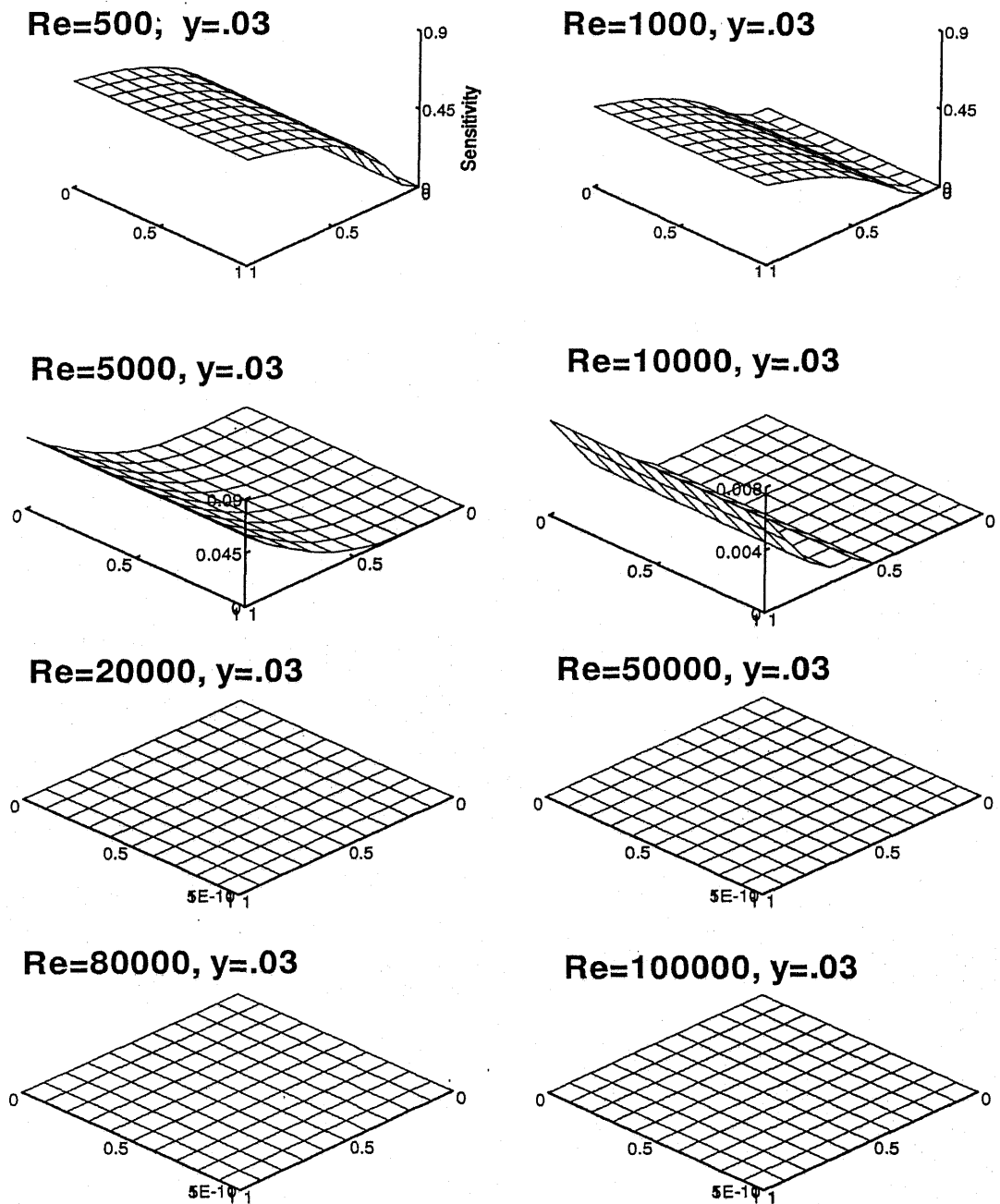Figure 7.17: Variation in the sensitivity coefficient for three dimensional parabolic problem. The studies have been carried out at $y = .01$.
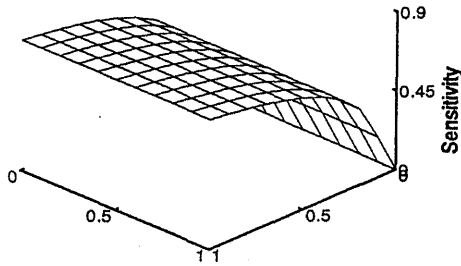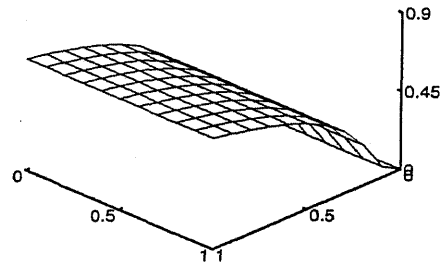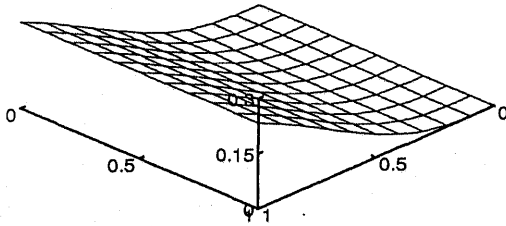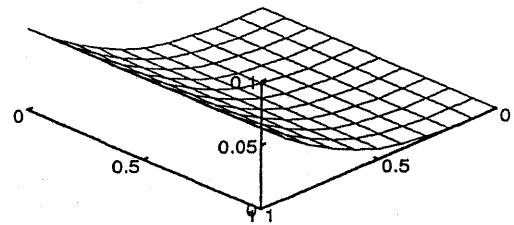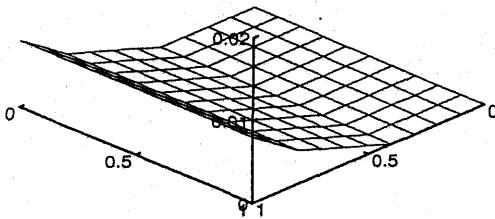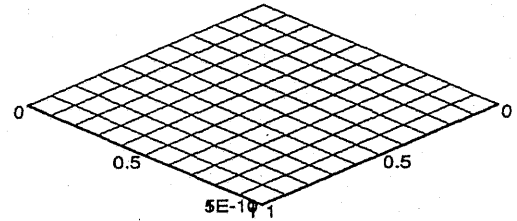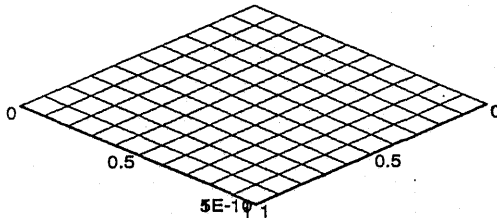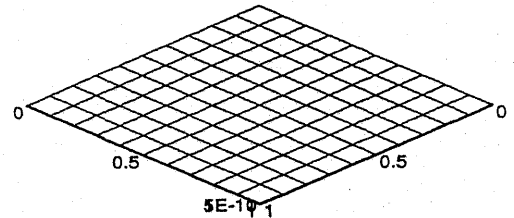
Figure 7.18: Variation in the sensitivity coefficient for three dimensional parabolic problem. The studies have been carried out at $y = .02$.

Figure 7.19: Variation in the sensitivity coefficient for three dimensional parabolic problem. The studies have been carried out at $y = .03$.

7.3 Three dimensional unsteady elliptic formulation

The performance of the inverse formulation is studied for three dimensional unsteady heat transfer from the flat plate (Figures 7.20 - 7.22). The intermediate direct problems have been numerically solved by an elliptic formulation[3]. The results from sensitivity analysis are shown in Figure 7.23.

The inverse formulation is shown to be less effective for small time but predicts well as the time progresses. The sensitivity studies show that the sensitivity coefficient at a point increases with time. This allows the inverse algorithm to extract more and more informations from a point as the time progresses. The specific observations of this part of the study are:

1. Unsteady inverse technique becomes more efficient as time progresses.

2. For noise level and measurement plane remaining same, inverse estimation quality degrades with the increase in Reynolds number.

3. The sensitivity analysis complies with the inverse estimations.

---

[3]A parabolic solver in space and time could also have been used, but would be inapplicable for flow past a rib that is discussed in chapter 8.
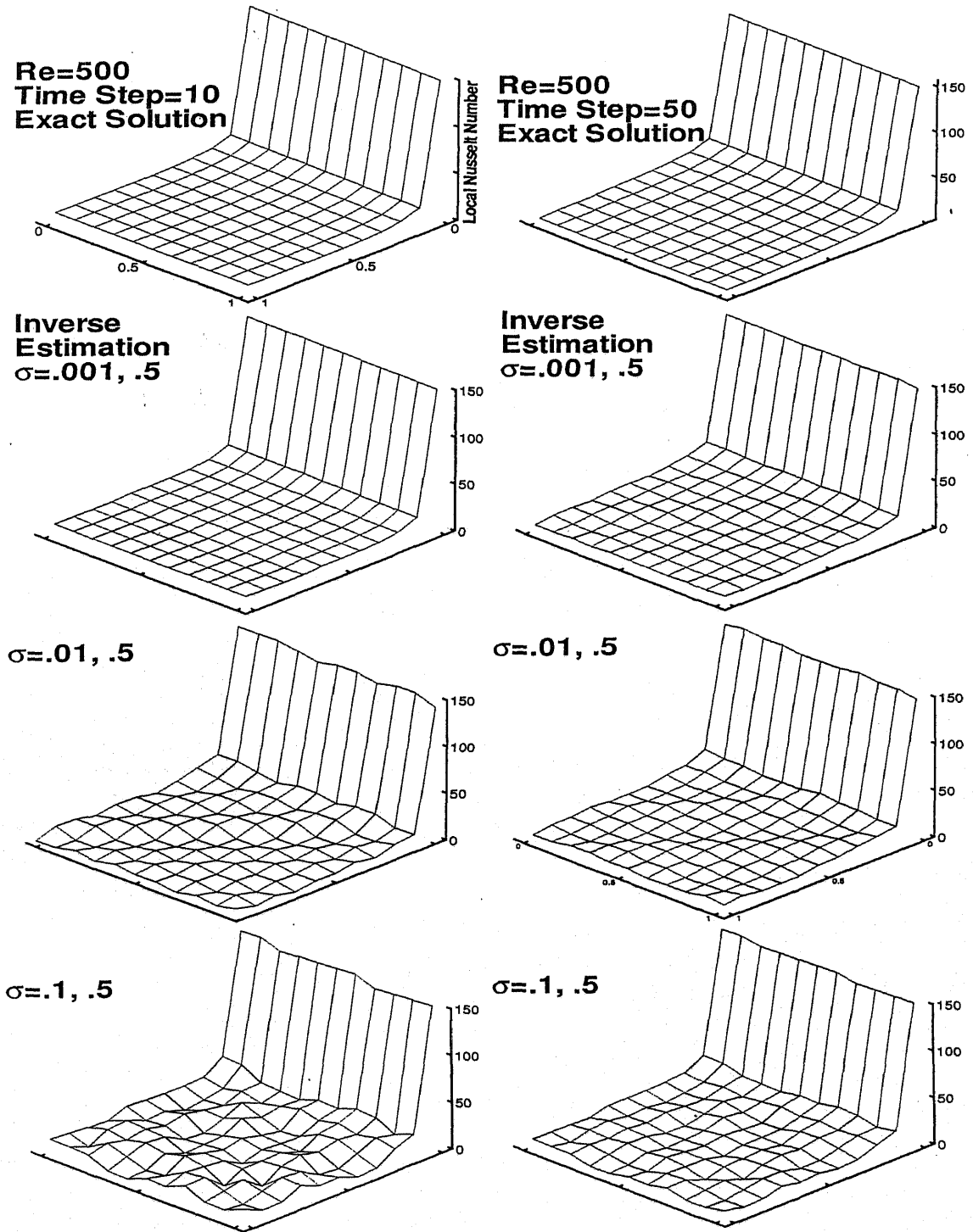
Figure 7.20: Comparison of inverse and direct solution. Scatter in plate temper-ature is $\sigma=0.5$. Scatter in interior temperature varies from $\sigma=0.001$ to $\sigma=0.1$. Only 50% interior temperatures are available at $y = 0.01$. The temperature field has been obtained from an elliptic formulation. A two-dimensional parabolic solver is used for the flow field.
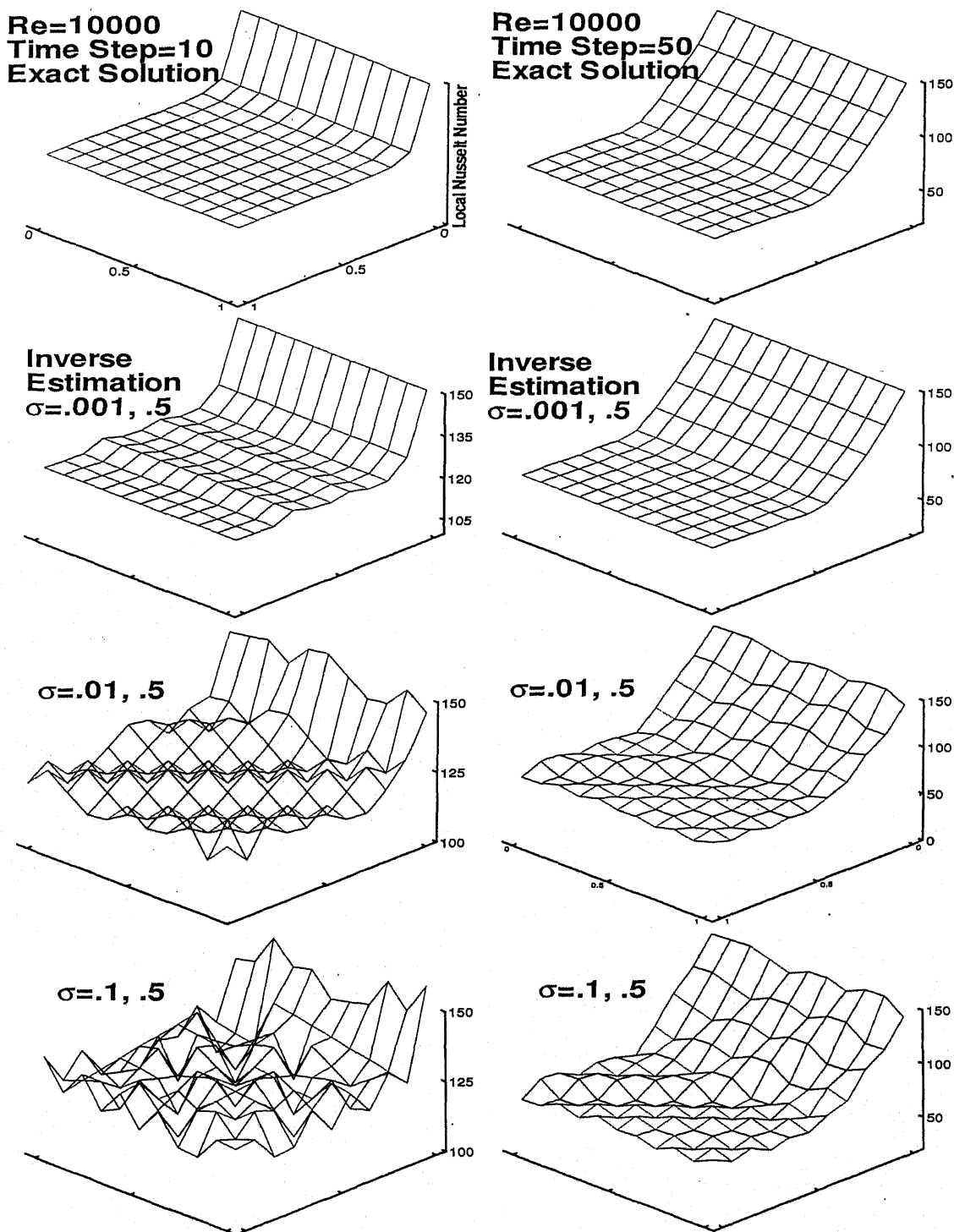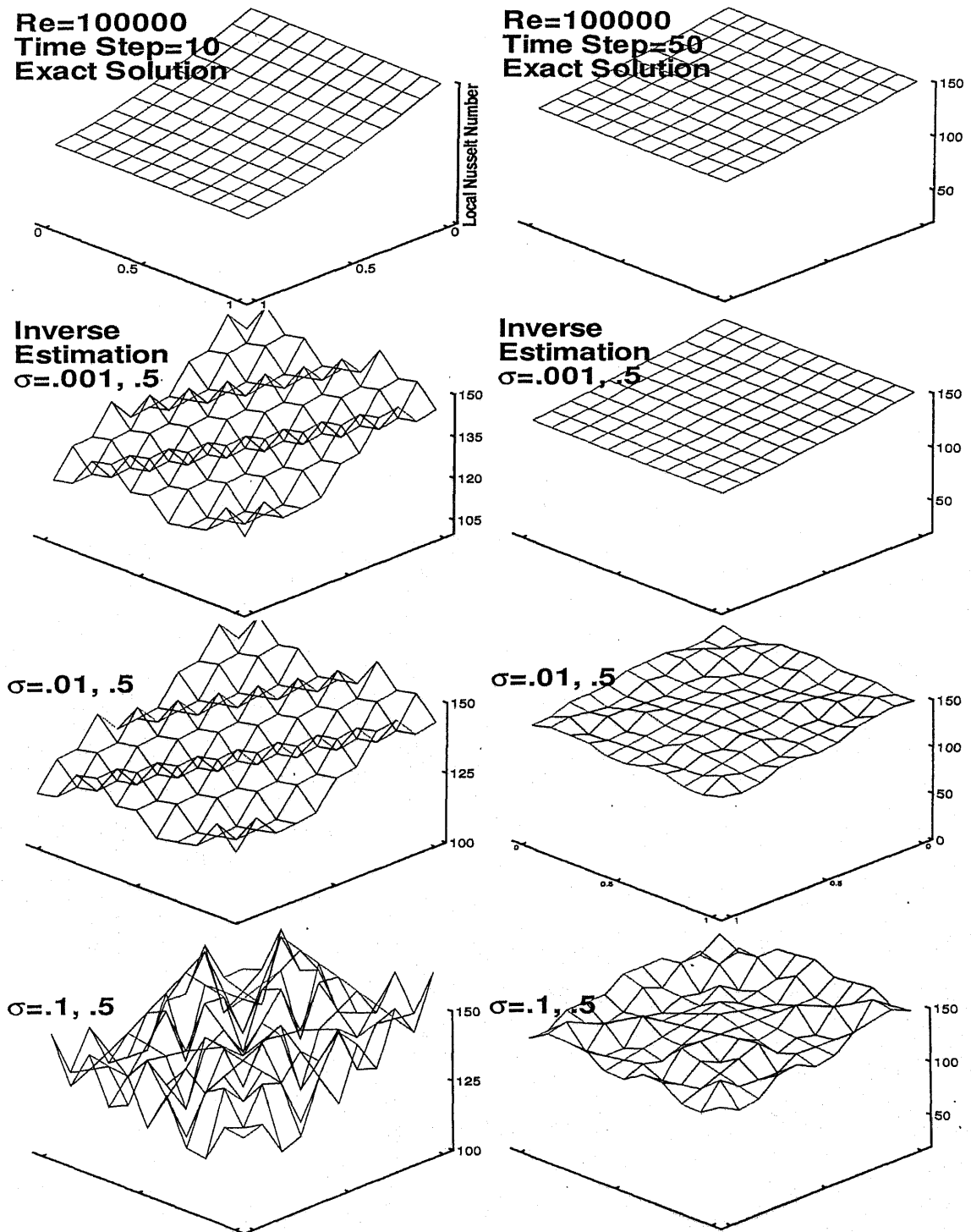
Figure 7.21: Comparison of inverse and direct solution. Scatter in plate temperature is $\sigma=0.5$. Scatter in interior temperature varies from $\sigma=0.001$ to $\sigma=0.1$. Only 50% interior temperatures are available at $y=0.01$. The temperature field has been obtained from an elliptic formulation. A two-dimensional parabolic solver is used for the flow field.
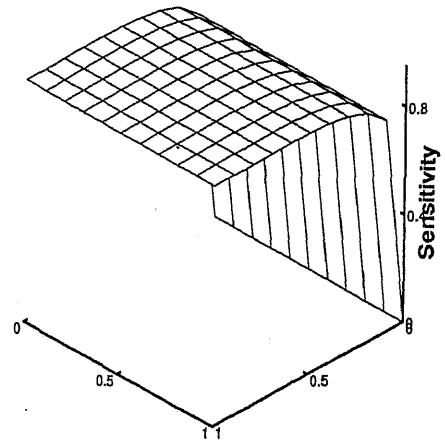
Figure 7.22: Comparison of inverse and direct solution. Scatter in plate temperature is $\sigma=0.5$. Scatter in interior temperature varies from $\sigma=0.001$ to $\sigma=0.1$. Only 50% interior temperatures are available at $y = 0.01$. The temperature field has been obtained from an elliptic formulation. A two-dimensional parabolic solver is used for the flow field.
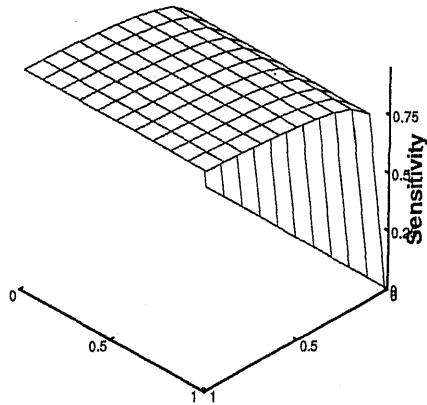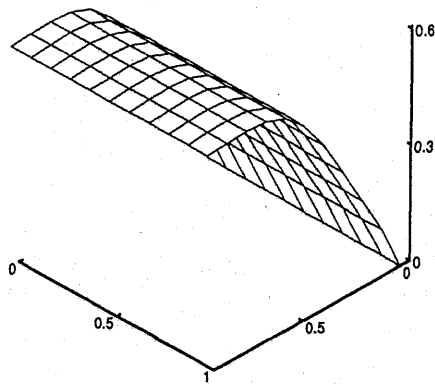
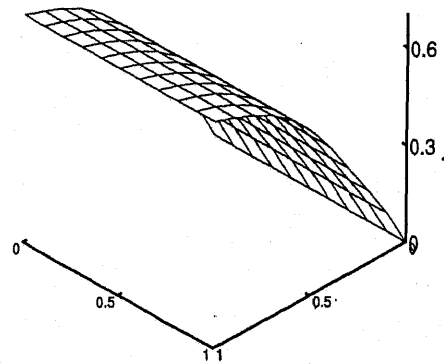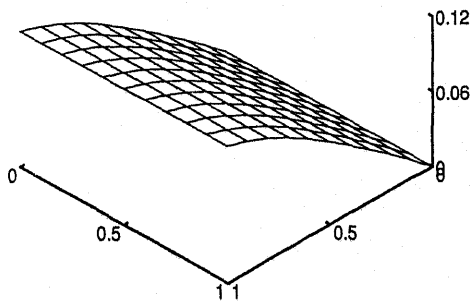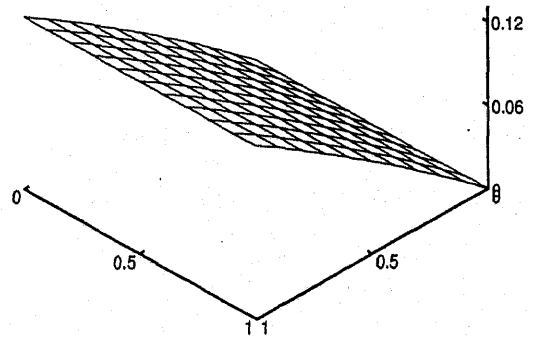Figure 7.23: Variation of sensitivity coefficient with time and Reynolds number for three dimensional elliptic problem. The studies are carried out at a plane $y = 0.01$.

Chapter 8

Convective Heat Transfer from a Flat Plate with a Rib

This chapter presents the outcome of applying the inverse technique to predict the local Nusselt number for flow over a surface with a solid rib mounted over it. Three different solvers are used namely: (1) Unsteady two dimensional formulation with a steady plate temperature, (2) Unsteady three dimensional formulation with a steady plate temperature, (3) unsteady two dimensional formulation with experimentally determined time varying surface temperature. Detailed formulations are furnished in Chapter 4 and the numerical issues are discussed in Appendices A and B. Inverse solutions of (1) and (2) contain the following steps:

1. Solve direct problem assuming a meaningful plate temperature distribution. The plate temperature is steady but may vary with position over the plate. This step will generate interior fluid temperature field and the local Nusselt number variation over the surface. The solution of this problem is termed as *exact solution*.

2. Select interior temperature on certain planes for inclusion in the functional.

3. Perturb the plate temperature and the interior temperatures of step 2 with zero mean Gaussian noise (Appendix C). Thus each perturbed temperature fall in the range

$$\theta|_{\text{perturbed}} = \theta|_{\text{exact}} \pm \Gamma\sigma \qquad (8.1)$$

where σ is the standard deviation of the Gaussian distribution. Γ indicates the confidence interval. For present analysis a 99% confidence interval is

maintained by keeping $-2.576 < \Gamma < 2.576$. It is expected in practice that the standard deviation of the interior temperature is much smaller than that of the surface temperature.

4. Filter the plate and interior point temperatures by Gram orthogonal polynomial smoothing.

5. Solve the complete inverse problem to estimate the local Nusselt number distribution.

6. Compare the Nusselt number distribution with the exact solution of step 1.

For the transient plate temperature problem, the noise level of the experimental data is not known exactly. The stopping criterion based on additional data is used to stabilized the solution. No data smoothing technique has been incorporated for this part of the study.

8.1   Two Dimensional Formulation

The effectiveness of the inverse formulation is revealed for the two dimensional geometry in Figures 8.1 - 8.3. The results of the sensitivity analysis has also been presented in Figure 8.4.

The sensitivity at the interior points is higher than for the flat plate case. This is attributed to the presence of rib, that influences the flow field to a greater extent, than a boundary-layer. This phenomenon serves as the reason for better prediction of the unsteady local Nusselt number as compared to a flat plate. Specific observations in this section are:

1. Transient prediction of the solver is superior than the flat plate one.

2. For noise level and measurement plane remaining same, inverse estimation quality degrades with the increase in Reynolds number.

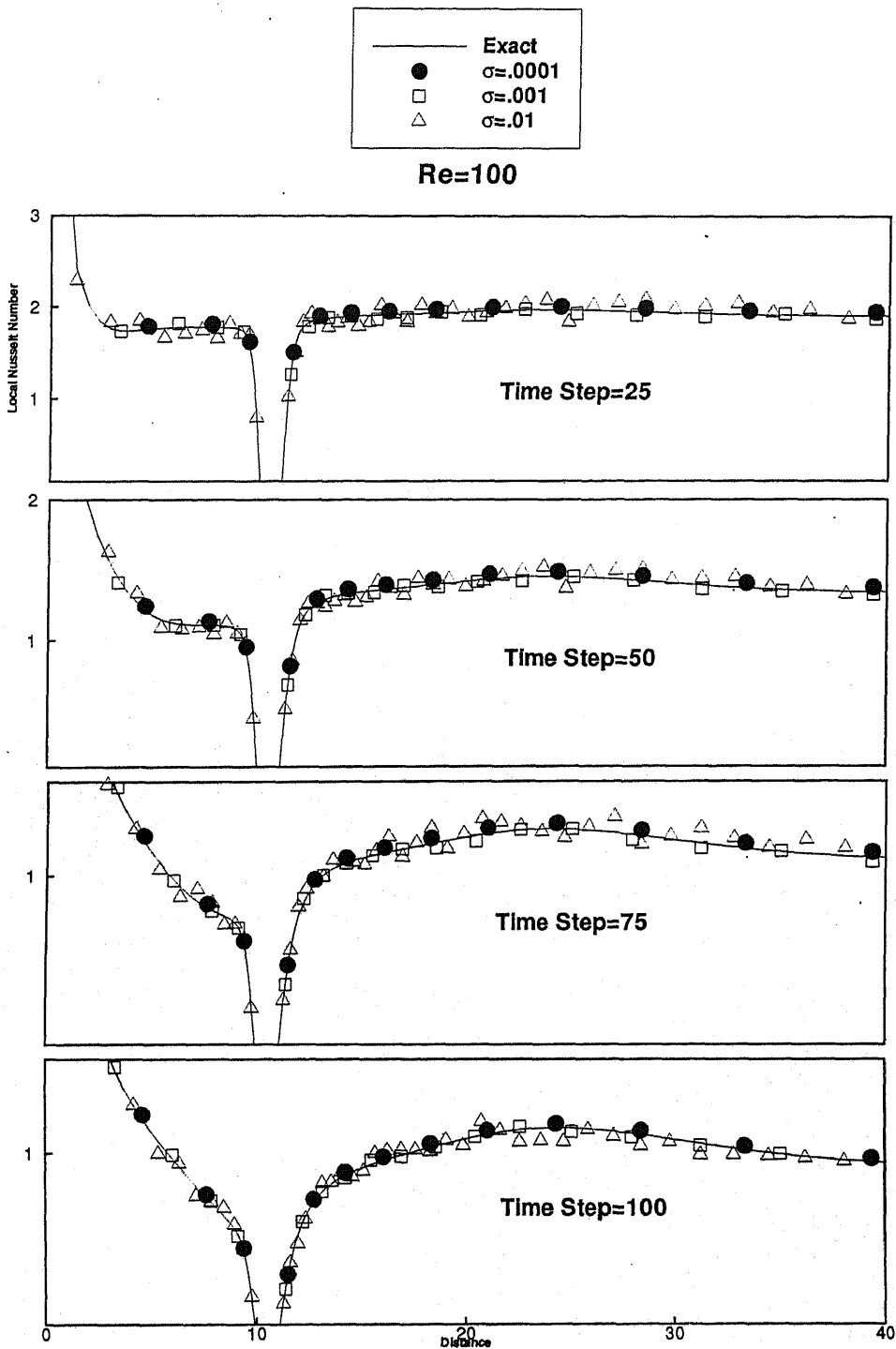3. The sensitivity analysis complies with the inverse estimations.

Figure 8.1: Comparison of inverse and direct solutions. Scatter in plate temperature is $\sigma=0.5$. Scatter in interior temperature is varying from .0001 to .01. Only 50% interior temperatures are available at $y = 0.01$. Velocity and temperature have been obtained from an elliptic formulation.
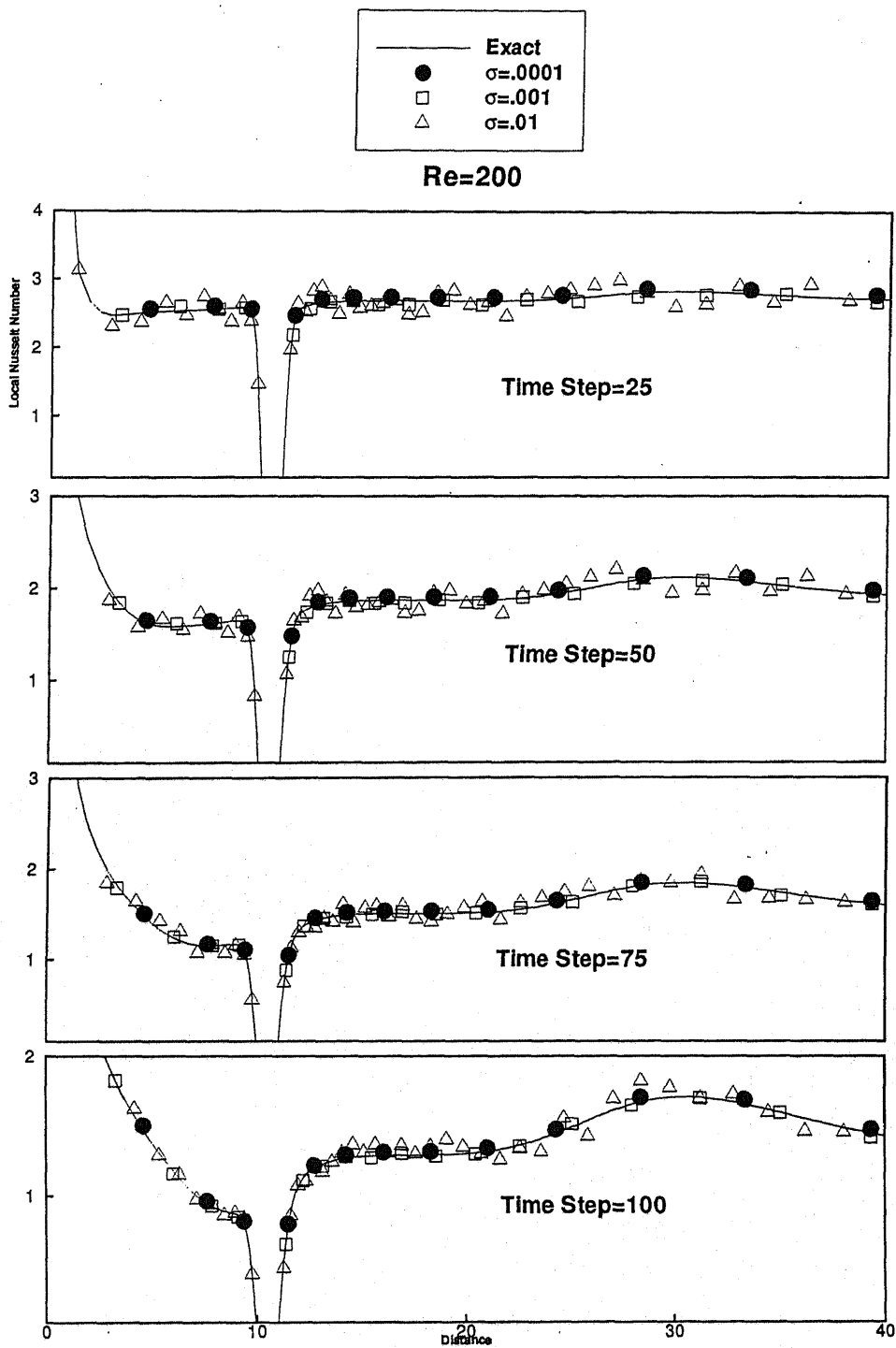
Figure 8.2: Comparison of inverse and direct solutions. Scatter in plate temperature is $\sigma=0.5$. Scatter in interior temperature is varying from .0001 to .01. Only 50% interior temperatures are available at $y = 0.01$. Velocity and temperature have been obtained from an elliptic formulation.

Figure 8.3: Comparison of inverse and direct solutions. Scatter in plate temperature is $\sigma=0.5$. Scatter in interior temperature is varying from .0001 to .01. Only 50% interior temperatures are available at $y = 0.01$. Velocity and temperature have been obtained from an elliptic formulation.
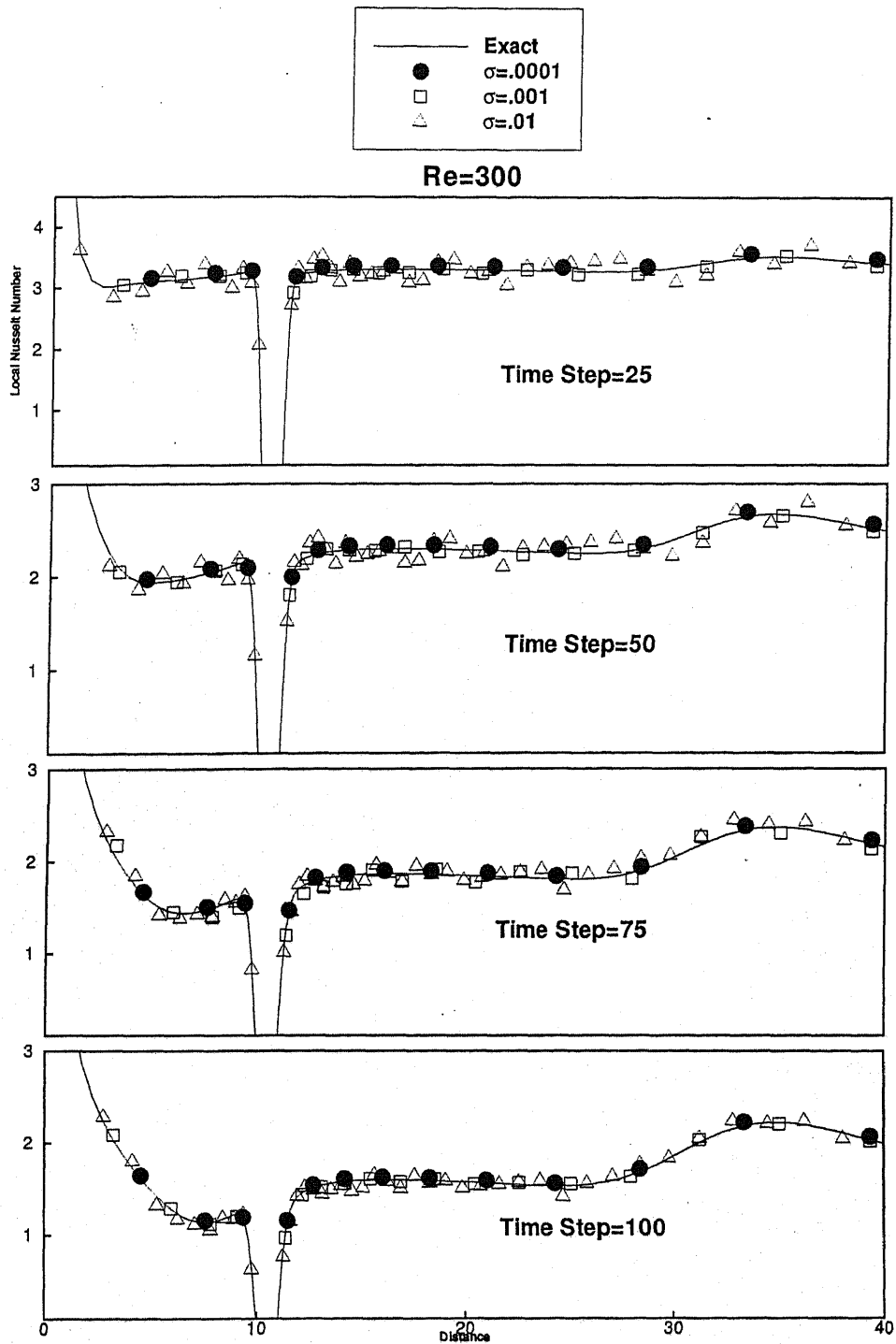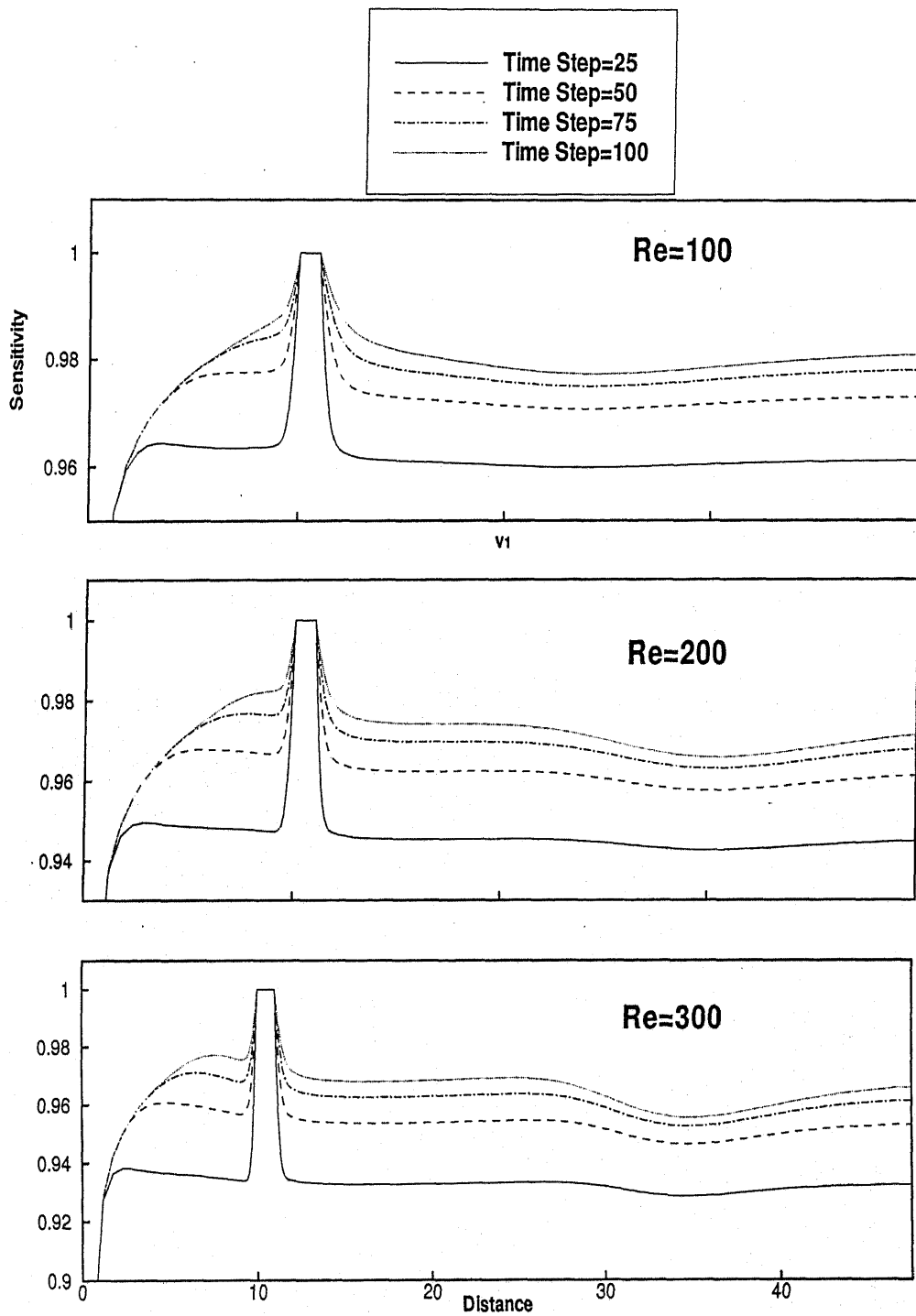
Figure 8.4: Variation in the sensitivity coefficient with time. The studies have been carried out at $y = 0.01$.

8.2   Three Dimensional Formulation

The effectiveness of the inverse formulation is revealed for the two dimensional geometry in Figures 8.5 - 8.7. The results of the sensitivity analysis has also been presented in Figure 8.8.

The sensitivity at the interior points is higher than for the flat plate case. This is attributed to the presence of rib, that influences the flow field to a greater extent, than a boundary-layer. This phenomenon serves as the reason for better prediction of the unsteady local Nusselt number as compared to a flat plate. Specific observations in this section are:

1. Transient prediction of the solver is superior than the flat plate case. Behavior of the three dimensional solver matches with the two dimensional one.

2. For noise level and measurement plane remaining same, inverse estimation quality degrades with the increase in Reynolds number.

3. The sensitivity analysis complies with the inverse estimations.

Figure 8.5: Comparison of inverse and direct solutions. Scatter in plate temperature is $\sigma=0.5$. Scatter in interior temperature is $\sigma=0.01$. Only 50% interior temperatures are available at $y = 0.01$. Velocity and temperature have been obtained from an elliptic formulation. The flow field is two dimensional with three dimensional temperature field.
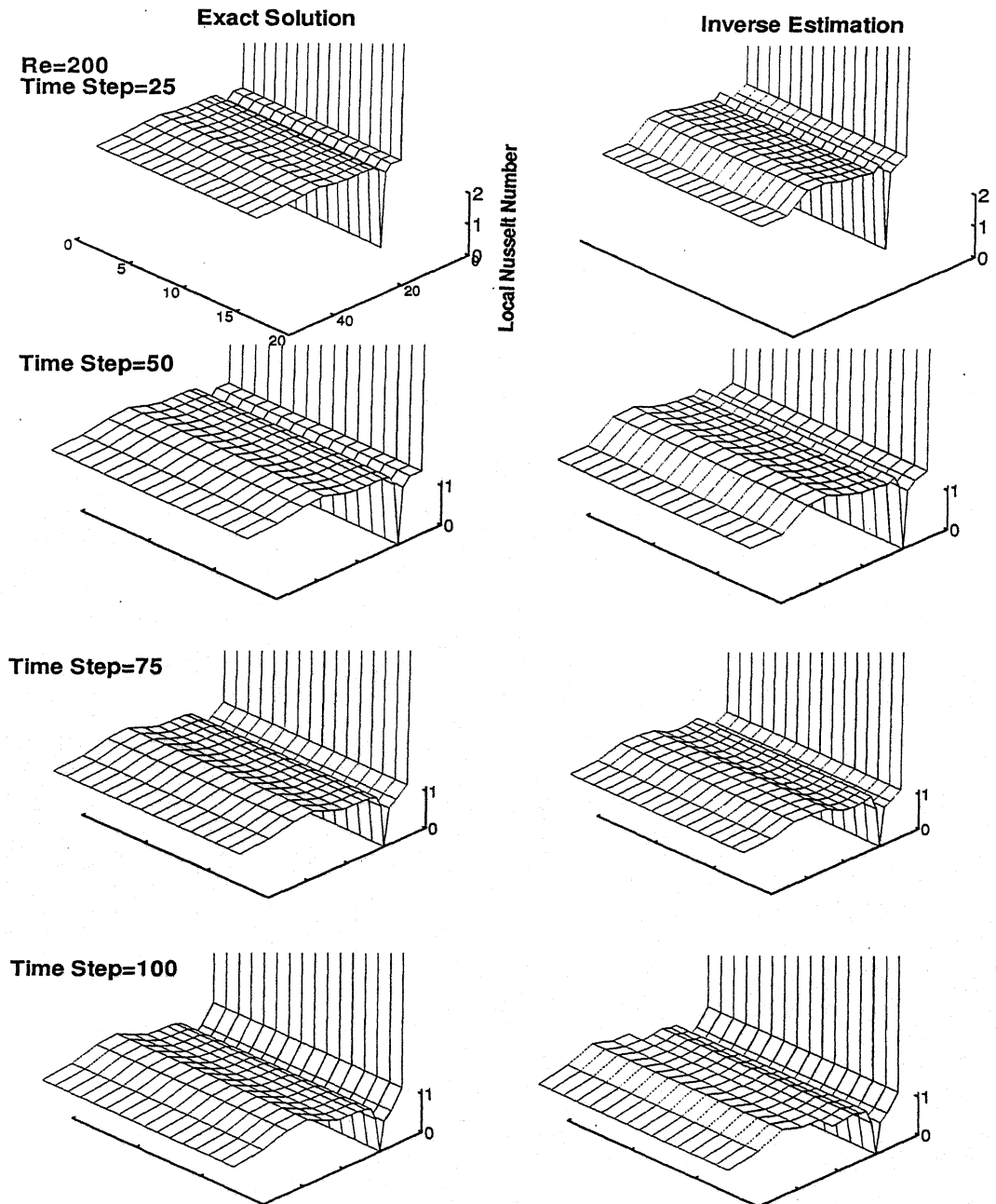
Figure 8.6: Comparison of inverse and direct solutions. Scatter in plate temperature is $\sigma=0.5$. Scatter in interior temperature is $\sigma=0.01$. Only 50% interior temperatures are available at $y = 0.01$. Velocity and temperature have been obtained from an elliptic formulation. The flow field is two dimensional with three dimensional temperature field.
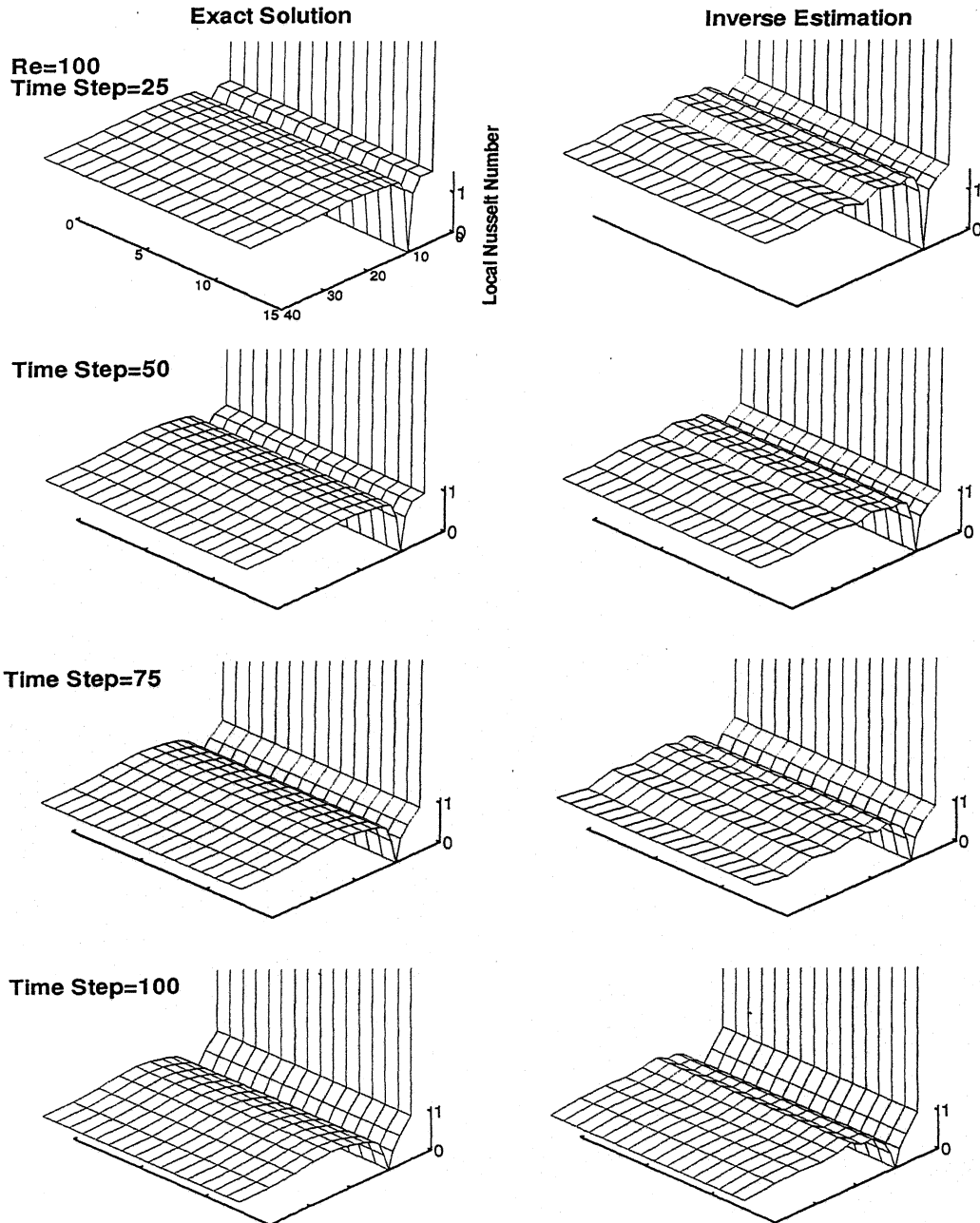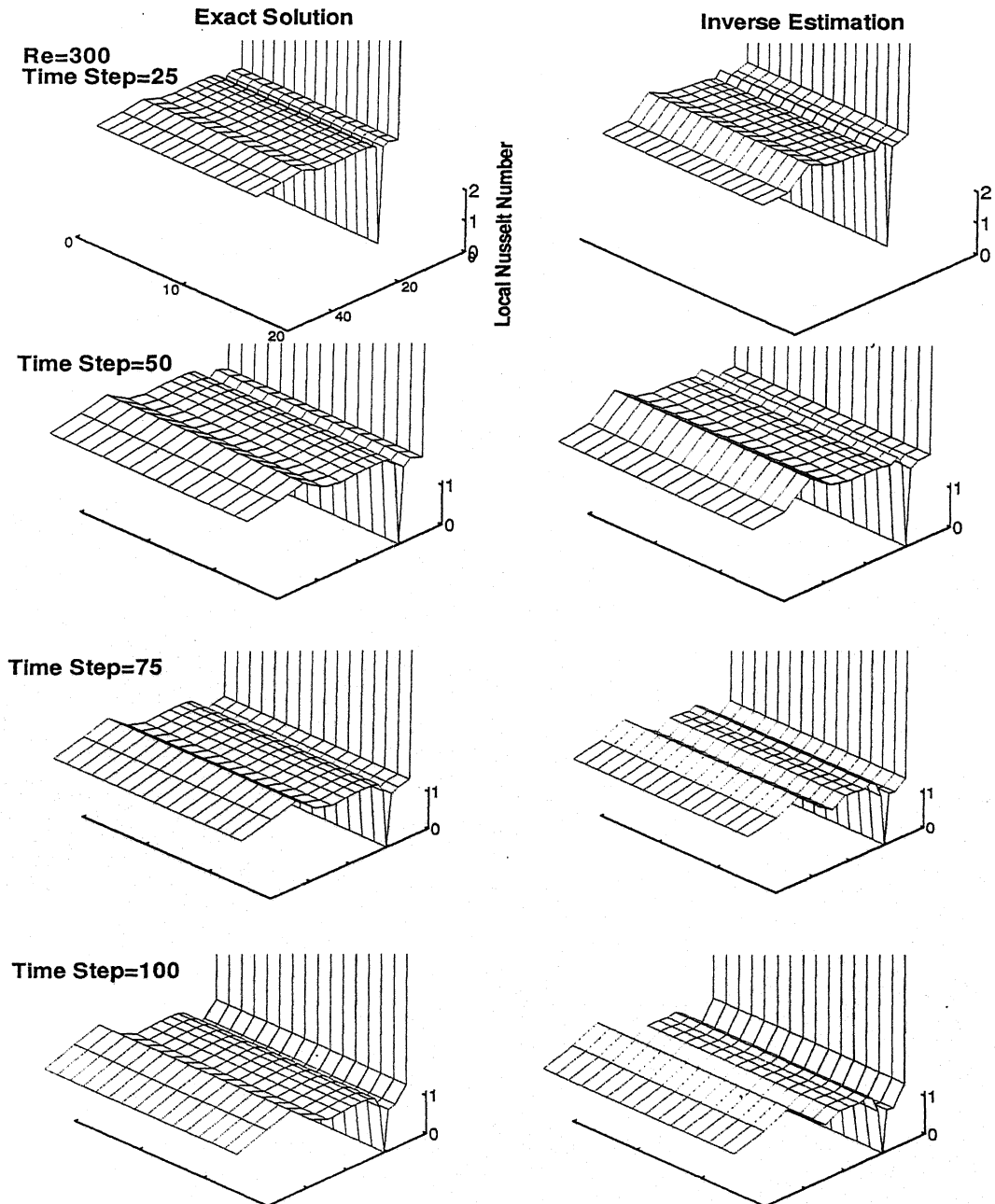
Figure 8.7: Comparison of inverse and direct solutions. Scatter in plate temperature is $\sigma=0.5$. Scatter in interior temperature is $\sigma=0.01$. Only 50% interior temperatures are available at $y = 0.01$. Velocity and temperature have been obtained from an elliptic formulation. The flow field is two dimensional with three dimensional temperature field.
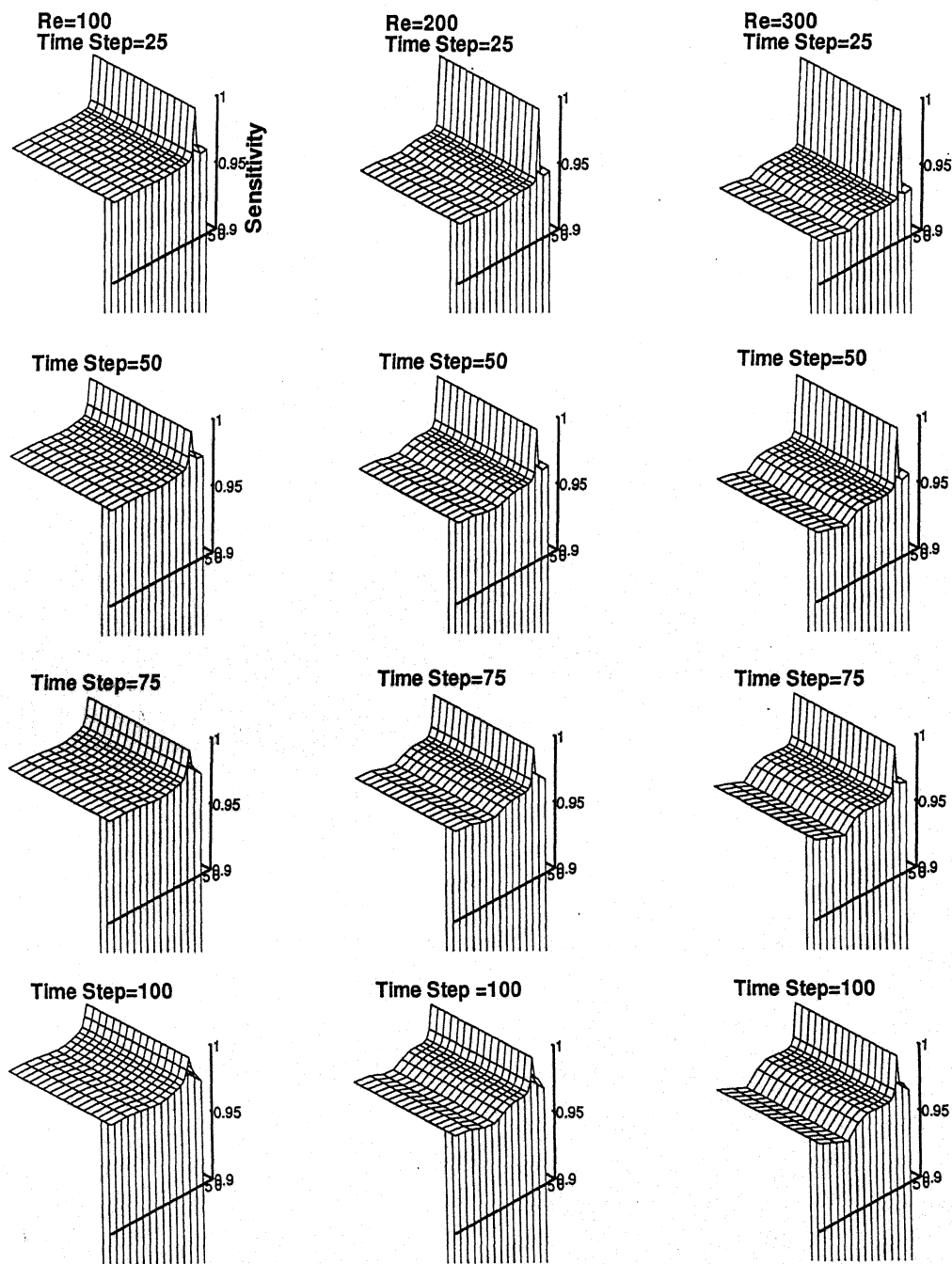
Figure 8.8: Variation in sensitivity coefficient with time and Reynolds number for inverse estimation of local Nusselt number over a ribbed surface.
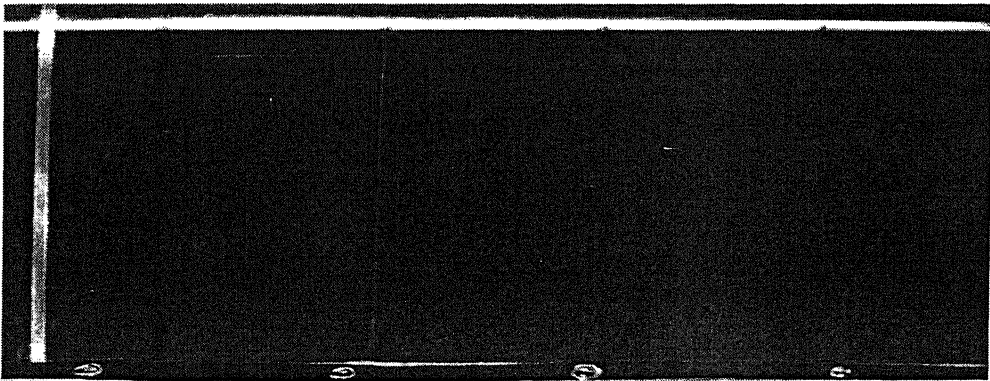
Figure 8.9: LCT image at time 0, Re=260.
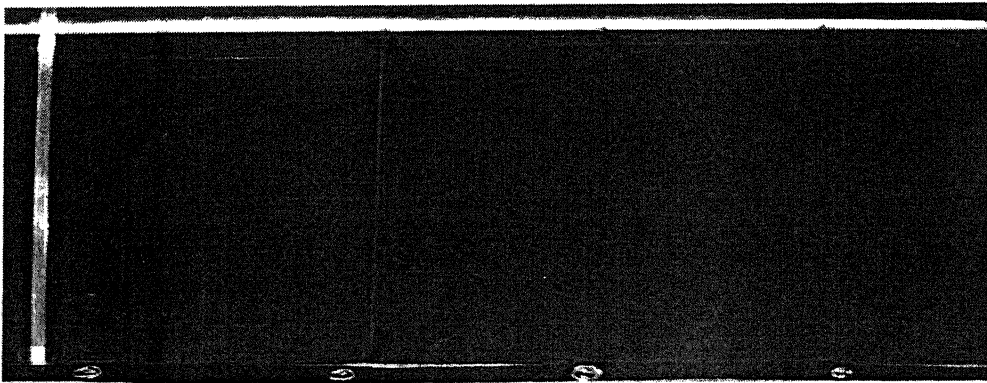
Figure 8.10: LCT image after 20 sec, Re=260.
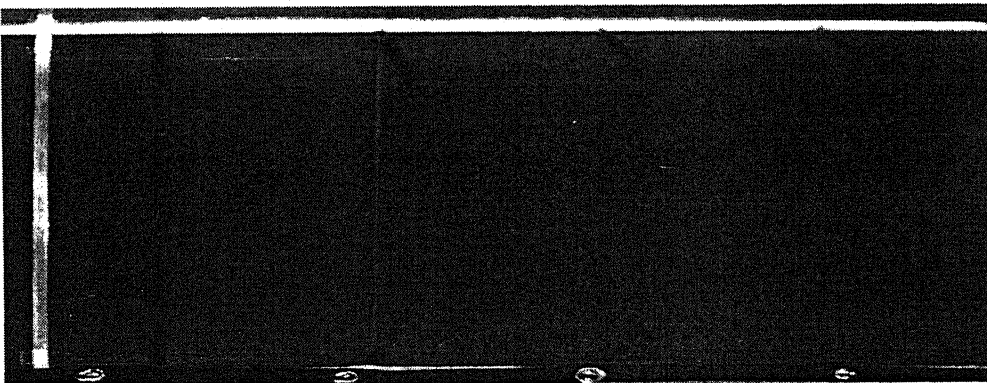
Figure 8.11: LCT image after 45 sec, Re=260.
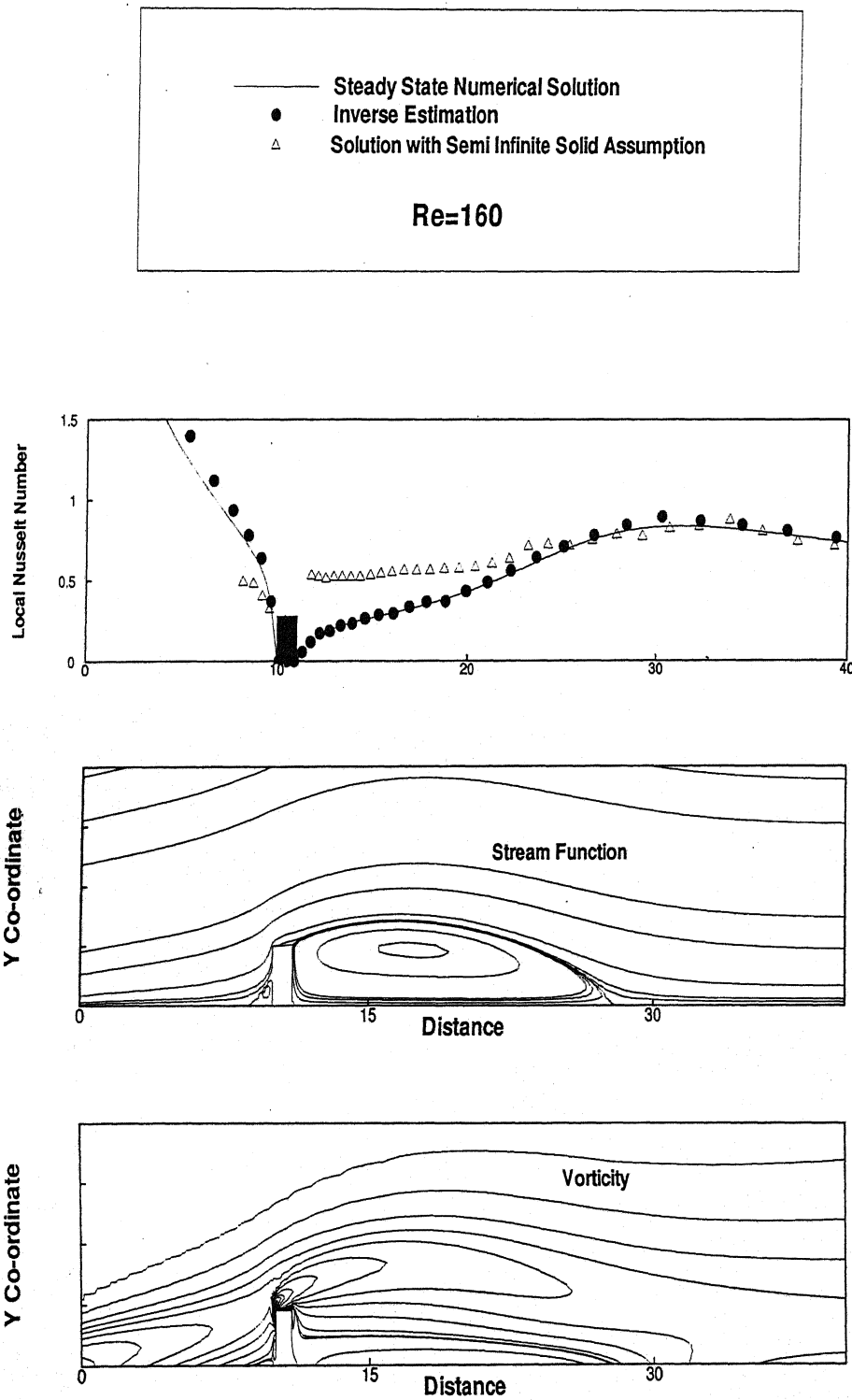
Figure 8.12: Local Nusselt number estimation using inverse technique with transient LCT data.
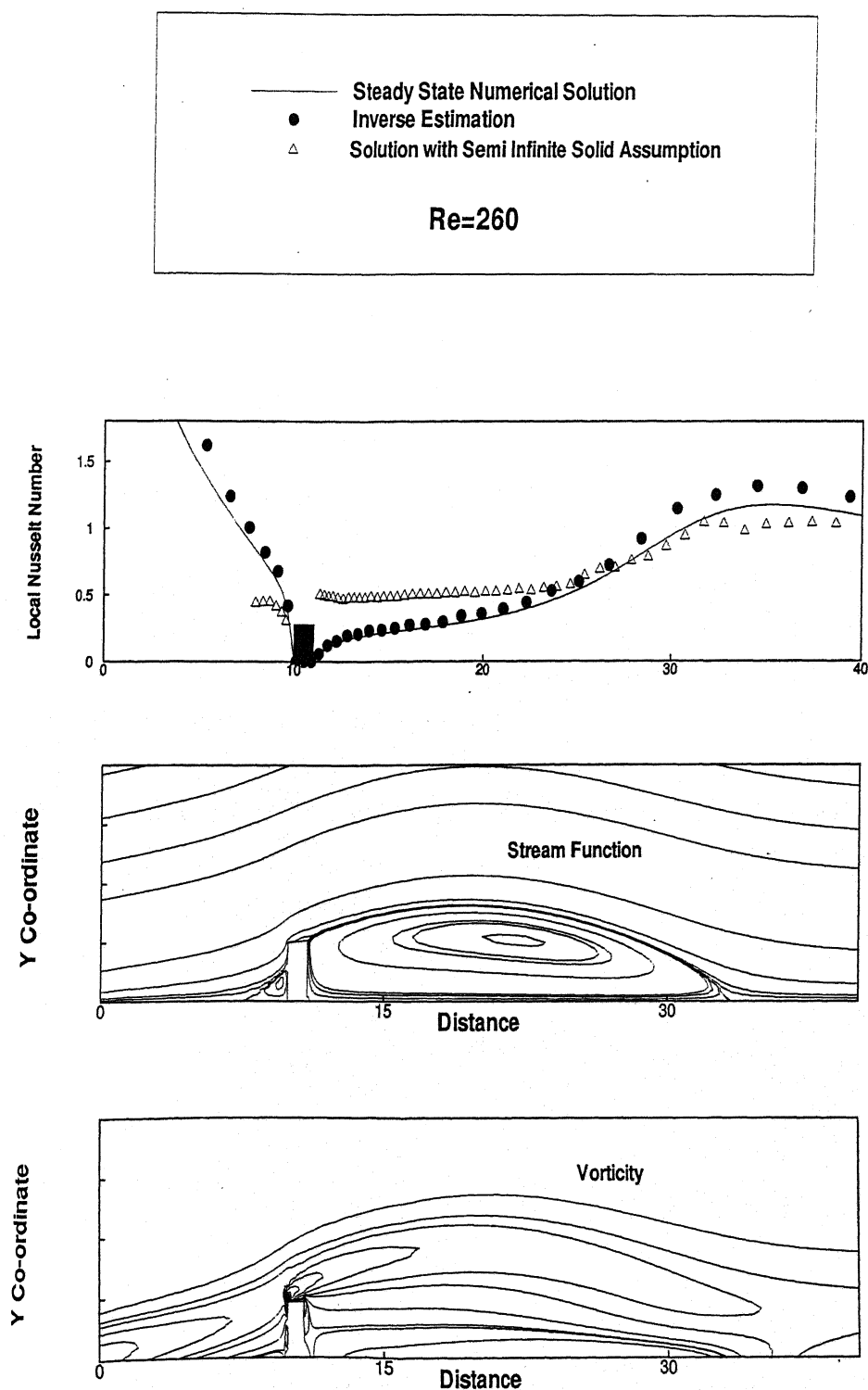
Figure 8. 13: Local Nusselt number estimation using inverse technique with transient LCT data.

Chapter 9

Conclusions and Scope for Future Work

9.1 Conclusion

An inverse function estimation technique for two and three dimensional forced convective heat transfer from a flat plate has been discussed in the present work. The focus of the research is towards determining the local Nusselt number distribution over the flat surface, and the effect of a surface mounted rib. The input to the calculation is the surface temperature variation as well as selected temperatures in the fluid phase. The study supports the conjugate gradient method as an efficient approach for the solution of inverse convection equations. The procedure also suppresses within limits the effect of initial guess in the final solution and scatter in the input data. Sensitivity study, required during the inverse procedure is seen to be a useful tool for designing an experiment.

The inverse forced convection modeling has also been found to be useful for extracting information from noisy experimental data. The results show that the tool is promising and deserves further exploration. Certain advantages and disadvantages are to be noted regarding the conjugate gradient approach:

Advantages

1. The procedure is accurate and the exact solution is realized if the data given is exact.

2. The procedure yields a qualitatively good prediction when noise in the

interior data is less than 0.1, namely 10%.

3. The technique subdues substantial surface temperature scatter (0.4) provided the interior data is of superior quality.

4. The number of iterations needs to minimize the functional is not high, mostly falling in the range of 3 to 50.

5. The procedure does not need *a priori* information about the unknown function, the Nusselt number in the present context.

Disadvantages

The computational cost increases rapidly with the increase of problem complexity, Reynolds number, problem dimensions and grid fineness. All computer programs were executed in a Pentium4 PC with 512 SDRAM. A comparison of CPU times is given in the following table (Reynolds number is 10000 for flat plate and 260 for the ribbed surface).

Formulation	CPU time
Two dimensional parabolic, flat plate	30 seconds
Three dimensional parabolic, flat plate	3 hours
Three dimensional elliptic, flat plate (upto 50 time steps)	2 days
Two dimensional elliptic, ribbed plate (upto 50 time steps)	4 days
Three dimensional elliptic, ribbed plate (upto 50 time steps)	9 days
Two dimensional elliptic, transient plate temperature, ribbed surface (upto 19000 time steps)	18 days

The CPU time needed for the velocity computations are not included in the above table. The CPU time for velocity computation varies from 60 seconds (for two dimensional parabolic problem) to 4 days (vorticity-stream function formulation).

9.2   Scope for Future Work

The present work has opened up new areas of exploration. Following challenges are recommended for future researchers.

1. An extensive assessment of the applicability of inverse forced convection techniques against life experiments.

2. The relative performance study of different inverse convection techniques in extracting useful informations from noisy experimental data.

3. Acceleration techniques to decrease the CPU time.

4. An inverse procedure for obtaining the skin friction coefficient from velocity data.

5. Identification of dynamic filters for transient problems.

References

[1] Alifanov, O. M., *Inverse Heat Transfer Problems*, Springer-Verlag, New York, 1994.

[2] Bakushinsky, A. and Goncharsky, A., *Ill-Posed Problems: Theory and Applications*, Kluwer Academic Publishers, netherlands, 1989.

[3] Beck, J. V., Blackwell, G. and Clair, C. R. St., *Inverse Heat Conduction: Ill-Posed problems*, Wiley, New York, 1985.

[4] Boer, J. B., Fische, D., *Interior Lighting*, Philips Tecnical Library, Kluwer Technical Books, New York, 1981.

[5] Burggraf, O. R., An Inverse Analysis For Estimating The Time-varying Inlet Temperature In Laminar Flow Inside A Parallel Plate Duct,*Int. J. Heat Mass Transfer*, Vol. 38, pp. 39-45, 1995.

[6] Camci, C., Kim, K. and Hippensteele, S. A., A New Hue Capturing Technique for the Quantitative Interpretation of Liquid Crystal Images Used in Convective Heat Transfer Studies, *ASME J. Turbomachinery*, Vol. 114, pp. 765-775, 1992.

[7] Chan, T. L., Ashforth-Frost, S. and Jambunathan, K., Calibrating for Viewing Angle Effect During Heat Transfer Measurements on a Curved Surface, *Int. J. Heat Mass Transfer*, Vol. 44, pp. 2209-2223, 2001.

[8] Colaco, M. J. and Orlande, H. R. B., Inverse Forced Convection Problem Of Simultaneous Estimation Of Two Boundary Heat Fluxes In Irregularly Shaped Channels, *Numerical Heat Transfer, Part A*, Vol. 39, pp. 737-760, 2001.

[9] Engl, H. W., Hanke, M. and Neubauer, A., *Regularization of Inverse Problems*, Kluwer Academic Publishers, netherlands, 1990.

[10] Farina, D. J., Ahcker, J. M., Moffat, J. and Eaton, J. K., Illumination Invariant Calibration of Thermochromic Liquid Crystals, *Exp. Therm. Fluid Sci.*, Vol. 9, pp. 1-12, 1994.

[11] Gartling, D. K., A Test Problem for Outflow Boundary Conditions - Flow over a Backward Facing Step, *International Journal for Numerical Methods in Fluids*, Vol. 11, pp. 953-967, 1990.

[12] Gilyazov, S. K. and Gol'dman, N. L., *Regularization of Ill-Posed Problems by Iteration Methods*, Kluwer Academic Publishers, netherlands, 2000.

[13] Glasko, V. B., *Inverse Problems of Mathematical Physics*, American Institute of Physics, New York, 1988.

[14] Hadamard, J., *Lectures on the Cauchy Problem in Linear Partial Differential Equations*, Yale University Press, New Haven, 1923.

[15] Hanke, M., *Conjugate Gradient Type Methods for Ill Posed Problems*, Longman Scientific and Technical, U.K., 1995.

[16] Huang, C. H. and Ozisik, M. N., Inverse Problem of Determining Unknown Wall Heat Flux in Laminar Flow Through a Parallel Plate Duct, *Numerical Heat Transfer, Part A*, Vol. 21, pp. 55-70, 1992.

[17] Huang, C. H. and Chen, W. C., A Three-Dimensional Inverse Forced Convection Problem In Estimating Surface Heat Flux By Conjugate Gradient Method, *Int. J. Heat Mass Transfer*, Vol. 43, pp. 3171-3181, 2000.

[18] Huang, C. H. and Wang, S. P., A Three-Dimensional Inverse Heat Conduction Problem In Estimating Surface Heat Flux By Conjugate Gradient Method, *Int. J. Heat Mass Transfer*, Vol. 42, pp. 3387-3403, 1999.

[19] Ireland, P. T. and Jones T. V., Response time of a surface thermometer employing encapsulated thermochromic liquid Crystals, *J. Phys.*, Vol. 20, pp. 1195-1199, 1987.

[20] Jarny, Y., Ozisik, M. N. and Bardon, J. P., A General Optimization Method Using Adjoint Equation For Solving Multidimensional Inverse Heat Conduction, *Int. J. Heat Mass Transfer*, Vol. 34, No. 11, pp. 2911-2919, 1991.

[21] Keller, J. B., Inverse Problems, *Am. Math. Mon.,*, Vol. 83, pp. 107-118, 1976.

[22] Khachfe R. A. and Jarney, Y., Numerical Solution Of 2-D Nonlinear Inverse Heat Conduction Problems Using Finite-Element Method, *Numerical Heat Transfer, Part B*, Vol. 37, pp. 45-67, 2000.

[23] Khalidy, N. A., A General Space Marching Algoritm Of Two-Dimensional Boundary Inverse Heat Conduction Problem, *Numerical Heat Transfer, Part B*, Vol. 34, pp. 339-360, 1998.

[24] Khalidy, N. A., On The Solution Of Parabolic And Hyperbolic Inverse Heat Conduction Problem, *Int. J. Heat Mass Transfer* , Vol. 41, pp. 3731-3740, 1998.

[25] Kirsch, A., *An Introduction to the Mathematical Theory of Inverse Problems*, Springer-Verlag, New York, 1996.

[26] Korn, G., Korn, T., *Mathematical Handbook For Scientists And Engineers*, McGraw-Hill Book Company, U.S.A., 1968.

[27] Kozodoba, L. A. and Krukovsky, P. G., *Methods for Solving Inverse Heat Transfer Problems*, Naukova Dumka, Kiev 1982.

[28] Kurpisz, K. and Nowak, A. J.,*Inverse Thermal Problems*, Computational Mechanics Publications, Southampton, U.K., 1995.

[29] Leonard, B. P., Stability of Explicit Advection Schemes. The Balance Point Location Rule,*International Journal For Numerical Methods in Fluids*, Vol. 38, pp. 471-514, 2002.

[30] Leung, C. W., Chen, S. and Jarney, Y., Numerical Simulation of Laminar Forced Convection of Laminar Forced Convection in an Air-Cooled Hori-

zontal Printed Circuit Board Assembly, *Numerical Heat Transfer, Part A*, Vol. 37, pp. 373-393, 2000.

[31] Li, H. Y. and Yan, W. M., Inverse Convection Problem For Determining Wall Heat Flux In Annular Duct Flow, *ASME Journal of Heat Transfer*, Vol. 122, pp. 460-464, 2000.

[32] Lin, M. and Wang, T., A Transient Liquid Crystal Method Using a 3-D Inverse Transient Conduction Scheme, *Int. J. Heat Mass Transfer*, Vol. 45, pp. 3491-3501, 2002.

[33] Minkowycz, W. J., Sparrow, B. M., Scheider, G. E., Pletcher, R. H., *Handbook of Numerical Heat Transfer*, J. Wiley & Sons Inc., U.S.A., 1988.

[34] Moutsoglou, A., An Inverse Convection Problem, *Journal of Heat Transfer*, Vol. 111, pp. 37-43, 1989.

[35] Moutsoglou, A., Solution of An Elliptic Inverse Convection Problem Using a Whole Domain Regularization Technique, *J. Thermophysics*, Vol. 4, pp. 341-349, 1990.

[36] Ozisik, M. N. and Orlande, H. R. B., *Inverse Heat Transfer: Fundamentals and Applications*, Taylor and Francis, New York, 2000.

[37] Peyret, R. and Taylor, T. D., *Computational Methods for Fluid Flow*, Springer-Verlag, New York, 1983.

[38] Press, W. H., Tukolsky, S. A., Vetterling, W. T. and Flannery, B. P., *Numericals Recipes in FORTRAN*, Cambridge University Press, India, 2000.

[39] Taler, J. and Zima, W., Solution of Inverse Heat Conduction Problems Using Control Volume Approach, *Int. Comm. Heat Mass Transfer*, Vol.42, pp. 1123-1140, 1999.

[40] Roche, P. J., *Computational Fluid Dynamics*, Hermosa Publishers, Albuquerque, 1976.

[41] Tannehill, J. C., Anderson, D. A. and Pletcher, R. H., *Computational Fluid Mechanics and Heat Transfer*, Second Edition, Taylor & Francis, Washington, 1997.

[42] Tariq, A. and Panigrahi, P. K., Flow and Heat Transfer in a Rectangular Duct with Single-rib and Two-ribs Mounted on the Bottom Surface, *Journal of Enhanced Heat Transfer*, in press.

[43] Tikonov, A. N., Goncharsky, A. V., Stepanov, V. V. and Yagola, A. G., *Numerical Methods for the Solution of Ill-Posed Problems*, Kluwer Academic Publishers, Netherlands, 1990.

Appendix A

Discretization and Numerical Algorithm

A.1 Solution of Velocity Field

In the present work steady, laminar two-dimensional flow of incompressible, Newtonian fluid is addressed. Two different solution methodologies have been applied for computing the velocity field.

1. Two dimensional boundary-layer approximation.

2. Vorticity - stream function formulation.

The appropriate differential equations have been solved by the method of finite differences. The numerical solution has been developed on uniform and non-uniform grids.

A.1.1 Two Dimensional Boundary Layer Flow

Recalling the formulation presented in Chapter 3, we have the following governing equations for a flat plate boundary-layer:

$$\frac{\partial u}{\partial x} + \frac{\partial v}{\partial y} = 0 \tag{A.1}$$

$$\frac{\partial (u^2)}{\partial x} + \frac{\partial (uv)}{\partial y} = \frac{1}{\text{Re}} \frac{\partial^2 u}{\partial y^2} \tag{A.2}$$

The boundary conditions are:

$$x = 0, \ u = 1, \ v = 0 \tag{A.3}$$

Figure A.1: Flow over a Flat Plate
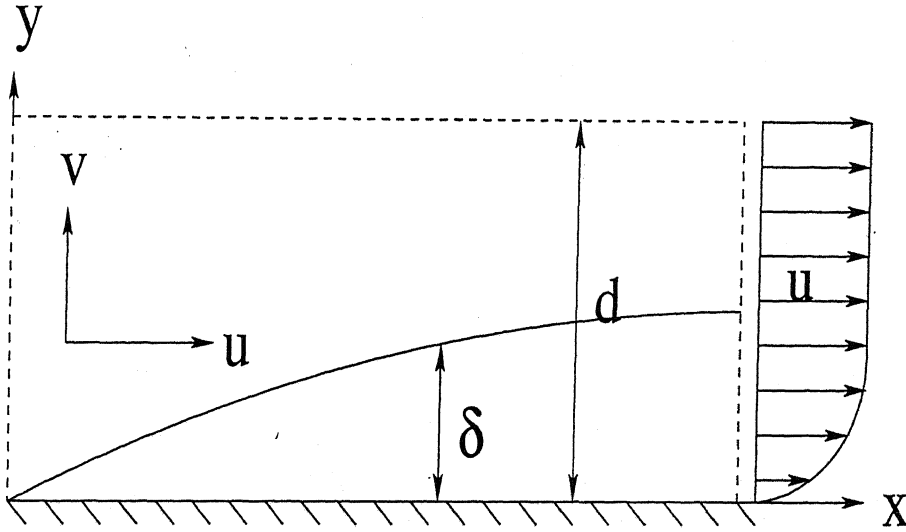
$$y = 0, \ u = 0, \ v = 0 \qquad\qquad (A.4)$$

$$y = d, \ u = 1 \qquad\qquad (A.5)$$

The momentum equation is solved by the Crank-Nicolson scheme, using central-difference discretization for both advection and diffusion terms. Hence

$$\frac{(u^2)_j^{i+1} - (u^2)_j^i}{\Delta x} + \frac{1}{2}\left[\frac{(uv)_{j+1}^{i+1} - (uv)_{j-1}^{i+1}}{2\Delta y} + \frac{(uv)_{j+1}^i - (uv)_{j-1}^i}{2\Delta y}\right] =$$
$$\frac{1}{2\mathrm{Re}}\left(\frac{u_{j+1}^{i+1} - 2u_j^{i+1} + u_{j-1}^{i+1}}{\Delta y^2} + \frac{u_{j+1}^i - 2u_j^i + u_{j-1}^i}{\Delta y^2}\right) \qquad (A.6)$$

This leads to a tridiagonal system of equations:

$$Au_{j-1}^{i+1} + Bu_j^{i+1} + Cu_{j+1}^{i+1} = D \qquad\qquad (A.7)$$

with the following boundary conditions (Figure A.1)

$$y = 0, \ u_j^{i+1} = 0 \qquad\qquad (A.8)$$

$$y = d, \ u_j^{i+1} = 1 \qquad\qquad (A.9)$$

The coefficients in Equation A.7 are

$$A = -\frac{v_{j-1}^{i+1}}{4\Delta y} - \frac{1}{2\mathrm{Re}\Delta y^2} \qquad\qquad (A.10)$$

$$B = \frac{u_j^{i+1}}{\Delta x} + \frac{1}{\mathrm{Re}\Delta y^2} \qquad\qquad (A.11)$$

$$C = \frac{v_{j+1}^{i+1}}{4\Delta y} - \frac{1}{2\text{Re}\Delta y^2} \tag{A.12}$$

$$D = \frac{(u^2)_j^i}{\Delta x} - \frac{1}{4}\left[\frac{(uv)_{j+1}^i - (uv)_{j-1}^i}{\Delta y}\right] + \frac{1}{2\text{Re}}\left(\frac{u_{j+1}^i - 2u_j^i + u_{j-1}^i}{\Delta y^2}\right) \tag{A.13}$$

From the continuity equation, we can determine the y component of velocity as

$$v = -\frac{\partial}{\partial x}\int u\,dy \tag{A.14}$$

In finite difference form,

$$v_j^{i+1} = \frac{-3\left[\int_1^j u\,dy\right]_i + 4\left[\int_1^j u\,dy\right]_{i-1} - \left[\int_1^j u\,dy\right]_{i-2}}{2\Delta x} \tag{A.15}$$

For $i = 1$

$$v_j^{i+1} = \frac{-\left[\int_1^j u\,dy\right]_i + \left[\int_1^j u\,dy\right]_{i-1}}{\Delta x} \tag{A.16}$$

and

$$y = 0, \quad v_j^{i+1} = 0 \tag{A.17}$$

Thus knowing the values of u and v at the i-th position, we can find the values of u and v at the $i+1$-th position. However, the non-linearity and the coupling of the above equations leads to an iterative solution comprising of the following steps:

1. Set $i = 1$ and assign u^i and v^i for all j from the given initial condition.

2. Compute D.

3. Assign iteration counter $k = 0$ and set$[u^{i+1}]^k = u^i$, $[v^{i+1}]^k = v^i$.

4. Set $u^{i+1} = [u^{i+1}]^k$ and $v^{i+1} = [v^{i+1}]^k$ for all j to compute A, B, C

5. Solve the tridiagonal system of equations using Thomas algorithm to find u^{i+1} for all j.

6. Find v^{i+1} for all j using Equation A.13 or A.14.

7. Set $[u^{i+1}]^{k+1} = u^{i+1}$ and $[v^{i+1}]^{k+1} = v^{i+1}$ for all j.

8. Compute the global convergence quantity J

$$J = \sum_{j=1}^{j=n} \left(\left[(u_j^{i+1})^k - (u_j^{i+1})^{k+1} \right]^2 + \left[(v_j^{i+1})^k - (v_j^{i+1})^{k+1} \right]^2 \right)$$

9. If $J < \epsilon$ (ϵ is a small real number close to zero),
   set $u^{i+1} = [u^{i+1}]^{k+1}$ and $v^{i+1} = [v^{i+1}]^{k+1}$

10. Else, set $k = k + 1$ and go to 4.

11. Set $i = i + 1$ and go to 2.

A.1.2   Vorticity - Stream Function Formulation
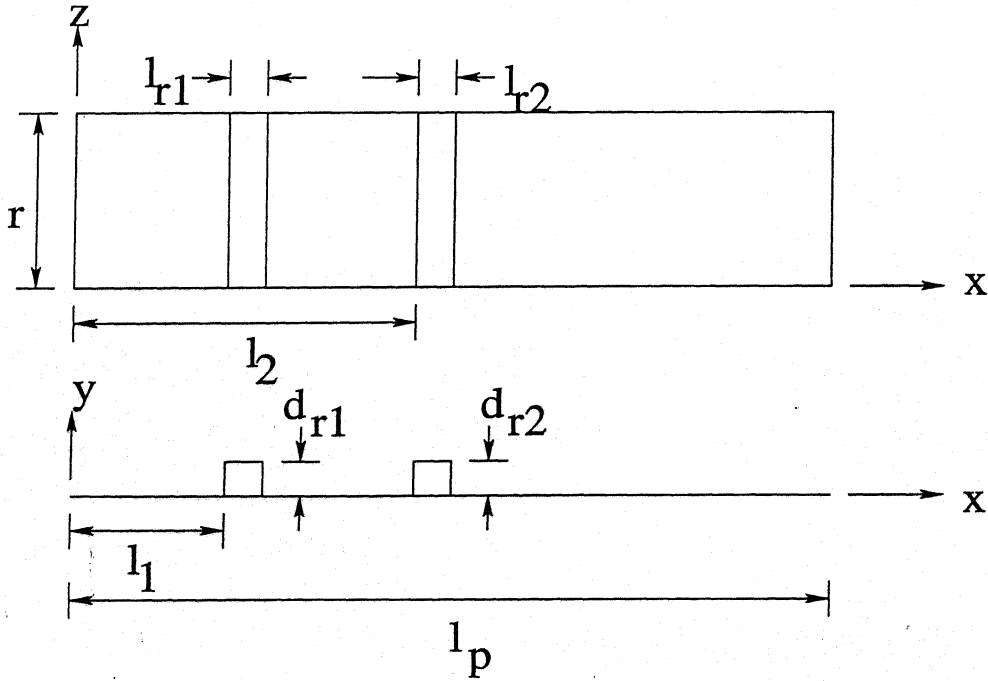
Figure A.2: Plate with Single Rib

Recalling the formulation presented in Chapter 4, we have the following governing equations for steady, two dimensional, incompressible flow:

$$\frac{\partial \omega}{\partial t} + \frac{\partial (u\omega)}{\partial x} + \frac{\partial (v\omega)}{\partial y} = \frac{1}{\text{Re}} \left(\frac{\partial^2 \omega}{\partial x^2} + \frac{\partial^2 \omega}{\partial y^2} \right) \tag{A.18}$$

$$\frac{\partial^2 \psi}{\partial x^2} + \frac{\partial^2 \psi}{\partial y^2} = -\omega \tag{A.19}$$

$$u = \frac{\partial \psi}{\partial y} \tag{A.20}$$

$$v = -\frac{\partial \psi}{\partial x} \tag{A.21}$$

For a surface mounted rib (Figure A.2) the initial and boundary conditions are:

$$t = 0, \ \omega = 0, \ \psi = y, \ u = 1, \ v = 0 \tag{A.22}$$

$$x = 0, \ \omega = 0, \ \psi = y, \ u = 1, \ v = 0 \tag{A.23}$$

$$x = l_p, \ \frac{\partial \omega}{\partial x} = 0, \ \frac{\partial^2 \psi}{\partial x^2} = 0, \ \frac{\partial u}{\partial x} = 0, \ \frac{\partial v}{\partial x} = 0 \tag{A.24}$$

$$y = 0, \ \omega = -\nabla^2 \psi, \ \psi = 0, \ u = 0, \ v = 0 \tag{A.25}$$

$$y = d, \ \omega = -\nabla^2 \psi, \ \psi = y, \ u = 1 \tag{A.26}$$

$$x = l_1, \text{ and } y \le d_{r1}, \ \omega = -\nabla^2 \psi, \ \psi = 0, \ u = 0, \ v = 0 \tag{A.27}$$

$$x = l_1 + l_{r1}, \text{ and } y \le d_{r1}, \ \omega = -\nabla^2 \psi, \ \psi = 0, \ u = 0, \ v = 0 \tag{A.28}$$

$$x < l_1 + l_{r1}, \text{ and } x > l_1, \text{ and } y = d_{r1}, \ \omega = -\nabla^2 \psi, \ \psi = 0, \ u = 0, \ v = 0 \tag{A.29}$$

For nodes falling within the rib

$$x \le l_1 + l_{r1}, \text{ and } x \ge l_1, \text{ and } y \le d_{r1}, \ u = 0, \ v = 0 \tag{A.30}$$

An explicit time-marching scheme is applied for the vorticity transport equation. The Poisson equation for the stream function is solved in each time step using Gauss-Seidel iterative method with successive over-relaxation. The convective terms are discretized by QUICK scheme (Quadratic Upstream Interpolation for Convective Kinematics) [Leonard, 2002, Minkowycz et al., 1988] and central differencing has been used for the diffusion terms.

The discretized form of the vorticity transport equation can be expressed as follows. The following notation has been employed: superscripts and subscripts denote time and space co-ordinates respectively

$$
\begin{aligned}
\omega_{i,j}^{n+1} &= \omega_{i,j}^n + \Delta t \left[\frac{1}{\text{Re}} \left(\frac{\omega_{i+1,j}^n - 2\omega_{i,j}^n + \omega_{i-1,j}^n}{\Delta x^2} + \frac{\omega_{i,j+1}^n - 2\omega_{i,j}^n + \omega_{i,j-1}^n}{\Delta y^2} \right) \right] \\
&\quad - \Delta t \left(\frac{u_{i+\frac{1}{2},j}^n \omega_{i+\frac{1}{2},j}^n - u_{i-\frac{1}{2},j}^n \omega_{i-\frac{1}{2},j}^n}{\Delta x} + \frac{u_{i,j+\frac{1}{2}}^n \omega_{i,j+\frac{1}{2}}^n - u_{i,j-\frac{1}{2}}^n \omega_{i,j-\frac{1}{2}}^n}{\Delta y} \right)
\end{aligned} \tag{A.31}
$$

The boundary conditions for the surface mounted rib geometry are

$$x = 0, \quad \omega_{i,j}^{n+1} = 0 \tag{A.32}$$

$$x = l_p, \quad \omega_{i,j}^{n+1} = \frac{4\omega_{i-1,j}^{n+1} - \omega_{i-2,j}^{n+1}}{3} \tag{A.33}$$

$$y = 0, \quad \omega_{i,j}^{n+1} = -\frac{\psi_{i,j+1}^{n+1}}{(\Delta y)^2} \tag{A.34}$$

$$y = d, \quad \omega_{i,j}^{n+1} = -\frac{\left(\psi_{i+1,j}^{n+1} - 2\psi_{i,j-1}^{n+1} + \psi_{i-1,j}^{n+1}\right)}{(\Delta x)^2} \tag{A.35}$$

$$x = l_1, \text{ and } y \leq d_{r1}, \quad \omega = -\frac{\psi_{i-1,j}^{n+1}}{(\Delta x)^2} \tag{A.36}$$

$$x = l_1 + l_{r1}, \text{ and } y \leq d_{r1}, \quad \omega_{i,j}^{n+1} = -\frac{\psi_{i+1,j}^{n+1}}{(\Delta x)^2} \tag{A.37}$$

$$x < l_1 + l_{r1}, \text{ and } x > l_1, \text{ and } y = d_{r1}, \quad \omega^{n+1}i,j = -\frac{\psi_{i,j+1}^{n+1}}{(\Delta y)^2} \tag{A.38}$$

The stream function equation can be discretized as

$$\frac{\psi_{i+1,j}^{n+1} - 2\psi_{i,j}^{n+1} + \psi_{i-1,j}^{n+1}}{(\Delta x)^2} + \frac{\psi_{i,j+1}^{n+1} - 2\psi_{i,j}^{n+1} + \psi_{i,j-1}^{n+1}}{(\Delta y)^2} = -\omega_{i,j}^{n+1} \tag{A.39}$$

The Poisson equation is solved within every time step for the stream function. The appropriate boundary conditions are:

$$\text{For uniform incoming flow } x = 0, \quad \psi_{i,j}^{n+1} = y \tag{A.40}$$

$$x = l_p, \quad \psi_{i,j}^{n+1} = 2\psi_{i-1,j}^{n+1} - \psi_{i-2,j}^{n+1} \tag{A.41}$$

$$y = 0, \quad \psi_{i,j}^{n+1} = 0 \tag{A.42}$$

$$y = d, \quad \psi_{i,j}^{n+1} - \psi_{i,j-1}^{n+1} = dy \tag{A.43}$$

$$x = l_1, \text{ and } y \leq d_{r1}, \quad \psi_{i,j}^{n+1} = 0 \tag{A.44}$$

$$x = l_1 + l_{r1}, \text{ and } y \leq d_{r1}, \quad \psi_{i,j}^{n+1} = 0 \tag{A.45}$$

$$x < l_1 + l_{r1}, \text{ and } x > l_1, \text{ and } y = d_{r1}, \quad \psi_{i,j}^{n+1} = 0 \tag{A.46}$$

After computing the values of the stream function, the velocity components can be found from the following expressions:

$$u_{i,j}^{n+1} = \frac{\psi_{i,j+1}^{n+1} - \psi_{i,j-1}^{n+1}}{2\Delta y} \tag{A.47}$$

$$v_{i,j}^{n+1} = \frac{\psi_{i-1,j}^{n+1} - \psi_{i+1,j}^{n+1}}{2\Delta x} \tag{A.48}$$

$$x = 0, \ u_{i,j}^{n+1} = 1, \ v_{i,j}^{n+1} = 0 \tag{A.49}$$

$$x = l_p, \ u_{i,j}^{n+1} = \frac{4u_{i-1,j}^{n+1} - u_{i-2,j}^{n+1}}{3}, \ v_{i,j}^{n+1} = \frac{4v_{i-1,j}^{n+1} - v_{i-2,j}^{n+1}}{3} \tag{A.50}$$

$$y = 0, \ u_{i,j}^{n+1} = 0, \ v_{i,j}^{n+1} = 0 \tag{A.51}$$

$$y = d, \ u_{i,j}^{n+1} = 1 \tag{A.52}$$

$$x \leq l_1 + l_{r1}, \ \text{and} \ x \geq l_1, \ \text{and} \ y \leq d_{r1}, \ u_{i,j}^{n+1} = 0, \ v_{i,j}^{n+1} = 0 \tag{A.53}$$

The sequence of calculations for obtaining the velocity distribution has the following steps:

1. Specify initial values for ω and ψ at time $t = 0$

2. Find u and v at $t = 0$

3. Solve the vorticity transport equation for ω at all interior points at the next time step.

4. Solve Poisson equation for stream function within the time step.

5. Find the velocity components $u = \psi_y$ and $v = -\psi_x$.

6. Determine the values of ω at the boundaries.

7. Return to step 2 for the next time step.

A.2   Solution of Energy Equation

In the present work, forced convection alone from the heated wall to the fluid has been considered. Three different strategies have been applied for the solution of the energy equation.

1. Steady solution with two dimensional boundary-layer approximation.

2. Steady solution with three-dimensional boundary layer approximation.

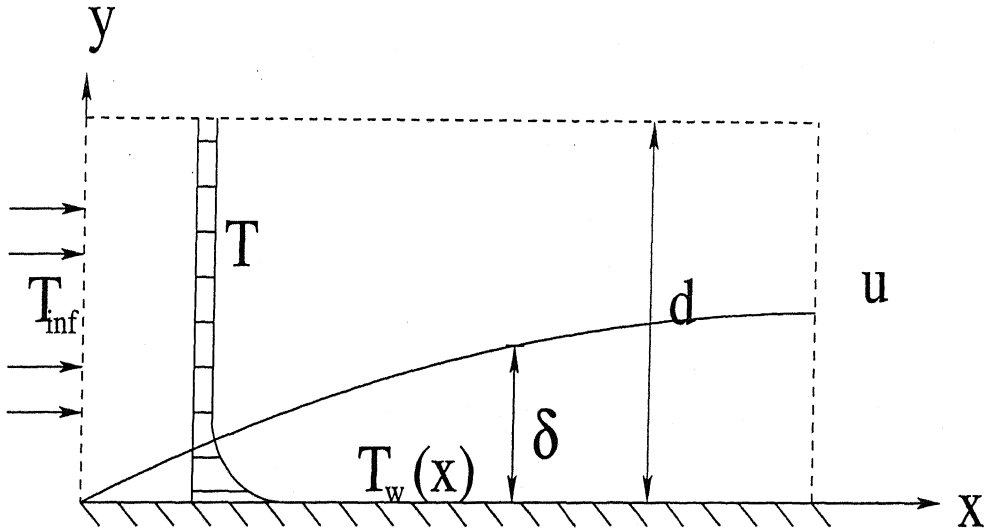3. Unsteady solution of the elliptic form of the energy equation.

Figure A.3: Heat Transfer over a Flat Plate

All the three methodologies have been applied to the flat plate geometry; only the third one is applicable for the ribbed plate. Finite difference method of discretization has been used to solve the differential equations. Both uniform and non-uniform grids are used.

A.2.1 Two Dimensional Boundary Layer Solution

Recalling the formulation presented in Chapter 3, we have the following governing equation for heat transfer from a heated flat plate:

$$\frac{\partial(u\theta)}{\partial x} + \frac{\partial(v\theta)}{\partial y} = \frac{1}{\text{Pe}}\frac{\partial^2\theta}{\partial y^2} \tag{A.54}$$

The boundary conditions are:

$$x = 0, \ \theta = 0 \tag{A.55}$$

$$y = 0, \ \frac{\partial\theta}{\partial y} = -\text{Nu} \tag{A.56}$$

$$y = d, \ \theta = 0 \tag{A.57}$$

where Nu is the Local Nusselt number.

The equation is solved by the Crank-Nicolson scheme, using central differences

for both advection and diffusion terms. Thus

$$\frac{(u\theta)_j^{i+1} - (u\theta)_j^i}{\Delta x} + \frac{1}{2}\left[\frac{(v\theta)_{j+1}^{i+1} - (v\theta)_{j-1}^{i+1}}{2\Delta y} + \frac{(v\theta)_{j+1}^i - (v\theta)_{j-1}^i}{2\Delta y}\right] =$$
$$\frac{1}{2\text{Pe}}\left(\frac{\theta_{j+1}^{i+1} - 2\theta_j^{i+1} + \theta_{j-1}^{i+1}}{\Delta y^2} + \frac{\theta_{j+1}^i - 2\theta_j^i + \theta_{j-1}^i}{\Delta y^2}\right) \quad \text{(A.58)}$$

This leads to a triadiagonal system of equation:

$$A\theta_{j-1}^{i+1} + B\theta_j^{i+1} + C\theta_{j+1}^{i+1} = D \qquad \text{(A.59)}$$

with the following boundary conditions (A.3)

$$y = 0, \ \theta_j^{i+1} = 1 \qquad \text{(A.60)}$$

$$y = d, \ \theta_j^{i+1} = 0 \qquad \text{(A.61)}$$

The coefficients of Equation A.59 are

$$A = -\frac{v_{j-1}^{i+1}}{4\Delta y} - \frac{1}{2\text{Pe}\Delta y^2} \qquad \text{(A.62)}$$

$$B = \frac{u^{i+1} - j}{\Delta x} + \frac{1}{\text{Pe}\Delta y^2} \qquad \text{(A.63)}$$

$$C = \frac{v_{j+1}^{i+1}}{4\Delta y} - \frac{1}{2\text{Pe}\Delta y^2} \qquad \text{(A.64)}$$

$$D = \frac{(u\theta)_j^i}{\Delta x} - \frac{1}{4}\left[\frac{(v\theta)_{j+1}^i - (v\theta)_{j-1}^i}{\Delta y}\right] + \frac{1}{2\text{Pe}}\left(\frac{\theta_{j+1}^i - 2\theta_j^i + \theta_{j-1}^i}{\Delta y^2}\right) \quad \text{(A.65)}$$

The above tridiagonal system of equation is solved by Thomas algorithm. Thus knowing the i-th values of θ, the $i+1$-th values of θ can be computed. The complete algorithm for the temperature field computations is as follows:

1. Set $i = 1$ and assign θ^i for all j from the given initial condition.

2. Compute coefficients A, B, C, D.

3. Solve the tridiagonal system of equations (A.59-A.60) using Thomas algorithm to find θ^{i+1} for all j.

4. Set $i = i + 1$ and go to 2.

A.2.2   Three Dimensional Boundary Layer Solution

Recalling the formulation presented in Chapter 3, we have the following governing equation for steady three dimensional flat plate boundary layer:

$$\frac{\partial(u\theta)}{\partial x} + \frac{\partial(v\theta)}{\partial y} = \frac{1}{\text{Pe}}\left(\frac{\partial^2\theta}{\partial y^2} + \frac{\partial^2\theta}{\partial z^2}\right) \tag{A.66}$$

The boundary conditions are:

$$x = 0, \ \theta = 0 \tag{A.67}$$

$$y = 0, \ \frac{\partial\theta}{\partial y} = -\text{Nu} \tag{A.68}$$

$$y = d, \ \theta = 0 \tag{A.69}$$

$$z = 0, \ \frac{\partial\theta}{\partial z} = 0 \tag{A.70}$$

$$z = r, \ \frac{\partial\theta}{\partial z} = 0 \tag{A.71}$$

where Nu is the Local Nusselt number. In the inverse calculation, the local values of Nusselt number are updated iteratively.

The equation is solved by the ADI scheme. The discretized form of the governing equation is as follows:

For i to $i + \frac{1}{2}$:

$$\frac{(u\theta)_{j,k}^{i+\frac{1}{2}} - (u\theta)_{j,k}^{i}}{\frac{\Delta x}{2}} + \frac{(v\theta)_{j+1,k}^{i+\frac{1}{2}} - (u\theta)_{j-1,k}^{i+\frac{1}{2}}}{2\Delta y} =$$

$$\frac{1}{\text{Pe}}\left[\frac{\theta_{j+1,k}^{i+\frac{1}{2}} - 2\theta_{j,k}^{i+\frac{1}{2}} + \theta_{j-1,k}^{i+\frac{1}{2}}}{(\Delta y)^2} + \frac{\theta_{j,k+1}^{i} - 2\theta_{j,k}^{i} + \theta_{j,k-1}^{i}}{(\Delta z)^2}\right] \tag{A.72}$$

For $i + \frac{1}{2}$ to $i + 1$:

$$\frac{(u\theta)_{j,k}^{i+1} - (u\theta)_{j,k}^{i+\frac{1}{2}}}{\frac{\Delta x}{2}} + \frac{(v\theta)_{j+1,k}^{i+\frac{1}{2}} - (u\theta)_{j-1,k}^{i+\frac{1}{2}}}{2\Delta y} =$$

$$\frac{1}{\text{Pe}}\left[\frac{\theta_{j+1,k}^{i+\frac{1}{2}} - 2\theta_{j,k}^{i+\frac{1}{2}} + \theta_{j-1,k}^{i+\frac{1}{2}}}{(\Delta y)^2} + \frac{\theta_{j,k+1}^{i+1} - 2\theta_{j,k}^{i+1} + \theta_{j,k-1}^{i+1}}{(\Delta z)^2}\right] \tag{A.73}$$

Equation A.72 produces tridiagonal system of equation in the y direction. For the frame at $i + \frac{1}{2}$ we can have the solution by sweeping in the z direction and
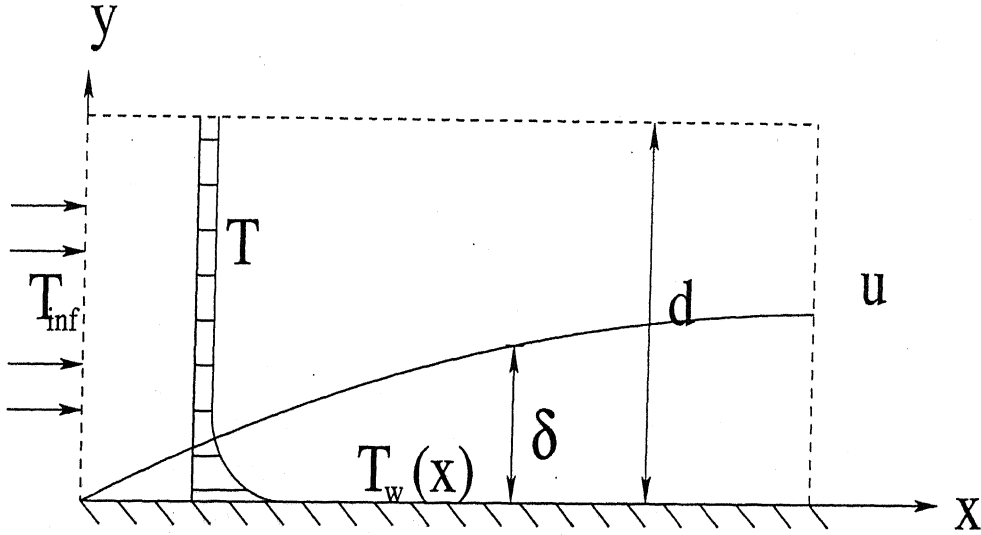
Figure A.4: Heat Transfer over a Flat Plate

solving tridiagonal matrix at each z location. Similarly, Equation A.73 produces a tridiagonal system of equation in the z direction. So for the frame at $i+1$ we can have the solution by sweeping in y direction and solving tridiagonal system of equation at each y location.

A.2.3   Unsteady Energy Equation Solution

Recall the formulation presented in Chapter 3, we have the following governing equation for unsteady three dimensional flow over a heated surface (Figure A.2, A.4).

$$\frac{\partial \theta}{\partial t} + \frac{\partial (u\theta)}{\partial x} + \frac{\partial (v\theta)}{\partial y} = \frac{1}{\text{Pe}} \left(\frac{\partial^2 \theta}{\partial x^2} + \frac{\partial^2 \theta}{\partial y^2} + \frac{\partial^2 \theta}{\partial z^2} \right) \tag{A.74}$$

The initial and boundary conditions for the geometry of Figure A.2 are:

$$t = 0, \ \theta = 0 \tag{A.75}$$

$$x = 0, \ \frac{\partial \theta}{\partial x} = 0 \tag{A.76}$$

$$x = 1, \ \theta = 0 \tag{A.77}$$

$$y = 0, \ \frac{\partial \theta}{\partial y} = -\text{Nu} \tag{A.78}$$

$$y = d, \ \theta = 0 \tag{A.79}$$

$$z = 0, \ \frac{\partial \theta}{\partial z} = 0 \tag{A.80}$$

$$z = r, \ \frac{\partial \theta}{\partial z} = 0 \tag{A.81}$$

where Nu represents the local Nusselt number distribution over the heated boundary.

A fully implicit finite difference procedure has been employed. The convective terms are discretized bu the QUICK[33,29] algorithm. Central differencing has been applied for the diffusion terms. The discretized form of the governing equation is as follows:

$$\frac{u_{i,j,k}^{n+1} - u_{i,j,k}^{n}}{dt} + \frac{(u\theta)_{i+\frac{1}{2},j,k}^{n+1} - (u\theta)_{i-\frac{1}{2},j,k}^{n+1}}{\Delta x} + \frac{(v\theta)_{i,j+\frac{1}{2},k}^{n+1} - (v\theta)_{i,j-\frac{1}{2},k}^{n+1}}{\Delta y} =$$
$$\frac{\theta_{i+1,j,k}^{n+1} - 2\theta_{i,j,k}^{n+1} + \theta_{i-1,j,k}^{n+1}}{Pe\Delta x^2} + \frac{\theta_{i,j+1,k}^{n+1} - 2\theta_{i,j,k}^{n+1} + \theta_{i,j-1,k}^{n+1}}{Pe\Delta y^2} + \frac{\theta_{i,j,k+1}^{n+1} - 2\theta_{i,j,k}^{n+1} + \theta_{i,j,k-1}^{n+1}}{Pe\Delta z^2} \tag{A.82}$$

The initial and boundary conditions for the geometry of the figure can be written as

$$t = 0, \ \theta_{i,j,k}^{n+1} = 0 \tag{A.83}$$

$$x = 0, \ \theta_{i,j,k}^{n+1} = 0 \tag{A.84}$$

$$x = 1, \ \theta_{i-2,j,k}^{n+1} - 4\theta_{i-1,j,k}^{n+1} + 3\theta_{i,j,k}^{n+1} = 0 \tag{A.85}$$

$$y = 0, \ 3\theta_{i,j,k}^{n+1} - 4\theta_{i+1,j,k}^{n+1} + \theta_{i+2,j,k}^{n+1} = 2\Delta y Nu_{i,j,k}^{n+1} \tag{A.86}$$

$$y = d, \ \theta_{i,j,k}^{n+1} = 0 \tag{A.87}$$

$$z = 0, \ 3\theta_{i,j,k}^{n+1} - 4\theta_{i,j,k+1}^{n+1} + \theta_{i,j,k+2}^{n+1} = 0 \tag{A.88}$$

$$z = r, \ \theta_{i,j,k-2}^{n+1} - 4\theta_{i,j,k-1}^{n+1} + 3\theta_{i,j,k}^{n+1} = 0 \tag{A.89}$$

Equations have been solved by G-S iteration. The solution methodology consists of the following steps [Roche, 1976, Tannehill *et al.*, 1997]:

1. Specify initial values for $\theta_{i,j,k}^{n+1}$ at time $t = 0$

2. Solve equations A.79 to A.86 for $\theta_{i,j,k}^{n+1}$ at time $t = t + \Delta t$ using the Gauss-Seidel iterative method.

3. Continue marching in time till $t = t + \Delta t$ reaches its specified limit or the change in the local two successive time steps is negligible.

A.3   Solution of the Adjoint Problem

The adjoint problem differs from the direct in the following sense.

1. It contains a source term.

2. It contains a negative diffusion term.

3. It contains a final condition instead of an initial one.

Let us consider a typical adjoint equation arising from the three-dimensional unsteady temperature field. Recalling the formulation presented in Chapter 3, we have the following adjoint equation and boundary conditions:

$$\frac{1}{\text{Pe}}\left(\frac{\partial^2\lambda}{\partial x^2}+\frac{\partial^2\lambda}{\partial y^2}+\frac{\partial^2\lambda}{\partial z^2}\right)+\frac{\partial(u\lambda)}{\partial x}+\frac{\partial(v\lambda)}{\partial y}+\frac{\partial\lambda}{\partial t}+2(\theta-Y)\delta(y-y_1)=0 \quad \text{(A.90)}$$

$$t=t_f,\ \lambda=0 \quad\quad \text{(A.91)}$$

$$x=0,\ \lambda=0 \quad\quad \text{(A.92)}$$

$$x=1,\ \frac{\partial\lambda}{\partial x}+u\lambda\text{Pe}=0 \quad\quad \text{(A.93)}$$

$$y=0,\ \frac{\partial\lambda}{\partial y}=-2w\text{Pe}(\theta_w-Y_w) \quad\quad \text{(A.94)}$$

$$y=d,\ \lambda=0 \quad\quad \text{(A.95)}$$

$$z=0,\ \frac{\partial\lambda}{\partial z}=0 \quad\quad \text{(A.96)}$$

$$z=r,\ \frac{\partial\lambda}{\partial z}=0 \quad\quad \text{(A.97)}$$

Letting $\tau=t_f-t$ we have the following transformed system:

$$\frac{\partial\lambda}{\partial\tau}-\frac{\partial(u\lambda)}{\partial x}-\frac{\partial(v\lambda)}{\partial y}=\frac{1}{\text{Pe}}\left(\frac{\partial^2\lambda}{\partial x^2}+\frac{\partial^2\lambda}{\partial y^2}+\frac{\partial^2\lambda}{\partial z^2}\right)+2(\theta-Y)\delta(y-y_1) \quad \text{(A.98)}$$

$$\tau=0,\ \lambda=0 \quad\quad \text{(A.99)}$$

$$x=0,\ \lambda=0 \quad\quad \text{(A.100)}$$

$$x=1,\ \frac{\partial\lambda}{\partial x}+u\lambda\text{Pe}=0 \quad\quad \text{(A.101)}$$

$$y=0,\ \frac{\partial\lambda}{\partial y}=-2w\text{Pe}(\theta_w-Y_w) \quad\quad \text{(A.102)}$$

$$y=d,\ \lambda=0 \quad\quad \text{(A.103)}$$

$$z = 0, \quad \frac{\partial \lambda}{\partial z} = 0 \qquad (A.104)$$

$$z = r, \quad \frac{\partial \lambda}{\partial z} = 0 \qquad (A.105)$$

The equation is now reduced to an initial value problem. The solution methodology of the direct problem can now be used. However, the negative advection terms and the Dirac Delta function must have to be treated carefully.

A.4 Discretization of Convective Terms

In the parabolic problems, the convective terms have been discretized by a central difference scheme. For the elliptic equations, two and three dimensional QUICK schemes have been used. The QUICK algorithm (Quadratic Upstream Interpolation for Convective Kinematics) is based on local upstream-weighted quadratic interpolation in estimating numerical cell face values and gradients of all field variables undergoing simultaneous convection and diffusion. For pure convection, the scheme is third order accurate.

To elaborate the scheme, let us consider one dimensional convection and diffusion of a scalar ϕ; its transport is governed by the equation

$$\frac{\partial \phi}{\partial t} + u \frac{\partial \phi}{\partial x} = \Gamma \frac{\partial^2 \phi}{\partial x^2} \qquad (A.106)$$

where u is the convective velocity in the x direction and Γ is the diffusion coefficient. Considering a uniform grid the term $\frac{\partial \phi}{\partial x}$ can be written as

$$\frac{\partial \phi}{\partial x} = \frac{\phi_{i+\frac{1}{2}} - \phi_{i-\frac{1}{2}}}{\Delta x} \qquad (A.107)$$

now

$$\phi_{i-\frac{1}{2}} = \phi_{\text{LIN}} - \frac{1}{8} \text{CURV} \Delta x^2 \qquad (A.108)$$

where

$$\phi_{\text{LIN}} = \frac{1}{2} (\phi_i + \phi_{i-1}) \qquad (A.109)$$

and

$$\text{CURV} = \frac{\phi_i - 2\phi_{i-1} + \phi_{i-2}}{\Delta x^2}, \text{ if } u_{i-\frac{1}{2}} > 0 \qquad (A.110)$$

$$\text{CURV} = \frac{\phi_{i+1} - 2\phi_i + \phi_{i-1}}{\Delta x^2}, \text{ if } u_{i-\frac{1}{2}} < 0 \qquad (A.111)$$

For two and three dimensions (i.e. if the scalar is a function of all three dimensions) the Equation A.105 becomes

$$\phi_{i-\frac{1}{2},j} = \phi_{\text{LIN}} - \frac{1}{8}\text{CURV}\Delta x^2 + \frac{1}{24}\text{CURVTY}\Delta y^2 \qquad (A.112)$$

and

$$\phi_{i-\frac{1}{2},j,k} = \phi_{\text{LIN}} - \frac{1}{8}\text{CURV}\Delta x^2 + \frac{1}{24}\text{CURVTY}\Delta y^2 + \frac{1}{24}\text{CURVTZ}\Delta z^2 \quad (A.113)$$

where

$$\text{CURVTY} = \frac{\phi_{i-1,j+1} - 2\phi_{i-1,j} + \phi_{i-1,j-1}}{\Delta y^2}, \text{ if } u_{i-\frac{1}{2},j} > 0 \qquad (A.114)$$

$$\text{CURVTY} = \frac{\phi_{i,j+1} - 2\phi_{i,j} + \phi_{i,j-1}}{\Delta y^2}, \text{ if } u_{i-\frac{1}{2},j} < 0 \qquad (A.115)$$

$$\text{CURVTZ} = \frac{\phi_{i-1,j,k+1} - 2\phi_{i-1,j,k} + \phi_{i-1,j,k-1}}{\Delta z^2}, \text{ if } u_{i-\frac{1}{2},j,k} > 0 \qquad (A.116)$$

$$\text{CURVTZ} = \frac{\phi_{i,j,k+1} - 2\phi_{i,j,k} + \phi_{i,j,k-1}}{\Delta z^2}, \text{ if } u_{i-\frac{1}{2},j,k} < 0 \qquad (A.117)$$

This discretization scheme of the convective terms has been employed in all elliptic direct, adjoint and sensitivity problems and in the vorticity transport equation. The scheme is found to be free of any oscillation for the range of grid sizes, Reynolds numbers and Peclet numbers studied.

A.5   Time Step Estimation

For accuracy of numerical simulation, the mesh size must be chosen small enough to resolve the expected spatial variations in all dependent variables. Once a mesh has been chosen, the condition on the time step necessary to prevent numerical instabilities are determined from the combination of Courant-Friedrichs-Lewy (CFL) criterion and the restriction of the grid Fourier number. According to the CFL condition, the distance the fluid travels in one time increment must be less than one space increment. This leads to a constraint on the time step in the form

$$\Delta t < \left[\frac{\Delta x}{|u|}, \frac{\Delta y}{|v|}\right] \qquad (A.118)$$

The grid Fourier number restriction can be applied as

$$\Delta t < \frac{\text{Re}}{2}\left[\frac{(\Delta x \Delta y)^2}{(\Delta x)^2 + (\Delta y)^2}\right] \qquad (A.119)$$

The minimum of this two is the upper limit of time step for explicit computation. For implicit formulation the time step is taken less than 10 times of the corresponding explicit time step.

Appendix B

Grid Independence and Code Validation

B.1   Grid Independence Test

The performance of any numerical scheme with respect to accuracy is highly dependent on the size of grid chosen. In the present study extensive numerical experiments have been performed to finalize the grid size for computation. It is observed that as the Reynolds number increases, the grid size has to be made smaller to have a grid independent solution.

For the flat plate, the domain size is 1×1. The Reynolds number range is 500 to 100000. A uniform grid is used with mesh size varies from from $.01 \times .01$ to $.001 \times .001$ has been used.

For ribbed surface, the domain length is 47.5×6.5. The grid is non-uniform, varying in a geometric progression. For a Reynolds number up to 845, it is observed that a grid points of 251×71 is sufficient. The same fineness has been maintained in the present work for all Reynolds number, ranging from 100 to 300. The grid size varies from .01 close to the rib to .6 away from it, as shown in Figure B.1.

A grid independence test result for the two dimensional energy equation is shown in Figure B.2. The Reynolds number for this plot is 300 (based on the rib height). The local Nusselt number distribution has been plotted and three grid sizes are tested.
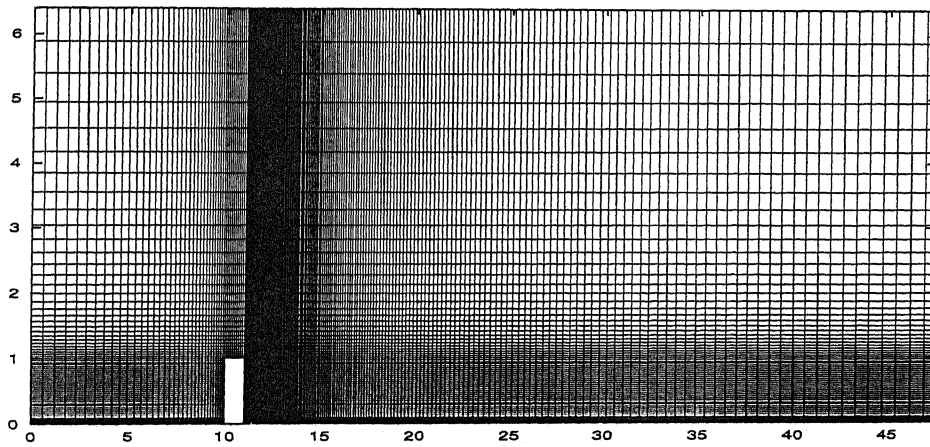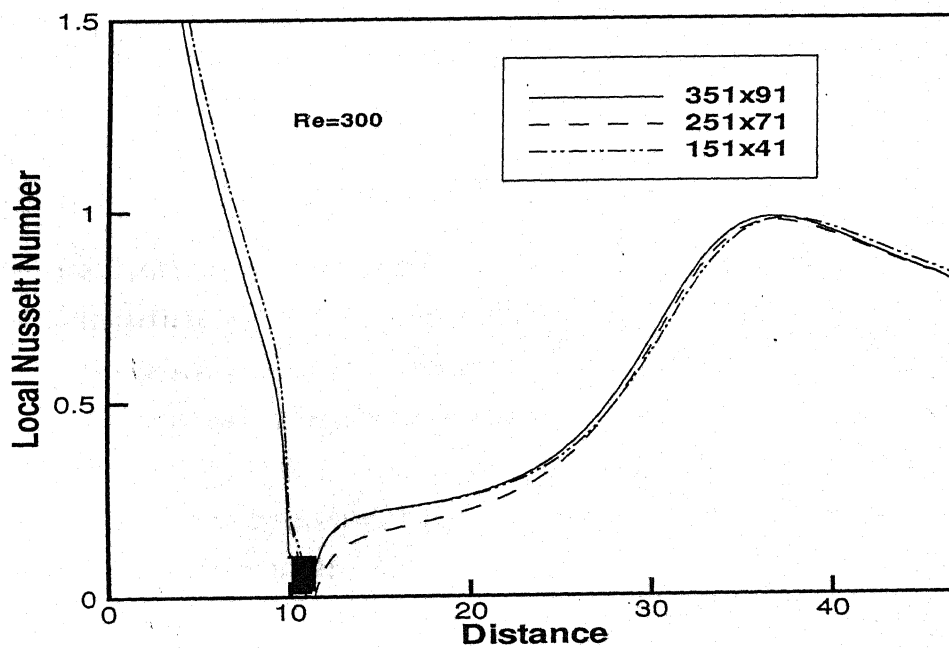
Figure B.1: Grids for a Ribbed Surface.

Figure B.2: Grid independence test for two dimensional energy equation.

B.2   Code Validation

All the computer programs have been extensively validated against analytical, experimental and published numerical results.

B.2.1   Two Dimensional Boundary Layer Solution

Two dimensional velocity and temperature field can be solved analytically with the boundary-layer approximation. This gives the following expressions for skin friction coefficient and the local Nusselt number:

$$C_f = 0.644 \mathrm{Re}_x^{-\frac{1}{2}} \tag{B.1}$$

$$\mathrm{Nu}_x = 0.332 \mathrm{Pr}^{\frac{1}{3}} \mathrm{Re}_x^{\frac{1}{2}} \tag{B.2}$$

The numerical solutions were compared with these analytical solutions and are shown shown in figure B.3

B.2.2   Three Dimensional Boundary Layer Solution

To validate the three dimensional boundary layer solution of the energy equation, a constant temperature over the whole plate was utilized. The solution along the mid-plane (along z direction) has been compared with the analytical and two dimensional boundary-layer solutions in Figure B.3

B.2.3   Vorticity-Stream Function Solution

The two dimensional velocity field has been solved by the vorticity-stream function formulation in a non-uniform grid shown of Figure B.1. The velocity code is validated against experimental results and published numerical simulations.

The comparison is against the numerical solution of backward facing step problem [Gartling, 1990]. The Reynolds number of flow being based on channel height is 800. The backward facing step height is half the channel height. The inlet velocity profile is parabolic.

The experimental validation has been conducted in the wind tunnel described in Chapter 5. Hot wire anemometry (single wire probe) is used to measure the streamwise velocity distribution. As the hot wire anemometer is unable to capture the direction of velocity, near rib region region shows a mismatches.

The comparisons are presented in Figure B.4.

B.2.4   Two Dimensional Elliptic Energy Equation Solution

The two dimensional elliptic energy equation solver has been compared with experimental and published numerical results in Figure B.5. The numerical result has been compared with a laminar flow solution past a heat generating obstacle [Leung *et al.*, 2000] at three different Reynolds numbers. Here the obstacle is placed in an insulated channel. The channel height is considered as the characteristic length. The zero gradient condition has been applied on the outflow plane.

Experimental validation has been carried out in the wind tunnel described in Chapter 5. For this validation, flow is established over the plate while the heating is on. After a long time the temperature field becomes steady. Temperature profiles at selected locations have been measured using RTD, and compared with the numerical simulation [Figure B.5].

B.2.5   Three Dimensional Elliptic Energy Equation Solution

Three dimensional elliptic energy equation is solved for constant plate temperature and mid plane results are compared with two-dimensional energy equation solver. The results are shown in Figure B.6.
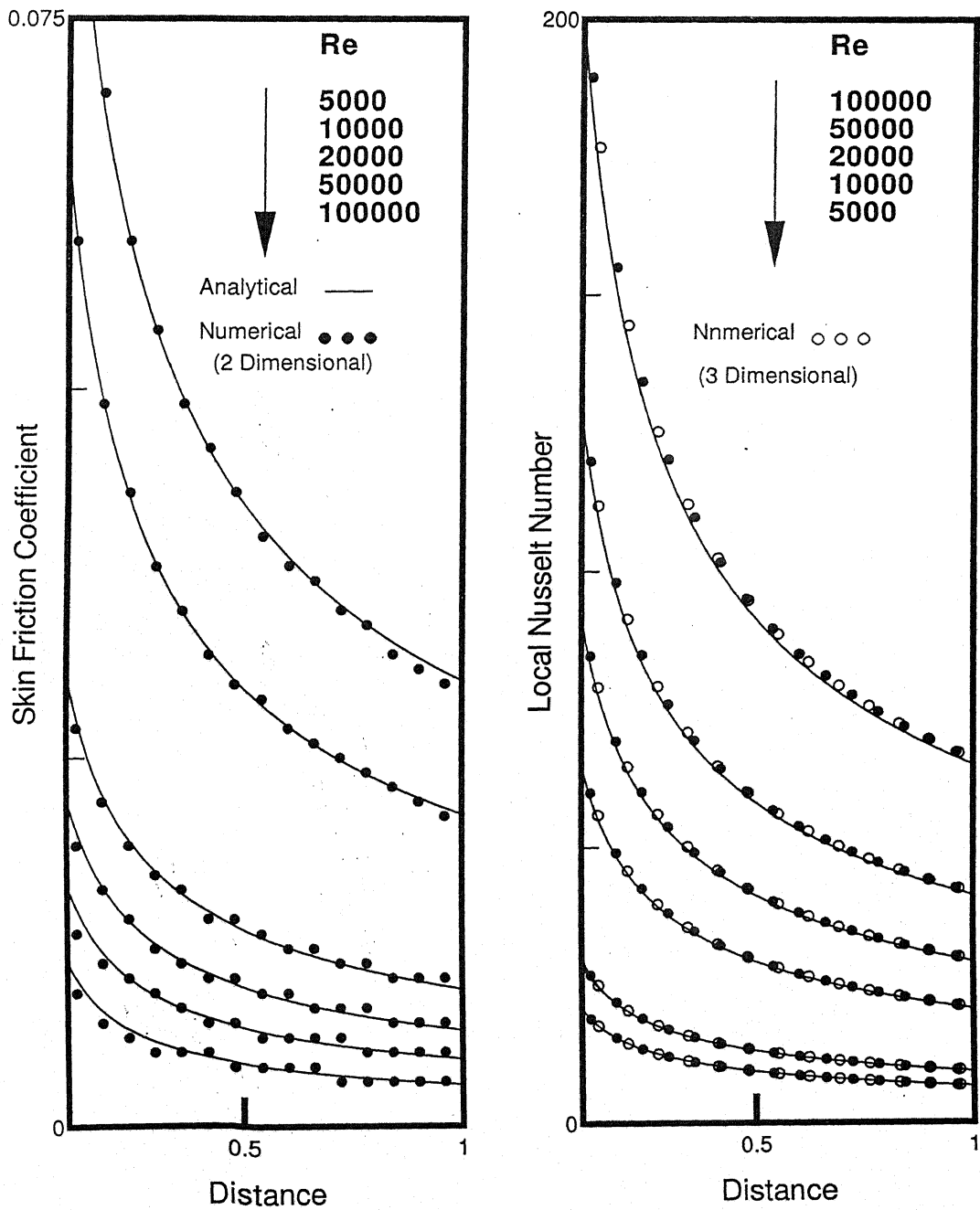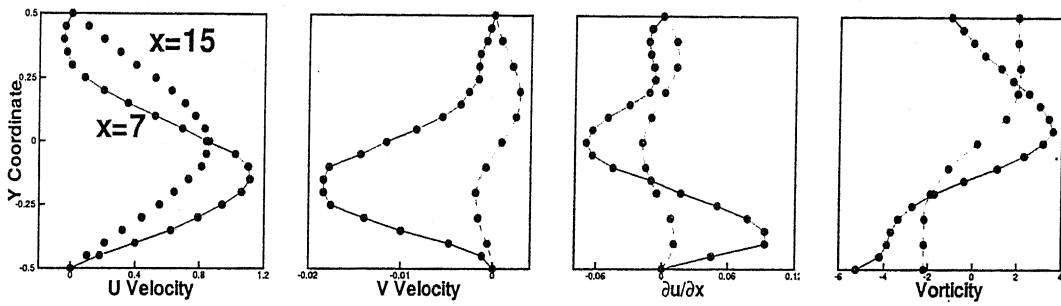
Figure B.3: Comparison of analytical and numerical solutions of two dimensional momentum and two/three dimensional energy equation.

Numerical Comparison with Backward Facing Step Problem
Re=800
● ● ● ● Present Solution

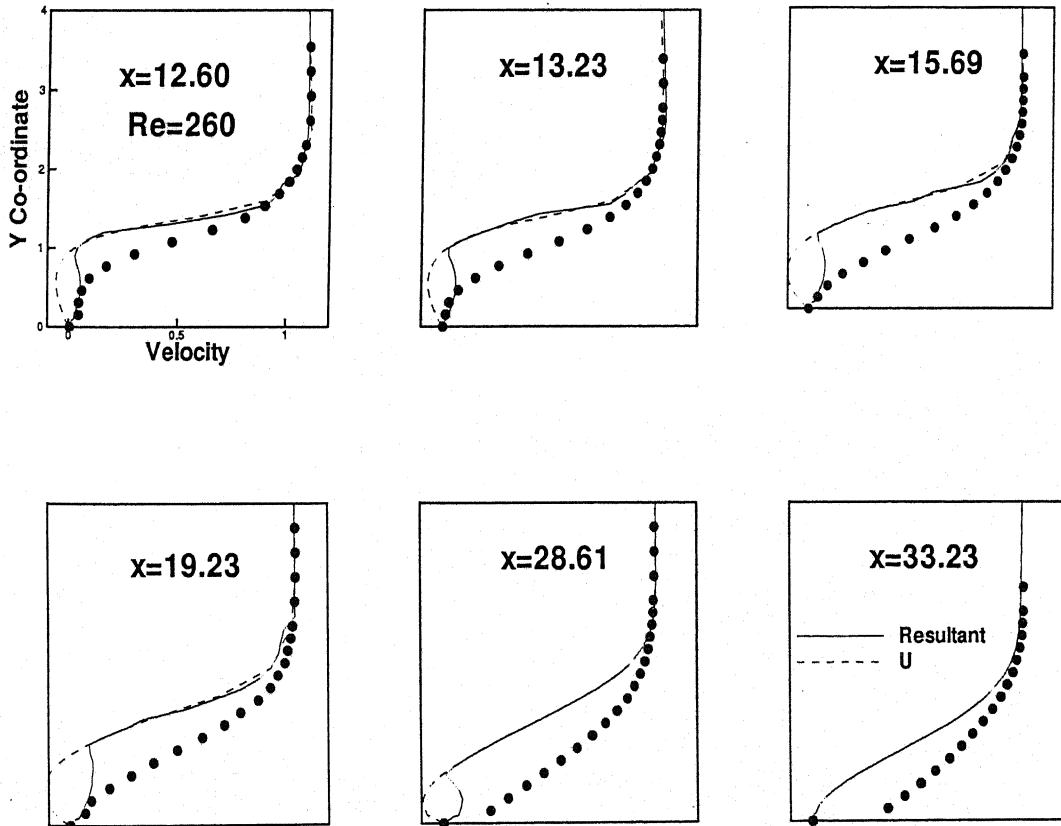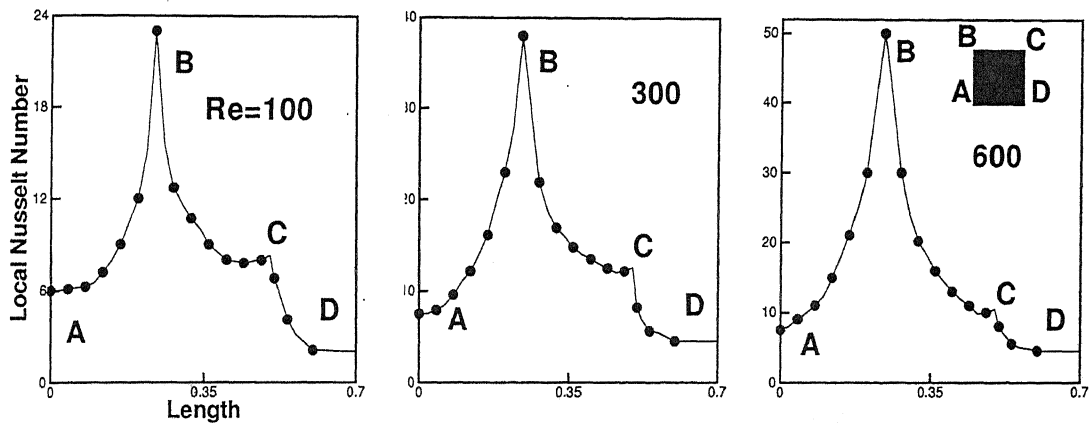## Comparison with Experimental Results
● ● ● ● Experimntal

Figure B.4: Validation of the stream function-vorticity solution.

Present Solution ⊕ ⊕   Published Solution ————————

Comparison with Numerical Results
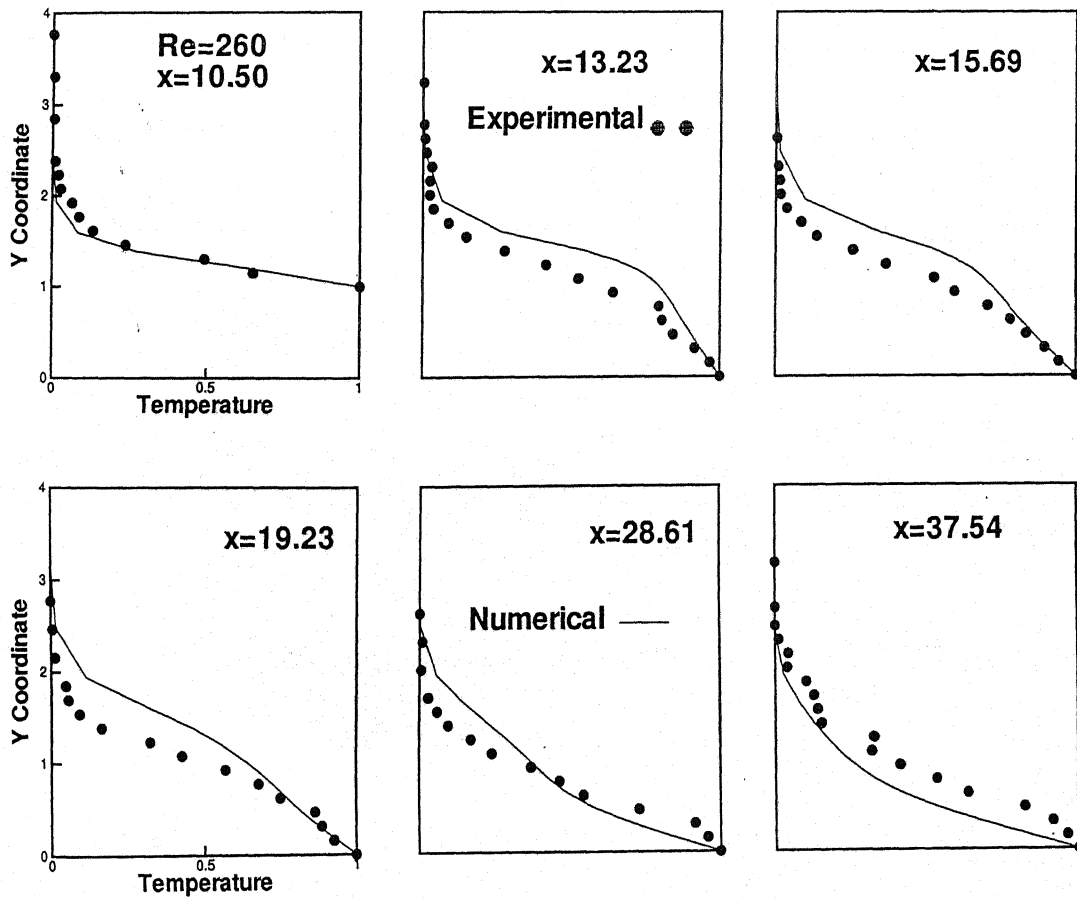

Comparison with Experimental Results

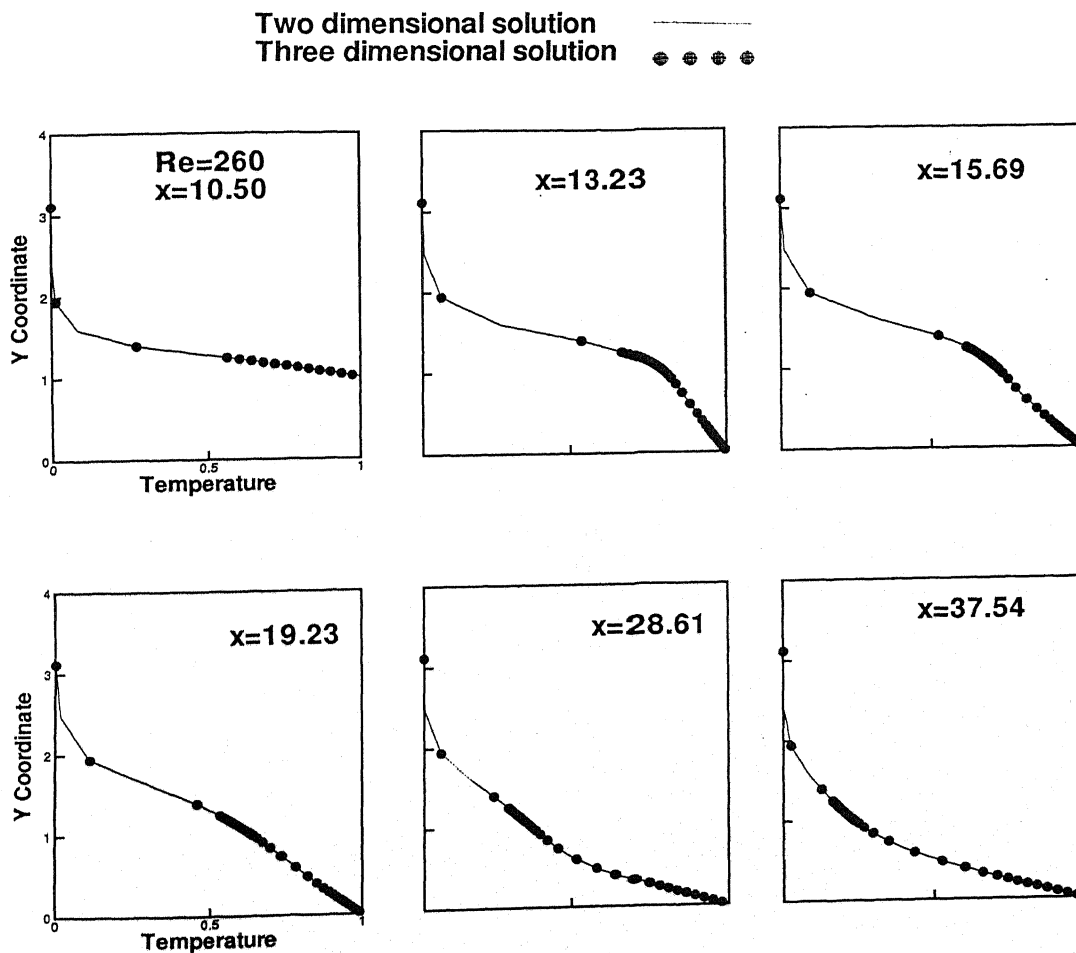Figure B.5: Validation of the two-dimensional energy equation.

Figure B.6: Comparison of two and three dimensional elliptic energy equation solution.

Appendix C

Gaussian Random Number Generation

The scatter in temperature measurement has been assumed to have a Gaussian probability distribution. For simulating experimentally derived scatter, the Box-Muller method is used to transform white noise to Gaussian noise [Press *et al.*, 2000]. White noise has a uniform variate and is obtained from built-in function RAND of the FORTRAN library. A brief outline of the Box-Muller method is given here.

If $x_1, x_2, \ldots$ are random deviates with a joint probability distribution of $p(x_1, x_2, \ldots) dx_1 dx_2 \ldots$ and if $y_1, y_2, \ldots$ are each function of all the $x_1, x_2, \ldots$ (same number of $y_1, y_2, \ldots$ as $x_1, x_2, \ldots$), then the joint probability distribution of the $y_1, y_2, \ldots$ is

$$p(y_1, y_2, \ldots) dy_1 dy_2 \ldots = p(x_1, x_2, \ldots) \left| \frac{\partial(x_1, x_2, \ldots)}{\partial(y_1, y_2, \ldots)} \right| dy_1 dy_2 \ldots \qquad (C.1)$$

where $|\partial()/\partial()|$ is the Jacobian determinant of the $x_1, x_2, \ldots$ with respect to the $y_1, y_2, \ldots$ (or reciprocal of the Jacobian determinant of the $y_1, y_2, \ldots$ with respect to the $x_1, x_2, \ldots$).

An important example of the use of equation (C.1) is the Box-Muller method for generating random deviates with a normal (Gaussian) distribution, namely

$$p(y) dy = \frac{1}{\sqrt{2\pi}} e^{-\frac{y^2}{2}} dy \qquad (C.2)$$

Considering the transformation between two uniform deviates on (0,1), x_1, x_2 and two quantities y_1, y_2 we get

$$y_1 = \sqrt{-2 \ln x_1} \cos 2\pi x_2 \qquad (C.3)$$

$$y_2 = \sqrt{-2\ln x_1}\sin 2\pi x_2 \qquad (C.4)$$

Equivalently we can write

$$x_1 = \exp[-\frac{1}{2}(y_1^2 + y_2^2)] \qquad (C.5)$$

$$x_2 = \frac{1}{2\pi}\arctan\frac{y_2}{y_1} \qquad (C.6)$$

Now the Jacobian can readily be calculated

$$\frac{\partial(x_1, x_2)}{\partial(y_1, y_2)} = \begin{vmatrix} \frac{\partial x_1}{\partial y_1} & \frac{\partial x_1}{\partial y_2} \\ \frac{\partial x_2}{\partial y_1} & \frac{\partial x_2}{\partial y_2} \end{vmatrix} = -\left[\frac{1}{\sqrt{2\pi}}e^{-\frac{y_1^2}{2}}\right]\left[\frac{1}{\sqrt{2\pi}}e^{-\frac{y_2^2}{2}}\right] \qquad (C.7)$$

Since this is the product of a function of y_2 alone and a function of y_1 alone, we see that each y is independently distributed according to the normal distribution (C.7).

There is an easy way of implementation of this algorithm as shown by Press *et al.* [2000]. This calls for the following steps:

1. Choose two uniform variate (v_1 and v_2) within the unit circle (not unit square), so that their sum of squares ($R^2 = v_1^2 + v_2^2$) is within the circle.

2. Define a uniform variate $x_1 = R^2$.

3. Define $v_1/v_2 = 2\pi x_2$ which gives cosine and sine in Equations C.3 and C.4 as v_1/R and v_2/R respectively.

4. Using Equations C.3 and C.4 find the corresponding Gaussian random number y_1 and y_2.

A 144549